UNIVERSITY OF CALABRIA

DEPARTMENT OF CHEMISTRY AND PHYSICS

"B. Telesio – Doctorate School of Science and Technique"

Mesophase and Molecular materials

(STM^3) – XXV Cycle

CHIM/03

Ph. D. Thesis

"Hydrophilic Ir(III) complexes suitable for the construction of functional mesoporous materials"

School Director

Prof. Roberto Bartolino

Supervisor

Prof. Mauro Ghedini

Curriculum Coordinator

Prof. Carlo Versace

Candidate

Yogesh Jivajirao Yadav

Academic year: 2011 - 2012

UNIVERSITÁ DELLA CALABRIA

DIPARTIMENTI DI CHIMICA E FISICA

Scuola Di Dottorato – B. Telesio
"Scienze e Tecnologie delle Mesofasi e dei Materiali Molecolari"
(STM^3) – XXV Ciclo
CHIM/03

Ph. D. Thesis

"Hydrophilic Ir(III) complexes suitable for the construction of functional mesoporous materials"

Direttore della Scuola
Prof. Roberto Bartolino

Supervisore
Prof. Mauro Ghedini

Curriculum Coordinatore
Prof. Carlo Versace

Candidato
Yogesh Jivajirao Yadav

Anno Accademico: 2011 – 2012

To my family

&

Dr. Elisabeta Ildyko Szerb

Acknowledgement

It is a privilege to express my greatest gratitude to the people, who have helped and supported me throughout PhD course. It is very tough to remember all the peoples who have contributed to my life during these three years.

Foremost, I would like to express my sincere gratitude to my Prof. Mauro Ghedini for his supervision, inspiration, immense knowledge and for providing me such a wonderful opportunity to accomplish my PhD.

I would like to convey my very special thanks to Dr. Elisabeta Ildyko Szerb for her valuable and constructive suggestions and consistent encouragement, which I received throughout my research work. Without her guidance I would have been unable to complete my thesis. She did lots of things in every aspect of my PhD thesis. She is very caring, loving and kind person I have seen ever in my life. I don't have words to express thankfulness to her.

I would like to thanks Dr. Anna Maria Talarico for her help on photophysical properties of my complexes. Thanks to Dr. Teresa F. Mastropietro for her assistance on structural characterization of my complexes. I am also grateful for the extraordinary help regarding my permit stay and accommodation in Italy given by Dr. Nicolas Godbert and Dr. Paoletta Ciancio.

I would like to acknowledge Prof. Alessandra Crispini, Prof. Daniella Pucci, Dr. Iolinda Aiello and Massimo La Deda for their great support and suggestions.

My sincere thanks go to our collaborators Dr. Bertrand Donnio and Dr. Heinrich Benoit for providing me an opportunity to do research work at IPCMS - Département des Matériaux Organiques (DMO), University of Strasbourg, France.

I would like to extend my thanks to Prof. Carlo Versace, coordinator of this PhD course, and Prof. Roberto Bartolino, chairman of the doctorate school of B. Telesio who were always available towards all Ph. D. students, whenever required.

I would like to acknowledge Prof. Prof. Giuseppina De Luca for her assistance regarding the H NMR studies.

I would like to extend my thanks to my labmate, Dr. Barbara Sanz, who helped me in completing my thesis. I wish to thanks Dr. Loredana Ricciardi, Dr. Andreeea Ionescu, Dr. Paola Liguori, Dr. Sante Pirillo, Dr. Luigi Rizzuti, Eugenio Giorno, Valentinea Febbraio and my friends from India, Italy and around the globe who appreciated me and motivated me for my work.

Eventually, I want to thank my family members for their support, who inspired me and encouraged me to complete my project.

Finally, I would like to thanks god for gifting me such kind, cooperative, loving and supportive peoples who helped me a lot in my life.

Thanks once again to all

Summary

Nowadays, intensive efforts have been carried out on the design of novel advanced molecular materials, which can self-assemble in a strong, directional and reversible way to construct supramolecular materials with specific properties. The rational design and preparation of supramolecular assemblies through the coordination of metal ions with organic ligands has attracted attention for developing novel crystalline materials with interesting structural topologies and promising applications, and has evolved as an interesting research. The metals used in these complexes can serve as structural components and/or as a source of properties (e.g., magnetic, catalytic, optoelectronic, etc).

Cyclometallated Ir(III) octahedral complexes possess fascinating properties used in various applications such as luminescent and electrochemiluminescent labeling reagents for biological substrates[1], sensors[2], or electronic devices[3,4]. Recently, the interest in ionic Ir(III) complexes is growing rapidly because not only high internal quantum efficiency (~100%) can be achieved in principle, but also tunable emission wavelengths over the entire visible spectrum can be successfully obtained through ingenious modification of ligands. In particular, Ir(III) complexes based on the chelating ligand 2,2'-bipyridine (*bpy*) have been successfully applied in light-emitting electrochemical cells (LECs) and sensors.[5]

The theoretically calculated phosphorescence yield (Φp) of the Ir(III) complexes are close to unity in solution.[6] The solution investigations have made great contributions to the fundamental understanding of luminescence processes at molecular level. The conclusions drawn from the dilute solution data, however, cannot commonly be extended to the concentrated solutions. Indeed, many Ir(III) complexes show very different light-emitting behaviors in dilute and concentrated solutions and respectively in the solid state. The luminescence is often weakened or quenched at high concentrations, a phenomenon widely known as "concentration quenching". A main cause for the quenching process is mechanistically associated with the "formation of aggregates", which is probably why the concentration quenching effect has frequently been referred to as "aggregation-caused quenching" (ACQ).

On the other hand "aggregation-induced phosphorescent emission" (AIPE) is an unusual phenomenon existing also in transition metal complexes, which have no emission in solution but

enhanced emission in the solid state.[7] There are some examples of AIPE, most of them in neutral Ir(III) complexes.[8, 9, 10, 11, 12]

The main strategies to avoid unpleasant quenching phenomena are based on the dispersion of the chromophore. Mainly, two strategies are employed: engineering at molecular level by introducing functionalities able to electronically disconnect the chromophores (bulky groups or functionalities capable to construct hard crystalline or soft dynamic supramolecular assemblies) or isolating the active molecules in different host matrices (host-guest systems).[13] In particular, the dispersion of a chromophore into mesoporous materials not only prevents the aggregation phenomena but also provides increased thermal, chemical and mechanical stability to the final materials.

Mesoporous materials are ordered porous materials with periodic distribution of pores, high surface area, controllable large pore sizes in the range of 2 – 50 nm and variable topology of the pores. The inorganic matrixes may be made up of SiO_2, TIO_2, ZrO_2, Al_2O3, Nb_2O_5 etc.

Basically, the synthesis of ordered functional mesoporous materials is based on the condensation of an inorganic scaffold on the organised structure formed in water by surfactant molecules. Two different strategies may be employed, the cooperative self-assembly mechanism (CSA) and the true liquid crystal templating' (TLCT) mechanism.[14] The functionalization of the mesoporous material may be done in both cases by inserting the chromophore into the primarily water solution. Therefore, ***water soluble chromophores*** may guarantee a better compatibility with the surfactant/water system, whereas a proper functionalization on the molecular structure of the chromophore that permit the self-assembly into supramolecular ordered water assemblies, will allow to use the chromophores directly as structure directing agents (SDAs).

Since the photophysical properties of the ionic complexes are influenced profoundly by the surroundings of the molecule both in solution and in condensed states, it is fundamental to study the behavior of such complexes in these different states, in order to achieve a fine tuning of the properties as a function of their structure and order in the final material.

The knowledge gained in the assembling of supramolecular materials using non-covalent bonds may be used for the construction of ordered systems in water. This strategy will permit the one-step synthesis of functional mesoporous materials, and to control the order of the final material controlling the order in water of the functional Ir(III) complexes.

In particular, the molecular fragments that one can change to achieve the desired properties in the final ionic Ir(III) complexes are the cyclometallating or coordinating ligands, and respectively the counterion. My research therefore is focused on the design and synthesis of hydrophilic ionic Ir(III) complexes with flexible or rigid ancillary ligands and use of different counterions, all suitable for

controlling the supramolecular assembly in the solid state, and to transfer the knowledge gained into obtaining ordered structures in water, or water-surfactant systems, necessary for the synthesis of mesoporous materials with defined properties.

The ionic octahedral Ir(III) complexes synthesised during this thesis and their classification in different classes are presented in the figure S1.

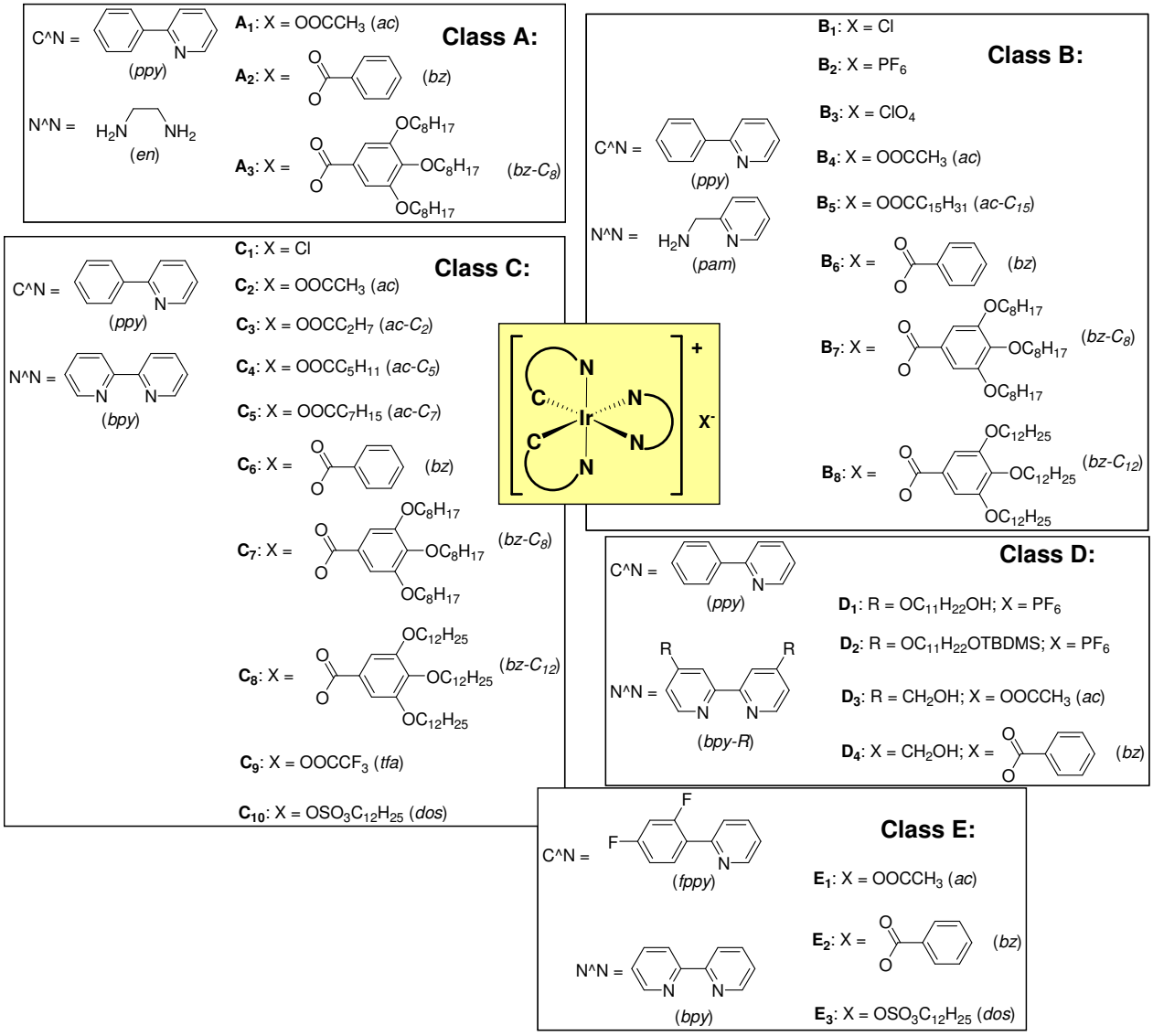

Scheme S1. Chemical structure of the ionic octahedral complexes synthesized.

I. Introduction

Luminescent materials are known to human being from ancient times and as time passes its importance has been enhanced in various fields. Nowadays, luminescent materials have seen the opening of many new research fields in which luminescent molecular materials have been forced, through chemical ingenuity, to acquire fundamental properties which are associated with classic materials. Moreover, the excited states and photophysical properties of transition metal complexes have fascinated chemists and physicists from an intellectual point of view for several decades, but this field has now taken on added importance because of several recent significant discoveries. In particular, luminescent transition metal complexes have interesting photophysical properties and are intensively researched for practical applications in a large variety of fields. Precisely, they can be used as photo-sensitizers in solar energy conversion[15], in chemo/electroluminescent systems[16], emissive dopants in organic light emitting devices (OLEDs)[17,18], photo catalysts for CO_2 reduction[19], luminescent sensors[20], biological labels[21] and biological probes[22]. These applications have focused mainly on a few key 2nd and 3rd row transition metals [*i.e.* Re(I), Ru(II), Os(II), Pt(II), Rh(III) and Ir(III)].

In particular, the chemistry of cyclometalated Ir(III) complexes is a current topic of investigation because of their unique photophysical properties and applications in light emitting devices such as *organic light emitting diodes* (OLEDs) for neutral complexes, and *light emitting electrochemical cells* (LEECs) for ionic complexes.

Recently, the OLEDs have evolved as the best candidate in the generation of full color flat panel display with potential application in display technology. State-of-the-art OLEDs are typically made of multiple layers of organic materials, sandwiched in between an anode, typically a transparent oxide film, such as indium–tin oxide (ITO), and an air-unstable cathode (Ca, Ba) often coupled with an electron-injection layer (Figure I.1.a). Such complex architectures are necessary to provide a balanced injection of positive and negative charges across the device, which must precisely recombine in the light-emitting layer, to grant the physical integrity of the whole device under the applied bias for hundreds of hours.[23] Nowadays, OLEDs can be utilized for display and illumination but their manufacturing still needs costly and complex procedures in an inert environment that must be followed by a rigorous encapsulation of the final device, particularly because of the presence of

low work-function metals or doped injection layers which are extremely sensitive to ambient oxygen and moisture. The multilayer structure, additionally, makes large-area processing extremely difficult, and ultimately imposes a production cost of OLEDs still incompatible with widespread applications in the general lighting market.

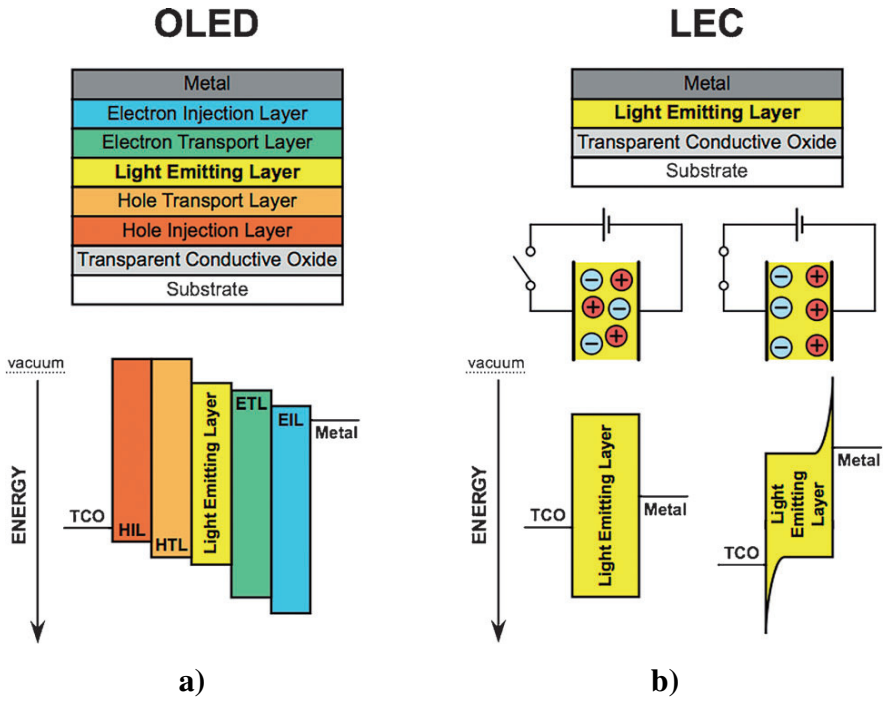

Figure I.1 Schematic representations of a typical a) OLED and b) LEC.

Furthermore, alternative to OLEDs are the *light-emitting electrochemical cells* (LECs), that have emerged as promising candidates for next-generation of solid-state lighting sources[24] having several advantages over OLEDs *i.e.* single-layer, solution-process, air-stable cathodes and low driving voltages, etc. Indeed, LECs have a much simpler architecture, are processed from solution and do not rely on air-sensitive charge-injection layers or metals for electron injection (Figure I.1.b). The concept of LEC was introduced in 1995 by Pei et al., who mixed an inorganic salt to a mixture of a conjugated luminescent polymer and an ionic conductive polymer whose chemical structure are presented in Figure I.2.a (MEH-PPV=poly[5-(2'-ethylhexyloxy)-2-methoxy-1,4-phenylene vinylene], PEO = poly-(ethylene oxide) and $[CF_3SO_3]^-Li^+$ = lithium trifluoromethanesulfonate).[25] Soon after this seminal contribution, an alternative approach was proposed by Maness et al., who utilized the Ru (II) ionic transition-metal complex presented in Figure I.2.b (poly-$[Ru(vbpy)_3]^{2n+}$, *vbpy* = 4-vinyl-4'-methyl-2,2'-bypiridine). In this approach, the Ru(II) complex and its counterion

[PF_6] play several key roles: promotion of charge injection from the electrodes, electron and hole transport through the device and, thanks to the intrinsic orange emission, luminescence.

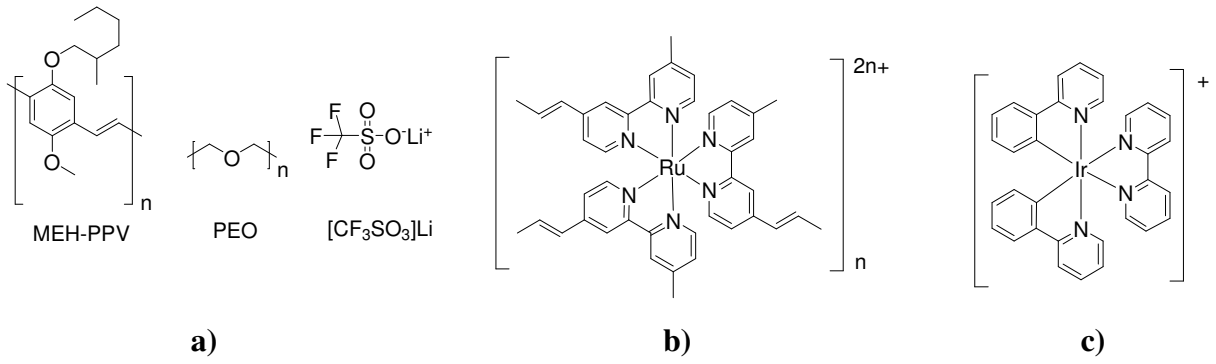

Figure I.2 Chemical structure of materials used in the first LECs a) MEH-PPV, PEO and [CF_3SO_3]Li, b) poly-[Ru(*vbpy*)$_3$]$^{2n+}$ and c) [Ir(*ppy*)$_2$(*bpy*)]$^+$.

Nowadays, the *ionic transition metal complexes based LECs* (iTMC-LECs) are mostly based on luminescent ionic biscyclometalated Ir(III) complexes.[26] The archetypal complex of this large family of Ir(III)-iTMCs used in LECs is [Ir(*ppy*)$_2$(*bpy*)]$^+$, in which *ppy* = 2-phenylpyridine and *bpy* = 2,2'-bipyridine (Figure I.2.c), as the single active component in the light-emitting layer.[27] This type of complexes, like the original Ru(II) complex, may sustain charge injection and transport while affording, at the same time, light emission.

A crucial benefit in the use of ionic compounds is the processability: iTMCs dissolve in polar benign solvents, allowing the devices to be prepared by facile coating or printing processes. In addition, the use of iTMCs allows novel device fabrication processes, such as soft-contact lamination[28], as well as the development of large-area illumination panels that do not require any patterning. Finally, the insensitivity of LEC devices to the work function of the electrode material allows air-stable metals to be used as anode and cathodes greatly decreasing the severe technical requirements for the encapsulation of devices. Taken in concern, these characteristics facilitate large-area processing and might give entry to flat electroluminescent devices at more affordable costs.

LECs are prepared by solution-based processes with benign solvents. Most devices reported to date consist of one or two active layers sandwiched in between one transparent and one reflecting electrode (Figure I.3.a).

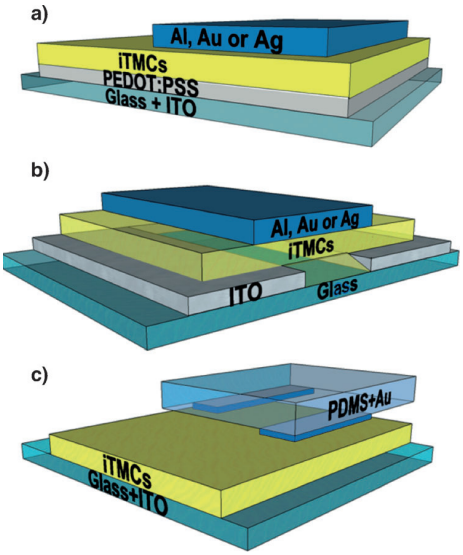

Figure I.3 Schematic layout of a sandwiched (a), cascaded (b), and laminated LEC (c).

Materials most commonly used for electrodes are ITO (transparent anode) and Au, Al, and Ag (air-stable reflecting cathode). Double layer LECs, besides the film of the light-emitting iTMC, entail a hole injection layer, generally composed of PEDOT:PSS [poly(3,4-ethylenedioxythiophene):polystyrenesulfonate]. Such a layer is deposited to smoothen the ITO surface and, as a result, increases the yield of device preparation. An inert polymer or an ionic liquid is frequently added to the iTMC core component to facilitate the formation of the film and to enhance the device performances. In most cases, the top metal contact is thermally evaporated; there are few examples in which it was prepared by soft contact lamination liquid top contacts are also reported.[29]

Bernards et al.[30] and Slinker et al.[31] have made LEC arrays powered directly by a standard US outlet (120 V, 60 Hz), without the use of transformers. These lighting panels consist of several LECs that were placed in series in such a way that the anode of a given device acts also as cathode for the next one (Figure I.3.b). Bernards et al. showed that iTMC-LECs with ITO anodes and laminated Au cathodes (Figure I.3.c) exhibit comparable performance to those fabricated with evaporated top contacts. These devices were made by evaporating the Au electrode onto a polydimethylsiloxane (PDMS) stamp, followed by softcontact lamination onto an iTMC-layer deposited on a patterned ITO substrate. Light emission output is uniform over the whole device area, indicating a high-quality mechanical and electrical contact.

LEC materials can be either conjugated light-emitting polymers or ionic transition-metal complexes, the related devices are termed polymer-LECs (PLECs)[32] or iTMC-LECs,[33] respectively. Both types of LECs have been studied for over 15 years, throughout which many materials, device concepts, and driving schemes have been tested. This research has led to notable achievements in

color, efficiency, turn-on time, and stability. iTMC-LECs differ from PLECs in that the iTMCs are intrinsically ionic and do not need auxiliary charged species to drive the device. In particular, LECs containing the octahedral ionic Ir(III) complexes because of their excellent extraordinary properties like high phosphorescence quantum yield, relatively short life times and color tuning through ligand modification and structure have gained a hot spot in this field. Additionally, iTMCs are typically phosphorescent triplet emitter, which allows for higher electroluminescence efficiencies compared to singlet emitters.[34] iTMCs also allow for easy solubilization in benign solvents and environmentally friendly wet device-preparation processes.[18] Early works on iTMC-LECs focused on differently substituted Ru(II) complexes, such as the archetype $[Ru(bpy)_3][PF_6]_2$; these devices achieved external quantum efficiencies up to 5.5%.[35] However, LECs based on ruthenium chromophores offer limited color tuning because the emission band is placed across the orange–red part of the visible spectrum and this restriction strongly limits the applicative potential for lighting and display technologies, which require wider color tunability. Using luminescent iTMCs based on different metal centers opened the route to the whole color scale[36] and, in this regard, the by far most versatile family of iTMCs is that of Ir(III) (Ir-iTMCs)[37]. These compounds, thanks to a unique combination of physical and chemical properties, provide a huge variety of stable complexes, covering the whole visible spectrum all the way from blue to red. In particular, changing the metal center from a second-row (e.g., Ru) to a third-row (Ir) transition element, the stability of the related complexes is generally improved by 1) increasing the metal–ligand bond strength and 2) by raising the ligand-field splitting energy (LFSE) and making dissociative metalcentered (MC) excited states less thermally accessible compared to Ru(II) analogues.[38] LFSE is further increased, relative to Ru(II) complexes, thanks to the higher electric charge of the Ir ion and by the presence of anionic cyclometalating ligands (C^N), typically used with Ir(III) centers.

All these combined features of Ir-iTMCs can lead to very high emission quantum efficiencies of virtually any color and impart good photochemical stability.[24] The first example of a LEC based on an ionic Ir(III) transition-metal complex was reported by Slinker et al. in 2004.[39] It was a single-layer device emitting yellow light that exhibits a photoluminescence quantum yield (PLQY) in oxygen-free acetonitrile solution of 23.5%.

I.1 Octahedral Ir(III) complexes as luminescent materials

An appropriate active material for practical applications in LEDs require high emission quantum yields, good photophysical, thermal and chemical stability, straightforward and cheap synthesis and ease of processability. Phosphorescent Ir(III) cyclometallated complexes are among the most promising active molecular materials in the research field of electroluminescent devices mostly because of their high phosphorescent efficiencies and tuneable colour over the whole visible spectrum. Nevertheless, these complexes are highly sensitive on molecular environment and dynamics, and often they lose the desired properties while processing. Indeed, the properties of the final material do not only depend on the molecular structure of the 'active molecule' but also on the molecular dynamics and the environment in which is accommodated: the assembly in random or ordered arrangements, rigid or dynamic structures with free or restricted molecular motions and the possibility to form specific intermolecular interactions. In particular, the light emitting processes may be influenced by aggregation in both destructive and constructive mode: the excited states of the aggregates may decay via non-radiative pathways, which is notoriously known as aggregation-caused quenching effect (ACQ) in the condensed phase, or an induction or enhancement of emission may be achieved mostly by restriction of intramolecular rotation (RIR) known as aggregation induced emission (AIE).[40]

Two main strategies were used to overcome the quenching effect: engineering at molecular level by introducing functionalities able to electronically disconnect the chromophores (bulky groups or functionalities capable to construct hard crystalline or soft dynamic supramolecular assemblies) or isolating the active molecules in different host matrices (host-guest systems).[41]

These strategies can provide alternative feasible approaches for improving the molecular-based devices performance. In particular, the devices containing Ir(III) complexes are targeted for electroluminescence studies because of the increased theoretical limit for emission efficiency from triplet emitting complexes (nearly 100% over singlet emitters 25%). The area of luminescent Ir(III) complexes has experienced a huge growth in recent years, prompted by the report in 1998 by Thompson *et al*. that luminescent bis- and tris-cyclometallated Ir(III) complexes can be used as phosphors in OLEDs.[42] They often show intense phosphorescence at room temperature with life times of microseconds (t ~μs). A wide variety of cyclometallated (C^N) ligands and bidentate (N^N) ligands have been used to obtain Ir(III) complexes. By changing either the cyclometallated ligands and/or the ancillary ligands on the metal and also the substituents on the ligands, the

emission wavelength can be controlled and hence a wide region of the visible spectrum can be covered.

The OLEDs that are constructed with neutral complexes typically consist of the luminescent chromophore embedded in an organic matrix sandwiched between multiple layers of charge transport materials and capped with a low work function cathode and a transparent anode. These neutral Ir(III) complexes are widely used as triplet emitters in OLEDs featuring external quantum efficiencies up to nearly 20%. Adachi *et al.*[43] presented a green-emitting device containing [Ir(*ppy*)$_2$(*acac*)] as dopant featuring a maximum external efficiency η_{ext} = 19.0% and a luminous power efficiency of η_p = (60±5) lm·W^{-1}. Recently Zhou *et al.*[44] prepared OLEDs with [Ir(*R*-*ppy*)$_2$(*acac*)] where different main group elements were introduced as substituents at the cyclometallating ligands. Depending on the nature of the substituent, emission color ranging from bluish green (-OPh as substituent) to red (-B(mesityl)$_2$ as substituent) could be realized. When incorporated into devices, good power efficiencies (η_p = 26.8 to 28.6 lm·W^{-1}) and external quantum efficiencies (η_{ext} = 10.3 to 11.1%) were achieved. Furthermore, one of the best true red color device emissions could be obtained by Ho *et al*. using neutral acetoacetone complexes with 9-arylcarbazole motivs in the cyclometallated ligands.[45] These devices showed remarkable external quantum efficiencies η_{ext} = 12% and power efficiencies η_p = 5.3 lm·W^{-1}. Furthermore, using the complex [Ir(*dfppy*)(*fppz*)$_2$] (*dffpyH*:2-(2,4-difluorophenyl)pyridine, *fppzH*:5-(2-pyridyl)-3-trifluoromethyl-pyrazole) as dopant enabled the construction of a deep blue OLED high η_{ext} of up to 8.5% and a power efficiency η_P of 8.5 lm·W^{-1} could be obtained.[46]

Furthermore, cationic Ir(III) complexes have emerged in LECs applications alternative to OLEDs due to their ability to electroluminescence from a single-layer of neat complex sandwiched directly between two air-stable electrodes. This simple device geometry is made feasible by the presence of mobile counterions that redistribute in the presence of an applied potential and facilitate charge injection at the electrodes. Additionally, charge transport occurs through a hopping mechanism, which enables low turn-on voltages (<3 V) and device operation from an alternating current (AC) power source. During the operation of iTMC-based LECs, severe excited-state self-quenching always occurs because complexes in the active layers of LECs are closely packed.[47] To resolve the excited-state-quenching problem and improve the electroluminescence efficiency of LECs, steric hindrance or bulky side groups are introduced into the ancillary ligands of ionic iridium complexes.[48] By enhancing the steric hindrance of ancillary ligand, Su *et al*.[49] developed a highly efficient green-emitting [Ir(*fppy*)$_2$(*bpy*-*R*)](PF$_6$) yielding η_{ext} of 7.1% and a peak power efficiency η_p as high as 26.2 lm·W^{-1}. Following the strategy to stabilize the HOMOs, Bolink *et al*.[6] synthesized

[Ir(*fppy*)$_2$(*tert-Bu-bpy*)](PF$_6$), the LEC based on this complex exhibited a high peak η_{ext} of 14.9% and power efficiency η_p of 39.8 lm·W^{-1}, which represents the most efficient LEC to date.

I.1.1 Classification of Ir(III) octahedral complexes

The Ir(III) octahedral complexes consists mainly of one core of Ir atom and three bidentate ligands. There are two main classifications. Firstly, regarding the molecular structure, Ir(III) complexes may be homoleptic (all ligands are identical) or heteroleptic (having different ligands in the molecular structure). Secondly, Ir(III) complexes may be neutral (formed by three cyclometallating ligands) or charged (principally formed by two cyclometallating ligands and one coordinating ligand). The latter are cationic Ir(III) complexes intensively researched for their applications in LECs. There are known in literature also anionic complexes, formed by two cyclometallating ligands and two monodentate ligands (CN, NCS or NCO). Usually, the atoms in the cyclometallating ligand, which are bonded to the Ir are C and N, where C has a formal negative charge. The most popular ligand used is 2-phenylpyridine. However, there are much fewer examples of complexes of the type [Ir(N^N)$_3$] (N^N) = 1-(2,4-diflurophenyl) parasol and 3-(trifluoromethyl)-5-(2-pyrazole)[50], due to their difficult synthesis and purification.

Primarily there are 4 main types of tris-bidentate homoleptic and heteroleptic Ir(III) complexes discussed in the literature: [Ir(C^N)$_3$], [Ir(C^N)$_2$(O^O)], [Ir(C^N)$_2$(N^N)]$^+$ and [Ir(C^N)$_2$(X)$_2$]$^-$ shown in Figure I.4.

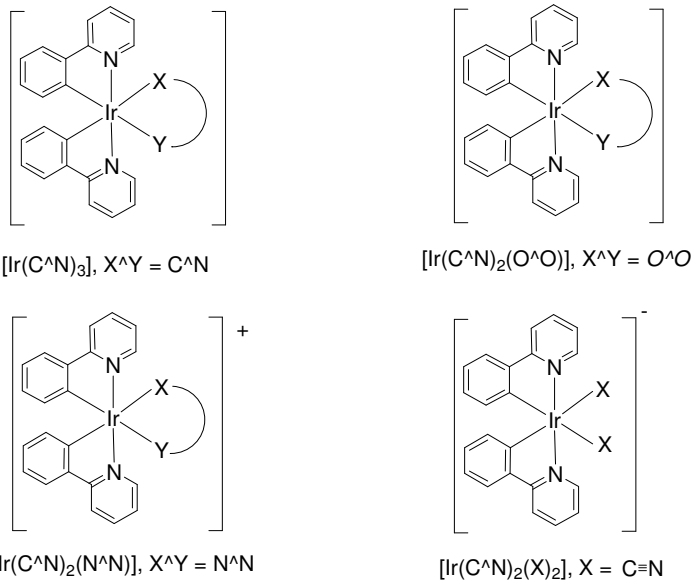

Figure I.4 General types of cyclometallated Ir(III) complexes.

I.1.1.1 Neutral Ir(III) complexes [Ir(C^N)$_3$](n = 0)

The neutral Ir(III) complexes consists of one core of Ir atom and three monoaninoic bidentate ligands. Usually, the atoms in the ligand, which are bonded to the Ir are C and N, where C has a formal negative charge. The most popular ligand used is 2-phenylpyridine (*ppy*). In particular, since the coordination arrangement of a neutral Ir(III) complex is octahedral, it can have two geometric isomers facial (*fac*-) and meridional (*mer*-) (Figure I.5).

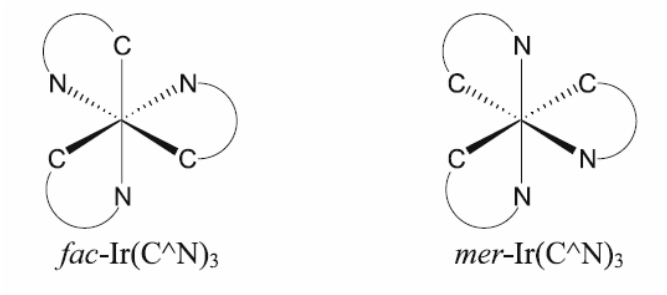

Figure I.5 Possible isomers of neutral Ir(III) complexes [Ir(C^N)$_3$].

Thompson *et al.* have demonstrated that controlling the reaction conditions can impart significant control on the isomer ratio (*fac/mer*).[51] In general, the *fac*-isomer is preferred at higher temperatures (>150°C) and the *mer*-isomer at lower temperature (<150°C). At high temperatures, the *mer*-isomer can be efficiently converted into the *fac*-species, demonstrating that the *fac*-isomer is the thermodynamically more stable isomer, while the *mer* moiety is a kinetic product. Because of the differing *trans* influence of phenyl and pyridyl ligands, the *mer*- and *fac*-isomers exhibit slightly different structural properties. In a *fac*-isomer the Ir – C and Ir – N bonds have nearly identical length; for the corresponding *mer*-isomer, the bonds *trans* to the Ir – C bond are slightly longer than those *trans* to the Ir – N bonds.[52] A practical consequence is that *fac*- and *mer*-isomers may show different electrochemical and spectroscopic properties.[26] Therefore, *fac*-and *mer*-isomers of [Ir(C^N)$_3$] are easily distinguished by ^{1}H NMR spectroscopy since the *fac*-isomers have C_3-symmetry, so, give only one set of ligand signals.

Nevertheless since the *fac*-isomer has higher phosphorescence quantum yield (Φp) is preferred with respect to *mer*-isomers. The different types of ligands used in the synthesis of neutral Ir(III) complexes as cyclometallating (C^N) ligands or charged/anionic (X^Y)ligands are presented in Figure I.6.

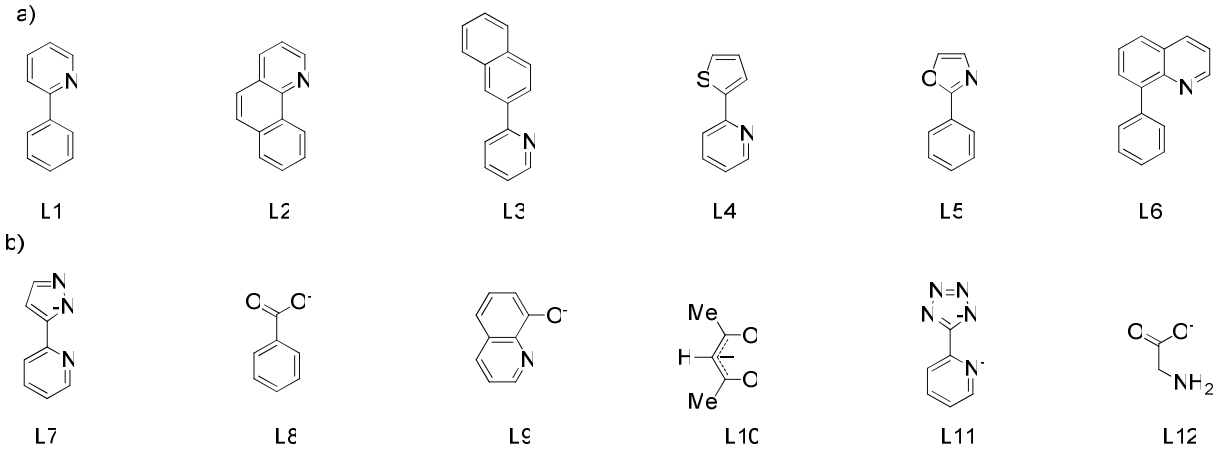

Figure I.6 a) Cyclometallating ligands (C^N), b) Charged ligands (X^Y) used in neutral Ir (III) complex chemistry.

Hence, an enormous number of possible neutral Ir(III) complexes can be made through judicious choice of cyclometallating C^N or charged /anionic X^Y ligands. The excited states of both neutral homoleptic and charged heteroleptic Ir(III) complexes can be tuned to display all three primary colors (red, blue and green).[53]

It has been well demonstrated that structural changes in the skeletal as well as the substituent groups of the cyclometallating ligand afford significant color tuning and efficiency improving the electrophosphorescence. Therefore, many studies have been enthusiastically done on the design and synthesis of novel cyclometallating ligands.

I.1.1.2 Cationic Ir(III) octahedral complexes $[Ir(C^N)_2(N^N)]^n$ (n = +1)

The charged Ir(III) complexes consists of one core of Ir atom, two cyclometallating ligands and one neutral N^N donor ligand. The most popular N^N donor ligand used is the 2, 2'-bipyridine (*bpy*). In particular, since the coordination arrangement of a neutral Ir(III) complex is octahedral there can exist three geometric isomers A, B and C (Figure 1.7).

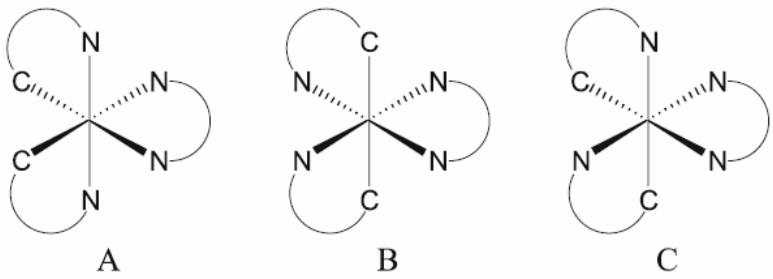

Figure I.7 Possible geometric isomers of charged Ir(III) complexes $[Ir(C^N)_2(X^Y)]^+$.

Nevertheless, it is well-established that the cyclometallating carbons of the $[(C\hat{}N)_2Ir(N\hat{}N)]^+$ center occupy mutually *cis* positions[54], which are in turn *trans* to the nitrogen atoms of the (N^N) coordinating ligand, configuration A. The reasons for this outcome appear related to a so-called *trans* effect of the Ir – C bonds. These induce a preferential labilization of the bonds located *trans* to them, which results in the stereochemical positioning of Ir – C and Ir –N bonds *trans* to one another. Such an effect is clearly observed for the stepwise reaction of Ir(*acac*)$_3$ with 2-phenylpyridine (*ppy*).[55] Here, after the first replacement of a *ppy* ligand for an *acac* unit, the subsequent substitution steps are *trans* directed and only *trans* C – Ir – N bonds form until the final *fac*-Ir(*ppy*)$_3$ complex is obtained.

Some examples of neutral N^N donor ligands used in the synthesis of charged Ir(III) complexes are presented in the Figure I.8.

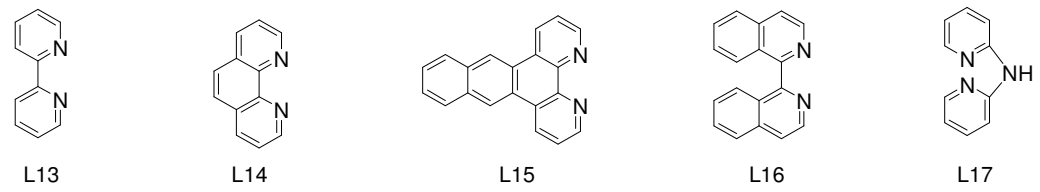

Figure 1.8 N^N donor ligands used in charged Ir (III) complex chemistry.

I.1.1.3 Anionic Ir(III) octahedral complexes $[Ir(C\hat{}N)_2(X)_2]^n$ (n = -1)

The anionic Ir(III) complexes consists of one core of Ir atom, two cyclometallating ligands and two monodentate ligands (CN, NCS or NCO). The Ir metal with two cyclometallating forms a configuration in which the two pyridine groups are trans to each other and the phenyl groups are trans to the anionic ligands, resulting in two electronically equivalent pyridines and phenyl groups.[56, 57, 58] There is no significant change in the ^{1}H NMR spectral pattern between the starting precursor [Ir(*ppy*)$_2$]$_2$-μCl$_2$ and the complexes indicating that the cleavage of the chloride bridge and the subsequent substitution of the chloride ligands by anionic ligands takes place without change in the geometry of the iridium octahedral complex (Figure I.9).

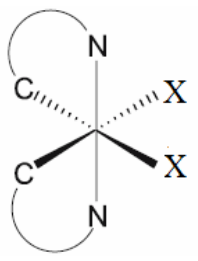

Figure I.9 Possible geometric isomer of anionic Ir(III) complexes $[Ir(C\hat{}N)_2(X)_2]^-$.

There are only few examples of anionic Ir(III) complexes found in the literature[59, 60] having the anionic ligands used for their preparation shown in Figure I.10.

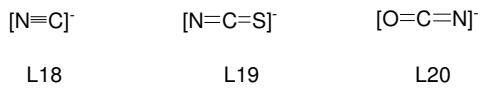

Figure I.10 Anionic ligands used in charged Ir (III) complex chemistry.

I.1.2 Synthesis of octahedral Ir(III) complexes

A widely followed path to prepare Ir(III) cyclometallated complexes is based on the use of dichloro-bridged Ir(III) dimers, in turn obtained from $IrCl_3$ and a (C^N) ligand. The synthesis of $[Ir(C^N)_2]_2$-μCl_2 is presented in Scheme I.1.

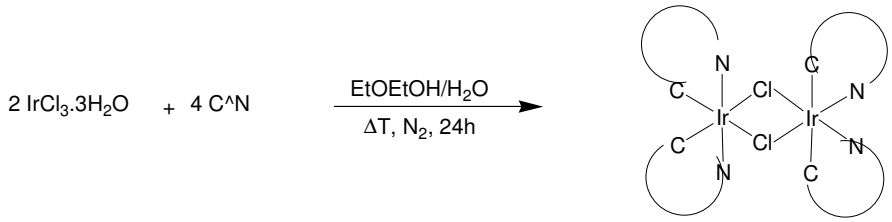

Scheme I.1 The synthesis of dichloro-bridged Ir(III) dimeric precursors, $[Ir(C^N)_2]_2$-μCl_2.

Furthermore, both types of neutral Ir(III) cyclometallated complexes can be obtained by reacting the precursor $[Ir(C^N)_2]_2$-μCl_2 using either a cyclometallating ligand (C^N) of same type (for the synthesis of homoleptic neutral complexes) or a different cyclometalling ligand (C^N) (for the synthesis of heteroleptic neutral complexes). Moreover, reacting the precursor $[Ir(C^N)_2]_2$-μCl_2 with a coordinating N,N-donor ligand, heteroleptic complexes having Cl^- as counterion are obtained. The general synthesis of the different type of Ir(III) complexes is presented in Scheme I.2.

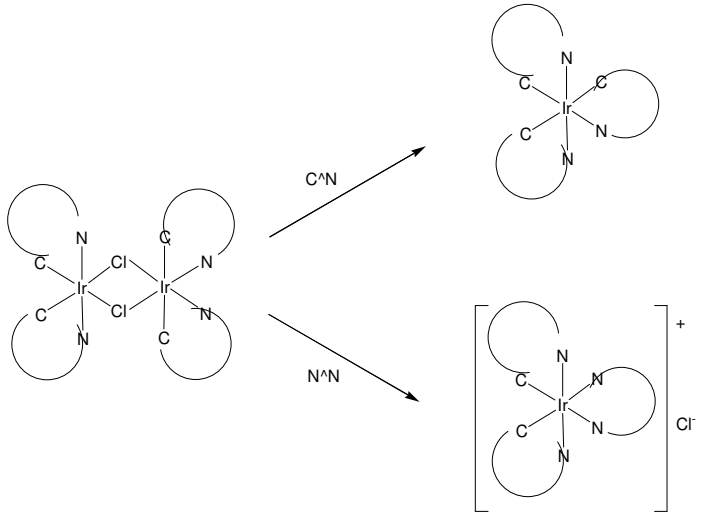

Scheme I.2 Synthesis of neutral and charged Ir(III) complexes.

The change of the counterion is easily done by metathesis with an excess of a salt that contains the desired counterion (Scheme I.3).

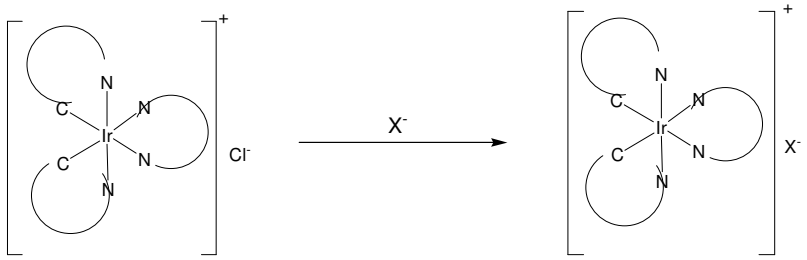

Scheme I.3 Metathesis in Ir(III) charged complexes.

The anionic Ir(III) cyclometallated complexes can be obtained by same methods used for the synthesis of neutral and cationic Ir (III) complexes. In particular, by reacting dimer $[Ir(C\text{^}N)_2]_2$-μCl_2 with an excess of a suitable anionic ligand (X) presented in figure I.10, the anionic Ir(III) octahedral complexes are obtained. The synthesis of anionic Ir(III) complexes is presented in Scheme I.4.

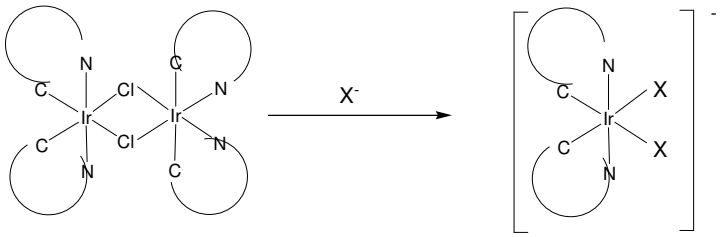

Scheme I.4 Synthesis of anionic Ir(III) complexes.

I.1.2.1 Synthesis of neutral Ir(III) complexes containing 2-phenylpyridine [Ir(*ppy*)$_3$](n = 0)

In general, the synthesis of Ir(III) neutral complexes requires relatively harsh conditions due to the kinetic inertness associated with the low-spin d^6 electronic configuration of the 3+ metal centre.[61] Tris-cyclometallated neutral Ir(III) complexes containing [Ir(*ppy*)$_3$] can be prepared directly by reaction of either Ir(*acac*)$_3$[62] or $IrCl_3 \cdot 3H_2O$[63] with a large excess of the cyclometallating ligand in glycerol at reflux temperatures, or in two steps by isolation of the intermediate bis-cyclometallated complexes [Ir(*ppy*)$_2$(acac)][64] or [Ir(*ppy*)$_2$]$_2$-μCl$_2$[65] respectively (Scheme I.5).

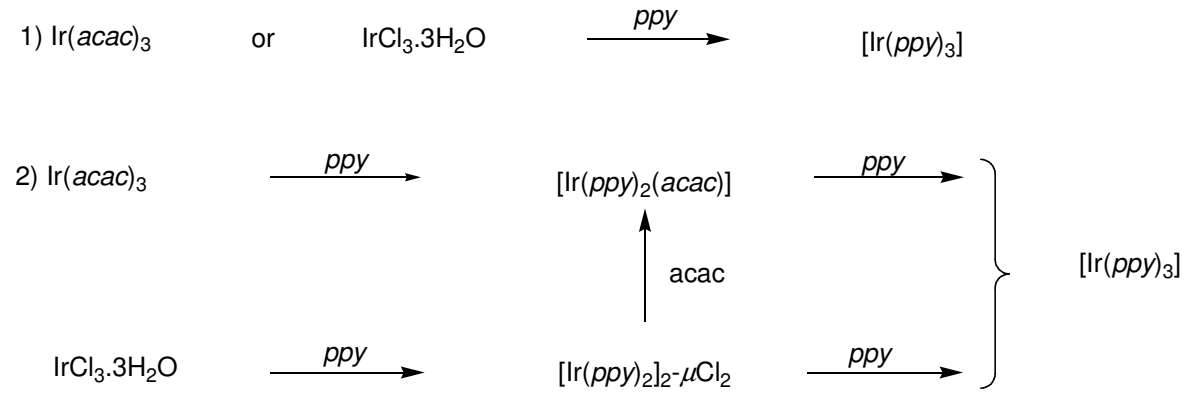

Scheme I.5 General synthesis of Ir(III) neutral complexes.

The route involving the use of the chloro-bridged dimers [Ir(*ppy*)$_2$]$_2$-μCl$_2$[66] is much more efficient than going via [Ir(*acac*)$_3$] which itself is prepared from $IrCl_3 \cdot 3H_2O$ but only in low yields (<20%).[67] Preparing [Ir(*ppy*)$_3$] in two steps from $IrCl_3 \cdot 3H_2O$ gives overall yields between 75 and 80% vs 45-60% using an one pot method. In addition, the second step from [Ir(*ppy*)$_2$]$_2$-μCl$_2$ can be carried out at much lower temperatures using silver salts.[68] Also, the one pot method uses a much larger excess of the cyclometallating ligand as solvent (up to 60 times 95) compared with only 2-3 times excess in each step during the two step procedure.[69] Hence, the two step method starting from $IrCl_3 \cdot 3H_2O$ is the preferred method.

In particular the chloro-bridged dimer [Ir(*ppy*)$_2$]$_2$-μCl$_2$ is easily prepared in high yields as a yellow powder, by heating $IrCl_3 \cdot 3H_2O$ with 2-phenylpyridine (*ppy*) in ethoxyethanol/water at reflux for 24 hours at 135°C.[70]

I.1.2.2 Synthesis of cationic Ir(III) octahedral complexes containing neutral ligands $[Ir(ppy)_2(N\hat{}N)]^n$ (n = +1)

A widely followed path to prepare charged Ir(III) cyclometallated complexes is based on the use of the same precursor as for the neutral complexes, the dichloro-bridged Ir(III) dimers $[Ir(ppy)_2]_2$-μCl_2 respectively. Specifically, the treatment of the dimeric precursor $[Ir(ppy)_2]_2$-μCl_2 with an excess of a suitable (N^N) ligand[51] gives the desired complexes usually with high yields. All these reactions occur under relatively mild condition in dichloromethane/methanol (3:1 v/v) under nitrogen atmosphere for 4 hours yielding the desired ionic Ir(III) cyclometallated complex, having Cl^- as counterion. Finally, the counterion can be changed by a simple methatesis reaction with an excess of a salt containing the desired counterion (Scheme I.6).

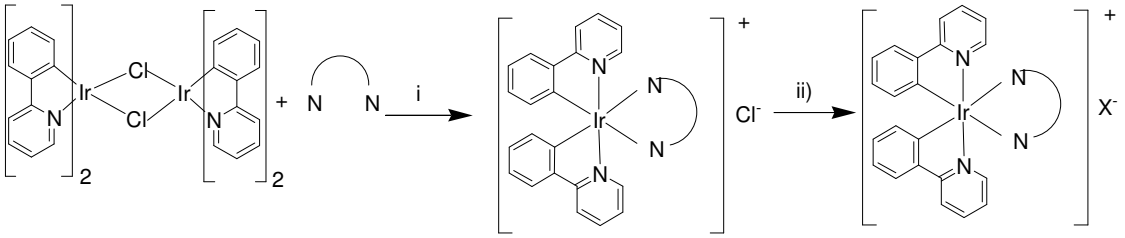

Scheme I.6 General synthesis of octahedral ionic Ir(III) complexes i) DCM : MeOH (3:1 v/v), ΔT, 4 hours, N_2, ii) X^-, ΔT, 3 hours, N_2.

By using this method a vast variety of charged Ir(III) octahedral complexes can be prepared through appropriate choice of the N^N ligands and counterions.

I.1.2.3 Synthesis of anionic Ir(III) octahedral complexes containing monodentate ligands $[Ir(ppy)_2(X)_2]^n$ (n = -1)

The anionic Ir(III) cyclometallated complexes can be obtained by the same method used for the synthesis of neutral and cationic Ir(III) complexes. In particular, by reacting the dimeric precursor $[Ir(C\hat{}N)_2]_2$-μCl_2 with an excess of suitable monodentate ligands (X) in dichloromethane solvent at reflux for 15 hr under nitrogen atmosphere, the anionic Ir(III) octahedral complexes are obtained. The synthesis of anionic Ir(III) complex containing cyanide(CN) ligand as shown in Scheme I.7.

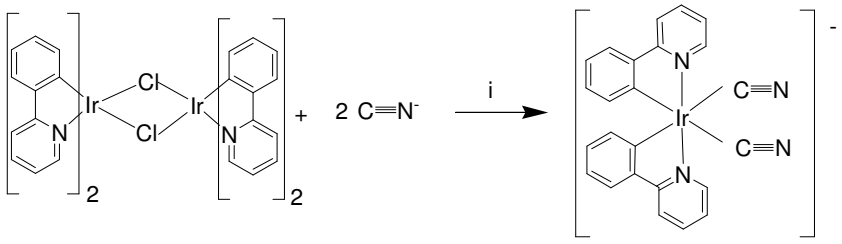

Scheme I.7 General synthesis of octahedral anionic Ir(III) complexes i) DCM , ΔT, 15 hours, N_2.

I.1.3 Properties of Ir(III) octahedral complexes

The Ir(III) octahedral complexes have been extensively studied and applied both the neutral for fabricating *organic light-emitting devices* (OLEDs) and charged one for *light-emitting electrochemical cells* (LECs). Their electrochemical and photophysical properties are in particular important because they highly satisfy the requirement for these devices comparatively with organic compounds. To understand the photophysical properties of Ir(III) complexes, it is useful to consider a localized molecular orbital model of the excited states. Figure I.10 shows the orbitals and spectroscopic states diagram for a low spin d^6 octahedral complex.[71] The octahedral crystal field of the ligands splits the five degenerate d-orbitals into a triply degenerate t_{2g} level and a doubly degenerate e_g* level. The magnitude of the splitting (Δ) is dependent on the crystal field strength of the ligands and the central metal ion. In the strong field configuration, the ground state is t_{2g}^6 and as all spins are paired it is a singlet (S_0). The lowest excited states are derived from promoting an electron to one of the unoccupied orbitals. There are three types of excited states: (a) metal centered d-d states, (b) ligand based π-π* states and (c) charge transfer states.

Metal centered d-d states arise from promoting a bonding electron from the t_{2g} level to e_g* level (t_{2g}^5 e_g^{*1}) and give rise to weak (Laporte forbidden) absorption bands (ε = *ca.* 100 $L \cdot mol^{-1} \cdot cm^{-1}$). Thus d-d emission is characterized by long radiative lifetimes and negligible quantum yields.

Ligand based π-π* states derive from promoting a bonding π-electron to an antibonding π* level. These transitions are highly intense and are localized on the ligands. Charge transfer states involve either metal to ligand charge transfer (MLCT) by promoting an electron from a metal orbital to a ligand orbital (t_{2g}^5 π^{*1}) or ligand to metal charge transfer (LMCT) which involves promoting an electron from a ligand to a metal orbital (π^1 e_g^1). These transitions have significant absorptions in the visible region (ε = *ca.* 20,000 – 25,000 $L \cdot mol^{-1} \cdot cm^{-1}$).

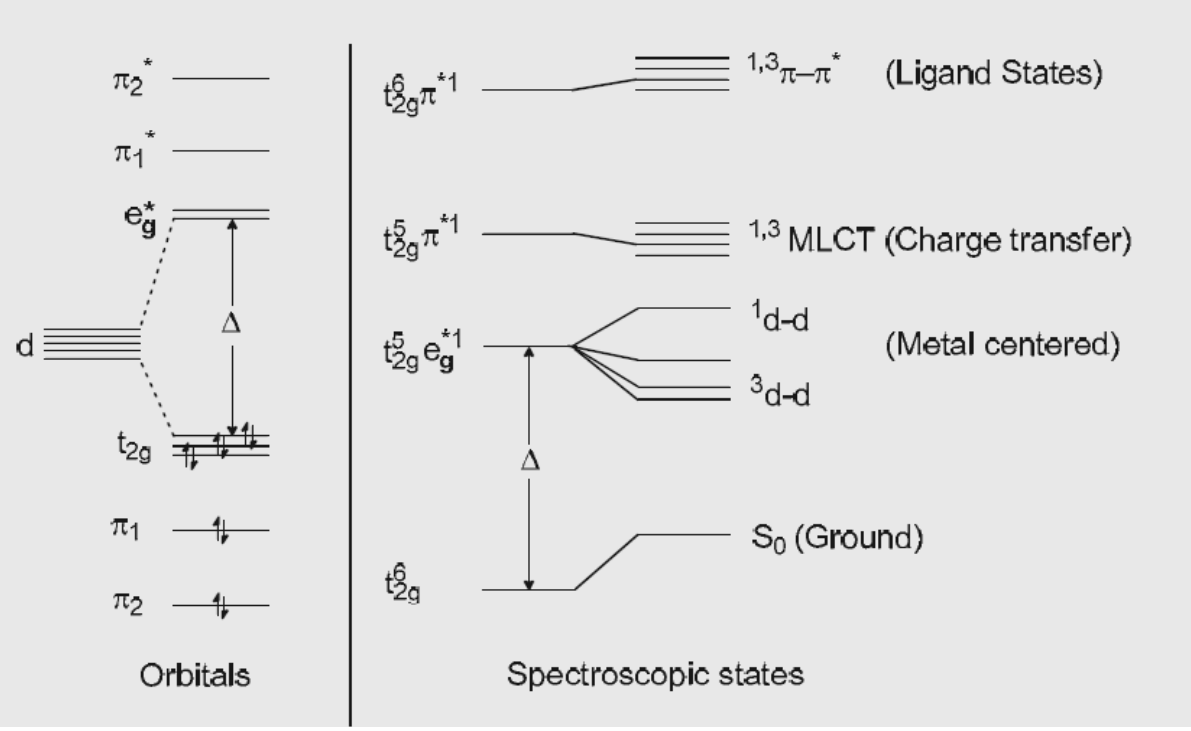

Figure I.10 Simplified orbital and state diagrams for a d^6 metal in an octahedral environment.

For a metal complex to be luminescent, it has to meet certain criteria:

(i) The lowest excited state must be either a charge transfer (CT) or ligand π-π*, this avoids photochemical instability associated with unstable d-d excited states;

(ii) Spin-orbit coupling should be high to enhance the emission to be more allowed and permit radiative decay to compete more effectively with non-radiative decay, which precludes first transition series complexes;

(iii) The crystal field should be strong enough to raise the d–d state above the MLCT state, to avoid thermal excitation.

For the cyclometallated Ir(III) complexes, the wave function of the excited triplet state, responsible for phosphorescence, is principally expressed as a combination of the LC and the MLCT excited triplet state. However, not all the complexes are highly luminescent because of the different deactivation pathways.[21] Furthermore, will be presented in detail the exploitable properties of the Ir(III) complexes and the strategies used for improving them.

I.1.3.1 Thermal and chemical stability

The Ir(III) octahedral complexes have high thermal and chemical stability because the atoms in the ligand, which are bonded to the Ir are the C and N, where C has a formal negative charge. The coordinative disposition around the Ir atom involves the formation of a 5- or 6- membered metalocyclic ring. The cyclometallated aromatics have been commonly used for assembling such luminescent compounds because as compared with other organic ligands, aromatic cyclometallates tend to form the strongest bonding interaction with transition-metal elements.

The *ppy* is a typical ligand structure in which the phenyl ring plays the role of the anionic part. The strong Ir–C and Ir-N bonds between the Ir(III) metal and these *ppy*-based ligands afford a five member metallacycle. That yields for the neutral Ir(III) complexes of general formula $[Ir(C\hat{}N)_3]$, a molecular structure with extensive electronic interactions between the d-orbital of Ir and π-orbital of the ligands that is characteristic of a good thermal stability. In the case of charged complexes, the neutral N^N donor ligands can serve to improve complex stability compared to the tris-cyclometallated systems and the presence of counterions may be beneficial for applications in electrooptical devices. Indeed, these counterions are mobile under the influence of an applied bias leading to accumulation of negative charge near one electrode and depletion near the other electrode. This ionic space charge creates high electric field at the electrodes which increases electron charge injection into the metal complexes.

A further increase of the thermal and chemical stability may involve the incorporation of sterically hindering dendrons at the periphery of the emitting core. This further may enhances the solubility in solvents and polymer matrices, offers better compatibility in solution processes, color tunability and higher photoluminescence quantum efficiency.[72]

1.1.3.2 Color Tuning

The most attracting property of Ir(III) complexes is that they have high color tuning. The color variation appears roughly related to the size of the ligand, *i.e*. a more extended electronic delocalization causes a lowering of the ligand centered LUMO, in turn resulting in lower-lying levels both of ^{3}MLCT and ^{3}LC nature. When sufficient overlap is present between the ^{3}LC and ^{3}MLCT states then only excited-state mixing occurs.[73] Furthermore it is possible to control the energy of the lowest excited state by deliberately adjusting the energy of metal and ligand orbitals, which can be achieved through substituent effects or by changing the ligand parent structure entirely (e.g., *ppy* vs. 1-phenylpyrazole, *ppz*).[26] In tris-cyclometallated complexes $[Ir(ppy)_3]$ the HOMO resides on the Ir and Ir-C σ-bond while the LUMO resides on the pyridyl ring of ppy ligand. Liu *et*

al. studied the effect of varying substituents on the pyridyl ring.[74] A strong electron withdrawing substituent (*e.g.* CN) lowers the LUMO decreasing the HOMO-LUMO gap leading to a red shift in emission with respect to the unsubstituted complex. In contrast, with OMe, the emission was relatively unaffected suggesting the HOMO-LUMO gap is relatively unchanged.

Tsuzuki and co-workers demonstrated that the position of the substituent also affects the emission.[75] Thus, the strongly electron withdrawing C_6F_5 substituent on the pyridine leads to a lowering of the LUMO energy and results in a red shift of emission with respect to the unsubstituted complex. DFT calculations suggest that the e LUMO is more concentrated on the *para*- position with respect to N; therefore, substitution on this position has a greater effect. This indicates that the emission wavelength is tunable according to the position as well as the electronic properties of the substituent. Lasker and co-workers reported complexes in which the effect of substituents on the phenyl and pyridine can be additive.[76] Thus, with F substituents *meta* to the metallated carbon lowers the HOMO level giving a blue shift compared to unsubstituted complex also contains an electron donating substituent on the pyridine ring which raises the LUMO giving an increased blue shift.

In the case of heteroleptic charged Ir(III) complexes, when both classes of ligands provide orbitals that participate in the excited-state transitions, the cyclometallating ligand tends to be associated with the ^{3}LC transition and the ancillary ligand with the ^{3}MLCT transition. In such cases, the excited state can be tuned directly through ligand modifications, because each ligand is linked to a different transition. By monitoring the effect of various ligand permutations within the coordination sphere, it is possible to gain insight into the factors that govern the photophysical and electrochemical behavior of heteroleptic charged Ir(III) complexes, and to tailor materials with specific excited-state properties.

The most effective methods for tuning the energy of the lowest excited state involves changing the degree of conjugation in the structure of the participating (cyclometallating and/or ancillary) ligands. As the coordination sphere becomes more diffuse, the corresponding orbitals are stabilized. It follows then, that the excited-state transitions can be tuned by altering the size of the ligands and also by localizing electron density in discrete regions of the molecule or by partially destroying ligand aromaticity. For example, bulky pendant groups can be used to distort a ligand from planarity, which will destabilize its π orbitals, and, as a result, increase the size of the associated ^{3}MLCT or ^{3}LC transition. Recently, Zhao *et al.*[77] synthesized a series of complexes [Ir(*piq*)$_2$(N^N)]PF_6 (*piq*= 1-phenylisoquinoline and N^N = *bpy*, *phen* derivatives) and studied the effect on emission of increasing conjugation of the N^N ligand. The emission wavelength of the

complexes varies from 586 to 659 nm. Hence, it is concluded that increasing the π-conjugation of the N^N ligand leads to a red shift in emission consistent with the LUMO being centered on the N^N ligand. These results also have been supported by density functional theory (DFT) calculations.

Another promising method for tuning (and fine-tuning) the excited-state properties of Ir(III) complexes involves deliberate functionalization of the ligands through the use of substituent groups. By modifying the symmetry and inductive influence of a ligand with different substituents, it is possible to control metal–ligand bonding as well as ligand orbital energies and, thus, to control the nature of the lowest excited state. Tremendous color versatility has been achieved with Ir(III) luminophores in this manner, and a broad range of excited-state lifetimes (from nanoseconds to several microseconds) as well as phosphorescent yields (approaching 100%) have been reported. In particular, electronic effects have been considered due to their profound influence on orbital energies as well as the relative ease with which electron-withdrawing (e.g., -F,-CF_3) and electron-donating (e.g., $(CH_3)_3$, -OCH_3) groups can be incorporated into the ligand structure. Electron-withdrawing substituents tend to stabilize the HOMO by removing electron density from the metal; whereas donating groups have an inverse effect.[72, 78, 79] This relationship is convoluted by the fact that withdrawing groups may also lower the energy of the LUMO (i.e., increasing the electron affinity of the parent ligand). Fortunately, the cyclometallating and ancillary ligands can be separately substituted with electron-withdrawing and electron donating groups in heteroleptic complexes, which enables deliberate control over the excited state.

In conclusion, the emission color of cyclometallated Ir(III) complexes can be tuned through the entire visible region and into the near infrared by varying either the C^N ligand and/or the X^Y ligand. Furthermore, the electronic effects of the substituents and their position can significantly influence the photophysical properties.

I.1.3.3 Phosphorescence quantum yield (Φp)

In pursuing Ir(III) complexes for the successful electrophosphorescence, the key requirement is to attain high quantum yield (Φp). Many novel highly phosphorescent Ir(III) complexes have been reported so far, and studied well to understand collective structure–property relationships for obtaining large Φp is literature and fully established. The judicious selection of ligand structures and their chelate disposition should be considered before synthesis in order to obtain high phosphorescence quantum yield**.**

The theoretically calculated Φp of the phosphorescent Ir(III) complexes (neutral/charged) are close to unity in solution. There are two opposite phosphorescences where passing from solution to solid state: aggregation induced quenching (ACQ) and aggregation induced phosphorescence emission (AIPE).

The solution investigations have made great contributions to the fundamental understanding of luminescence processes at molecular level. The conclusions drawn from the dilute solution data, however, cannot commonly be extended to the concentrated solutions. Indeed, many Ir(III) complexes show very different light-emitting behaviors in dilute and concentrated solutions. The luminescence is often weakened or quenched at high concentrations, a phenomenon widely known as "concentration quenching". A main cause for the quenching process is mechanistically associated with the "formation of aggregates", which is probably why the concentration quenching effect has frequently been referred to as "aggregation-caused quenching" (ACQ).

There is no "solvent" in the solid state, the "solute" molecules are located in the immediate vicinity. The aromatic rings of the neighboring fluorophores, especially those with disc-like shapes, experience strong π–π stacking interactions, which promotes the formation of aggregates with ordered or random structures. The excited states of the aggregates have tendency via non-radiative pathways, which is notoriously known as aggregation-caused quenching (ACQ) of light emission in the condensed phase. The concentration self-quenching associated with triplet–triplet annihilation within Ir(III) phosphors always happens due to the strong interactions between closely packed molecules[80], which limits the scope of their usage in optical devices. Until now, a variety of approaches have been taken in an effort to overcome the issue to some extent, such as attaching enhanced steric hindrance or bulky side groups into the complexes to separate chromophoric units.[48]

On the other hand aggregation-induced phosphorescent emission (AIPE) is an unusual phenomenon existing also in transition metal complexes, which have no emission in solution but enhanced emission in the solid state.[7] There are some examples of AIPE, most of them in neutral Iridium complexes.[8] The efforts have been made to investigate this property in Ir (III) complexes.[81]

In some cases, it has been observed that Φ_p of Ir(III) complexes in solid states such as frozen solutions, doped polymer alms or powdery states is increased by more than one order compared to that in solution states.[82] These observations indicate that motional relaxations imposed on the septic part of the molecular structure are responsible for hazardous non-radioactive transitions, thus resulting in low Φ_p in mobile states. For the structural origin of these behaviors, Ir–ligand stretching vibrations[83] C–C ring deformation[73] and C–H vibration in aryl rings[84] were suggested. These

vibrational motions aid strong coupling between vibronic levels in the potential energy surface of ground state and isoenergetic levels in the potential energy surface of excited states, thus facilitating faster non-radiative transitions.

The restricted intramolecular motions in the solid state are responsible for highly enhanced phosphorescence in the solid state for a heteroleptic Ir(III) complexes[85,86,87] containing chromophoric ancillary ligands. For Ir(III) complexes systems, it has been recently demonstrated that the phosphorescent AIE of heteroleptic Ir(III) complexes can be triggered by intermolecular excimer state, *i.e.*, metal-to-ligand-ligand charge-transfer (^{3}M(LL)CT) state[7] or restricted intramolecular relaxation[9] in the solid-state.

Since the octahedral structure of Ir(III) complex intrinsically prevents direct Ir(III)–Ir(III) interactions, the engineering of crystal packing structure through the modification of π-π interactions between the cyclometallated ligands could be a viable approach to the polymorphism-induced multiple AIEs of the Ir(III) complex.

I.2 World of porous materials

"With clay, we make a jar. But it is the empty space inside that we need." This ancient Chinese proverb resumes in few words the target of science about porous systems: create materials with empty spaces inside to use their cavities. Porous materials are well known since a long time and used for different applications, such as filtration, liquid adsorption and so other. Generally porous materials have porosity (volume ratio of pore space to the total volume of the material) between 0.2 - 0.95. Pores are classified into two types: open pores which connect to the surface of the material, and closed pores which are isolated from the outside**.** Porous materials can also be classified according to their degree of order: fully crystalline (zeolites), ordered on a mesoscopic length scale, but amorphous on the atomic length scale (surfactant-templated materials) or fully disordered (silica gels). During research and evolution of new porous systems a better control of pore size, a decrease of pore diameter and a well-organized structure are necessary to increase base properties.

If pore diameter has nanometric dimensions, we can speak of nanoporous materials. Nanoporous materials have unique surface, structural and bulk properties that enhance their application in various fields such as ion exchange, separation, catalysis, sensor, biological, molecular isolation and purification.[88, 89] The useful way to classify a nanoporous material is by the diameter size of their pores, because most of properties, interesting for applications of adsorption and diffusion, sensors, electronics etc., are dependent by this parameter. The prefix *nano* means a typical dimension between 1 and 100 nm. In this range, the material properties change drastically, overall for interaction and diffusion when materials interact with other molecules. If the two dimensions are similar we can expect that molecule-wall interactions will be prevalent respect to molecule-molecule interaction. By the other way, if guest molecules are smaller than pore size, there will be both molecule-wall and molecule-molecule interactions during the diffusion process.

There are different possible ways to classify nanoporous materials. According to the definition of the International Union of Pure and Applied Chemistry (IUPAC)[90] nanoporous materials are divided into three different classes, depending on their pore sizes.

- Microporous materials having pore diameter below 2 nm.
- Mesoporous materials with pore diameters lie in the range between 2 and 50 nm.
- Macroporous materials having pore diameter above 50 nm.

The prefix meso- means "in-between". Of course, it means in-between of nanometric range, but in this case also in-between molecular and solid-state physics, in-between molecular and *continuum* approach, in-between covalent chemistry and micromechanical techniques. Mesopores, in fact, are

enough large to host more than one molecule in their cross-section, but not large enough to let bulk properties become major than surface interactions. Therefore, mesostructures are at half way between single molecules and extended structures, so their properties (mechanical, electrical and magnetic), are different from each of the two extremes.

Some mesoporous materials are also mesostructured, because a monosized pore is coupled with long range ordered voids. Mesostructures depend by chemical and processing parameters; therefore a great number of characteristics can be tuned, as well large active surface area, pore dimension, and pore shape.[91] In general mesostructured materials are defined as mesoporous materials before calcination or chemical extraction i.e. materials in which the surfactants/block-copolymers are not removed.

Mesostructured materials are highly versatile substrates for the formation of functional materials. In particular silica and then titanium mesoporous materials have led to many promising applications in areas ranging from photovoltaic and photo catalysis to photo-electrochromics and sensors.[92]

I.2.1 Mesoporous materials

In recent years, ordered mesoporous materials with controllable pore architectures have attracted the interest of both scientific and industry due to their potential applications in adsorption technology, molecular separation, catalysis, electronics, gas sensors, etc.

The following characteristic properties of mesoporous materials affecting new challenge in the material research field made them most popular among all other porous materials:

- periodic distribution of pores
- high surface area (~1500 m^2/g)
- controllable and large pore size in the range of 2 ~ 50 nm
- variable topology of the pores (size and arrangement).

Therefore these materials represent new challenges in the materials research field. A significant breakthrough in the mesoporous materials research has come when Mobil[93,94] scientists in 1992 disclosed the M41S family of materials, prepared through surfactant templated synthesis. These silica-based mesoporous materials have large uniform pore structures, high specific surface areas and specific pore volumes, including hexagonal-MCM-41, cubic-MCM-48 and lamellar-MCM-50, as illustrated in Figure I.11.

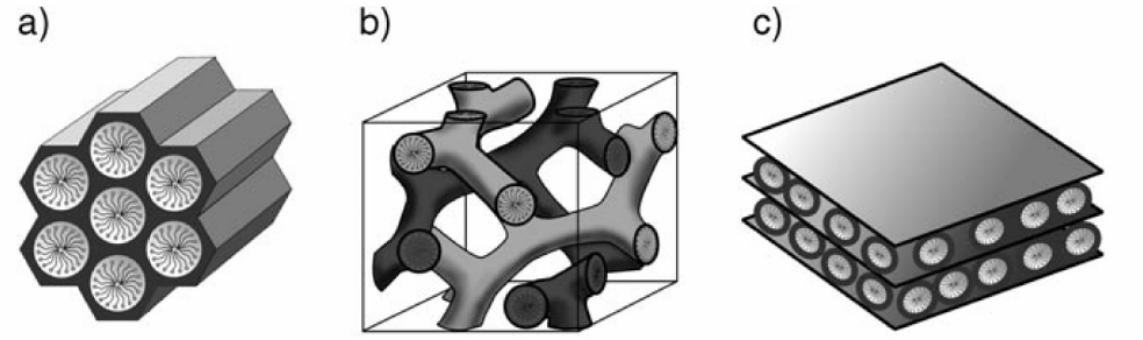

Figure I.11 Structures of mesoporous M41S materials: a) MCM-41 (2D hexagonal), b) MCM-48 (cubic) and c) MCM-50 (lamellar).

I.2.2 Synthesis of mesoporous materials

The synthesis of mesoporous materials is based on the sol gel condensation of the inorganic source on the micellar or lyotropic phase formed in water by a surfactant, used as *structure directing agent* (SDA). A number of models have been proposed to explain the formation of mesoporous materials and to provide a rational basis for the various synthesis routes. In-depth investigations into the formation process of these mesoporous materials have found two different mechanisms[95,96,97] involved: *cooperative self-assembly* (CSA) and *true liquid-crystal templating* (TLCT), respectively as shown in Figure I.12.

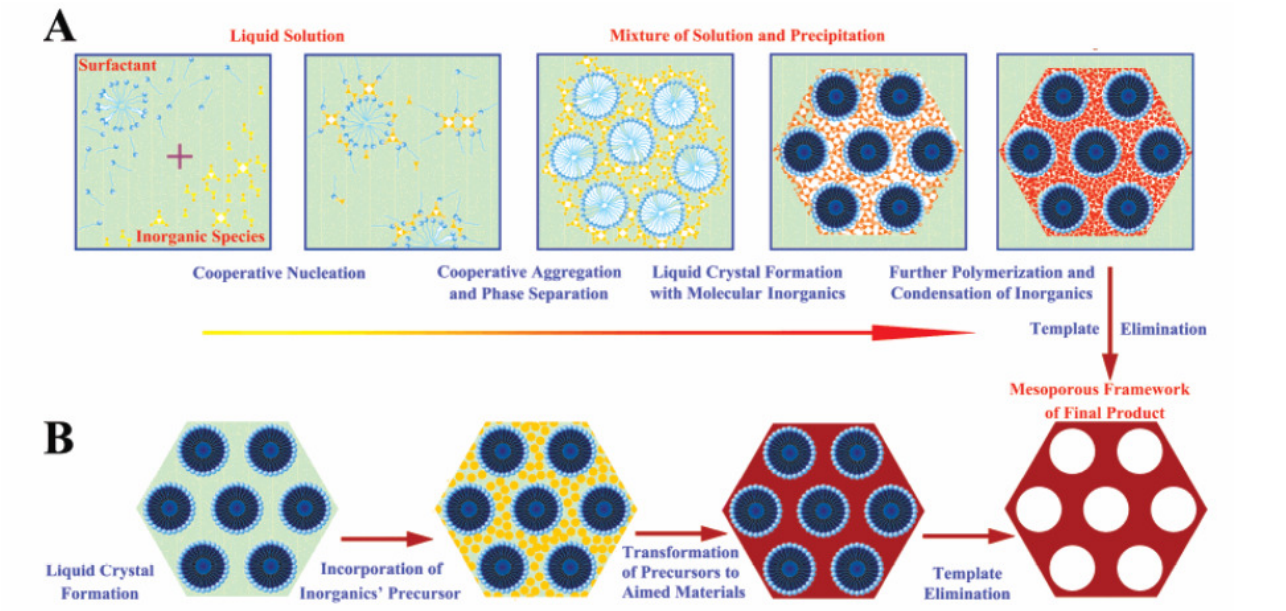

Figure I.12 Two synthetic strategies of mesoporous materials: (A) cooperative self-assembly (CSA), (B) "True" liquid-crystal templating process, (TLCT).

The self-assembly can be defined as "the ordering of molecules with no external effort". Asymmetric molecules such as surfactants are made-up of two distinct entities within the same molecule: hydrophilic head group and hydrophobic tail group. In aqueous medium, these molecules act as SDAs and change the structural orientation depending on their concentration.[98, 99,100]

Therefore, the surfactant self-assembly is particularly essential for the formation of highly ordered mesoporous materials. On the basis of the current knowledge on the surfactant self-assembly, the mesoporous materials can be rationally designed and the synthesis can be controlled.

I.2.2.1 Cooperative self-assembly

This pathway was established on the basis of cooperative assembly between organic surfactants and inorganic precursors forming mesoporous materials. It is well known that self-assembly occurs when molecules interact with one another through a balance of attractive and repulsive interactions. The self-assembly is driven by weak noncovalent bonds such as hydrogen bonds, van der Waals forces, and electrovalent bonds between the surfactants and inorganic species.

The condensation of the inorganic precursor is made in the micellar solution of common surfactants in water, therefore at low concentration of SDAs. In particular, the use of supramolecular aggregates of ionic surfactants (e.g. long-chain alkyltrimethylammonium halides) as SDAs was groundbreaking in the synthesis of these materials. In CSA, the surfactants molecules and the inorganic species undergo cooperative nucleation resulting in the formation of aggregates. These aggregates further undergo cooperative aggregation and phase separation leads to liquid crystals with molecular inorganic, which on further polymerization and condensation resulted in the mesoporous materials with template molecules. Finally template molecules are removed to obtain the mesoporous materials with empty opres.

On the most common level, these CSA model is predicated upon the presence of surfactants in a solution to guide the formation of the inorganic mesostructure from the solubilized inorganic precursors. Surfactants contain a hydrophilic head group and a long hydrophobic tail group within the same molecule and will self-organize in such a way as to minimize contact between the incompatible ends. How the inorganic precursor interacts with the surfactant is the issue whereby the type of interaction between the surfactant and the inorganic precursor will be seen as a significant difference in the resulting mesoporous materials.

I.2.2.2 True liquid-crystal templating (TLCT)

The alternative synthesis route to mesoporous materials uses direct templating by preformed lyotropic liquid crystal phases that are prepared under high surfactant concentrations, generally >20wt.%.[101,102,103,104,105,106] In this pathway, true liquid-crystal mesophases are involved in the surfactant templating assembly to synthesize ordered mesoporous solids. The concentration of the surfactant is so high that under the prevailing conditions (temperature, pH) a lyotropic liquid-crystalline phase is formed without requiring the presence of the precursor inorganic framework. The incorporation of inorganic precursor leads to transformation of precursor to aimed materials forming a mesoporous structure. The high concentration of surfactant required for direct liquid crystal templating is maintained throughout the whole process and the phase structure is preserved by the sol–gel formation of silica in the hydrophilic domains.

The synthesis takes place under conditions of controlled alkoxide hydrolysis and condensation, coupled with removal of the produced alcohol in order to prevent disruption of the liquid crystal phase structure. This results in a solid replica of the liquid crystal phase. Precipitation of a powder form product is avoided and macroscopic (monolithic) porous objects are obtained. The shape and size of the monoliths can be controlled.

I.2.3 Mechanism of the synthesis using tetraethoxy silane (TEOS)

There are a number of models proposed to explain the formation of mesoporous materials and to provide a rational basis for the various synthesis routes. In-depth investigations into the formation process of these composite materials have found different mechanisms. The polymerization is carried out in an aqueous solution by adding a catalyst and a source of silica. Silicate precursors that can be used to prepare ordered mesoporous silicas are diverse, for example, silica gels, colloidal sols, sodium silicates, silica aerogels, tetramethoxysilane (TMOS) or tetraethoxy silane (TEOS). Hydrothermal treatment is necessary to prepare ordered mesoporous silicates when they are used as silicate precursors. Mixed silicate precursors[93] were also used in the synthesis of mesoporous materials. It is found that TEOS is the most convenient and efficient silicate precursor in the laboratory.[107] Non-molecular silica sources are, for example, already polymerized sol-gel materials which lead to non-homogeneous solutions.[108]

The first step of polymerization is the formation of silanol groups by hydrolysis of the alkoxide precursors, the gel, in aqueous solution (Figure I.13). The general reactions for hydrolysis and the

polymerization occur through water (oxolations) or alcohol (alcoxolations) producing condensations.[109]

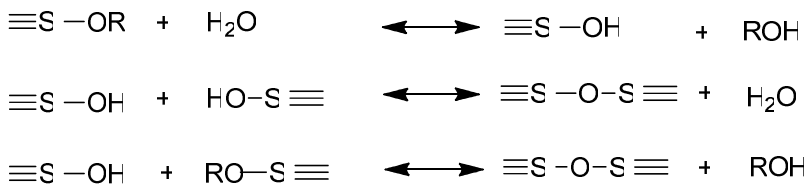

Figure I.13 Polymerisation of TEOS.

The process is catalyzed by acids or bases resulting in different reaction mechanisms (Figure I.14). The pH used therefore has an effect on the kinetics of the reaction.

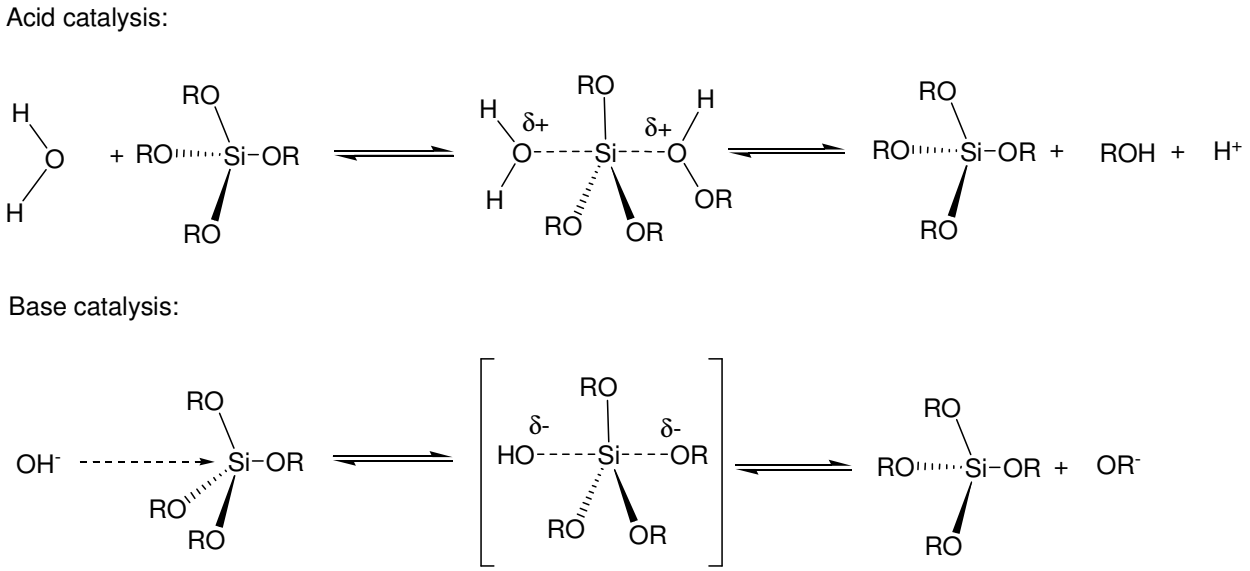

Figure I.14 Differences in mechanism depending on the type of catalyst used in the silicon-based sol–gel process.

Commonly used catalysts are HCl, NaOH or NH_4OH. The reaction is slowest at the isoelectric point of silica (between 2.5 and 4.5 depending on different parameters) and the speed increases rapidly on changing the pH. The pH not only plays a major role in the mechanism but also for the microstructure of the final material. Applying acid-catalyzed reactions, an open network structure is formed in the first step of the reaction leading to the condensation of small clusters afterwards. Contrarily, the base-catalyzed reaction leads to highly cross linked sol particles already in the first step. This can lead to variations in the homogeneity of the final materials.

Not only have the reaction conditions had a strong influence on the kinetics of the reaction but also the structure of the precursors. Generally, larger substituent decreases the reaction time due to steric hindrance. In addition, the substituent plays a mature role in the solubility of the precursor in the solvent. Water is required for the reaction and if the organic substituents are quite large usually the precursor becomes immiscible in the solvent. By changing the solvent one has to take into account that it can interfere in the hydrolysis reaction, for example alcohols can undergo *trans*-esterification reactions leading to quite complicated equilibrium in the mixture. Hence, for a well-defined material the reaction conditions have to be fine-tuned.

I.2.4 Common surfactants used as SDAs for the construction of the mesoporous materials

Generally a clear homogeneous solution of surfactants in water is required to get ordered mesoporous structures. Surfactants are amphiphilic molecules which consist of a hydrophilic, polar head group and a hydrophobic, non-polar tail. Due to their amphiphilic nature, surfactant molecules have a high affinity towards surfaces and interfaces, thereby the term "surfactant" which is an abbreviation for "surface active agent". The ambivalent nature of amphiphiles leads to a competition between the hydrophilic part attempting to increase their contact with water and the hydrophobic ones trying to avoid it. Such chemical incompatibility leads to the association of the molecules into micellar aggregates with defined topologies such as hollow spherical, rod-or disc-like micelles, in which these aggregations in space occurs, keeping unlike parts isolated from unlike solvent.

I.2.4.1 Assembly of surfactants

In aqueous solution at low concentration, surfactant molecules exist as mono molecules with non-ordered structures. When the concentration of surfactant increases, they aggregate together to form micelles. The micelle concentration, at which surfactant molecules aggregate to form isotropic micelles is called "critical micelle concentration" (CMC). Further increase in concentration of surfactant causes the formation of ordered structures.

In aqueous solutions micelles are called *normal,* meaning that the head of the amphiphilic molecules are in contact with water molecules, while the hydrocarbon tails entirely occupies the interior of the micelles (Figure I.15.a). Below a certain specific water content which appears to be

determined by the maximum capacity of the hydrophilic groups for binding water, the two parts of the amphiphilic molecule interchange position and micelles become *reversed* (Figure I.15.b).

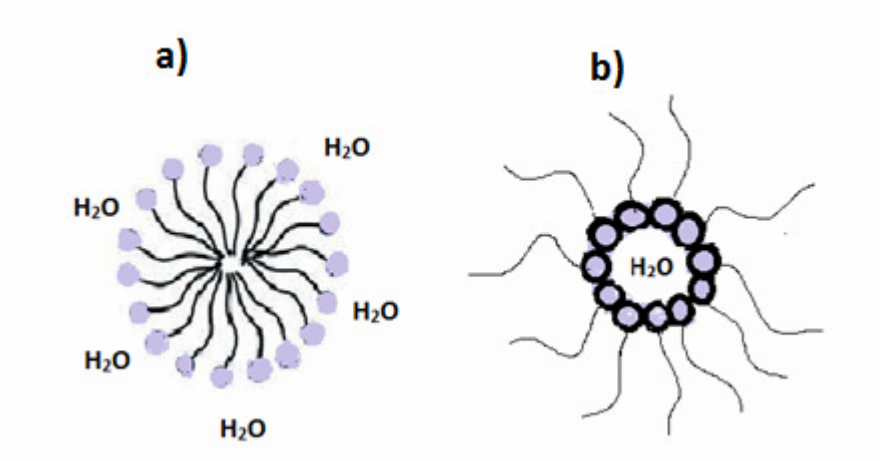

Figure I.15 Formation of a) normal micelle and b) reverse micelle in aquous solution.

Above the critical micelle concentration (CMC) and at a boundary temperature, referred to as the Krafft point or critical micelle temperature (CMT) below which micelles are not soluble, the micelles begin to interact and to self-assemble into ordered arrays of supramolecular aggregates or lyotropic mesophases. The occurrence of the mesophase is thus driven by the hydrophilic/hydrophobic balance, packing constraints (chain and surface areas) and solvent effects. The nature of the mesophase is strongly connected to the type of aggregation, and the curvature between the polar/apolar interfaces.

The most used surfactant for the construction of silica based mesoporous materials is cetyltrimethyl ammonium bromide (CTAB). The chemical structure of the surfactant is presented in Figure I.16. It is formed by a hydrophilic charged head group (trimethyl ammonium bromide) and a long alkyl chain that forms the hydrophobic part.

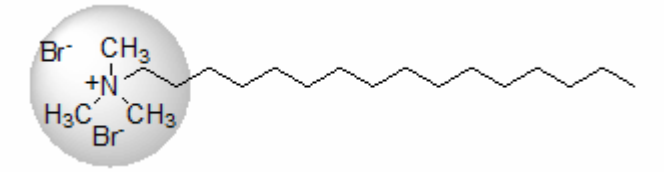

Figure I.16 Structure of cetyltrimethyl ammonium bromide (CTAB).

The schematic phase diagram of CTAB in water is shown in Figure I.17. Above the CMC, CTAB assemble into normal spherical micelles (CMC1). As the concentration of the surfactant increases, the spherical micelles can coalesce to form cylindrical micelles (CMC2).

Further increase of the surfactant concentration leads to liquid crystalline (LC) phases. The rod like micelles aggregate and form hexagonal close packed LC arrays. A further increase of the surfactant concentration can produce cubic bicontinuous LC phases and can even lead to LC lamellar phases.

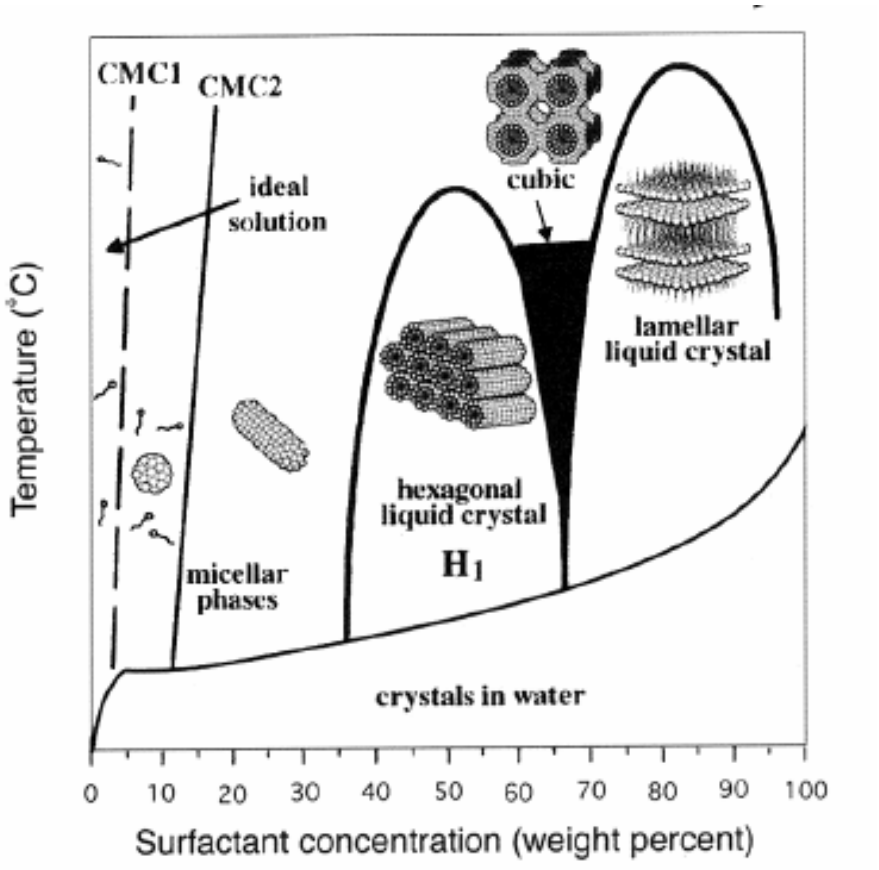

Figure I.17 Schematic phase diagram for CTAB in water.

I.2.5 Classification of surfactants

The surfactants used for the construction of mesoporous materials can be classified into cationic,[110, 111] anionic[107, 112, 113, 114] and neutral[101,115,116,117,118] respectively, as a function of their chemical structure. Their general chemical structure is shown in Figure I.18.

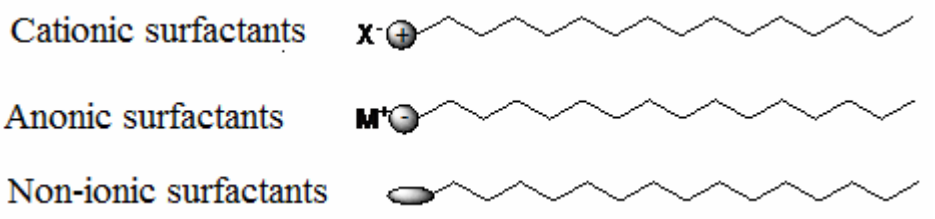

Figure I.18 Surfactants used in the synthesis of mesoporous materials: a) cationic, b) ionic and c) non-ionic.

Furthermore the synthesis of mesoporous materials will be presented as a function of the type of surfactant used.

I.2.5.1 Cationic surfactants as SDAs

Cationic surfactants have positive charged head groups. The mostly used for the construction of the mesoporous materials are quaternary cationic surfactants of the type: $C_nH_{2n+1}N(CH_3)_3Br$ (n =8-22). As mentioned before, the most frequently used cationic quaternary ammonium surfactant is CTAB. Gemini surfactants, bolaform surfactants, multiheadgroup surfactants, and recently reported cationic fluorinated surfactants can also be used as templates to prepare various mesostructures.[14]

Cationic surfactants have excellent solubility, have high critical micelle temperature (CMT) values, and can be widely used in acidic and basic media. But they are toxic and expensive.

If the reaction takes place under basic conditions whereby the silica species are present as anions, the synthetic pathway is termed S^+I^- (Figure I.19.a; S: surfactant; I: inorganic species). In this case surfactant (S^+) and inorganic precursor (I^-) are charged with opposite sign and interact by using electrostatic forces. The pore sizes are determined by aliphatic chain lengths and the pore walls are generally smooth and without large defects.

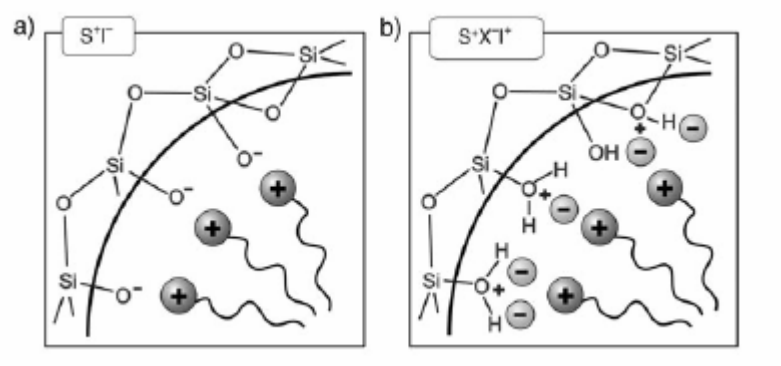

Figure I.19 Electrostatic interaction of cationic surfactants with inorganic precursor by a) S^+I^- and b) $S^+X^-I^+$ pathway.

The preparation can also be takes place under acidic conditions (below the isoelectric point of the Si-OH bearing inorganic species; pH =2), where the silica species are positively charged. To produce an interaction with the cationic surfactant, X^- ion is involved as usually a halide (X = Cl^-, Br^-, I^-, SO_4^{2-} or NO_3^-). The synthetic pathway is termed $S^+X^-I^+$ (Figure I.19.b; S: surfactant; I: inorganic species).

In a strongly acidic medium, the initial $S^+X^-I^+$ interaction through Coulomb forces or more exactly, double-layer hydrogen bonding interaction, gradually transforms to the $(IX)^-S^+$ one. Here anions affect the structures, regularity, morphologies, thermal stability, and porosities of mesoporous silicas. The acid-derived materials have thicker pore walls and a framework charge different from the base-derived mesoporous materials, due to the different precipitation conditions and charge balance requirements.

I.2.5.2 Anionic surfactants as SDAs

Anionic surfactants are typically weak acids or their conjugated salts. The chemical structure of the most common anionic surfactants used is presented in Figure I.20.

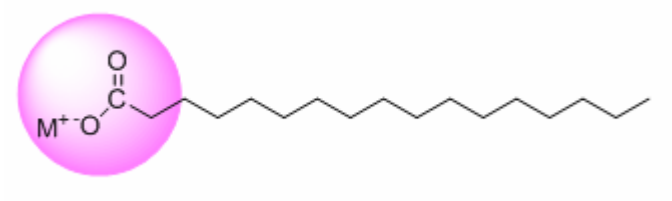

Figure I.20 Anionic surfactants.

Again two synthetic procedures can be used. If the reaction takes place under basic conditions the inorganic species are present as anions. To produce an interaction with the anionic surfactant, it is necessary to consider a mediator ion M^+ usually Na^+, K^+, Cr^{3+}, Ni^{2+}. In such cases surfactant and inorganic precursor, charged with same sign, interacts by using electrostatic coulomb forces. The synthetic pathway is termed $S^-M^+I^-$ (Figure I.21.a; S: surfactant; I: inorganic species).

If the preparation takes place under acidic conditions, where surfactants are negatively charged and the inorganic species are positively charged, the synthetic pathway is termed as S^-I^+ (Figure I.21.b; S: surfactant; I: inorganic species).

Thus, the dominating interactions in these pathways are of an electrostatic in nature.

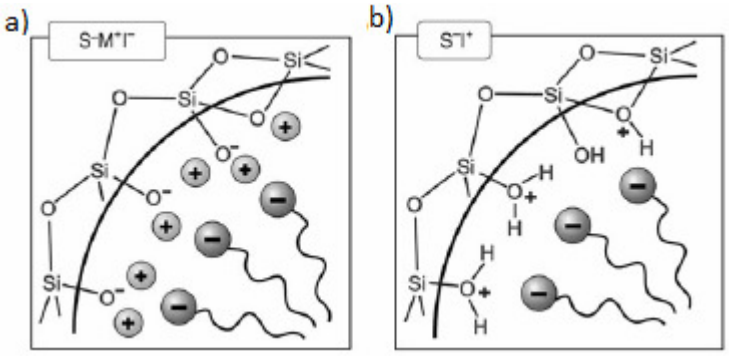

Figure I.21 Electrostatic interaction of anionic surfactants with inorganic precursor by a) $S^-M^+I^-$ and b) S^-I^+ pathway.

I.2.5.3 Nonionic surfactants as SDAs

Nonionic surfactants differ from both cationic and anionic surfactants in which the molecules are actually uncharged. The hydrophilic groups are made up of water soluble moieties, (e.g. water-soluble polymer chains) rather than charged head groups, while hydrophobic groups are made of water insoluble polymeric chains.

Nonionic surfactants are available in wide variety of different chemical structures. The most used nonionic surfactants are the Pluronic family polymers (Figure I.22). They consist of poly(ethylene oxide) (PEO) chains as hydrophilic groups and poly (propylene oxide) (PPO) as hydrophobic group. They are widely used in industry because of attractive characteristics like low price, nontoxicity, and biodegradability. In addition, the self-assembling of nonionic surfactants produces mesophases with different geometries and arrangements, becoming more and more popular and powerful in the syntheses of mesoporous solids.

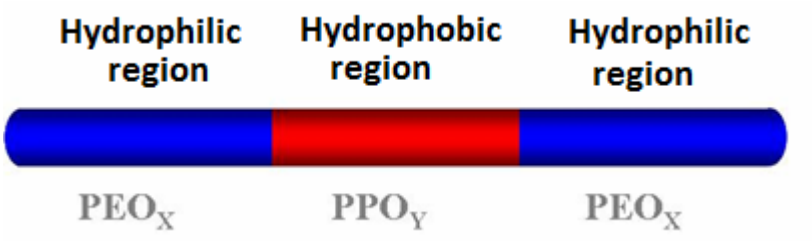

$$HO^-(CH_2\text{-}CH_2\text{-}O)_n^-(CH(CH_3)\text{-}CH_2\text{-}O)_m^-(CH_2\text{-}CH_2\text{-}O)_n$$

Pluronic PEO-PPO-PEO

Figure I.22 Nonionic surfactants.

When nonionic surfactants are used under neutral conditions, the attractive interactions are mediated through hydrogen bonds. The pathway is namely as N^0I^0 or S^0I^0, pathway (Figure I.23.a; N^0 are neutral amines, S^0 are nonionic surfactants and I^0 are hydrated silicate oligomers derived from TEOS).

Moreover, it is still possible for the attractive interactions to be mediated through hydrogen bonds. This is the case when nonionic surfactants are used, the ion pairs ($S^0(XI)^0$) pathway is presented Figure I.23.b.

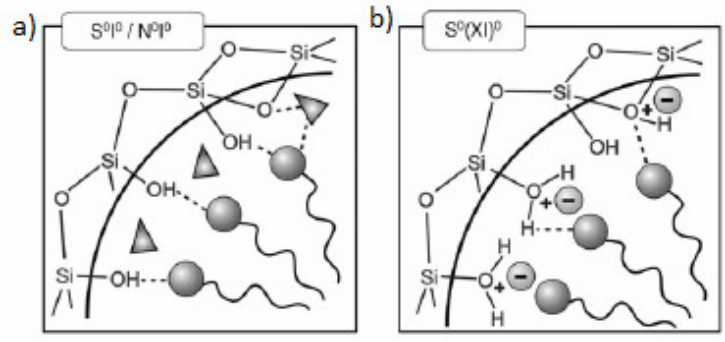

Figure I.23 Electrostatic interaction of nonionic surfactants with inorganic precursor by a) $S^0I^0/N^0I^0$and b) $S^0(XI)^0$ pathway.

II Chemical synthesis and characterization of new octahedral Ir(III) ionic complexes

II.1 Introduction

The interest in the chemistry of water-soluble cyclometallated complexes have been mainly from their potential application in various fields. The research has focused on the use of hydrophilic moieties in Ir(III) complexes for the promotion of water-solubility. The molecular fragments that one can change to achieve the desired properties in the final complex are the cyclometallating or coordinating ligands, and respectively the counterion. A coordinating ligand is a molecule with two or more potential electron-pair donor atoms, which attaches itself to a metal ion exhibiting a relatively high stability.

We started our work using as model complex [(*ppy*)$_2$Ir(*en*)]Cl presented in the Figure II.1. It has a hydrophilic ligand as ancillary ligand, the ethylene diamine (*en*), two cyclometalating ligands (*ppy*) and chloride (Cl^-) as counterion.

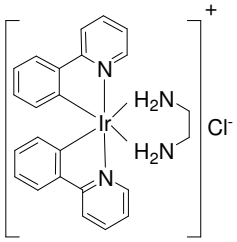

Figure II.1 Chemical structure of model complex [(*ppy*)$_2$Ir(*en*)]Cl

Only few examples of cyclometallated Ir(III) complexes formed by a non-aromatic diamine have been reported up until now.[119] The introduction of *en* into the cyclometalated Ir(III) framework introduces two NH_2 molecular functionalities, each able to generate H-bonding interactions, one of the means to control molecular assemblies during crystallization and to engineer the structures of the resulting crystalline materials.[120] Moreover the hydrogen bonding interactionsfacilitate controlled self-assembly allowing the targeted design of specific self-assembled structures.[121,122,123,124,125,126] The correlation between the supramolecular crystalline organization and the crystalline solid state photophysical properties introduce new properties in the final material.

They are also directionally specific, and this is distinctly advantageous in crystal design, wherein they are widely used. Furthermore, the complex resulted soluble in water.

A delicate balance of different competitive/cooperative factors is responsible for the final supramolecular organization; the ligand structure and counter anions plays a significant role in assembling these supramolecular architectures. Therefore, acetate and benzoate were introduced in the molecular structure of the model complex $[(ppy)_2Ir(en)]Cl$, changing thus the inorganic Cl^- with two moderately coordinating counterions. This choice was made also because these moieties may be easily functionalized with alkyl chains of variable lengths, therefore yielding to the final molecular structure of the complex, an amphiphilic character similarly to the surfactants.

The counterions were obtained as Ag(I) salts, by an easy two step synthesis in high yields. The general method of synthesis and chemical structure of the acetate and benzoate counterions is presented in Scheme II.1.

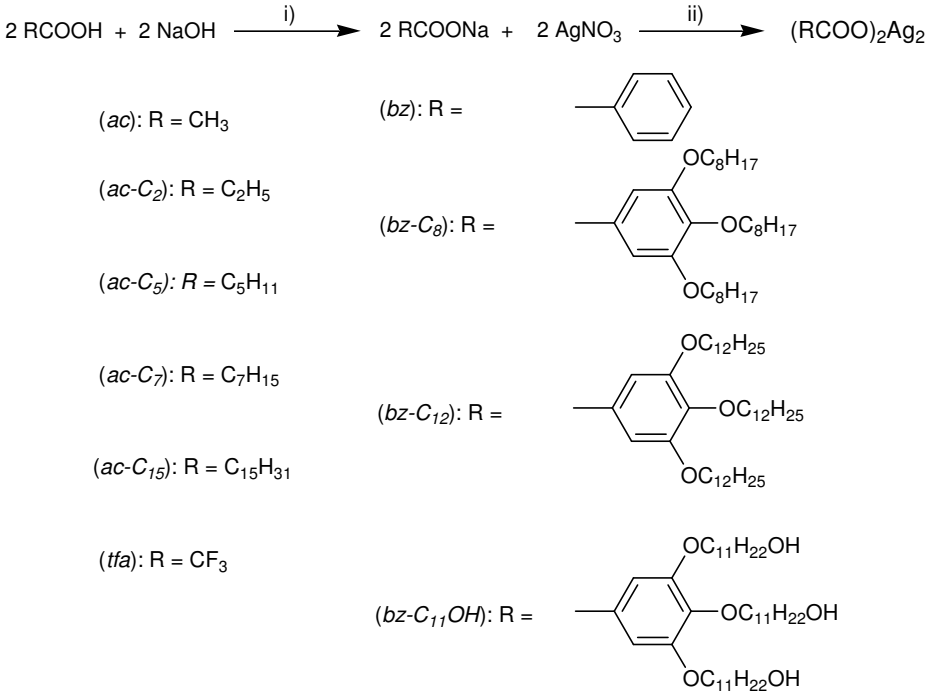

Scheme II.1 Synthesis and chemical structure of the new counterions used for the functionalization of the octahedral ionic complexes, i) H_2O/ EtOH, 2 hours, rt, ii) 2 hours, rt.

Initially we followed the change in the hydrophilicity which can be achieved through the changing of the counterions as shown in Figure II.2.

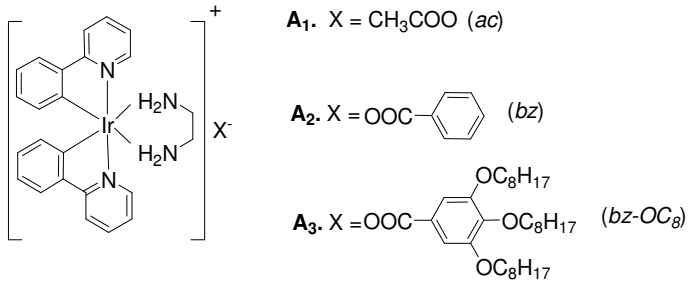

Figure II.2 Chemical structure of the octahedral Ir(III) ionic complexes from class A with the general formula [Ir(*ppy*)$_2$(*en*)](X), where X = acetate (*ac*), benzoate (*bz*) and 3,4,5-dodecyloxybenzoate (*bz-C$_8$*).

Subsequently, the change in the hydrophobicity was followed by changing the *en* ligand with 2-picolylamine (*pam*), reducing thus the number of the NH_2 groups and introducing an aromatic N donor moiety, obtaining complexes from class B (Figure II.3).

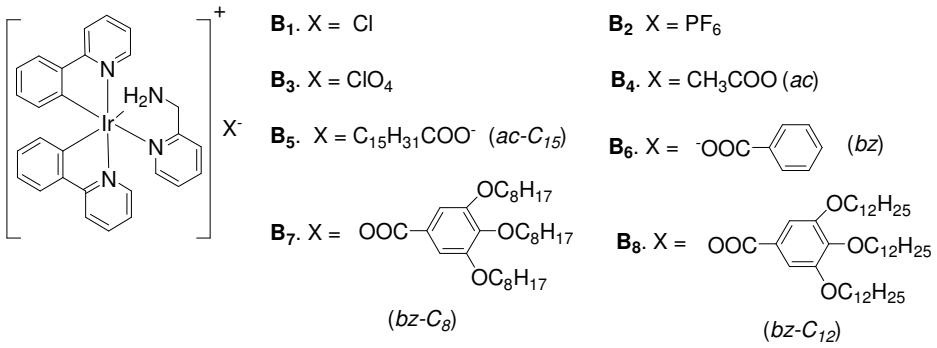

Figure II.3 Chemical structure of the octahedral Ir(III) ionic complexes of class B with the general formula [Ir(*ppy*)$_2$ (*pam*)](X), where X = chloride (Cl), hexaflourophosphate (PF_6), perchlorate (ClO_4), acetate (*ac*), hexadecanoate (ac-C_{15}), benzoate (*bz*), 3, 4, 5-tris-ocyloxybenzoate (bz-C_8) and 3,4,5-tris-dodecyloxybenzoate (*bz-C$_{12}$*).

The same inorganic counterion (Cl^-) was used initially as in the model complex (complex **B$_1$**), to probe the effects of this substitution on the resulting crystal structures and, hence, on the photophysical properties of the crystalline phases. Furthermore two new complexes with inorganic counterions, ClO_4 and PF_6 (complexes **B$_4$** and **B$_5$**) were synthesized. With respect to *en*, the *pam* ligand possess a single $–NH_2$ functionality and an aromatic group, able, in principle, to direct the assembly of the complex cations through both H-bonding and aromatic interactions. The supramolecular arrangement of functional molecules in the solid state can substantially affect the final organic optoelectronic device performance. In particular, controlling the self-assembly process of luminescent metal complexes into functional supramolecular organization, whose properties derive both from the structure of the metal complexes and their intermolecular interactions in the

ground and in the excited state, is fundamental for the development of advanced photoactive functional materials.

Furthermore, the effect of the counterion was followed within this class of complexes: alkyl chains were introduced through acetate counterions (complexes **B_2** and **B_3**), aromatic counterions and aromatic with long alkyl chains (complexes **B_6** and **B_7** and **B_8** respectively).

Another structure variation through ligand control was followed in the case of complexes from class C (**C_1-C_{10}**) were two N-donor aromatic moieties were introduced using the 2,2'-bipyridine (*bpy)* ligand. The resulting complexes may possess desired intramolecular π–π stacking between the *bpy* ligand and the phenyl rings of the cyclometallated ligand, which renders the supramolecular structures more stable. The same families of acetate and benzoate counterions were used as well as two new counterions: the trifluoroacetate (*tfa*) and dodecylsulfate (*dos*). The chemical structure of the complexes is shown in Figure II.4.

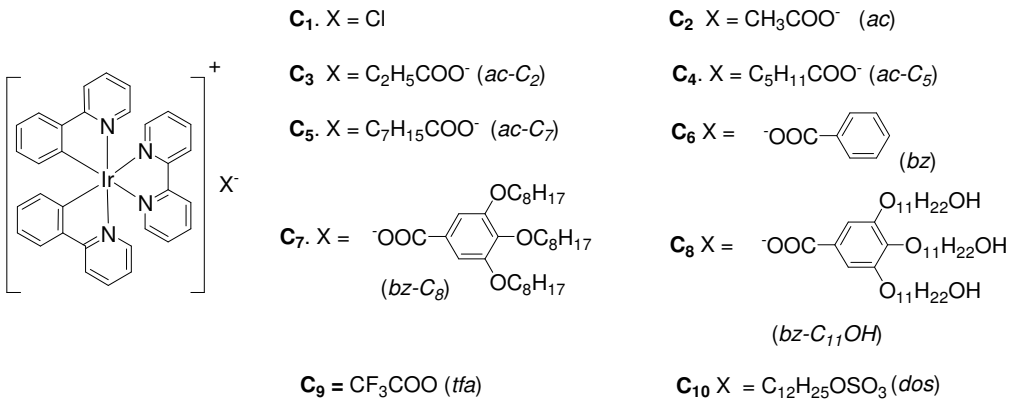

Figure II.4 Chemical structure of octahedral ionic Ir(III)complexes from class C with general formula [Ir(*ppy*)$_2$ (*ppy*)](X), where X = chloride (Cl), acetate (*ac*), propionate (ac-C_2), hexanoate (ac-C_5), octanoate (ac-C_7), benzoate (bz), 3,4,5-tris-ocyloxybenzoate (bz-C_8), 3,4,5-tris-dodecyloxybenzoate (*bz-C_{12}*), trifluoroacetate (*tfa*) and dodecylsulfate (dos).

Furthermore, to tune the redox, photophysical properties and supramolecular order of Ir(III) complexes through ligand modification, another strategy involving the functionalization of the ligands was employed, obtaining thus complexes from class D. In particular, the *bpy* ligand was functionalized in 4, 4'-positions with either alkyl chains ending with hydrophilic OH groups or alkyl chains ending with t-butyl-dimethylsilane (TBDMS) respectively. PF_6, *ac*, *bz* and *dos* were used as representative counterions to contra balance the charge. Thus, taking advantage of the experience in the synthesis of functionalized 2,2'-bipyridine as organic synthons for the formation of octahedral mesogenic transition metals, new Ir(III) complexes of class D (**D_1-D_4**) were prepared, their structure being shown in Figure II.5.

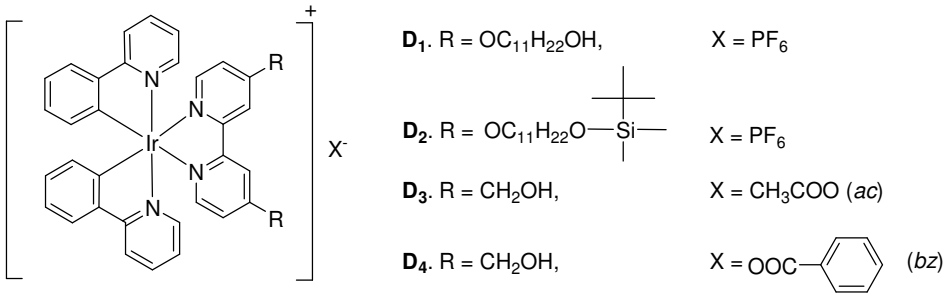

Figure II.5 Chemical structure of octahedral ionic Ir(III)complexes from class D with functionalized *bpy* ligands of general formula [Ir(*ppy*)$_2$(*bpy-R*)](X), where X = hexafluorophophate (PF_6), acetate(*ac*) and benzoate (*bz*).

The introduction of the F group on the *ppy* ligands may not only influence the structural organization of the final material, but also may favorable tune its photophysical properties. Therefore, F groups on 3rd and 5th positions of the cyclometallating *ppy* ligand were introduced. The new Ir (III) complexes of class E (**E$_1$**-**E$_3$**) were prepared (Figure II.6).

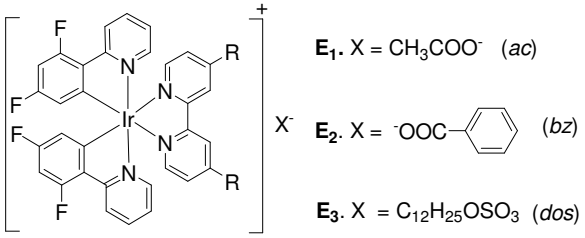

Figure II.6 Chemical structure of octahedral ionic Ir(III) complexes from class E with functionalized *fppy* ligands of general formula [Ir(*fppy*)$_2$(*bpy-R*)](X), where X = acetate(*ac*), benzoate (bz) and dodecylsulfate (*dos*).

Indeed, in *ppy*-based Ir(III) complexes, the emission is believed to originate from mixed triplet states possessing both intraligand (IL) $^3\pi$-π^* and metal-to-ligand charge transfer (^{3}MLCT) characters or states with greater contributions from ^{3}MLCT. From the view point of ligand chromophores, the lowest unoccupied molecular orbital (LUMO) and highest occupied molecular orbital (HOMO) energy levels are mainly located at the pyridyl portion and phenyl segment of the *ppy* ligand, respectively, which are affected by the electronic state of the ligand. In principle, in order to blue-shift the emission wavelength in iridium (III) complexes, the LUMO-HOMO energy gap should be increased, thereby stabilizing the HOMO and/ or destabilizing the LUMO energy levels.

Regarding the new functionalized *bpy* ligands, their reactivity versus transitional metal complexes was primarily tested, using Zn(II) salts. This strategy permitted to investigate the stability of the ligands in different reaction conditions and the versatility towards complexation, through an easy one-step reaction. Furthermore, Zn (II) salts among the different transition metal studied are one of

the most fascinating as it is very cheap and its 24th most abundant metal in the earth's crust. Zinc tends to form bonds with a greater degree of covalency and it forms much more stable complexes with N- donors.

Moreover, owing to the growing interest towards photoactive complexes based on less traditional but more abundant and cheaper metal elements, like the complexes containing metals with a d^{10} electronic configuration[127,128], a further goal of this investigation is the development of Zn(II) complexes based materials. Complexes of Zn(II) are mostly 4- or 6- coordinate although 5-coordinate complexes are known. Although in aqueous solution Zn(II) is coordinated to six water molecules[129], in both zinc –finger proteins and enzymes, zinc usually is tetrahedrally coordinated, but in some cases catalytic binding sites it is found penta-coordinated and rarely, hexacordinated.[130] Herein, Table II.1 a full list of the five classes of complexes prepared is presented.

Table II.1

Class	General formula of complexes	Counterions
A	[Ir(*ppy*)$_2$(*en*)]X	*ac*, *bz*, *bz-C$_8$*
B	[Ir(*ppy*)$_2$(*pam*)]X	Cl, PF_6, ClO_4, *ac*, ac-C_{15}, *bz*, *bz-C$_8$*, *bz-C$_{12}$*
C	[Ir(*ppy*)$_2$(*bpy*)]X	Cl, *ac*, ac-C_2, ac-C_5, ac-C_7, bz, bz-C_8, *bz-C$_{12}$*, *tfa*, dos
D	[Ir(*ppy*)$_2$(*bpy-R*)]X	PF_6, *ac*, *bz*
E	[Ir(*fppy*)$_2$(*bpy*)]X	*ac*, *bz*, dos

II.2 Complexes of class A, [(ppy)$_2$Ir(en)]X, where X = ac, bz, bz-C$_8$

As the model complex [Ir(*ppy*)$_2$(*en*)]Cl, the complexes of class A contain two *ppy* as cyclometallating ligands and ethylenediamine (*en*) as ancillary ligand. The *en* has two CH_2 groups and two NH_2 groups. It has outstanding ability form the stable complexes via 5 membered metallocyclic rings with Ir. The use of *en* into the Ir(III) framework introduces the NH_2 molecular functionality, suitable for the generation of H-bonding interactions, one of the means to control molecular assemblies during crystallization and to engineer the structures of the resulting crystalline materials. Therefore, the potential of this ligand in the construction of new highly luminescent crystalline materials is outstanding.

Furthermore, the counterions plays a significant role in assembling supramolecular architectures and slight change in the structure of counterions will influences the desired properties of final material.

Therefore, the first change in the molecular structure of the model complex [Ir(*ppy*)$_2$(*en*)]Cl was the substitution of the counterions with acetate (*ac*) and benzoate (*bz*) moieties. These are versatile derivatives, easily functionalisable with long alkyl chains, and therefore represent a simple and straightforward method to mimic the amphiphilic structure of surfactants, with respect to the functionalization of the ligands. Indeed, the counterions as Ag(I) salts were obtained in a two step synthesis, while more complicated and elaborated methods are used to functionalize the ligands.[131]

The different counterions used were *ac*, *bz* and *bz-C$_8$* respectively. Their chemical structure and proton numerotation is presented in Figure II.7.

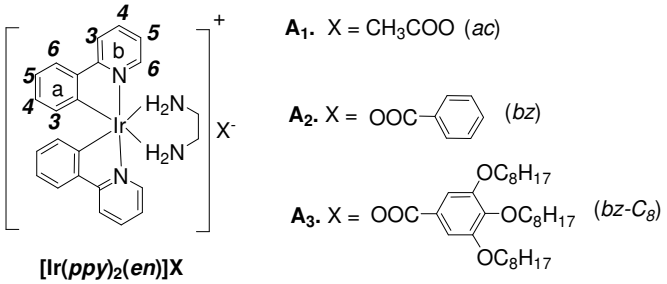

Figure II.7 Chemical structure of the complexes **A$_1$-A$_3$** with the general formula [Ir(*ppy*)$_2$(*en*)]X, where X = acetate(*ac*), benzoate (*bz*) and 3, 4, 5-tris-ocyloxybenzoate (*bz-C$_8$*).

II.2.1 Synthesis and characterization of complexes A_1 - A_3

II.2.1.1 Synthesis

For the synthesis of complexes of class A, previously a series of Ag(I) salts were prepared, by a modified synthetical procedure found in the literature.[132]

Synthesis of the counterions:

A series of Ag(I) salts of acetate, benzoate and benzoate functionalized with octyloxy-alkyl chains were obtained in order to be used for the synthesis of complexes of Class A. The synthesis and chemical structure of the counterions obtained is presented in Scheme II.2.

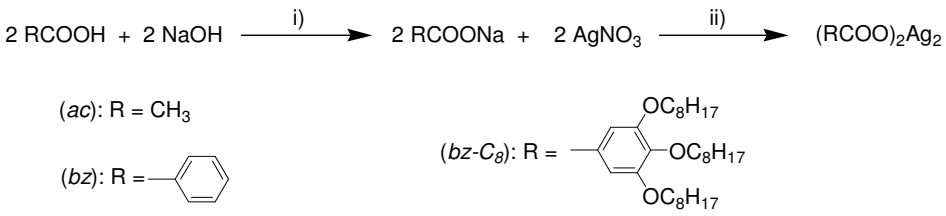

Scheme II.2 Synthesis and chemical structure of the new counterions used for functionalize class A complexes: i) EtOH/H_2O, rt, 2 hours, ii) rt, 2 hours.

In particular, the corresponding acid precursor (acetic acid, benzoic acid and 3,4,5-trioctyloxybenzoic acid respectively) were reacted with NaOH in EtOH/H_2O solution, (Scheme II.2). After two hours of stirring at r.t., an equimolecular amount of $AgNO_3$ was added and the mixture was further stirred for 2 hours. The product, formed as a white precipitate in the reaction mixture, was filtered out, washed with water, dried and used without further purification.

The crystal structure of Ag(I) salts of the acetic acid and benzoic acid found in the literature[133, 134] show that they exist in dimeric forms, by the formation of eight-membered rings involving two Ag atoms, with the carboxylate groups acting as bidentate bridging ligands, typical of this oxidation state of the complex forming metal. Therefore $R_2(COO)_2$ molecular formula will be used for all the Ag(I) salts of functionalized acetates and benzoates synthesized further.

For the synthesis of the functionalized benzoates, first the acids were obtained using the same method reported in literature[135]. In particular, the reaction of 3,4,5-trihydroxybenzoate with bromoalkane under basic conditions led to the related tri-alkoxybenzoic acid *H-bz-C_8*, after alkaline hydrolysis and an acidic workup. The synthesis is presented in Scheme II.3.

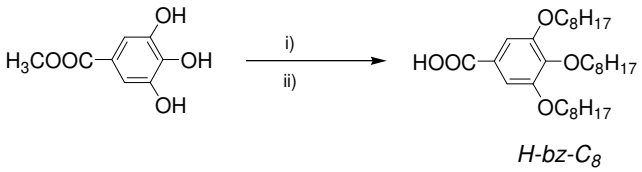

H-bz-C8

Scheme II.3 Synthesis of *H-bz-C*$_8$,: i) RBr, K_2CO_3, Cyclohexanone, 48 hours, ΔT; ii) KOH, EtOH, 4 hours, ΔT;

The Ag(I) salts thus prepared were further used for the synthesis of Ir(III) complexes of class A.

Synthesis of complexes

The synthesis of the ionic Ir(III) complexes of class A were carried out by using the same general method described in the introduction part. In particular, following the classical bridge-splitting reaction of the dimeric precursor $[Ir(ppy)_2]_2$-μCl_2 with 2.0 equivalents of *en* ligand, followed by subsequently addition of 2.2-fold excess of Ag(I) salts that contains the appropriate counterions acetate (*ac*), benzoate (*bz*) and 3,4,5-tris-ocyloxybenzoate (*bz-C*$_8$), complexes of series **A$_1$ - A$_3$** were obtained (Scheme II.4).

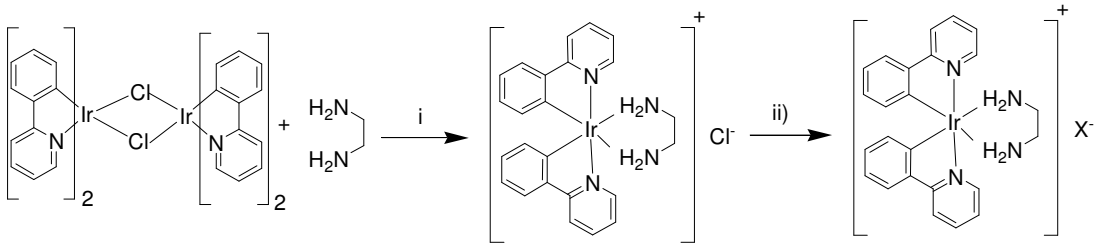

Scheme II.4 Synthesis of octahedral ionic Ir(III) complexes of class A: i) CH_2Cl_2/ MeOH (3:1 v/v), ΔT, 4 hours, N_2; ii) Ag_2X_2, ΔT, 3 hours, N_2.

All ionic species are obtained as microcrystalline yellow powder solids in good yields (82.3 %, 81.0%, and 75.0% respectively), and will be referred as complexes **A$_1$ - A$_3$** with the general formula $[Ir(ppy)_2(en)]X$, as illustrated in Scheme II.2.1. In particular, complex **A$_1$** was water soluble. The complexes were fully characterized by IR and ^{1}H NMR spectroscopies, conductivity measurements and elemental analysis. Furthermore, TGA and DSC analysis were performed in order to identify to possible solvents that are included in the molecular formula of the complexes.

Conductivity measurements conducted in acetonitrile solution for complexes **A$_1$** and **A$_2$**, assesed their 1:1 electrolyte nature. Indeed, the molar conductivities (127 $\Omega^{-1}\cdot cm^2\cdot mol^{-1}$ (**A$_1$**) and 103 $\Omega^{-1}\cdot cm^2\cdot mol^{-1}$ (**A$_2$**) respectively), are in the acceptable Λ_M ranges for univalent electrolytes in acetonitrile solution.[136] Furthermore, for solubility reasons, the conductivity measurements for

complex **A_3** were performed in methanol solution. Again the value obtained (61 $\Omega^{-1}\cdot cm^2\cdot mol^{-1}$) is in the range of univalent electrolytes in methanol solution.[136]

II.2.1.2 Spectroscopic characterization

IR spectroscopy

In the IR spectra of complex **A_1-A_3**, the characteristic bands of the stretching frequencies of the aliphatic chains were identified at 2926 cm^{-1} and 2855 cm^{-1}, more intense for complex **A_3** that has three long alkyl chains, whereas for complex **A_1** these bands are almost covered by the characteristic stretching's of N-H (broad band's at 3380 and 3250 cm^{-1}). Furthermore, the main bands of the C-O frequencies of the carboxylate anions are identified at 1562 cm^{-1} (C-O antisym. stretch.) and 1418 cm^{-1} (C-O sym. stretch.) for **A_1** and respectively around 1550 cm^{-1} (C-O antisym. stretch.) and 1380 cm^{-1} (C-O sym. stretch.) for the benzoate containing complexes **A_2** and **A_3**.

^{1}H NMR spectroscopy

The ^{1}H NMR spectra were recorded in CD_3OD for complexes **A_1 - A_2** and $CDCl_3$ for complex **A_3**. The aromatic region showed all 16 protons of the *ppy* in the range of 9.0 ppm to 6.0 ppm. Furthermore, in the aliphatic region, the signals attributed to the *en* ligand, 2 NH_2 protons and 2 CH_2 protons were identified in the range between 5.0 and 3.0 ppm.

Regarding the counterions, the singlet of the *ac* in complex **A_1** was found at 1.88 ppm. Furthermore, the ^{1}H NMR spectrum of complex **A_2** showed in the aromatic region the additional signals regarding the 5 protons from *bz* as overlapped peaks in the range of 7.40 -7.30 ppm. The spectrum of complex **A_3** showed the additional 2 aromatic protons from *bz-OC_8* as a singlet at 7.22 ppm and respectively the protons from the aliphatic chains of complex **A_3** were found in the range of 4.00 to 0.80 ppm.

II.2.1.3 Thermal analysis

TGA showed that all powder complexes contain solvent in their powder pristine solids. The desolvation processes in correspondence with endothermic peaks observed in the DSC trace reveals a relatively strong interaction between the Ir(III) complexes and the solvent molecules, identified as H_2O molecules from NMR spectra's. Furthermore, the number of co-crystallized water molecules differs from one complex to other, as determined by the weight mass loss in the TGA traces. Therefore, we will refer to this class as having the general formula $[Ir(ppy)_2(en)]X\cdot xH_2O$.

In particular, powder complex **A_1** has an experimental mass loss of 1.29 % corresponding to 1/2 molecules of water (calcd. 1.43%), in a relatively narrow range of temperature (35 – 70°C),

accompanied by an endothermic process in the DSC trace (ΔH = 8.4 kJ·mol^{-1}). Complex **A_2** has an experimental mass loss of 5.13 % (total loss) corresponding to 2 molecules of water (calcd. 5.06 %), in two steps in a broad range of temperature (35 – 230°C), accompanied by two endothermic processes in the DSC trace (ΔH_1 = 111.8 kJ·mol^{-1} and ΔH_1 = 7.3 kJ·mol^{-1}). Finally complex **A_3** has an experimental mass loss of 2.35 % corresponding to one and 1/2 molecules of water (calcd. 2.46%), in a relatively narrow range of temperature (70 – 100°C), accompanied by an endothermic process in the DSC trace (ΔH = 83.6 kJ·mol^{-1}).

As an example for Class A, in Figure II.8, the TGA and DSC traces are shown for **A_3**.

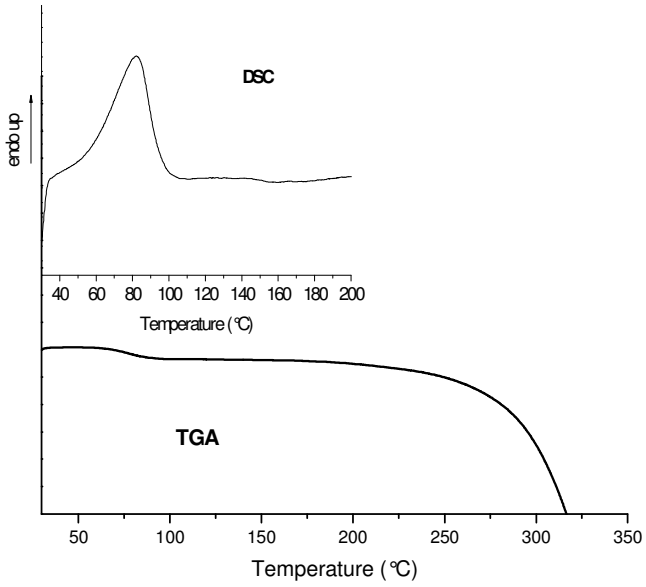

Figure II.8 TGA and DSC traces of powder complex **A_3.**

The TGA and DSC traces of powdered complexes **A_1** and **A_2** are shown in experimental section, Chapter III (Figure III.1 and Figure III.2).

II.2.2 Structural characterization of cation [Ir(ppy)$_2$(en)]$^+$

Furthermore, in order to check out the effects of the presence 2 NH_2 moiety in the modulation of supramolecular organizations and, therefore, the photophysical properties of crystalline materials, single crystals suitable for X-ray analysis were grown for all of the complexes **A_1 - A_3**.

The crystals of **A_1** were obtained directly by slow evaporation CH_2Cl_2 solution of the complex at room temperature, whereas crystals of **A_2** were obtained by the diffusion of hexane into the dichloromethane solution of the complex, followed by slow evaporation at room temperature.

The crystal structure of compounds **A_1** and **A_2** is built up of mononuclear $[(ppy)_2Ir(en)]^+$ cation, and uncoordinated acetate (**A_1**) or benzoate (**A_2**) anions. Two (**A_1**) or one (**A_2**) crystallization water molecules and a dichloromethane solvent molecule (**A_1**) are also presents in the crystalline structure of **A_1** and **A_2**. The compounds are not isostructural, most likely for the presence of the additional dichloromethane solvent molecule present in A_1. In particular, the cationic complexes in both compounds pack into two different monoclinic centrosymmetric space groups, namely C2/c and $P2_1/c$ for **A_1** and **A_2**, respectively.

The single X-ray crystal structure of complexes **A_1** showed that complexes was built up of mononuclear $[Ir(ppy)_2(en)]^+$ cation exhibiting a distorted octahedral geometry around the Ir metal centre, with two cyclometallated *ppy* and an *en* ancillary ligands drawing a IrC_2N_2 chromophore. A view of the molecular fragments of **A_1**, and that of the **A_2** should be same and therefore the adopted atomic labelling scheme is given in Figure II.9.

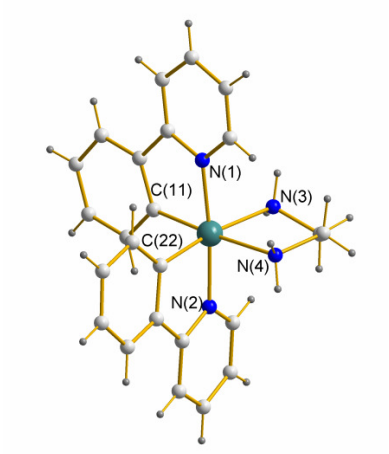

Figure II.9 View of the molecular fragments of class A showing the atomic labelling scheme.

The best equatorial plane is defined by the N(3)N(4)C(11)C(22) set of atoms, the Ir(1) atom slightly deviating from this plane. The two *ppy* ligands adopt the usual NN *trans* configuration, with Ir-N and Ir-C bond distances falling in the expected ranges[137, 138, 139] (Table II.2.1). The *en* ligand displays notably longer Ir-N distances, which can be attributed to the *trans*-influence of the strong Ir-C bonds of the *ppy* ligands[140, 141, 142, 143] (see Table II.1).

In both complexes **A_1** and **A_2**, the complex cation, the uncoordinated counterions (*ac* for **A_1** and *bz* for **A_2**) and a solvent water molecule are involved in hydrogen bonding interactions, as showed in Figure II.10.a for complex **A_2**.

Table II.2.1 Bond lengths [Å] and angles (°) for $\mathbf{A_1}$ and $\mathbf{A_2}$.

Compound	$\mathbf{A_1}$	$\mathbf{A_2}$
Ir(1)-C(11)	2.027(11)	2.015(4)
Ir(1)-C(22)	2.036(10)	2.020(4)
Ir(1)-N(1)	2.081(9)	2.060(3)
Ir(1)-N(2)	2.076(9)	2.064(3)
Ir(1)-N(3)	2.212(8)	2.195(3)
Ir(1)-N(4)]	2.217(9)	2.211(3)
N(1)-Ir(1)-N(2)	173.8(3)	174.01(13)
N(1)-Ir(1)-N(3)	88.2(3)	87.30(12)
N(1)-Ir(1)-N(4)	96.9(3)	97.76(12)
N(2)-Ir(1)-N(3)	96.5(3)	96.46(13)
N(2)-Ir(1)-N(4)	88.0(3)	87.58(13)
N(4)-Ir(1)-N(3)	78.9(3)	78.60(12)
C(11)-Ir(1)-C(22)	90.3(4)	91.60(17)
C(11)-Ir(1)-N(1)	80.5(4)	80.22(15)
C(11)-Ir(1)-N(2)	95.0(4)	94.63(15)
C(11)-Ir(1)-N(3)	96.0(4)	97.45(14)
C(11)-Ir(1)-N(4)	174.4(4)	175.68(14)
C(22)-Ir(1)-N(1)	94.9(4)	97.06(16)
C(22)-Ir(1)-N(2)	80.9(4)	79.92(17)
C(22)-Ir(1)-N(3)	173.3(4)	170.52(15)
C(22)-Ir(1)-N(4)	94.8(4)	92.44(15)

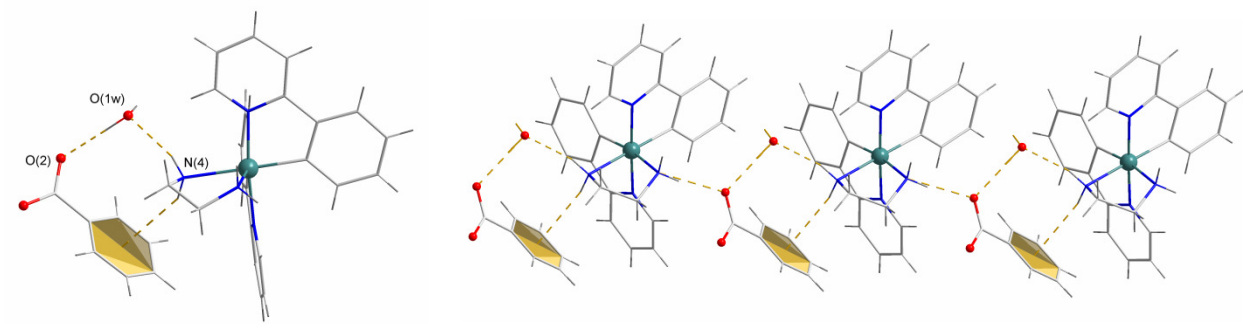

a) **b)**

Figure II.10 View of the hydrogen bonding interactions in $\mathbf{A_2}$; view of the 1D supramolecular structure along the *c* crystallographic direction.

In $\mathbf{A_1}$ the acetate anions acts as bridges between the Ir complexes assembling a 1D motif by means of hydrogen bonds involving the oxygen atom of the anion and the NH_2 group of the *en* ligand [O(2)···N(4) distance of 2.91(2) Å; N(4)-H(4B)···O(2) distance and angle of 2.05 Å and 159°, respectively; O(1*a*)···N(3) distance of 2.97(1) Å; N(3)-H(3B)···O(1*a*) distance and angle of 2.11 Å and 159°, respectively; *a* = -1/2+*x*, 1/2+*y*, *z*]. The crystallized water molecules also support this motif by establishing additional hydrogen bonding interactions with the anion and the *en* ligand

[N(3)···O(1w*b*) distance of 3.04(2) Å; N(3)-H(3AB)···O(1w*b*) distance and angle of 2.18 Å and 159°, respectively; O(2)···O(1W) 2.798 Å; O(1)···O(2W*c*) 2.780 Å; *b*= 1/2-x,3/2-y,-z and *c* =1-x,1-y,-z]. The crystal data and structure refinement for **A_1** are shown in Table II.2.

Table II.2 Crystal data and selected structure refinement parameters for complexes **A_1** and **A_2**

	A_1	**A_2**
Empirical formula	$C_{27}H_{33}Cl_2IrN_4O_4$	$C_{31}H_{31}IrN_4O_3$
Formula weight	740.67	699.80
Temperature	296(2) K	296(2) K
Wavelength	0.71073 Å	0.71073 Å
Crystal system	Monoclinic	Monoclinic
Space group	C2/c	P2(1)/c
Unit cell dimensions	a = 18.426(3) Å α = 90°. b = 9.7097(12) Å β = 101.209(13)°. c = 33.075(5) Å γ = 90°.	a = 9.8304(12) Å α = 90°. b = 9.7533(11) Å β = 97.797(4)°. c = 29.975(4) Å γ = 90°.
Volume	5804.7(14) $Å^3$	2847.4(6) $Å^3$
Z	8	4
Density (calculated)	1.695 Mg/m^3	1.632 Mg/m^3
Absorption coefficient	4.823 mm^{-1}	4.727 mm^{-1}
F(000)	2928	1384
Crystal size	0.08 x 0.06 x 0.04 mm^3	0.04 x 0.03 x 0.03 mm^3
Theta range for data collection	1.26 to 25.00°.	1.37 to 26.86°.
Index ranges	-21<=h<=21, -11<=k<=11, -39<=l<=39	-12<=h<=12, -12<=k<=12, -38<=l<=38
Reflections collected	41574	63867
Independent reflections	5125 [R(int) = 0.0509]	6107 [R(int) = 0.0583]
Completeness	to theta = 25.00° 99.9 %	to theta = 26.86° 99.4 %
Absorption correction	Semi-empirical from equivalents	Semi-empirical from equivalents
Max. and min. transmission	0.8305 and 0.6989	0.8712 and 0.8334
Refinement method	Full-matrix least-squares on F^2	Full-matrix least-squares on F^2
Data / restraints / parameters	5125 / 0 / 344	6107 / 3 / 358
Goodness-of-fit on F^2	1.150	1.162
Final R indices [I>2sigma(I)]	R1 = 0.0576, wR2 = 0.1525	R1 = 0.0251, wR2 = 0.0607
R indices (all data)	R1 = 0.0630, wR2 = 0.1558	R1 = 0.0403, wR2 = 0.0742
Largest diff. peak and hole	3.848 and -1.366 $e.Å^{-3}$	0.699 and -0.831 $e.Å^{-3}$

In **A_2** the solvent water molecule bridges the Ir complexes and the anion, acting as acceptor toward one of the hydrogen atoms of the *en* ligand [O(1w)···N(4) distance of 3.015(5) Å; N(4)-H(4A)···O(1w) distance and angle of 2.142(4) Å and 163.3(2)°], and as donor toward the carboxylate group of the anion [O(1w)···N(2) distance of 2.780(5) Å; O(1w)-H(1wA)···O(2) distance and angle of 1.83(3) Å and 174.4(3)°]. Moreover, the *en* ligand displays N-H···π interactions with the phenilic ring of the benzoate [N(4)-H(4B)···π_{centr} distance and angle of 2.7 Å and 147°]. Furthermore, the crystal data and structure refinement for **A_2** are shown in Table II.2.

An one-dimensional supramolecular structure is achieved in **A_2** by further hydrogen bonds involving the oxygen atom of the benzoate anion and the NH_2 group of the *en* ligand [O(2)···N(3) distance of 2.892(4) Å; N(3)-H(3A)···O(2) distance and angle of 1.999(3) Å and 171.0(2)°, respectively], which held together adjacent complexes along the *a* crystallographic direction (Figure II.10.b). Weaker Van der Waals and electrostatic interactions ensure the crystal cohesion.

II.2.3 Photophysical properties

II.2.3.1 Photophysical properties of [Ir(*ppy*)$_2$(*en*)]$^+$ cation

Since the photophysical properties of the complexes are independent from the counterions, the absorption and emission spectra of class A compounds are discussed taking into consideration the common [Ir(*ppy*)$_2$(*en*)]$^+$ cation. In particular, photophysical measurements have been conducted in acetonitrile solution (Figure II.11).

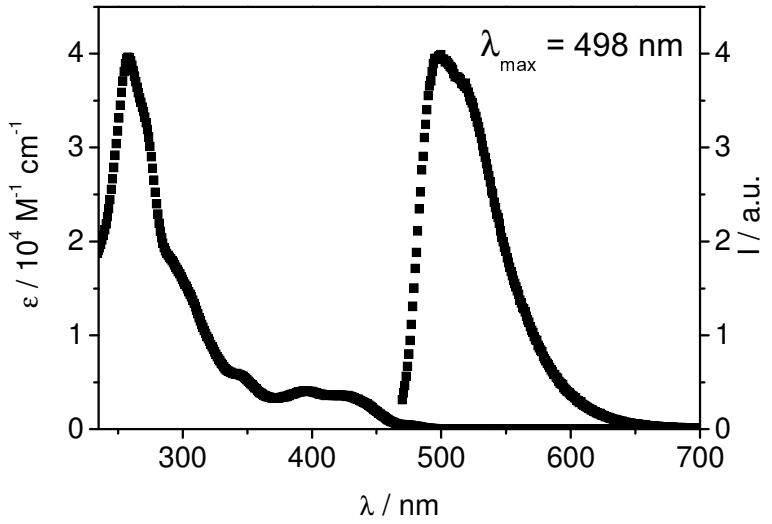

Figure II.11 The absorption and emission spectra of [Ir(*ppy*)$_2$(*en*)]$^+$ cation in acetonitrile deaerated solution.

The absorption spectrum show intense bands (molar extinction coefficient > 10^4 M^{-1} cm^{-1}) in the ultraviolet part of the spectrum between 200 nm and 333 nm. These bands are associated with ligand centered (LC) transitions. The LC bands are accompanied by weaker and broad bands (with molar extinction coefficients of ca. 1×10^3 to 7×10^3 M^{-1} cm^{-1}) that extend from 370 nm to slightly over 460 nm and are associated with both spin-allowed and spin-forbidden metal-to-ligand charge transfer (MLCT) transitions.

Moreover, luminescence properties of the [Ir(*ppy*)$_2$(*en*)]$^+$ cation, has been measured in deaerated acetonitrile solution. In the deoxygenated acetonitrile solution, [Ir(*ppy*)$_2$(*en*)]$^+$ cation shows a

brilliant blue-green ^{3}MLCT emission, with the emission maximum centered at 498 nm, luminescence quantum yield of 0.68 and emission lifetime about 1600 ns (Table II.3).

Table II.3 Phototophysical data of cation [Ir (*ppy*)$_2$(en)]$^+$

Complex	Absorption λ(nm) (ε x 10^4 M^{-1} cm^{-1})	λ_{max} (nm)	τ[ns]	Φ(%)
Class A[a]	257(4); 344(0.6); 395(0.4);429 (0.354);476(0.05)	498	τ = 1600	68.0

[a]Deaerated acetonitrile solution.

II.2.3.2 Photophysical properties of complex A_1 in water

Finally for the complex **A_1**, [Ir(*ppy*)$_2$(*en*)](*ac*), soluble in water, a full photophysical analysis was performed also in this solvent. The absorption and emission spectra of the [Ir(*ppy*)$_2$(*en*)](*ac*) is shown in Figure II.12.

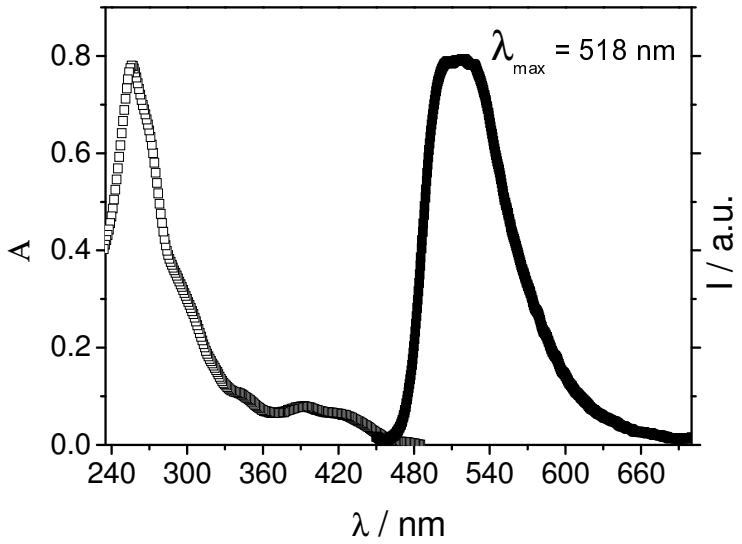

Figure II.12 The absorption and emission spectra of complex [Ir(*ppy*)$_2$(*en*)]*ac* in water.

The general photophysical data in solution of complex **A_1**, [Ir(*ppy*)$_2$(*en*)](*ac*) in water, are shown in Table II.4. In particular, complex **A_1** showed a slight red shifted emission maxima with respect to the corresponding acetone solution. Moreover, the luminescent decay resulted multiple exponential in nature. Both these experimental evidences strongly suggest the presence of aggregation phenomena in solution.

Table II.4 Photophysical data of complex $\mathbf{A_1}$, [Ir(*ppy*)$_2$(en)](*ac*), in water.

Complex	**Absorption λ(nm) (ε x 10^4 M^{-1} cm^{-1})**	**λ_{max} (nm)**	**τ[ns]**	**Φ(%)**
$\mathbf{A_1}$ = [Ir(*ppy*)$_2$(*en*)](*ac*)	425(0.187), 392(0.25), 345(0.312), 300(sh), 270(sh), 256(2.437)	515	τ_1 = 1220 (10.5%) τ_2 = 2250 (89.5%)	91

II.3 Complexes of class B, [Ir(ppy)$_2$(pam)](X), where X = Cl, PF$_6$, ClO$_4$, ac, ac-C$_{15}$, bz, bz-C$_8$ and bz-C$_{12}$

Subsequently, the change in the hydrophobicity was followed by changing the *en* ligand with 2-picolylamine (*pam*), reducing thus the number of the NH_2 groups and introducing an aromatic N donor moiety, obtaining complexes from class B. With respect to *en*, the *pam* ligand possess a single $–NH_2$ functionality and an aromatic group, able, in principle, to direct the assembly of the complex cations through both H-bonding and aromatic interactions. The substitution of a non-chromophoric ancillary ligand (*en*) with a flexible asymmetric ligand containing an aromatic moiety (*pam*) may boost expected supramolecular organizations and, therefore, the photophysical properties of crystalline materials. Thus, this ligand has marvelous ability in the construction of new highly luminescent crystalline materials.

Following, the substitution of the counterion was completed. In particular, three groups of complexes were prepared: complexes **B$_1$ – B$_3$** having inorganic counterions (Cl, PF_6 and ClO_4 respectively), complexes **B$_4$** and **B$_5$** having acetate and hexanoate as counterions (*ac* and *ac-C$_{15}$*) and complexes **B$_6$ – B$_8$** having benzoate and functionalized benzoates as counterions (*bz*, *bz-C$_8$* and *bz-C$_{12}$*). The chemical structure and respectively the proton numerotation of the new complexes is presented in Figure II.13.

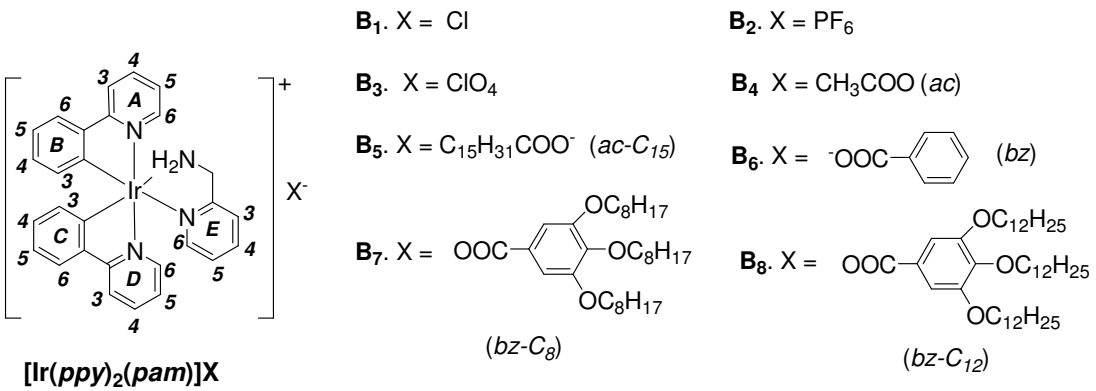

Figure II.13 Chemical structure of the octahedral Ir(III) ionic complexes of class B with the general formula [Ir(*ppy*)$_2$(*pam*)](X), where X = chloride (Cl), hexaflourophosphate (PF_6),perchlorate (ClO_4), acetate(*ac*), hexadecanoate (*ac-C$_{15}$*), benzoate (*bz*), 3, 4, 5-tris-ocyloxybenzoate (*bz-C$_8$*) and 3,4,5-tris-dodecyloxybenzoate (*bz-C$_{12}$*).

II.3.1 Synthesis and characterization of complexes B_1 – B_8

II.3.1.1 Synthesis

For the synthesis of complexes of class B, previously a series of Ag(I) salts were prepared, by a modified synthetical procedure found in the literature.[132]

Synthesis of the counterions:

The inorganic salts containing the appropriate counterions PF_6 and ClO_4 used for the synthesis of complexes **B_2** and **B_3** from commercial sources without further purification. The different organic counterions (carboxylates and benzoates) were prepared as Ag(I) salts by a modified synthetic process found in the literature[132], as reported previously for the complexes of class A.

The synthesis of the Ag(I) salt of *ac*, *bz* and *bz-C_8* were presented in the chapter II.2.1.1. Furthermore, two new Ag(I) salts were prepared, their synthesis being presented in Scheme II.5.

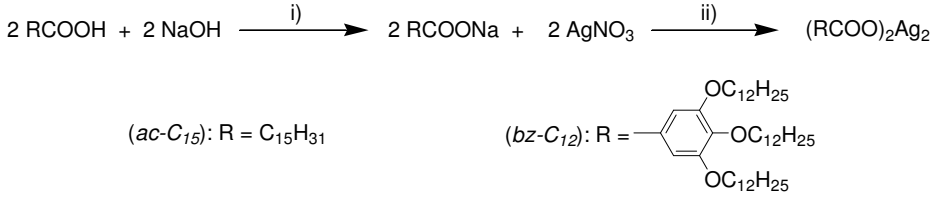

Scheme II.5 Synthesis and chemical structure of the two newcarboxylate Ag(I)salts used for functionalize class B complexes: i) NaOH, EtOH/H_2O, rt, 2 hours, ii) $AgNO_3$, rt, 2 hours.

In particular, the corresponding acid precursor (hexadecanoic acid and 3,4,5-dodecyloxybenzoic acid) were reacted with NaOH in EtOH/H_2O solution, (Scheme II.5). After two hours of stirring at r.t., an equimolecular amount of $AgNO_3$ was added and the mixture was further stirred for 2 hours. The products, formed as a white precipitates in the reaction mixture, were filtered out, washed with water, dried and used without further purification.

As for the other Ag(I) salts presented previously in chapter II.2.1.1, the similar features detected by spectroscopic analysis indicated the $R_2(COO)_2Ag$ as molecular structure.

For the synthesis of the functionalized benzoates, first the acids were obtained using the same method reported in literature.[13135] In particular, the reaction of methyl-3,4,5-trihydroxybenzoate with bromoalkane under basic conditions were led to the related tri-alkoxybenzoic acids, after alkaline hydrolysis and an acidic workup. The synthesis is presented in Scheme II.6.

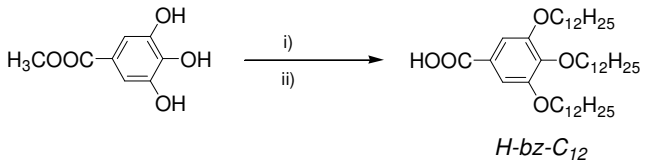

Scheme II.6 Synthesis of 3,4,5-trialkyloxybenzoic acid: i) RBr, K_2CO_3, cyclohexanone, 48 hours, ΔT; ii) KOH, EtOH, 4 hours, ΔT.

The Ag(I) salts thus prepared were further used for the synthesis of Ir(III) complexes of class B.

Synthesis of complexes

The synthesis of the ionic Ir(III) complexes of class B were carried out by using the same general method described in the introduction part (Scheme II.7). In particular, following the classical bridge-splitting reaction of the dimeric precursor $[Ir(ppy)_2]_2$-μCl_2 with 2.0 equivalents of *pam* ligand (Scheme II.7), complex **B_1** was obtained. The homologous complexes **B_2** – **B_3** were subsequently obtained by metathesis of complex **B_1** with a 5-fold excess of inorganic salts containing the appropriate counterions (NH_4PF_6 and $KClO_4$ respectively), whereas complexes **B_4** – **B_8** were obtained by reacting complex **B_1** with 1.1 equivalents of the Ag(I) salt of the appropriate carboxylate.

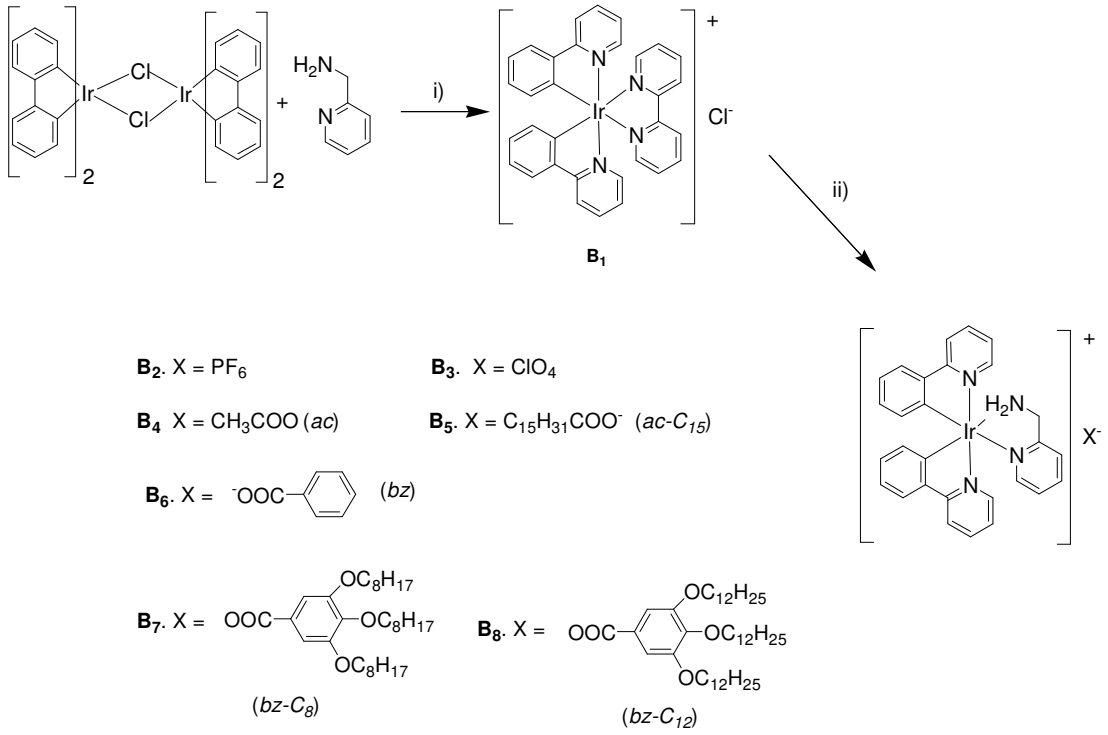

Scheme II.7 Synthesis of octahedral ionic Ir(III) complexes of class C: i) CH_2Cl_2/MeOH (3:1 v/v), ΔT, 4 hours, N_2; ii) Ag_2X_2, ΔT, 3 hours, N_2.

All ionic species are obtained as microcrystalline yellow powder solids in good yields (66 - 90%) and in particular complexes **B_1** and **B_4** were water soluble. The complexes were fully characterized

by IR and ^{1}H NMR spectroscopies, conductivity measurements and elemental analysis. Furthermore, TGA and DSC analysis were performed in order to identify to possible solvents that are included in the molecular formula of the complexes.

In particular, conductivity measurements, assesed their 1:1 electrolyte nature, the molar conductivities being in the acceptable Λ_M ranges for univalent electrolytes in acetonitrile solution.[136]

II.3.1.2 Spectroscopic characterization

IR spectroscopy

In the IR spectra of complexes of class **B** the characteristic bands of the stretching frequencies of N-H were identified as broad bands around 3400 and 3300 cm^{-1}.

Furthermore, for complexes containing inorganic counterions (**B$_2$** and **B$_3$**), the main stretching frequencies of the counterions were identified at 844 cm^{-1} (PF_6, complex **B$_2$**), and 1087 cm^{-1} (ClO_4, complex **B$_3$**) respectively.

In the IR spectra of complexes **B$_4$** and **B$_5$** that contains aliphatic carboxylate counterions (*ac* and *ac-C_{15}*), the characteristic bands of the stretching frequencies of the aliphatic chains were identified at 2919 cm^{-1} and 2851 cm^{-1}. The bands were more intense for complex **B$_5$** that has a long alkyl chain, whereas for complex **B$_4$** these bands are almost covered by the characteristic stretching's of N-H (broad band's at 3348 and 3259 cm^{-1}). Furthermore, the main bands of the C-O frequencies of the carboxylate anions are identified around 1562 cm^{-1} (C-O antisym. stretch.) and 1418 cm^{-1} (C-O sym. stretch.) for **B$_4$** and **B$_5$** respectively.

In the IR spectra of complex **B$_6$**, **B$_7$** and **B$_8$**, that contain benzoate and functionalized benzoates as counterions (*bz*, *bz-C_8* and *bz-C_{12}*), the characteristic bands of the stretching frequencies of the aliphatic chains were identified at 2925 cm^{-1} and 2853 cm^{-1}, more intense for complex **B$_7$** and **B$_8$** that have three long alkyl chains, whereas for complex **B$_6$** these bands are almost covered by the characteristic stretching's of N-H (broad bands around 3412 and 3250 cm^{-1}). Furthermore, the main bands of the C-O frequencies of the benzoate anions are identified at 1558 cm^{-1} (C-O antisym. stretch.) and 1382 cm^{-1} (C-O sym. stretch.) for **B$_6$** and respectively around 1558 cm^{-1} (C-O antisym. stretch.) and 1365 cm^{-1} (C-O sym. stretch.) for the functionalized benzoate containing complexes **B$_7$** and **B$_8$**.

^{1}H NMR spectroscopy

The aromatic region showed all 16 protons of the *ppy* in the range of 9.0 ppm to 6.0 ppm, with different chemical shifts for the two *ppy* fragments, induced by the unsymmetrical structure of *pam* ancillary ligand.

Surprisingly, different chemical shifts were observed for the doublet signal attributed to the proton 3E (See Figure II.13.). In complexes **B_2** and **B_3** (with PF_6 and ClO_4 as counterions), appears more upfield shifted (9.08 and 9.13 ppm) than in all other complexes (around 9.7 ppm). Consequently, one of the NH_2 protons of complex **B_1** and **B_3 – B_8**, also suffers a higher deshielding and shifts downfield, being identified as a broad multiplet at 7.26 ppm, whereas all *pam* aliphatic protons of complexes **B_2** and **B_3** appears in the aliphatic region in the range between 5.0 and 3.0 ppm. This suggest a lower coordination strain of the *pam* ligand around the metal center in the case of complexes **B_2** and **B_3**, having PF_6 and ClO_4 as counterions[57].

The ^{1}H NMR spectra of the complexes **B_6**, **B_7** and **B_8**, displays the aromatic signals in the region also the signals corresponding benzoate counterions as overlapped peaks in the range of 7.42-7.27 ppm regarding the 5 protons of *bz* for complex **B_6**, and respectively a singlet at 7.22 ppm regarding 2 protons of *bz*-C_8 and *bz*-C_{12} assigned for the complexes **B_6** and **B_8**.

In the aliphatic region, the signals attributed to the *pam* ligand, one NH proton and 2 CH_2 protons were identified in the range between 5.2 and 3.4 ppm.

Furthermore, in the aliphatic region, the protons of the counterions are correctly assigned as a singlet at 1.9 ppm for complex **B_4** (having *ac* as counterion) and a triplet centered at 2.18 ppm, two multiplets at 1.6 and 1.31 ppm and a triplet at 0.93 ppm for complex **B_5** (having *ac*-c_{15} as counterion). Finally, the spectrum of complexes **B_7** and **B_8** (with *bz*-C_8 and *bz*-C_{12} as counterion) showed a triplate at 3.9 ppm, two multiplates at 1.75 ppm and 1.35 ppm and a singlet at 0.87 ppm assigned to the alkyl chains of the counterions.

Lastly, the integrated ratio between aromatic protons of *ppy* and *pam* in complexes of class **B**, were showed the presence of 1 *pam* and 2 *ppy* moieties per Ir center, and respectively the integrated ratio between aliphatic protons and aromatic protons showed the presence of one anion per iridium center, in agreement with the proposed structure.

II.3.1.3 Thermal analysis

TGA showed that some of the pristine powder complexes contain solvent molecules. The number of the solvent molecules was determined by the experimental weight loss. The identification of the solvent was made on the basis of ^{1}H NMR spectra.

In particular, **B_1** powder complex contains solvent in its powder pristine solid, with an experimental mass loss of 2.78 % corresponding to 2 molecules of water (calcd. 2.72%), in a relatively narrow range of temperature (50 – 125 °C). On the contrary, no solvent molecules were detected for **B_2** and **B_3.**

Furthermore, in order to check out the effects of the presence of NH_2 moiety and one aromatic ring in the modulation of supramolecular organizations and, therefore, the photophysical properties of crystalline materials, single crystals suitable for X-ray analysis were grown for complex **B_1**. In particular, two different types of crystals were obtained: **B_{1a}** from diffusion of hexane in an ethanolic solution of **B_1**, and **B_{1b}**, obtained by aging crystals **B_{1a}** in the ethanol/hexane batch. Crystals of **B_1** have been isolated as a yellow solvated (**B_{1a}**) and an orange non-solvated (**B_{1b}**) crystalline form, dependent on crystallization time. Furthermore, TGA analysis revealed also for crystals **B_{1a}** a dessolvation process of one molecule of ethanol (experimental mass loss 6.54 %, calcd. 6.67%). The TGA scans of the pristine powder complex **B_1** and crystals **B_{1a}** are presented in Figure II.14.

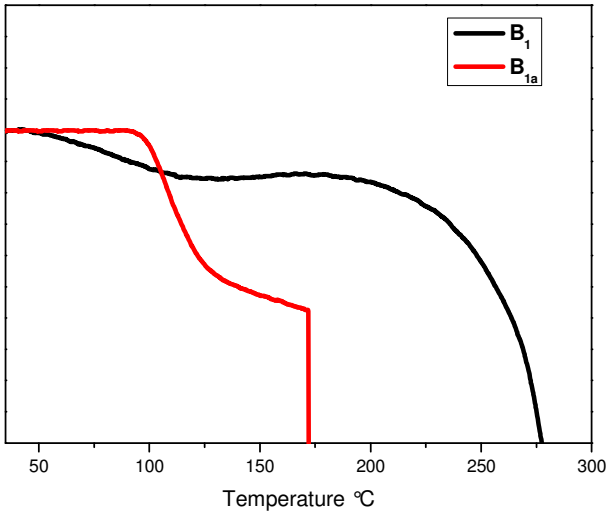

Figure II.3.14. TGA traces of powder complex **B_1** and crystals **B_{1a}**.

Both powder complexes **B_4** and **B_5** have an experimental mass loss corresponding to one and half molecules of water (**B_4**: exp. 3.83 %, calcd. 3.88%; **B_5**: exp. 2.99 %, calcd. 3.03%), in the range of temperature (35 – 100°C). TGA analysis showed for the powder complex **B_6** an experimental mass loss of 3.70 % corresponding to one and half molecules of water (calcd. 3.57 %), in a relatively narrow range of temperature (35 – 70°C), accompanied by an endothermic process in the DSC trace ($\Delta H = 41.1$ kJ·mol^{-1}). Complexes **B_7** and **B_8** have not showed experimental mass losses.

The TGA and DSC traces for complex **B_6** are shown in Figure II.15.

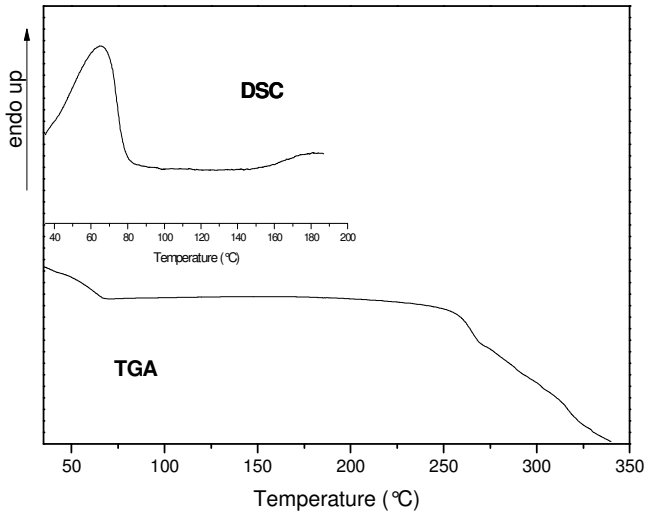

Figure II.15 TGA and DSC traces of powder complex **B_6.**

In addition, in order to probe the effects of the presence of *pam* as ancillary ligand and the benzoate counterionon the modulation of the supramolecular organizations and, therefore, the photophysical properties of crystalline materials, single crystals suitable for X-ray analysis were grown for some of the complexes from class B, their systematic structural analysis being presented further.

II.3.2 Structural characterization of cation $[Ir(ppy)_2(pam)]^+$

In order to check out the effects of the presence of NH_2 moiety and one aromatic ring in the modulation of supramolecular organizations and, therefore, the photophysical properties of crystalline materials, single crystals suitable for X-ray analysis were grown for the complexes **B_1**, **B_2**, **B_3**, **B_4** and **B_6**.

For complex **B_1**, two different types of crystals were obtained: **B_{1a}** from diffusionof hexane in an ethanolic solution of **B_1**, and **B_{1b}**, obtained by aging crystals **B_{1a}** in the ethanol/hexane batch. The crystals of **B_2** were obtained by diffusion of hexane into an acetone solution of the complex, followed by slow evaporation at room temperature, whereas crystals of **B_3** were obtained by the diffusion of water into the acetone solution of the complex, followed by slow evaporation at room temperature. Crystals of **B_1** have been isolated as a yellow solvated **(B_{1a})** and an orange non-solvated (**B_{1b}**) crystalline form, dependent on crystallization time. The crystal of **B_2** and **B_3** were isolated as unique orange colored crystalline phase. X-ray structural determination proved that **B_2** and **B_3** are isostructural.

Single crystals suitable for X-ray analysis were grown for the complex **B_4** by the diffusion of hexane into the dichloromethane solution of the complex, followed by slow evaporation at room temperature, and for complex **B_6**, by diffusion of ethanol into water solution of the complex, followed by slow evaporation at room temperature.

The single X-ray crystal structure analysis were collected at room temperature and studied well as below. As shown in Figure II.16 for **B_{1a}, B_{1b}**, the Ir(III) metal centre of complexes from class B is hexa-coordinated with two kinds of achiral bidentate ligands (two cyclometallated *ppy* and one *pam* ancillary ligands drawing a IrC_2N_2chromophore.

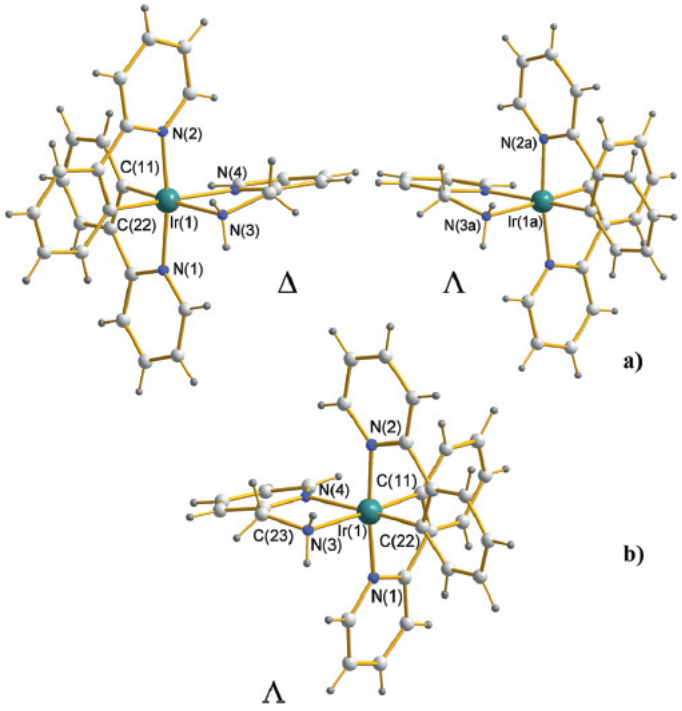

Figure II.16. View of the molecular fragments of class A showing the atomic labelling scheme.

In particular, the asymmetric unit of **B_{1a}, B_{1b}, B_2** and **B_3** is made up of a single cationic complex, which exhibits a distorted octahedral geometry around the Ir(III) metal centre. The best equatorial plane is defined by the N(3)N(4)C(11)C(22) set of atoms, the Ir(1) atom slightly deviating from this plane. The two *ppy* adopt the usual N,N *trans* configuration, with Ir–N and Ir–C bond distances falling in the expected ranges (Table II.5.).[137, 138, 139, 140, 141, 142, 143] The *pam* ligand displays notably longer Ir–N distances, which can be attributed to the *trans*-influence of the strong Ir–C bonds of the *ppy* ligands.

The five membered chelate ring defined by the *pam* ligand at the Ir(III) metal centre is not planar, the greater deviation being observed for the C(23) atom [value in the range 0.16(1) (1b)– 0.221(3) Å (3)]. According to the ring puckering analysis of PLATON,[144] the metallacycle conformation is

better described as an envelope form on N(3) (**B_{1a}, B_2** and **B_3**) or C(23) (**B_{1b}**)**.**[145]A greater degree of distortion is observed in **B_{1b}, B_2** and **B_3** with respect to **B_{1a}.**

Table II.5. Bond lengths [Å] and angles [°] for **B_{1a}, B_{1b}, B_2**and **B_3**.

Compound	B_{1a}	B_{1b}	B_2	B_3
Ir(1)-C(11)	2.026(7)	2.03(1)	2.041(5)	2.014(4)
Ir(1)-C(22)	2.022(8)	2.03(1)	2.046(6)	2.005(4)
Ir(1)-N(1)	2.101(6)	2.05(1)	2.072(4)	2.052(3)
Ir(1)-N(2)	2.065(6)	2.028(5)	2.072(5)	2.041(3)
Ir(1)-N(3)	2.229(5)	2.20(1)	2.207(5)	2.192(4)
Ir(1)-N(4)]	2.174(6)	2.15(1)	2.170(5)	2.124(2)
N(1)-Ir(1)-N(2)	172.8(2)	174.5(3)	174.1(2)	174.2(1)
N(1)-Ir(1)-N(3)	98.7(2)	97.5(3)	98.6(2)	98.8(1)
N(1)-Ir(1)-N(4)	88.8(2)	86.2(3)	87.1(2)	85.5(1)
N(2)-Ir(1)-N(3)	87.0(2)	86.6(3)	86.4(2)	86.8(2)
N(2)-Ir(1)-N(4)	96.7(3)	97.5(3)	97.0(2)	97.3(1)
N(4)-Ir(1)-N(3)	77.3(2)	77.9(3)	77.0(2)	77.6(1)
C(11)-Ir(1)-C(22)	90.0(3)	91.6(4)	87.4(2)	86.9(2)
C(11)-Ir(1)-N(1)	80.6(3)	80.5(4)	79.0(2)	79.6(1)
C(11)-Ir(1)-N(2)	94.1(3)	95.0(4)	96.1(2)	94.8(2)
C(11)-Ir(1)-N(3)	174.4(3)	174.4(4)	175.8(2)	177.0(1)
C(11)-Ir(1)-N(4)	97.1(3)	96.7(3)	99.4(2)	99.8(1)
C(22)-Ir(1)-N(1)	94.4(3)	96.6(4)	95.9(2)	97.7(1)
C(22)-Ir(1)-N(2)	80.6(3)	80.2(4)	80.4(2)	80.2(2)
C(22)-Ir(1)-N(3)	95.6(2)	93.9(4)	96.3(2)	95.9(1)
C(22)-Ir(1)-N(4)	172.6(2)	171.6(3)	172.9(2)	173.2(1)

In principle, without stereoselective synthesis pathways, the Δ and Λ enantiomers are both generated in a racemic mixture. As reported for many tris-chelated complexes,[146,147] the enantiomeric pairs usually crystallized as racemic salt. Accordingly, **B_{1a}, B_2** and **B_3** contain the same amount of Δ and Λ enantiomers, the cationic complexes packing into the P2(1)/c (**B_1**) or Pca2(1) space groups (**B_2** and **B_3**), respectively. On the contrary, **B_{1b}** crystallizes in the orthorhombic enantiomorphic space group P2(1)2(1)2(1) (**B_{1b}**). The absolute configuration has been also determined, and corresponds to the Λ form. Several crystals of **B_{1b}** have been tested, but we never found racemic crystals, proving that a spontaneous resolution occurs from the racemic solution.[148, 149, 150] Furthermore, the absolute structure has been determined satisfactorily, and can be verified by the Flack parameter of the single-crystal structure (Table II.6.)

Table II.6. Crystal data and selected structure refinement parameters for **B_{1a}, B_{1b}, B_2** and **B_3.**

Compound	B_{1a}	B_{1b}	B_2	B_3
empirical formula	$C_{30}H_{30}ClIrN_4O$	$C_{28}H_{24}ClIrN_4$	$C_{28}H_{24}F_6IrN_4P$	$C_{28}H_{24}ClIrN_4O_4$
Crystal system	Monoclinic	Orthorhombic	Orthorhombic	Orthorhombic
Space group	P2(1)/c	P2(1)2(1)2(1)	pca(2)1	pca(2)1
Z	4	4	4	4
fw	690.23	644.16	753.68	708.16
a , Å	14.2312(13)	9.8167(17)	11.0809(13)	11.0556(10)
b , Å	11.7771(11)	13.747(3)	15.5306(18)	15.2516(15)
c , Å	19.2326(18)	20.447(4)	16.1226(19)	15.3882(14)
α, β, γ, deg	90, 104.770(4), 90	90, 90, 90	90, 90, 90	90, 90, 90
V, Å^3	3116.9(5)	2759.3(9)	2774.6(6)	2594.7(4)
D_c, g cm^{-3}	1.471	1.551	1.804	1.813
μ, mm^{-1}	4.396	4.957	4.935	5.291
Independent reflections [R(int)]	6109 [0.0504]	4749 [0.0811]	4876 [0.0473]	5648 [0.0403]
Data/restraints/parameters	6109 / 0 / 361	4749 / 0 / 295	4876 / 1 / 358	5648 / 1 / 331
Goodness-of-fit on F^2	1.258	0.859	1.170	1.215
Absolute structure parameter	-	0.02(1)	0.087(8)	0.002(7)
[a]R1 [I > 2 σ (I)]	0.0372	0.0429	0.0261	0.0184
[b,c]wR2	0.1377	0.1017	0.0751	0.0474

The values of the puckering parameters calculated according to Cremer and Pople[151] are reported in Table II.7, together with the values relative to the N(3)–C(23)–C(24)–N(4) dihedral angle.

Table II.7 Geometrical parameters for the five membered Ir(1)–N(3)–C(23)–C(24)–N(4) metallacycle in **B_{1a}, B_{1b}, B_2** and **B_3**

	B_{1a}	B_{1b}	B_2	B_3
q (Å)	0.289(6)	0.24(1)	0.32(1)	0.34(1)
Φ (°)	215.4(2)	71(2)	43.8(1)	223.3(7)
N(3)–C(23)–C(24)–N(4) (°)	20.7(1)	30.2(1)	27.6(1)	30.1(1)

As already observed for the analogous en derivatives,[5] the supramolecular organization of **B_{1a}, B_{1b}, B_2** and **B_3** is principally managed by intermolecular interactions involving the NH_2 functionality of the *pam* ligands and the counterions. The solvated form **B_{1a}** shows noticeably long N–H···Cl interactions, developing along the *b* crystallographic axis, the N–H···Cl distance being outside the expected conventional range for hydrogen bonding interactions (Table II.8.).

Table II.8. N-H···Cl interactions in $\mathbf{B_{1a}}$.

	H···A	D···A	<(DHA)
N(3)-H(3a)···Cl(1)	2.646	3.46(1)	151.20
N(3)-H(3b)···Cl(1)^{i}	2.751	3.50(1)	141.85
O(1)-H(1a)···Cl(1)	2.273	3.09(1)	172.89
O(2)-H(2A)···Cl(1)^{ii}	1.879	2.69(1)	167.11
i = -*x*+2, *y*-1/2, -*z*+1/2 *ii* = -*x*+1, *y*-1/2, -*z*+1/2			

Cl–···π interactions concur in the construction of a supramolecular 1D zig-zag motif (Figure II.17.) (Cl–···aryl$_{centroid}$ distance and angle formed by the Cl–···aryl$_{centroid}$ axis with the aryl mean plane of 3.6 Å and 93°, respectively).[22] C–H···π interactions involving the aromatic rings of the *ppy* ligands are established between adjacent Ir(III) metal complexes [C(4)–H(4)···π_{centr} (C(17)C(22))^{i} 2.98 Å and 141°; i = 1 − x, 1/2 + y, 1/2 − z].

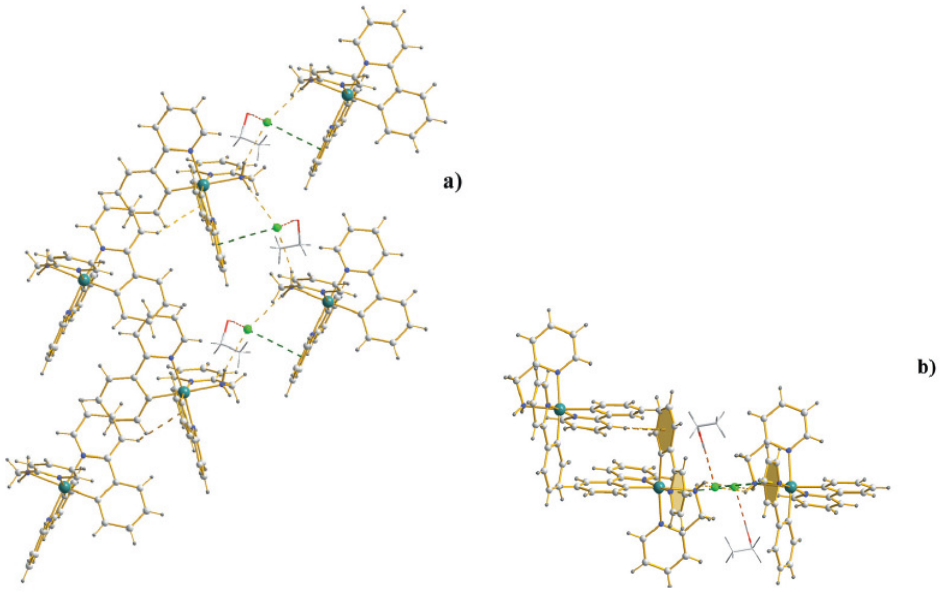

Figure II.17. Perspective (a) and side (b) views of the 1D supramolecularmotif in $\mathbf{B_{1a}}$. C–H···π interactions between the *ppy* rings are also shown.

B_{1b} shows a different supramolecular organization with respect to **B_{1a}** and an open-framework structure (Figure II.18.) containing minor empty voids (1.4% of potential solvent accessible area).

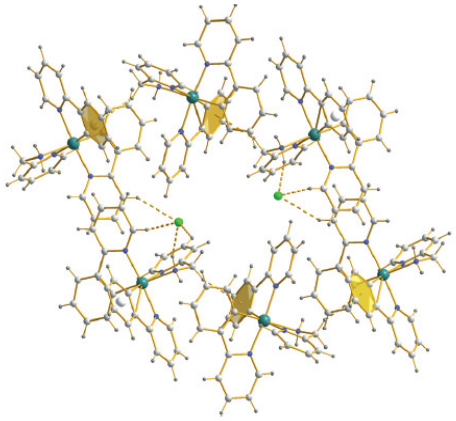

Figure II.18 View of the supramolecular open-framework organization in **B_{1b}**along the crystallographic direction. N–H···Cl, C–H···Cl and C–H···π interactions are shown.

Even if solvent molecules could reasonably play a templating role during the crystallization of **$4A^2$**, they are not retained in the final crystal structure. The supramolecular building is mainly sustained by N–H···Cl [N(3)···Cl(1)^{i} of 3.24(1), N(3)–H(3b)···Cl(1)^{i} distance and angle of 2.39 Å and 159°, respectively; i = 1 − x, −1/2 + y, 1/2 − z] and C–H···Cl interactions [C(1)–H(1)···Cl(1)^{ii} distance of 2.68 Å and angle of 164°; C(4)–H(4)···Cl(1)^{iii} distance of 2.84 Å and angle of 146°; with ii = −x + 2, y − 1/2, −z + 1/2 and iii = 1/2 − x, 1 − y, −1/2 + z]. Additional C–H···π interactions between the ppy rings and the exocyclic pam carbon atoms (C(23)–H(23b)···π_{centr} (C(17)C(22))^{i} 2.94 Å and 145°) concur in supporting the 3D supramolecular architecture. The same strong involvement of the –NH_2 fragment in intermolecular interaction seen in the case of $4\mathbf{A}^1$ is present in the crystalline organization of **B_2** and **B_3**. In **B_2**and **B_3** the N–H···X interactions involving the hexafluorophosphate (**B_2**) or the perchlorate (**B_3**) anions create a zig-zag 1D motif along the acrystallographic axis (Figure II.19).

The geometrical parameters relative to these interactions are reported in Table II.9. and 3.6 for **B_2** and **B_3** respectively. The aromatic rings of the *ppy* ligands that point at the outer surface of the supramolecular chain motif are involved in C–H···π interactions [C(4)–H (4a)···π_{centr} (C(17)C(22))^{iii} 2.82 and 144° in **B_4** and 2.79 Å and 146° in **B_5**; iii = −1/2 + x, − y, z)].

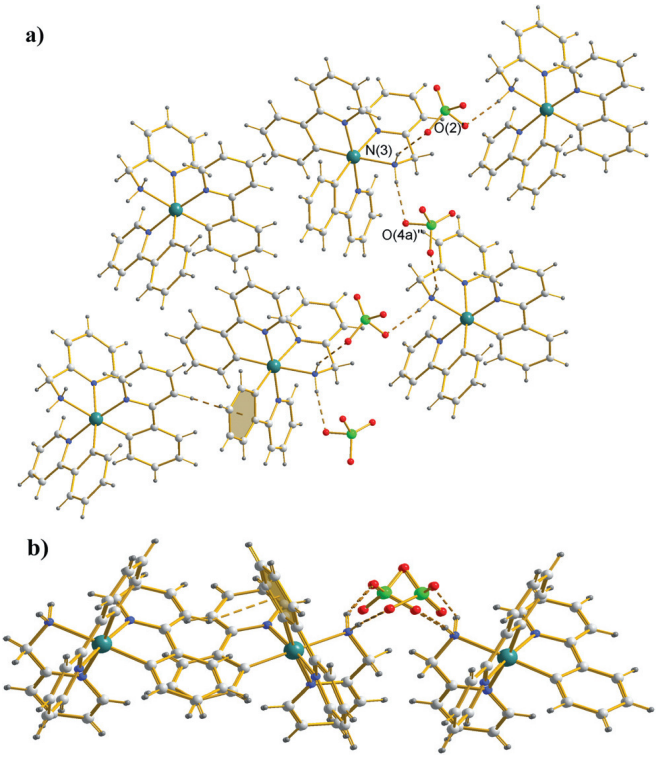

Figure II.19 Perspective (a) and side (b) views of the H-bonded 1D motif in 3. C–H···π interactionsbetween*ppy*of adjacent chains are also shown.

Table II.9. N–H···anion interactions in $\mathbf{B_2}$.

	H···A	D···A	<(DHA)
N(3)–H(3a)···F(4)^{i} N(3)–H(3b)···F(1)^{ii}	2.259 2.222	3.060(2) 2.089(1)	148.0 161.6
i = - x + 1/2, y + 1, z - 1/2. *ii = - x, - y, z - 1/2.*			

Table II.10. N-H···anion interactions in $\mathbf{B_3}$.

	H···A	D···A	<(DHA)
N(3)–H(3a)···O(2)^{i} N(3)–H(3c)···O(4a)^{ii}	2.230 2.140	3.039(7) 2.989(8)	148.7 156.7
i = - x + 1/2, y + 1, z - ½ *ii = - x, - y, z - 1/2.*			

The shorter N–H···X distances observed in $\mathbf{B_{1b}}$, $\mathbf{B_2}$ and $\mathbf{B_3}$ with respect to $\mathbf{B_{1a}}$ suggest the existence of more effective H-bonding interactions between the anions and the *pam* ligands in these crystalline species. The presence of the ethanol solvent molecules in $4\mathbf{A^1}$ most likely causes the weakening of the N–H···Cl^-interactions, separating the chromophores by adding steric effects and by establishing hydrogen bonding interactions with the chloride anion. Indeed, the ethanol solvent molecules and the chloride anions display short D···A separations [O(1)···Cl(1) 3.088 Å; O(1)–

H(1A)···Cl(1) distances and angle of 2.273 Å and 172.89°, respectively]. Therefore, the greater degree of puckering observed for the five membered metallacycle in **B_{1b}, B_2** and **B_3** can be seen as a result of the stronger N–H···X interactions present in these structures.

The crystal structures of compounds **B_4** and **B_6** are made up of mononuclear $[Ir(ppy)_2(pam)]^+$cation, and uncoordinated acetate (**B_4**) or benzoate (**B_6**) anions. Four crystallization solvent water molecules are also presents in both compounds.

In **B_6** the cationic complexes pack into the monoclinic centrosymmetric space group, $P2_1/c$. On the contrary, compound **B_4** crystallizes in the monoclinic non-centrosymmetric space groups Cc. The absolute structure has been determined satisfactorily, and can be verified by the Flack parameter of the single-crystal structure (Table II.11). Despite this difference, **B_4** and **B_6** are both racemic salts, containing the same amount of Δ and Λ enantiomers.

Table II.11 Crystal data and structure refinement for **B_4**and **B_6**

	B_4	**B_6**
Empirical formula	$C_{30}H_{37}IrN_4O_7$	$C_{35}H_{37}IrN_4O_6$
Formula weight	757.84	801.89
Temperature	296(2) K	296(2) K
Wavelength	0.71073 Å	0.71073 Å
Crystal system	Monoclinic	Monoclinic
Space group	Cc	P2(1)/c
Unit cell dimensions	a = 8.8188(8) Å α= 90° b = 33.863(4) Å β= 99.564(4)° c = 11.1443(11) Å γ = 90°	a = 20.085(2) Å α= 90°. b = 9.8689(11) Å β= 13.469(5)°. c = 18.862(2) Å γ = 90°.
Volume	3281.8(6) $Å^3$	3429.6(7) $Å^3$
Z	4	4
Density (calculated)	1.534 Mg/m^3	1.553 Mg/m^3
Absorption coefficient	4.117 mm^{-1}	3.942 mm^{-1}
F(000)	1512	1600
Crystal size	0.04 x 0.03 x 0.02 mm^3	0.08 x 0.06 x 0.02 mm^3
Theta range for data collection	1.20 to 27.10°.	1.11 to 24.41°.
Index ranges	-11<=h<=11, -43<=k<=43, -14<=l<=14	-23<=h<=23, -11<=k<=11, -21<=l<=21
Reflections collected	51235	68931
Independent reflections	7150 [R(int) = 0.0309]	5631 [R(int) = 0.0957]
Completeness	to theta = 27.10° 99.7 %	to theta = 24.41° 99.6 %
Absorption correction	Semi-empirical from equivalents	Semi-empirical from equivalents
Max. and min. transmission	0.9222 and 0.8526	0.9253 and 0.7433
Refinement method	Full-matrix least-squares on F^2	Full-matrix least-squares on F^2
Data / restraints / parameters	7150 / 17 / 410	5631 / 0 / 350
Goodness-of-fit on F^2	1.228	1.060
Final R indices [I>2sigma(I)]	R1 = 0.0169, wR2 = 0.0413	R1 = 0.0426, wR2 = 0.1151
R indices (all data)	R1 = 0.0211, wR2 = 0.0670	R1 = 0.0755, wR2 = 0.1336
Absolute structure parameter	0.002(7)	
Largest diff. peak and hole	0.679 and -0.999 $e.Å^{-3}$	1.155 and -0.980 $e.Å^{-3}$

A view of the molecular fragments of **B_4** and therefore also for the isostructural **B_5** (as demostrated by the similar features determined by ^{1}H NMR and IR spectroscopies) should be the adopted atomic labelling scheme given in Figure II.20.

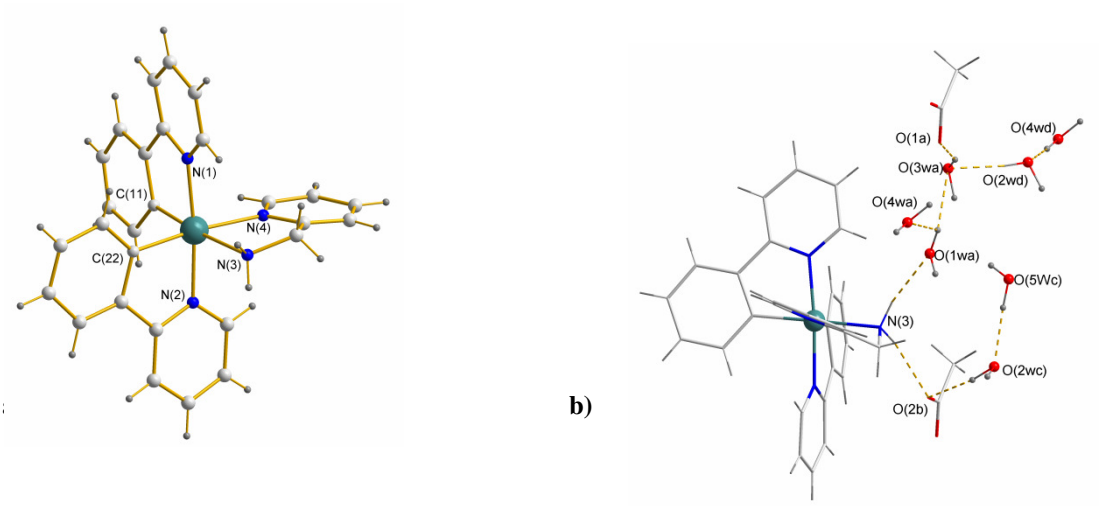

Figure II.20. View of the molecular fragments of **B_4** showing the atomic labelling scheme (a); details of the hydrogen bonding interactions(b).

Furthermore, compound **B_4** crystallizes in the monoclinic non-centrosymmetric space groups Cc, as a racemic salt, containing the same amount of Δ and Λ enantiomers. The absolute structure has been determined satisfactorily, and can be verified by the Flack parameter of the single-crystal structure (Table II.11).

The best equatorial plane is defined by the N(3)N(4)C(11)C(22) set of atoms, the Ir(1) atom slightly deviating from this plane. The two *ppy* ligands adopt the usual NN *trans* configuration, with Ir-N and Ir-C bond distances falling in the expected ranges.[137, 138, 139] The *pam* ligand displays notably longer Ir-N distances, due to the *trans*-influence of the strong Ir-C bonds of the *ppy* ligands.[140,141, 142, 143] The five membered chelate ring defined by the the *pam* ligand at the Ir(III) metal centre is not planar, the greater deviation being observed for the N(3) atom [0.24(1)]. According to the ring puckering analysis of PLATON[144], the metallacycle conformation is dubious, and can be better described as envelope on N(3). Furthermore, the bond lengths and angles for **B_4** are shown in Table II.12.

Table II.12. Bond lengths [Å] and angles [°] for **B_4** and **B_6**.

Compound	B_4	B_6
Ir(1)-C(11)	2.029(4)	2.039(8)
Ir(1)-C(22)	2.029(5)	2.045(7)
Ir(1)-N(1)	2.068(4)	2.169(6)
Ir(1)-N(2)	2.079(4)	2.167(6)
Ir(1)-N(3)	2.230(4)	2.098(6)
Ir(1)-N(4)	2.176(4)	2.073(7)
N(1)-Ir(1)-N(2)	171.65(15)	76.1(2)
N(1)-Ir(1)-N(3)	86.57(15)	91.1(2)
N(1)-Ir(1)-N(4)	97.01(15)	94.4(2)
N(2)-Ir(1)-N(3)	100.22(15)	96.0(2)
N(2)-Ir(1)-N(4)	89.40(14)	89.7(2)
N(4)-Ir(1)-N(3)	76.02(15)	172.9(2)
C(11)-Ir(1)-C(22)	88.30(18)	87.5(3)
C(11)-Ir(1)-N(1)	80.35(17)	97.5(2)
C(11)-Ir(1)-N(2)	93.90(17)	172.6(3)
C(11)-Ir(1)-N(3)	96.98(17)	80.0(3)
C(11)-Ir(1)-N(4)	172.71(17)	94.7(3)
C(22)-Ir(1)-N(1)	93.48(17)	172.9(3)
C(22)-Ir(1)-N(2)	80.22(17)	99.1(2)
C(22)-Ir(1)-N(3)	174.66(16)	94.6(3)
C(22)-Ir(1)-N(4)	98.68(16)	80.2(3)

As already observed for the analogous compounds containing Cl^-, ClO_4^- or PF_6^- as counterions and in the corresponding *en* derivatives from class **A**, the supramolecular organization of **B_4** is mainly directed by hydrogen bonding interactions involving the *pam* ligand and the counteranions.

In **B_4**, the complex cation, the uncoordinated acetate and the solvent water molecules are involved in an intricate net of hydrogen bonding interactions that involve the NH_2 functionality of the *pam* ligands, the carboxylate group of the acetate anions and the solvent water molecules.

Details of the hydrogen bonding interactions present in **B_4** are showed in Figure II.19b, and the geometrical parameters are given in Table II.13.

Table II.3.13 Hydrogen bonds in compound **B_4**.

D-H	d(D-H)	d(H···A)	<DHA	d(D···A)	A
N(3)-H(3B)	0.900	2.128	155.87	2.973	O(2*a*)
N(3)-H(3A)	0.900	2.161	154.52	2.999	O(1W*a*)
O(1w)-H(1wA)	0.964	2.134	118.47	2.729	O(4W)
O(1w)-H(1wA)	0.964	2.278	115.27	2.827	O(3W)
O(3w)-H(3wB)	0.961	1.858	151.49	2.741	O(1)
O(4w)-H(4wA)	0.958	1.996	172.46	2.948	O(2W)
O(2w)-H(2wA)	0.956	1.904	161.46	2.827	O(3W*b*)
O(2w)-H(2wB)	0.957	1.857	171.29	2.807	O(2*c*)
O(5w)-H(5wA)	0.959	1.902	164.22	2.837	O(2W)
Symmetry transformations used to generate equivalent atoms: *a= x-1/2, -y+1/2, z+1/2; b= x+1, y, z; c= x+1/2, -y+1/2, z+1/2.*					

The single X-ray crystal structure of complex **B_6** also reviewed a mononuclear $[Ir(ppy)_2(pam)]^+$cation exhibiting a distorted octahedral geometry around the Ir metal centre, with two cyclometallated *ppy* and a *pam* ancillary ligands drawing a IrC_2N_2chromophore,with a distorted octahedral geometry around the metal centre.

The best equatorial plane is defined by the N(3)N(4)C(11)C(22) set of atoms, the Ir(1) atom slightly deviating from this plane. The two *ppy* ligands adopt the usual NN *trans* configuration, with Ir-N and Ir-C bond distances falling in the expected ranges.[137, 138, 139] The *pam* ligand displays notably longer Ir-N distances, due to the *trans*-influence of the strong Ir-C bonds of the *ppy* ligands.[140,141, 142, 143]

The five membered chelate ring defined by the *pam* ligand at the Ir(III) metal centre is not planar, the greater deviation being observed for the N(3) atom [0.14(1) (**B_6**) Å]. According to the ring puckering analysis of PLATON[144], the metallacycle conformation is dubious, and can be better described as twisted on the N(3)-C(23) bond for **B_6**. Furthermore, the bond lengths and angles for **B_6** are shown in TableII.11.

In **B_6** the cationic complexes pack into the monoclinic centrosymmetric space group, $P2_1/c$. The absolute structure has been determined satisfactorily, and can be verified by the Flack parameter of the single-crystal structure (TableII.11) and contains the same amount of Δ and Λ enantiomers.

As already observed for the analogous compounds containing Cl^-, ClO_4^- or PF_6^- as counterions and in the corresponding *en* derivatives, the supramolecular organization of **B_6** is mainly directed by hydrogen bonding interactions involving the *pam* ligand and the counteranions.

In **B_6,** the complex cations, the uncoordinated *bz* and the solvent water molecules are involved in an intricate net of hydrogen bonding interactions that involve the NH_2 functionality of the *pam* ligands. In particular, in **B_6** the supramolecular bi-layered motif is assembled in the crystallographic *bc* plane, each layers being constituted by alternating, H-bonded complex cations and *bz* anions. The solvent water molecules are confined between the two layers and connected by several hydrogen bonds.

The supramolecular organization observed for compound **B_6** is showed in Figure II.21. In this case, the multiple and cooperative hydrogen bonding interactions play a key role in the structural formation and stabilization of discrete tetrameric $(H_2O)_4$ water clusters [O(1w)···O(4w) 3.00(1) Å; O(1w)···O(4wa) 2.92(2) Å] displaying the expected cyclic and planar conformation,[152, 153, 154, 155, 156] which are linked to the host lattice directly [N(3)···O(1wa) *a* =-*x*, 1-*y*, -*z*], 3.06(1) or *via* auxiliary water molecules [O(1w)···O(3w) 2.86(2) Å; O(4w)···O(2wa) 2.71(2) Å; O(2w)···O(2) 2.87(2) Å; O(3w)···O(2) 2.96(2) Å; N(3)···O(1) 2.82(2) Å].

No significant π···π stacking or C-H···π interactions are observed between the aromatic rings of the ligands in both compounds.

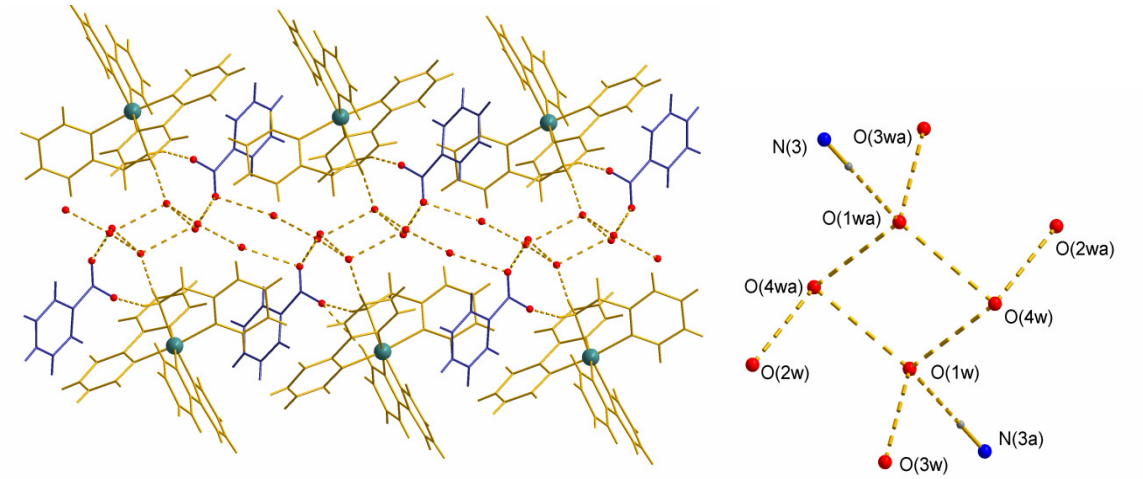

a) **b)**

FigureII.21. a) View of the hydrogen bonded bi-layer motif in $\mathbf{B_6}$ along the *b* crystallographic direction; b) A view of the tetrameric water cluster in its immediate environment [*a* =-*x*, 1-*y*, -*z*].

In particular, a supramolecular bi-layered motif is assembled in the crystallographic *bc* plane, each layers being constituted by alternating, H-bonded complex cations and acetate anions. The solvent water molecules are confined between the two layers and connected by several hydrogen bonds.

II.3.3 Photopysical properties

II.3.3.1 Photophysical properties of cation[Ir(*ppy*)$_2$(*pam*)]$^+$

Since the photophysical properties of the complexes are independent of the counterions, the absorption and emission spectra of class **B** (complexes $\mathbf{B_1}$–$\mathbf{B_8}$) compounds are discussed taking into consideration the common [Ir(*ppy*)$_2$(*pam*)]$^+$cation. In particular, photophysical measurements have been conducted in dichloromethane solution (Figure II.22.).

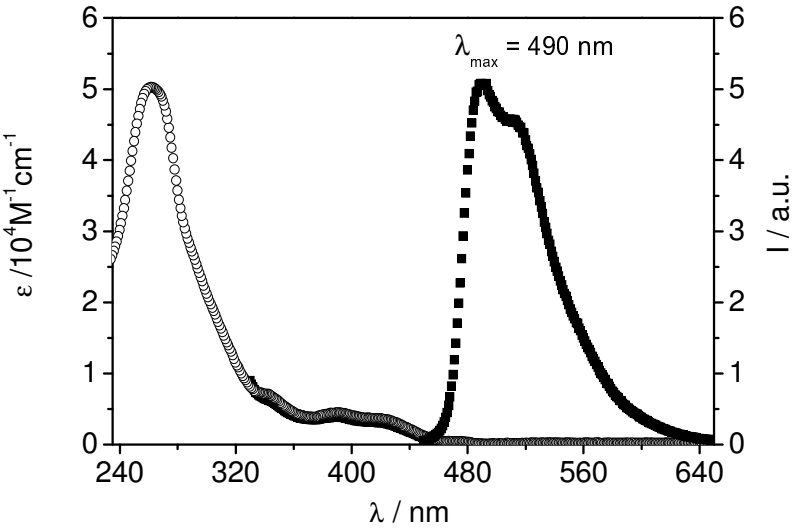

Figure II.22. Absorption and emission spectra of cation $[Ir(ppy)_2(pam)]^+$ in dichloromethane solution.

The absorption spectrum showed intense bands (molar extinction coefficient $>10^4 M^{-1} \cdot cm{-}1$) in the ultraviolet part of the spectrum between 200 nm and 320 nm. These bands are associated withligand centered (LC) transitions. The LC bands are accompanied by weaker and broad bands (with molar extinction coefficients of ca. 1×10^3 to 7×10^3 $M^{-1} \cdot cm^{-1}$) that extend from 350 nm to slightly over 470 nm and are associated with both spin-allowed and spin-forbidden metal-to-ligand charge transfer (MLCT) transitions.

Moreover, luminescence properties of the $[Ir(ppy)_2(pam)]^+$ cation, has been measured in deaerated dichloromethane solution. In the deoxygenated dichloromethane solution, $[Ir(ppy)_2(pam)]^+$ cation shows a brilliant blue-green ^{3}MLCT emission, with the emission maximum centered at 490 nm, luminescence quantum yield of 0.39 and emission lifetime about 800 ns (Table II.14)

Table II.14 Phototophysical data of cation $[Ir(ppy)_2(pam)]^+$.

Complex	**Absorption λ(nm) (ε x 10^4 M^{-1} cm^{-1})**	**λ_{max} (nm)**	**τ[ns]**	**Φ(%)**
Class B[a]	261(5); 281(2.5); 336(0.7); 378(0.38);449(0.17)	490	τ = 800	39.0

[a]Deaerated DCM solution.

II.3.3.2 Photophysical properties of complex B_4 in water

Finally for the complexes [Ir(*ppy*)$_2$(*pam*)](*ac*) soluble in water a full photophysical analysis was performed. The absorption and emission spectra of the [Ir(*ppy*)$_2$(*pam*)](*ac*) in water solution is shown in Figure II.23.

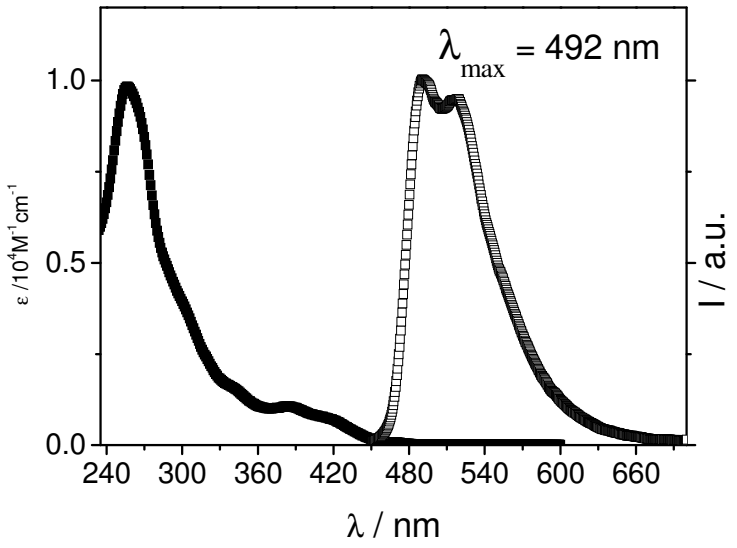

Figure II.23 The absorption and emission spectra of complex **B_4** [Ir(*ppy*)$_2$(*pam*)]*ac* in water.

The general photophysical data in solution of complex [Ir(*ppy*)$_2$(*pam*)](*ac*) in water is shown in Table II.15. In particular, complex **B_4** showed a slight red shifted emission maxima with respect to the corresponding acetone solution. Moreover, the luminescent decay resulted multiple exponential in nature. Both these experimental evidences strongly suggest the presence of aggregation phenomena in solution.

TableII.15. Photophysical data of complex **B_4**, [Ir(*ppy*)$_2$(pam)](*ac*), in water.

Complex	Absorption λ(nm) (ε x 10^4 M^{-1} cm^{-1})	λ_{max} (nm)	τ[ns]	Φ(%)
B_4= [Ir(*ppy*)$_2$(*pam*)](*ac*)	420(0.242), 385(0.357), 342(0.535), 300(sh), 256(3.5)	510	τ_1 = 1030 (10.8%) τ_2 = 1860 (89.2%)	64

II.4 Complexes of class C, [Ir(ppy)$_2$(bpy)]X, where X = Cl, ac, ac-C$_2$, ac-C$_5$, ac-C$_7$, bz, bz-C$_8$, bz-C$_{11}$OH, tfa and dos

Subsequently, the change in the hydrophobicity was followed by the replacing the *en* ligand of class **A** and *pam* of class **B** with the aromatic ancillary ligand 2,2'-bipyridine (*bpy*).

The *bpy* ligand has totally different chemical structure than that of the *en* and *pam* respectively. The *bpy* have two nitrogen donor atoms separated by two carbons and have outstanding capability to form five-membered ring with a metal center, which are the most stable structures. Furthermore, *bpy* is a particularly attractive oligopyridine a building block, being one of the most versatile ligand used for the preparation of supramolecular structures by coordinating a transitional metal centre. This is because *bpy* and respectively ligands based on *bpy*, easily form well defined chelate complexes with many metals. Hence, rather complicated and exotic structures, such as polycanter systems, dendrimers, well-defined helicates, and nanocyclic architectures have been built up in recent years. Additionally, many of their transition metal complexes give rise to interesting paramagnetic, nonlinear optical, photophysical and redox properties which can be controlled by the rational design of the ligand. Furthermore, oligopyridines may acts as efficient proton acceptors in hydrogen bonding and they can interact through π-stacking with other aromatic systems. Thus, they provide many different intermolecular interactions useful for designing well-ordered arrays of functional supramolecules.

Furthermore, unusual organizations and additional functionalities may be introduced by using different counterions in ionic Ir(III) complexes for which both photo and electronic peculiarities of the metal centre and the metal–ligand bond interactions, allow the formation of unique nanostructured materials. In addition, counterions are versatile systems that are able to promote different structures depending on the overall geometry of the new molecules, solvent, reaction conditions, coordination mode. The structure and the proton and carbon numerotation of the new complexes of class **C** synthesized is presented in Figure II.24.

Initially, the synthesis of complex **C$_1$** having the general formula [Ir(*ppy*)$_2$(*bpy*)]Cl was performed, being the analogues of the model complex [Ir(*ppy*)$_2$(*en*)]Cl, in order to follow the changes in the structural and photophysical properties by modifying the ancillary ligand. Furthermore, a series of Ir(III) octahedral ionic complexes containing carboxylate and functionalized carboxylates as counterions were prepared (complexes **C$_2$** – **C$_5$**). Following, the change of the counterion was performed and complexes **C$_6$ - C$_8$** containing benzoate and functionalized benzoates with long alkyloxy chains (*bz, bz-C$_8$ and bz-C$_{11}$OH*) were obtained. Finally, complexes **C$_9$ – C$_{10}$** containing as

counterions the dodecylsolphate and trifluoroacetate (*dos* and *tfa*) were synthesized. Their chemical structure and proton and carbon numerotation is presented in Scheme II.8.

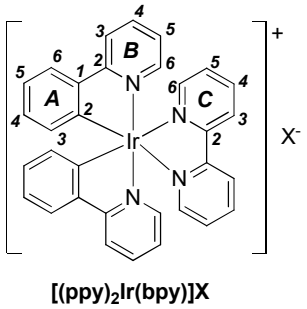

[(ppy)$_2$Ir(bpy)]X

C$_1$. X = Cl

C$_2$ X = CH_3COO^- (*ac*)

C$_3$ X = $C_2H_5COO^-$ (*ac-C$_2$*)

C$_4$. X = $C_5H_{11}COO^-$ (*ac-C$_5$*)

C$_5$. X = $C_7H_{15}COO^-$ (*ac-C$_7$*)

C$_6$ X = 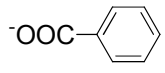 (*bz*)

C$_7$. X = 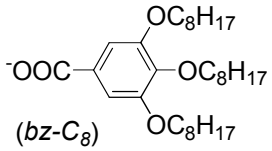 (*bz-C$_8$*)

C$_8$ X = 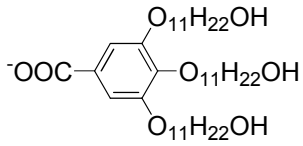 (*bz-C$_{11}$OH*)

C$_9$ = CF_3COO (*tfa*)

C$_{10}$ X = $C_{12}H_{25}OSO_3$ (*dos*)

Figure II.24 Chemical structure of octahedral ionic Ir(III)complexes from class C with general formula [Ir(*ppy*)$_2$(*ppy*)]X, where X = chloride (Cl), acetate (*ac*), propionate (*ac-C$_2$*), hexanoate (*ac-C$_5$*), octanoate (*ac-C$_7$*), benzoate (*bz*), 3,4,5-tris-ocyloxybenzoate (*bz-C$_8$*), 3,4,5-tris-dodecyloxybenzoate (*bz-C$_{12}$*), trifluoroacetate (*tfa*) and dodecylsulfate (*dos*).

II.4.1 Synthesis and characterization of complexes C$_1$-C$_{10}$

II.4.1.1 Synthesis

For the synthesis of class **C** complexes, previously a series of Ag(I) carboxylates were prepared, by a modified synthetical procedure found in the literature.[132]

Synthesis of the counterions:

The different organic counterions (carboxylates and benzoates) were prepared as Ag(I) salts by a modified synthetic process found in the literature[132], as reported previously for the complexes of class **A** and class **B**. The synthesis of the Ag(I) salt of *ac*, *bz* and *bz-C$_8$* were presented in the chapter II.2.1.1. Furthermore, two new Ag(I) salts were prepared, their synthesis being presented in Scheme II.8.

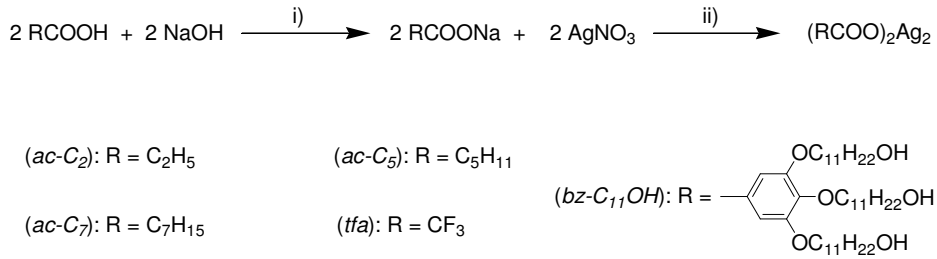

Scheme II.8 Synthesis and chemical structure of the two new carboxylates Ag(I) salts used for the synthesis of complexes of class **C**: i) NaOH, EtOH/H_2O, r.t., 2 hours, ii) $AgNO_3$, r.t., 2 hours.

In particular, the corresponding acid precursor (trifluoroacetic acid and 3,4,5-tris((hydroxyundecyl)oxy)benzoic acid respectively) were reacted with NaOH in EtOH/H_2O solution. After two hours of stirring at r.t., an equimolecular amount of $AgNO_3$ was added and the mixture was further stirred for 2 hours. The product, formed as a white precipitate in the reaction mixture, was filtered out, washed with water, dried and used without further purification.

The reported structures of the Ag(I) carboxylates[70] consist of dimeric pairs of silver bridged by the carboxylate ligand $Ag_2(OOCR)_2$.[132] The IR spectra of the Ag(I) salts synthesized *ac*, *ac-C*$_2$, *ac-C*$_5$, *ac-C*$_7$, *bz*, *bz-C*$_8$ and *bz-C*$_{11}$*-OH* suggest a similar molecular structure.

For the synthesis of the functionalized benzoates, first the acids were obtained using the same method reported in literature[135]. In particular, the reaction of methyl-3,4,5-trihydroxybenzoate with bromoalkane under basic conditions led to the related tri-alkoxybenzoic acids, after alkaline hydrolysis and an acidic workup. The synthesis of the *H-bz-C*$_8$ and *H-bz-C*$_{12}$ were presented previously, whereas the synthesis of the *H-bz-C*$_{11}$*-OH* is presented in Scheme II.9.

The Ag(I) salts thus prepared were further used for the synthesis of Ir(III) complexes **C**.

.

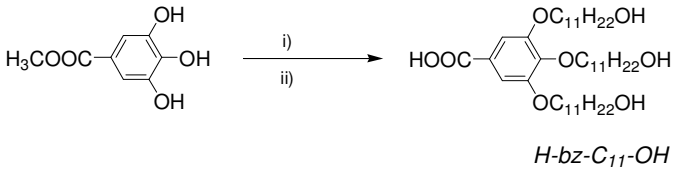

Scheme II.9 Synthesis of *H-bz-C*$_{11}$*-OH*: i) RBr, K_2CO_3, cyclohexanone, 48 hours, ΔT; ii) KOH, EtOH, 4 hours, ΔT.

Synthesis of complexes

The synthesis of the new Ir(III)complexes of class **C** was carried out using the same general classical method reported in the introduction part. In particular, the bridge-splitting reaction of the dichloro-precursor $[Ir(ppy)_2]_2$-μCl_2 with the *bpy* ligand (Scheme II.4.3) yields complex $\mathbf{C_1}$. The homologous complexes $\mathbf{C_2}$**-** $\mathbf{C_9}$ were subsequently obtained by metathesis of complex $\mathbf{C_1}$ with an 1.1 fold excess of Ag(I) salt containing the desired counterions *ac*, *ac-*C_2, *ac-*C_5, *ac-*C_7 C_7, *bz*, *bz-*C_8, *bz-*C_{11}*-OH* and *tfa* respectively, whereas complex $\mathbf{C_{10}}$ was obtained by the metathesis of complex $\mathbf{C_2}$ with a 5 fold excess of inorganic salt containing *dos* counterion (Scheme II.10.)

.

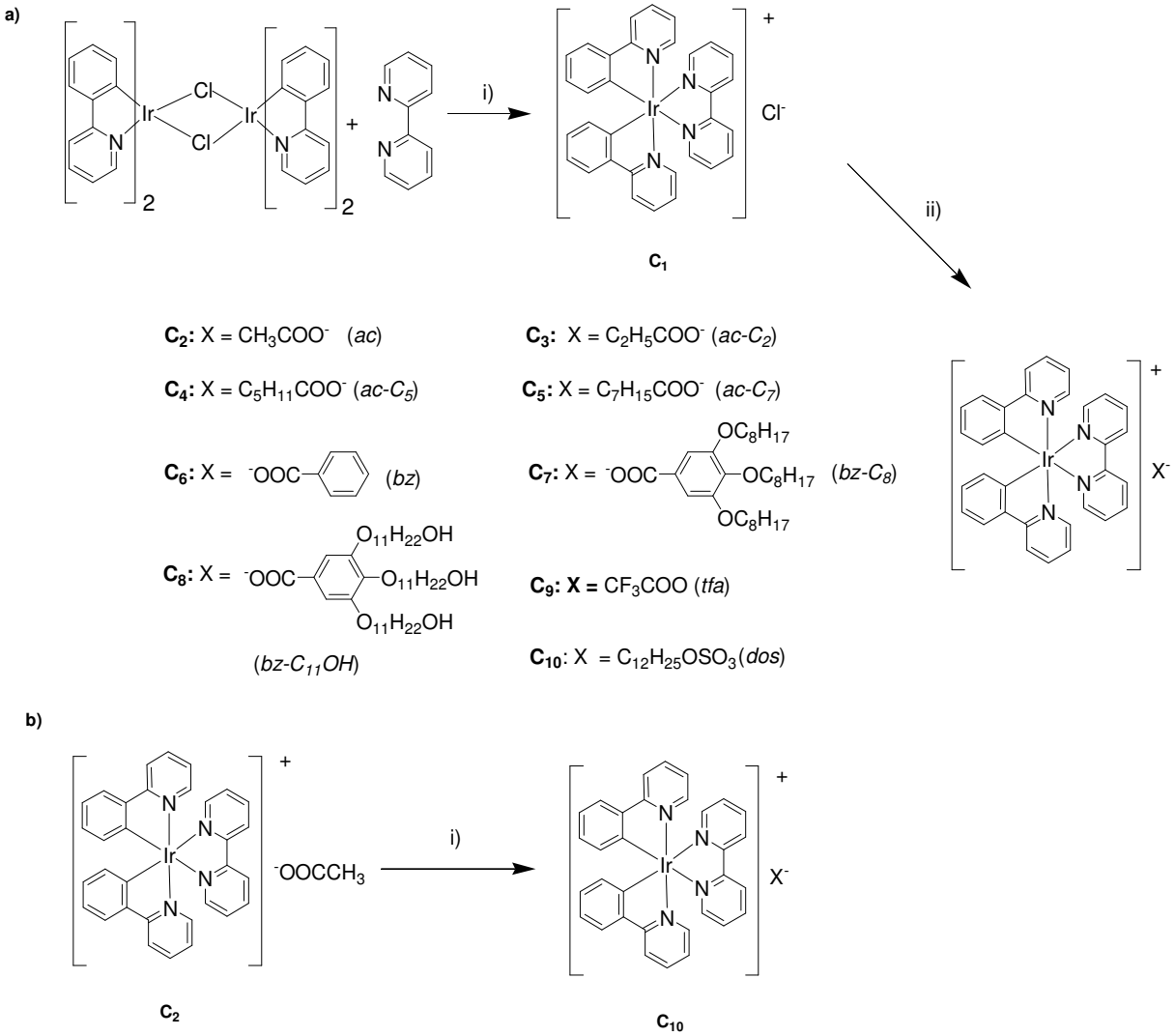

Scheme II.10 Synthesis of octahedral ionic Ir(III) complexes of class A: (a) i) CH_2Cl_2/ MeOH (3:1 v/v), ΔT, 4 hours, N_2; ii) Ag_2X_2, ΔT, 3 hours, N_2, (b) $C_{12}H_{25}OSO_3Na$, MeOH, ΔT, 24 hours, N_2.

All Ir(III) complexes **C_1 – C_{10}** were obtained in relatively high yields (68.0 - 87.5%) as yellow-orange, air-stable solids and were fully characterized by IR and ^{1}H NMR spectroscopies and elemental analysis. Additionally complexes **C_2 – C_5** where characterized by ^{13}C NMR spectroscopy. Furthermore, TGA and DSC analysis were performed in order to identify to possible solvents that are included in the molecular formula of the complexes.

The ionic natures for all complexes of class **C** were determined by conductivity measurements in acetonitrile solution for complexes **C_1 – C_5** and **C_8 - C_{10}** and in methanol for complexes **C_6 – C_7** for solubility reasons. The molar conductivities are characteristic for univalent electrolytes.[136]

Complexes **C_2** – **C_4**, containing acetate and alkylcarboxylates as counterions resulted soluble in water, at least macroscopically. The conductivity measurements performed in water solution for these complexes show lower Λ_M values in water. Indeed, while in acetonitrile the values found for complexes for complexes **C_2 – C_4** are in the range of 110 – 125 $\Omega^{-1}\cdot cm^2\cdot mol^{-1}$, the conductivity measurements performed in water solution, at the same concentration (10^{-5} mol/L), shows Λ_M values in the range of 40 – 55 $\Omega^{-1}\cdot cm^2\cdot mol^{-1}$. Except the differences derived from the physical chemical properties of the solvents, this lowering of the Λ_M in water may be due to some kind of aggregation similar to the behavior of surfactants over the critical micelle concentration (*cmc)*.

II.4.1.2 Spectroscopic characterization

IR spectroscopy

The IR spectra of the complexes **C_2 – C_5** show the corresponding frequencies for the carboxylate counterion at around 1560 cm^{-1} ($\nu_{as}(COO^-)$) and respectively at 1390 cm^{-1} ($\nu_s(COO^-)$). Furthermore, in the 3000 – 2840 cm^{-1} region, the C-H stretching vibrations of the methyl and/or methylene groups can be detected, whereas a strong broad band centred at 3400 cm^{-1} that remains after several days of drying the powders at the *vacuum* pomp, maybe only attributed to the presence of some crystallisation water molecules.

IR spectra of complexes **C_6 – C_8** containing the benzoate and functionalized benzoates as counterions, show the corresponding frequencies for the carboxylate around 1560 cm^{-1} (C-O antisym. stretch.) and respectively 1390 cm^{-1} (C-O sym. stretch.). Again, for complexes **C_7** and **C_8** containing long alkyl chains, the 3000 – 2840 cm^{-1} region of the IR spectra contain the C-H stretching vibrations of the methyl and/or methylene groups.

Furthermore, the main bands of the C-O frequencies of the *tfa* counterion were identified at 1687.9 cm^{-1} (C-O antisym. stretch.) and 1445.8 cm^{-1} (C-O sym. stretch.) for complex **C_9** and respectively for complex **C_{10}** the symmetric stretchings of SO_2 were identified at 1247.8 and 1227.3 cm^{-1}.

^{1}H NMR spectroscopy

The ^{1}H NMR spectra were recorded in $CDCl_3$ for all the complexes. In the aromatic region of the ^{1}H NMR spectra all 20 protons belonging to the two *ppy* and one *bpy* fragments were correctly identified and assigned in the range of 9.7 to 6.29 ppm. The chemical shifts indicate pure stereoisomeric forms with *cis* carbons and *trans* nitrogen atoms of the *ppy* ligands.[57]

Furthermore, a full assignment of carbons in the ^{13}C NMR spectra was made (Experimental Section, Chapter III).

The ^{1}H NMR spectra of the complexes **C_2 – C_4**, having aliphatic carboxylates as counterions, contain in the aliphatic region the signals of the alkyl chain protons of the counterions, with the intensity of the signals indicating a 1:1 ratio between the two molecular fragments. Indeed, the aliphatic region of the ^{1}H NMR spectra of complex **C_2** (having *ac* as counterion) contains a singlet centered at 2.03 ppm accounting for 3 protons; the ^{1}H NMR spectra of complex **C_3** (having *ac-C_2* as conterion) contains in the aliphatic region a quartet at 2.32 ppm and singlet at 1.13 ppm accounting for 2 and respectively 3 protons. The ^{1}H NMR spectra of complex **C_4** and **C_5** (having *ac-C_5* and *ac-C_7* as counterion respectively) show in the aliphatic region a triplet centered at 2.28 ppm, two multiplates at 1.68 ppm and 1.28 ppm and singlet at 0.83 ppm respectively, with the integrals showing the correct number of protons according to the molecular structure presented.

The complex **C_6** (having *bz* as counterion) showed in the aromatic region the additional signals regarding the 5 protons as overlapped peaks at 7.30 ppm. Furthermore, the spectrum of complex **C_7** (having *bz-C_8* as counterion) and **C_8** (*bz-$C_{11}OH$* as counterion) showed in the aromatic region the additional signals regarding the 2 aromatic protons and respectively the protons from the aliphatic chains that were found in the range of 4.00 to 0.80 ppm. The spectrum of complex **C_{10}** (*dos* as counterion) showed the protons from the aliphatic chains in the range of 4.00 to 0.80 ppm.

In conclusion, the integrated ratio between aromatic protons of *ppy* and *bpy* in complexes of class C, showed the presence of 1 *bpy* and 2 *ppy* moieties per Ir center, and respectively the integrated ratio between aliphatic protons and aromatic protons showed the presence of one anion per iridium center, in agreement with the proposed structure.

The ^{13}C NMR spectra were recorded in $CDCl_3$ for all the complexes **C_1 – C_4** also support the proposed structure.

II.4.1.3 Thermal analysis

For some of the complexes of class **C**, the presence of crystallization water in the molecular structure was supported by TGA analysis. The identification of the nature of solvent was made on the basis of ^{1}H NMR spectroscopy.

In particular, complex $\mathbf{C_1}$, having Cl as counterion has an experimental mass loss of 5.01 % corresponding to two molecules of water (calcd. 4.95 %). The dessolvation process is accompanied by a strong endotermic enthalpy variation (77.7 $kJ \cdot mol^{-1} \cdot K^{-1}$) observed in the DSC scan in the same range of temperatures (35 – 100°C), indicating a relatively strong interaction of the solvent molecules with the Ir(III) complex.

For the series of complexes containing aliphatic carboxylates as counterions $\mathbf{C_2 – C_5}$, the number of the water molecules that the pristine powder complexes contains, differs from one complex to other, by repeating synthesis of the same complex or by keeping them in air, indicating a highly hygroscopic nature. This hygroscopic nature is well illustrated in figure II.25, where the TGA scans recorded for complex C_2 are presented after different drying processes. It can be observed that there are always three weight loss processes occurring in the same range of temperatures, but the percentage of water losses are different. Therefore, we will refer to these complexes as having the general formula $[Ir(ppy)_2(bpy)](ac\text{-}C_x)\cdot xH_2O$.

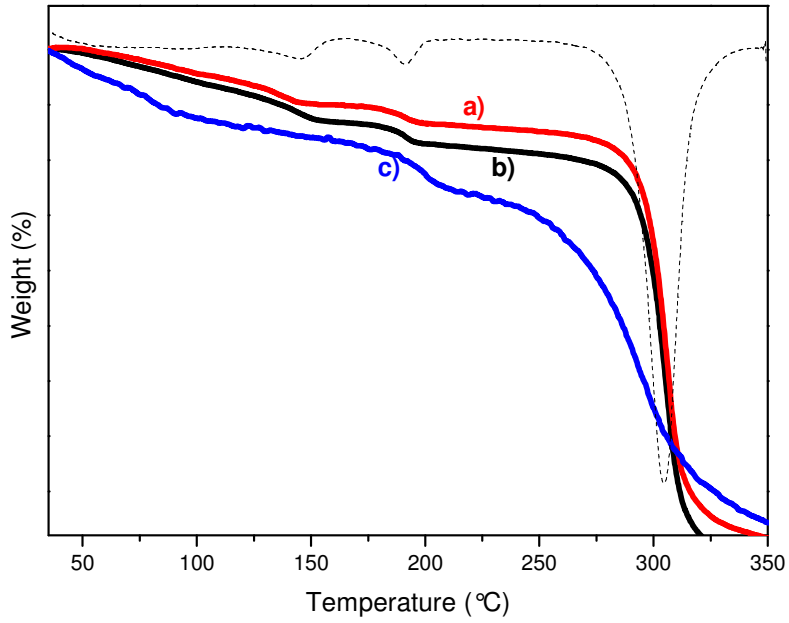

Figure II.25 TGA conducted on complex $\mathbf{C_2}$: a) and b) two different synthesis, after drying at *vacuum* pump for 48 hours; c) drying at 60°C for 24 hours.

After several days of drying under *vacuum*, TGA traces reveal for complexes **C_2 – C_4** three dessolvation processes in correspondence with endothermic peaks observed in the DSC scans, indicating relatively strong interactions between the Ir(III) complexes and the solvent molecules (Figure II.26). In particular, powder complex **C_2** has an experimental mass loss of 4.75 % corresponding to 2 molecules of water (calcd. 4.79%), occurring in three steps in a broad range of temperature (35 - 200°C). The processes are accompanied by endothermic enthalpy variation detected in the DSC trace (total ΔH_1 = 69.26 kJ·mol^{-1}), as presented in Figure II.25. Complex **C_3** has an experimental mass loss of 4.65 % corresponding to 2 molecules of water (calcd. 4.71), in a broad range of temperature (35 - 200°C), accompanied by endothermic processes in the DSC trace with a total ΔH_1 =43.26 kJ·mol^{-1}. Complex **C_4** has an experimental mass loss of 2.29 % corresponding to one molecule of water (calcd. 2.30%), in a relatively broad range of temperature (100 - 250°C), accompanied by endothermic processes in the DSC trace (total ΔH_1 = 74.7mol^{-1}). Finally, complex **C_5** has an experimental mass loss of 2.08 % corresponding to one molecule of water (calcd. 2.20%), in a relatively broad range of temperature (100 - 160°C), accompanied by an endothermic process in the DSC trace (ΔH = 80 kJ·mol^{-1}).

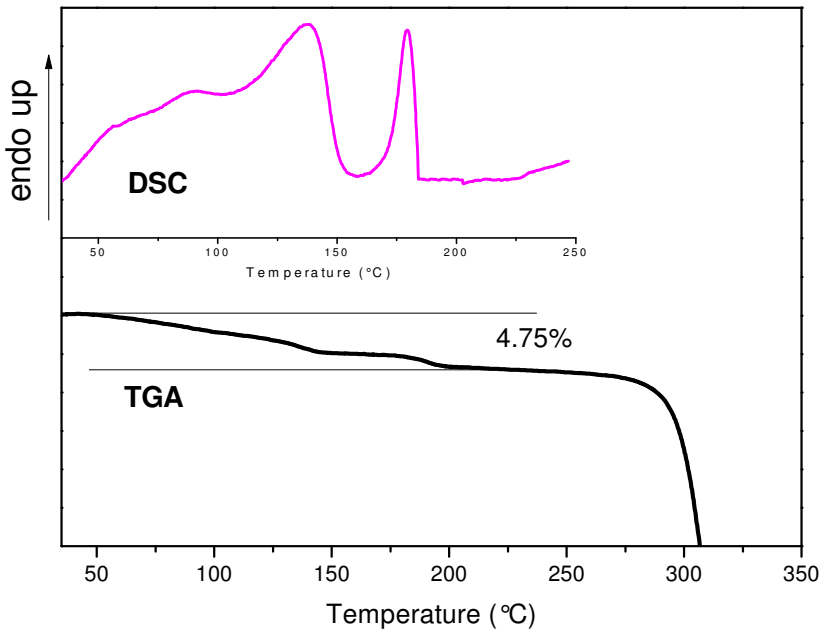

Figure II.26 TGA and DSC scans for complex **C_2**: experimental weight loss of 4.75 % corresponding to 2 molecules of water (calcd. 4.79 %).

Also complexes **C_6** – **C_7** having as benzoate and functionalised benzoates as counterions contain water molecules in their pristine solid powders. Indeed, the TGA traces of complex **C_6** shows an experimental mass loss of 2.42 %, corresponding of one molecule of water (calcd. 2.26 %). For complex **C_7** an experimental mass loss of 3.73 % was observed, corresponding to two and half molecules of water (calcd. 3.73 %).

II.4.2 Structural characterization of cation $[Ir(ppy)_2(bpy)]^+$

In order to check out the effects of the presence of *bpy* moiety in class a complexes as compared to class **A** and class **B** in the modulation of supramolecular organizations and, therefore, the photophysical properties of crystalline materials, single crystals suitable for X-ray analysis were grown for the complexes **C_1**.

The single crystal structure of **C_1** is made up of cationic $[Ir(ppy)_2(bpy)]^+$ complexes, chloride anions and crystallization water and dichloromethane molecules. The $[Ir(ppy)_2(bpy)]^+$ cation exhibits a distorted octahedral geometry around the Ir metal centre, the two cyclometallated *ppy* and the *bpy* ancillary ligands drawing a IrC_2N_2 chromophore. A view of the molecular fragments of **C_1** showing the atomic labelling scheme is given in Figure II.27.

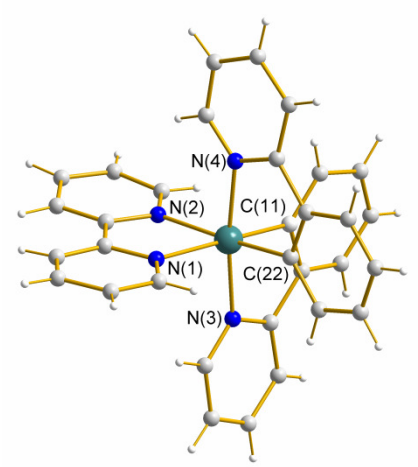

Figure II.27 View of the molecular fragments of the Λ enantiomer in **C_1** showing the atomic labelling scheme.

The best equatorial plane is defined by the N(1)N(2)C(11)C(22) set of atoms, the Ir(1) atom slightly deviating from this plane. The two *ppy* ligands adopt the usual NN *trans* configuration, with Ir-N and Ir-C bond distances falling in the expected ranges.[137, 138, 139] The *bpy* ligand displays notably

longer Ir-N distances, which can be attributed to the *trans*-influence of the strong Ir-C bonds of the *ppy* ligands[140, 141, 142, 143] (see Table II.16).

In principle, without stereoselective synthesis pathways, the Δ and Λ enantiomers of **C_1** are both generated in a racemic mixture. As reported for many tris-chelated complexes[146, 147], the enantiomeric pairs usually crystallized as racemic salts.

On the contrary, compound **C_1** crystallizes in a chiral tetragonal space group. The absolute structure has been determined satisfactorily, and can be verified by the Flack parameter of the single-crystal structure (Table II.16). The absolute configuration has been also determined, and corresponds to the Λ form.

Table II.16 Bond lengths [Å], bond angles (°), crystal data and structure refinement for **C_1**.

Bond lengths [Å]	**Bond angles (°)**	**The crystal data**	**Structure refinement**
Ir(1)-C(11)	2.039(8)	Empirical formula	$C_{32.50}H_{25}Cl_2IrN_4O_2$
Ir(1)-C(22)	2.045(7)	Formula weight	766.67
Ir(1)-N(4)	2.073(7)	Temperature	296(2) K
Ir(1)-N(3)	2.098(6)	Wavelength	0.71073 Å
Ir(1)-N(2)	2.167(6)	Crystal system	Tetragonal
Ir(1)-N(1)	2.169(6)	Space group	I-4
		Unit cell dimensions	a = 21.570(5) Å α= 90°. b = 21.570(5) Å β= 90°. c = 13.852(4) Å γ = 90°.
C(11)-Ir(1)-C(22)	87.5(3)	Volume	6444(3) $Å^3$
C(11)-Ir(1)-N(4)	94.7(3)	Z	8
C(22)-Ir(1)-N(4)	80.2(3)	Density (calculated)	1.580 Mg/m^3
C(11)-Ir(1)-N(3)	80.0(3)	Absorption coefficient	4.343 mm^{-1}
C(22)-Ir(1)-N(3)	94.6(3)	F(000)	3000
N(4)-Ir(1)-N(3)	172.9(2)	Crystal size	0.09 x 0.06 x 0.04 mm^3
C(11)-Ir(1)-N(2)	172.6(3)	Theta range for data collection	1.34 to 25.71°.
C(22)-Ir(1)-N(2)	99.1(2)	Index ranges	-26<=h<=26, -26<=k<=26, -16<=l<=16
N(4)-Ir(1)-N(2)	89.7(2)	Reflections collected	61343
N(3)-Ir(1)-N(2)	96.0(2)	Independent reflections	6148 [R(int) = 0.0735]
C(11)-Ir(1)-N(1)	97.5(2)	Completeness to theta = 25.71°	99.8 %
C(22)-Ir(1)-N(1)	172.9(3)	Absorption correction	Semi-empirical from equivalents
N(4)-Ir(1)-N(1)	94.4(2)	Max. and min. transmission	0.8454 and 0.6959
N(3)-Ir(1)-N(1)	91.1(2)	Refinement method	Full-matrix least-squares on F^2
N(2)-Ir(1)-N(1)	76.1(2)	Data / restraints / parameters	6148 / 2 / 380
		Goodness-of-fit on F^2	1.153
		Final R indices [I>2sigma(I)]	R1 = 0.0291, wR2 = 0.0759
		R indices (all data)	R1 = 0.0363, wR2 = 0.0932
		Absolute structure parameter	0.004(9)
		Largest diff. peak and hole	0.936 and -0.709 e.$Å^{-3}$

The crystal packing consists of a columnar organization of stacked complexes (Figure II.28). The Ir metal centres are not aligned along the axe of the columns, but they design a sort of zig-zag motif, with the *bpy* ligands substantially segregated within the columns. Weak C-H···Cl interactions [intermolecular contacts in the range 2.8-3.0 Å] as well as the hydrophobic character of the *bpy* ligands are most likely responsible of this organization. The Ir···Ir distance along the column is ~8.2 Å, while the distance between stacked complexes is ~6.9 Å, i. e. the half of the *c* lattice parameter.

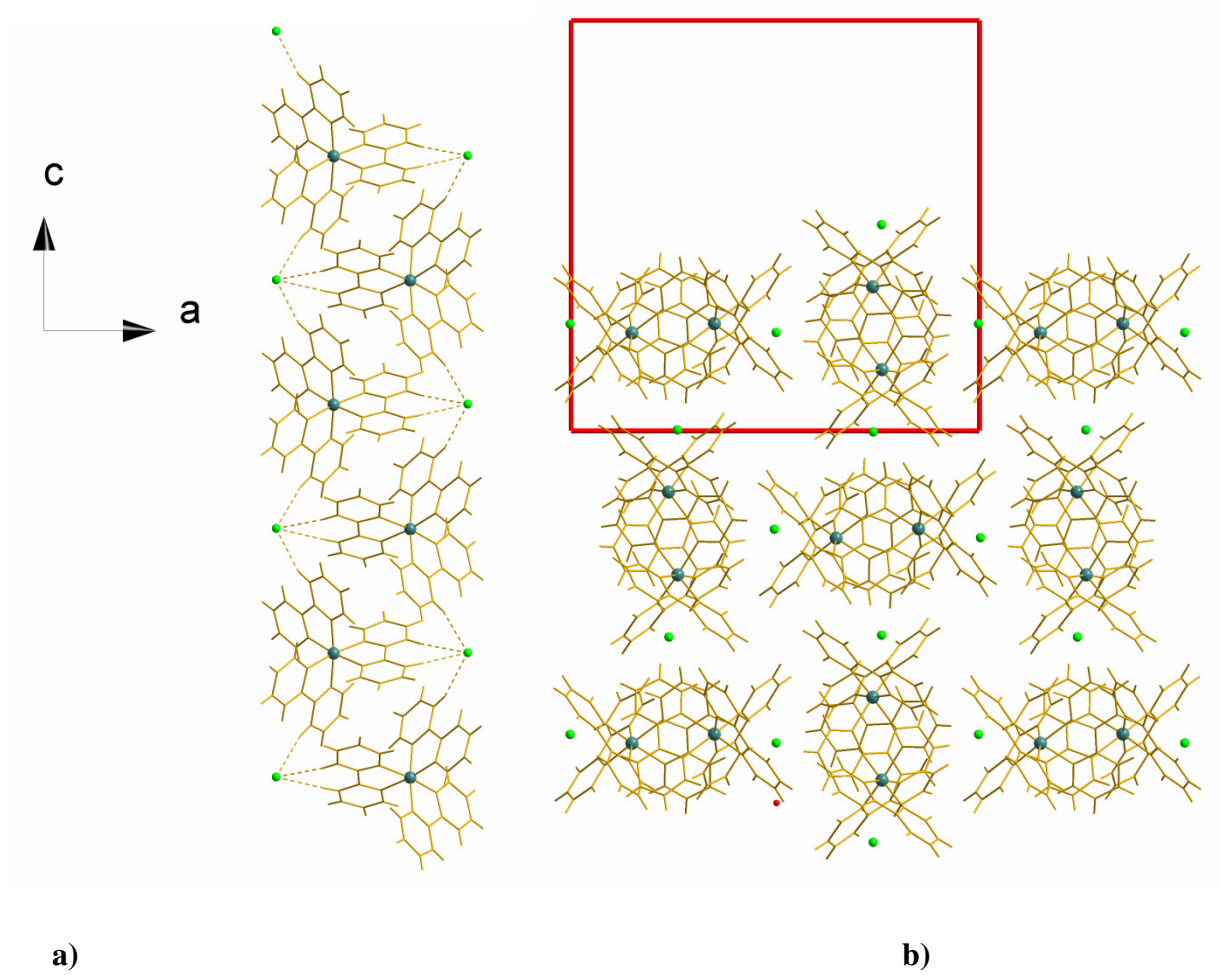

a) **b)**

Figure II.28 Side view of a single column (a); View along the crystallographic *c* directions of the columnar organization of $\mathbf{C_1}$ (b). Solvent molecules are not showed for clarity.

As clearly showed in Figure II.29, the supramolecular organization of $\mathbf{C_1}$ designs channel along the *a* crystallographic direction, that are filled by the counterions and the solvent (water and dichloromethane) molecules.

C-H···Cl interactions [C(7)-H(7A)··· $Cl(1)^{i}$ distance and angle of 2.82 Å and 170°; C(29)-H(29A)···$Cl(1)^{ii}$ 2.76 Å and 155°; *i*= 1/2-*y*,1/2+*x*,1/2-*z*, *ii* = *y*,-*x*,-*z*] as well as C-H···π interactions

involving the phenyl rings of the cyclometalated *ppy* ligands [C(25)-H(25A)···π_{centr} C(22)C(27)^{ii} distance and angle of 2.90 Å and 167.34°, respectively] support the three-dimensional architecture.

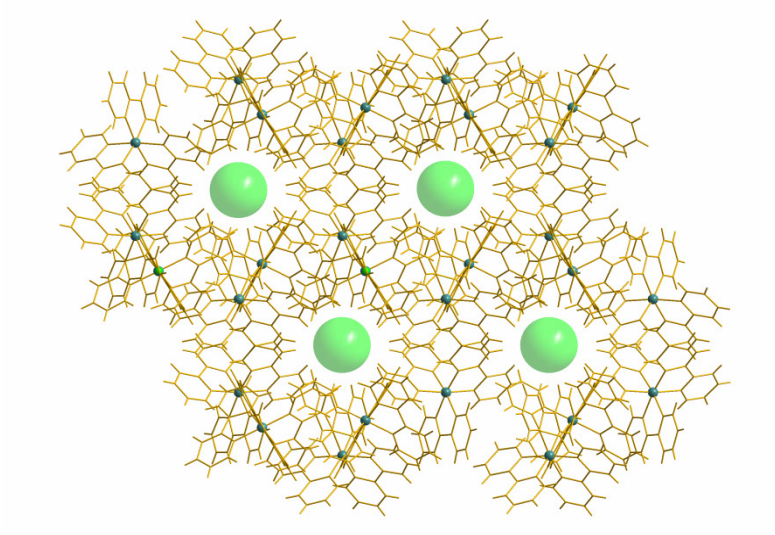

Figure II.29 View along the crystallographic *a* direction of the supramolecular channelled structure of $\mathbf{C_1}$ (b). Solvent molecules are not showed for clarity.

II.4.3 Characterization of the organization in water for complex C_2 – C_4

Complexes $\mathbf{C_2}$ – $\mathbf{C_4}$ that have carboxylate and alkyl carboxylates as counterions (*ac*, *ac-**C**$_1$* and *ac-**C**$_5$*) form highly viscous phases at low concentrations in water. On increasing the alkyl chain length of the counterion to *ac-C*$_7$, the hydrophobicity of the final complex increases, and hence complex $\mathbf{C_5}$ resulted insoluble in water.

Furthermore, highly birefringent textures were observed under polarized optical microscope (POM) that may be an indication of some kind of order. The ascertain of the concentration on which the complexes starts to show birefringence in water was determined approximately by preparing different concentration samples and observing them under POM. The initial concentration on which birefringence is observed was >1.0 % w/w for all three complexes $\mathbf{C_2}$ – $\mathbf{C_4}$.

Supramolecular ordered structures formed in water by low molecular weight compounds (LMWC) may be encountered in liotropic, chromonic or hydrogel systems. All three types of derivatives undergo self-organization in water by using non-covalent (physical) interactions like hydrogen bonding, solvophobic, charge transfer and van der Waals. The differences consist principally in the molecular structure of the LMWC and modality of self-organization.[157]

Lyotropic molecules are usually amphiphilic in nature (dual hydrophilic/hydrophobic character) leading to a competition between the hydrophilic parts attempting to increase their contact with water and the hydrophobic ones trying to avoid it. Hence the association of the molecules into micellar aggregates with defined topologies (hollow spherical, rod- and disk-like micelles) occurs, keeping unlike parts isolated from unlike solvent.

Chromonic systems are formed by charged organic flat (disklike or planar molecular shape) molecules that, when are dispersed in water, show a strong tendency to aggregate into stacks, which may become ordered at higher concentrations. The driving force for aggregation in this case is thought to be mainly enthalpic (which is different from conventional surfactants), resulting from strong attractive dispersion forces between aromatic groups and also, in some cases, from unlike charge attractions between ionic groups on the periphery. The relationship between the structure of the *chromonic* molecules and the bulk phase behaviour is still obscure. Seemingly small differences in structure can have large effects on the phase diagram. Several of the *chromonic* mesophases have structures not found for surfactants (e.g., hollow pipes).

Hydrogels are materials with three-dimensional, water swollen structures composed of mainly hydrophylic polymers, oligomers or roads, self-assembled from low molecular weight gelators (LMWG). Gelators are a class of molecules that can undergo self-organisation in a particular solvent to yield a fine fibrous structure. *Hydrogels* are rendered insoluble due to the presence of chemical of physical crosslinks that can be entanglements, crystallites or weak associations formed by van der Waals interactions, π-π-stackings or hydrogen bonds. The crosslinks provide the network structure and physical integrity.

Furthermore, *hydrogels* have a high percentage of water, some may contain until 99% in their structure, whereas usually lyotropic and *chromonic* phases forms at higher concentration of low molecular weigh molecules.

II.4.3.1 POM studies

The textures of phases can be observed by placing the thin sample between two crossed polarises, crossed at 90^{o} to each other. When light passes through the first polariser it becomes polarised, this has the effect that when the polarised light then passes through the sample, due to the birefringence, the light will be refracted in two different directions and hence will interfere. The light then passes through a second polariser which is also known as an analyser, where the interference pattern can be viewed using an optical microscope as a characteristic texture (Figure II.30).

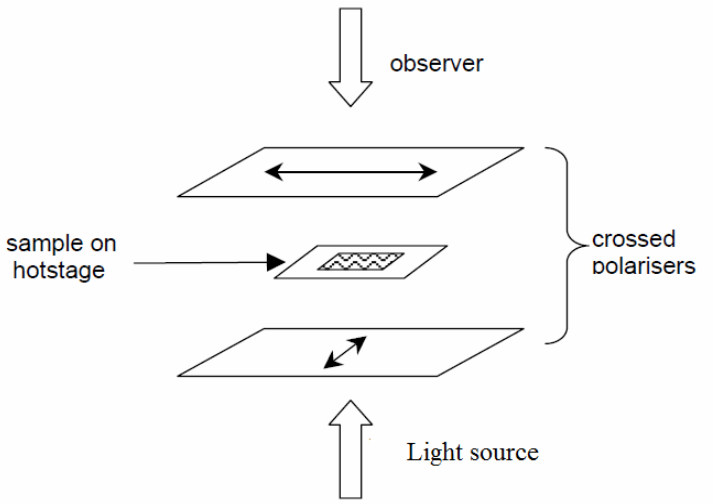

Figure II.30 Schematic of polarised optical microscope.

The complexes showed all similar textures on POM at room temperature, comparable to the optical textures of the N and M phases developed by chromonic compounds.[158,159] In particular, a schlieren texture is characteristic of low-concentrated phases (that starts to form around 1.2 % w/w), as it can be observed in Figure II.31 a) and b) where the textures developed by complexes **C_2** and **C_3** at 1.5% are presented. On increasing concentration (2.5 %), grainier textures may indicate a higher degree of ordering, and a herringbone texture is beginning to develop (Figure II.31.c, d).

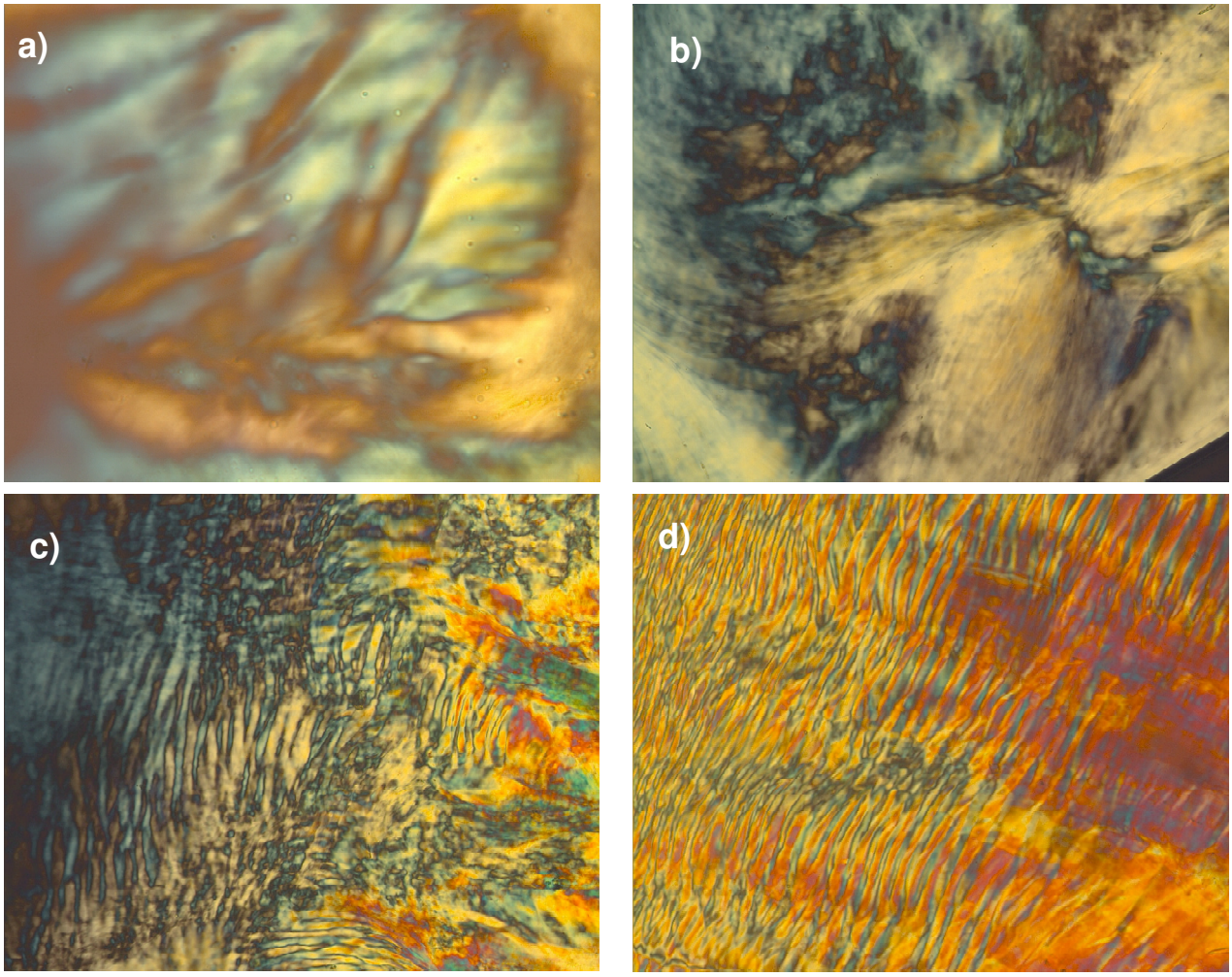

Figure II.31 POM micrographs of the phases formed in water by complexes $\mathbf{C_2}$ and $\mathbf{C_3}$ at room temperature: a) $\mathbf{C_2}$ at 1.5 %; b) $\mathbf{C_3}$ at 1.5 %; c) $\mathbf{C_2}$ at 2.5 % and d) $\mathbf{C_3}$ at 2.5 %.

II.4.3.2 ^{2}H NMR and ^{1}H NMR studies

When deuterated water is used as a solvent in ordered systems, it can serve as a probe to study the phase equilibrium. The ^{2}H NMR spectrum of ^2H_2O is dominated by the interaction of the deuteron quadrupolar moment with the electric field gradients in the nucleus. For an anisotropic sample the quadrupolar interaction is manifested as a doublet. In an isotropic solution, on the other hand, this interaction is averaged to zero as a result of rapid molecular motions, and ^{2}H spectrum consists of a sharp singlet.

The gel birefringent phases formed in water by complexes $\mathbf{C_2}$, $\mathbf{C_3}$ and $\mathbf{C_4}$ were investigated by ^{2}H NMR spectroscopy at variable temperatures at the concentration 2.5 % w/w in water. In order to investigate also the influence of the concentration, for complex $\mathbf{C_2}$ was prepared also a sample with the concentration of 3.0 % w/w.

As shown in figure II.32, the ^2H NMR spectra of complex $\mathbf{C_2}$ at 2.5 % w/w in water at temperatures below 40°C show two sharp peaks, indicating that the ^2H nucleus is in an anisotropic environment, that is, an aligned ordered phase upon exposure to the NMR magnetic field. On further heating, at 41.5°C, a singlet in the middle of the doublet peaks gradually emerged at the expense of the doublet intensity. At 42°C, only a singlet signal remained. These changes are indicative of a transition from an ordered phase to the isotropic phase.

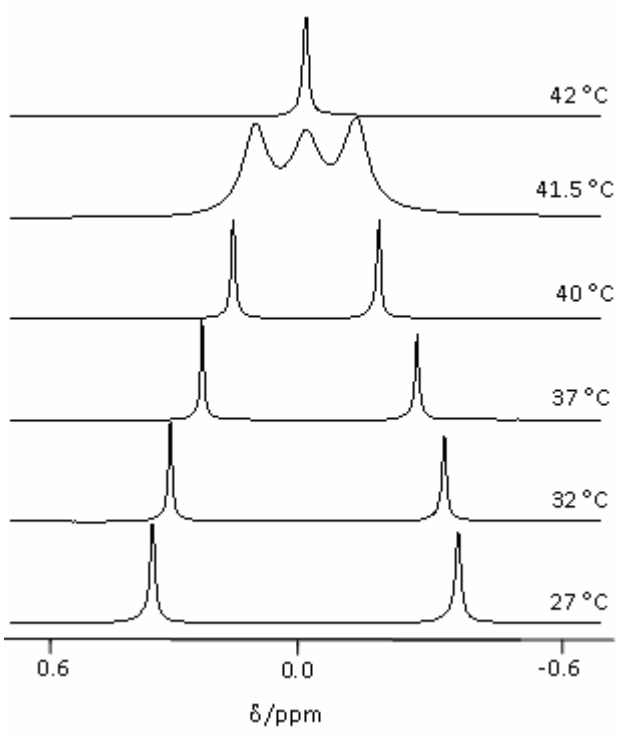

Figure II.32 Variable temperature ^2H NMR spectra of a ^2H_2O solution of complex $\mathbf{C_2}$ (2.5 % w/w).

Similar phase transitions were detected also for complexes $\mathbf{C_3}$ and $\mathbf{C_4}$ (both 2.5 % w/w in ^2H_2O), as showed in Figure II.32. Surprisingly, there seem to not be a correlation between the transition temperatures and the counterion chain length (like in thermotropic systems). Indeed, while for complex $\mathbf{C_2}$ the transition temperature to the isotropic phase was 42°C, for complex $\mathbf{C_3}$, at 45°C it can be still detected a co-existence of the ordered phase with the isotropic phase (Figure II.4.10 a), the true isotropic phase being observed at 46°C. Instead for complex $\mathbf{C_4}$, a smaller temperature range of the ordered phase existence can be observed, the system being already isotropic at 39°C (Figure II.33 b).

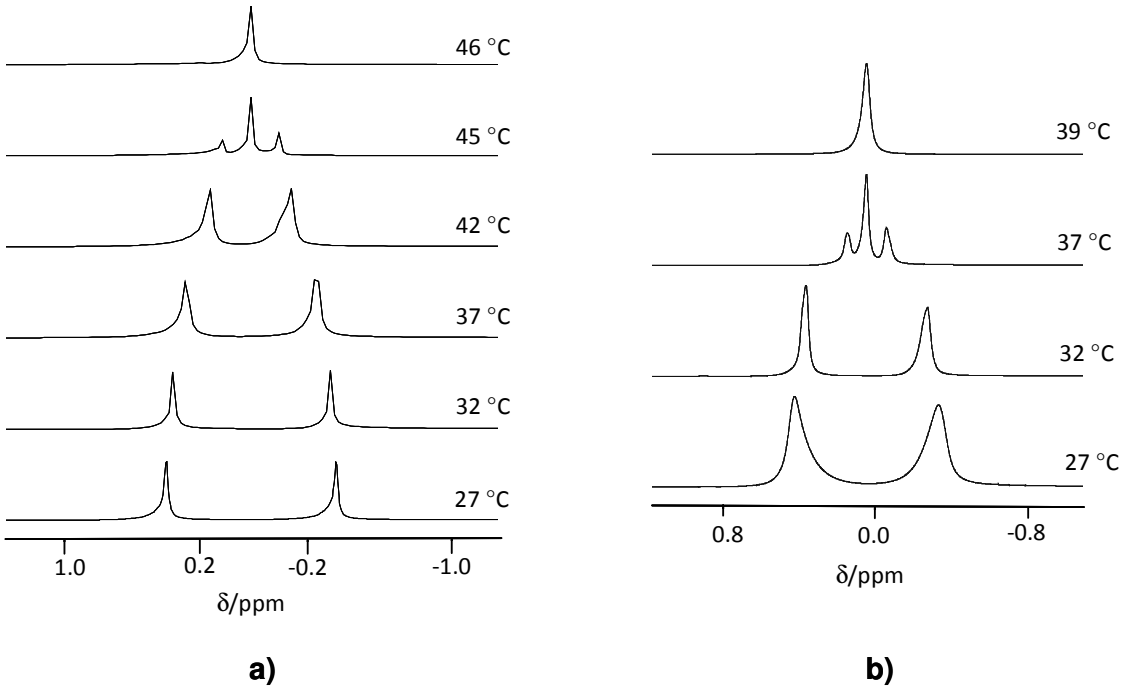

Figure II.33 Variable temperature ^2H NMR spectra of a ^2H_2O solution of complex a) $\mathbf{C_3}$ (2.5 % w/w) and b) $\mathbf{C_4}$ (2.5 % w/w).

Furthermore, a broadening of the two peaks of the ^2H NMR spectra of the gel phases at 2.5 % w/w can be observed on passing from complex $\mathbf{C_2}$ to complex $\mathbf{C_3}$ and $\mathbf{C_4}$ (Figure II.34). This suggests a lowering of the motion degree in the fluid phase. Since only the alkyl chain length of the counterion differs from one complex to other, this difference may be an indication of the fact that the counterion is included somehow in the fluid phase, contributing to its mobility.

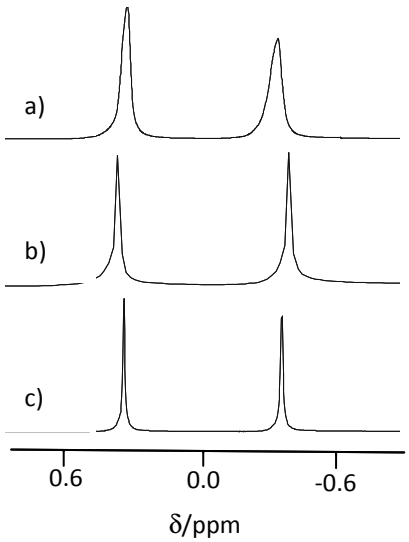

Figure II.34 ^2H NMR spectra of a ^2H_2O solution of complex a) $\mathbf{C_4}$ (2.5 % w/w) and b) $\mathbf{C_3}$ (2.5 % w/w) and c) $\mathbf{C_2}$ (2.5 % w/w) in water at 32°C.

Regarding the ^{1}H NMR spectra, the gel phase of complex **C_2** (2.5% w/w in water) was recorded at variable temperatures, keeping the same steps as for the ^{2}H NMR experiments, as it is showed in Figure II.35. At room temperature the spectra shows the expected broadening signals of the aromatic protons, whereas on increasing temperature the lines are narrowing.

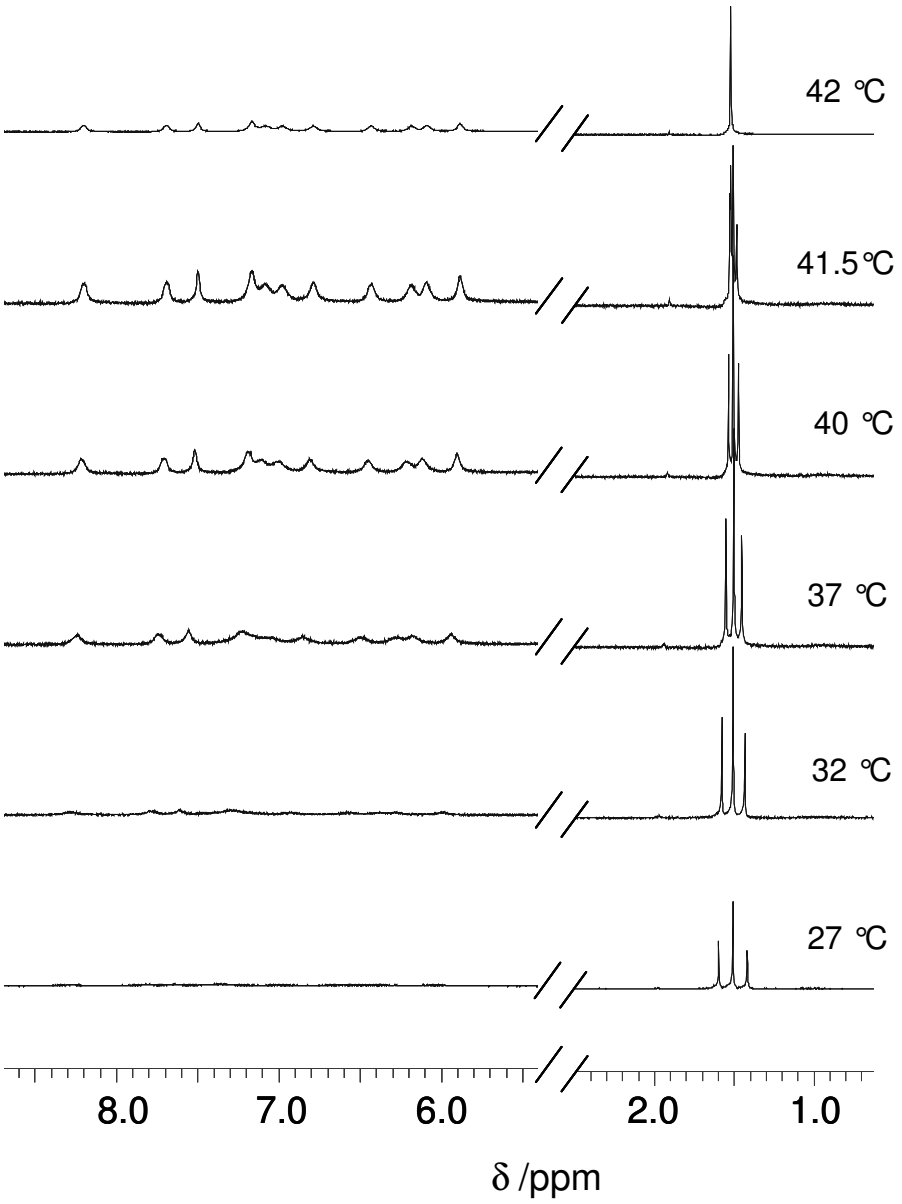

Figure II.35 Variable temperature ^{1}H NMR spectra of the gel phase of complex **C_2** (2.5 % w/w) in water.

The line width of an NMR signal depends on the internal mobility of the respective chemical group and the overall tumbling of the molecule. Spectra of isotropic liquids result in narrow lines, because the molecular motion averages dipolar couplings of nuclear spins and chemical shift anisotropy to isotropic values. In contrast, in ordered systems like gels, liquid crystals and solids, the motion of

certain segments of the molecules is strongly hindered, thus their dipolar interactions cannot be averaged out and their NMR lines become broadened. Therefore, the broadening and subsequent disappearance of signals of the aromatic protons suggests involvement of strong intermolecular interactions leading to self-organization of the molecules in the ordered state.

Furthermore, the single signal of the three aliphatic protons of the counterion that should appear in an isotropic phase, become a triplet in the ordered phase as can be seen in Figure II.34. This happens because in anisotropic environment dipolar couplings between magnetically equivalent nuclei are experienced, hence the proton NMR spectrum of an isolated methyl group will be observed as a triplet. In this case the dipolar coupling, D_{HH}, between the germinal protons can be derived from the following equation:

$$D_{HH} = 1/3T_{HH}$$

where T_{HH} is the total coupling measured directly from the splitting between two adjacent peaks of the triplet.

On increasing temperature, a decrease of the T_{HH} value occurs, similar with the decrease of the ^2H quadrupolar splitting, until reaching the isotropic phase at 42°C where only a singlet can be observed.

II.4.3.3 WAXS, SAXS and SANS

An accurate structural investigation of the gel phase formed by complex C_2 in water at 2.5% w/w and respectively of the isotropic solution at 1.0 % w/w was done by Wide Angle X-Ray Diffraction (WAXS), Small Angle X-Ray Diffraction (SAXS) and Small Angle Neutron Scattering (SANS) experiments.

Reference bulk structure and estimated molecular volume

In the single crystal structure of the analogue $[Ir(ppy)_2(bpy)]PF_6$ (structure HULVEQ in Cambridge database), the complexes arrange in an orthorhombic cell, consisting in a lamello-columnar type of organization with rows of complexes stacked in columns alternating with layers of counter-ions. The a×c plane of the orthorhombic cell includes 4 columns distributed in 2 rows with an intra-row spacing of 9.22 Å and an inter-row spacing of 9.89 Å, designing a bi-dimensional sub-lattice close to a single-column organization of oblique symmetry (a_0 = 9.22 Å, b_0 = 10.77 Å, γ_0 = 113.4°, S = 91.2 Å^2, Z_0 = 1). Along the columns axes, the distance between stacked complexes is of 7.91 Å, i.e. the half *b* lattice parameter. In the HULVEQ structure, the molecular volume of the complex including the counterion is of 721.6 Å^3, from which the molecular volume of the complex **C_2**, [Ir

(*ppy*)$_2$(*bpy*)](ac), is estimated to V_{Mol} ≈711 Å^3 by assuming partial molecular volume additivity and using density reference data.

Following, solutions of complex **C$_2$**, in deuterated water were prepared and investigated by WAXS, SAXS and SANS (X_M and X_V are the sample mass and volume fractions of solutions):

Complex **C$_2$**: 2.5 % w/w = 1.50 % v/v: X_M=0.02256; X_V=0.01502

Complex **C$_2$**: 1.0 % w/w = 0.61 % v/v: X_M=0.00924; X_V=0.00612

The viscosity of the diluted solution is comparable to the solvent, whilst the concentrated solution is in a birefringent gel phase.

Results and discussion

The WAXS pattern of the diluted solution nearly superposes with the one of the solvent at large angles but deviates upwards at low angles, due to the presence of large scattering objects dispersed in the solution (see Figure II.36). The same logically applies for the concentrated solution and a similar but more pronounced upward shift evidences the more abundant objects. In addition, a quite sharp peak appears at intermediate angles (d ≈ 7.6 Å; π ≈ 200 Å from Scherrer formula) and reveals the setting up of interaction between the closer objects in connection with the gelling. Interestingly, the location of this peak almost coincides with the stacking distance of complexes in the HULVEQ structure.

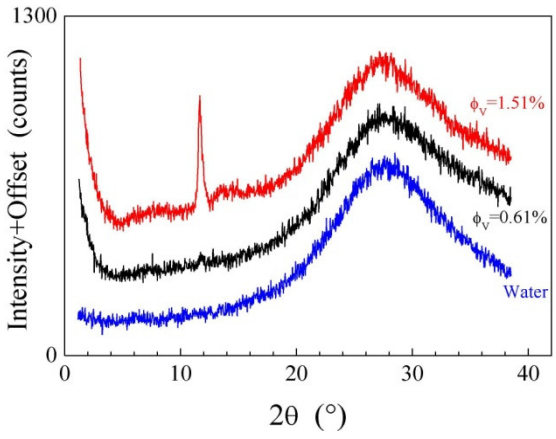

Figure II.36 WAXS pattern of the solvent (H_2O) and of the diluted (X_v = 0.61%) and gelled (X_v = 1.50%).

The similarity of the renormalized SAXS and SANS intensity variation between the diluted solution and the gel (see Figure II.37.), with in particular a form factor oscillation at the same location, shows that the objects are quite mono-disperse and that their size and shape do not significantly change with gelling. Nevertheless several structure factor peaks are observed for the gel at small q

vectors beyond the one visible in the WAXS pattern. The locations of the structure factor peaks are logically the same in SAXS and SANS curves, as the contrast change affects scattering intensities but not intermolecular distances.

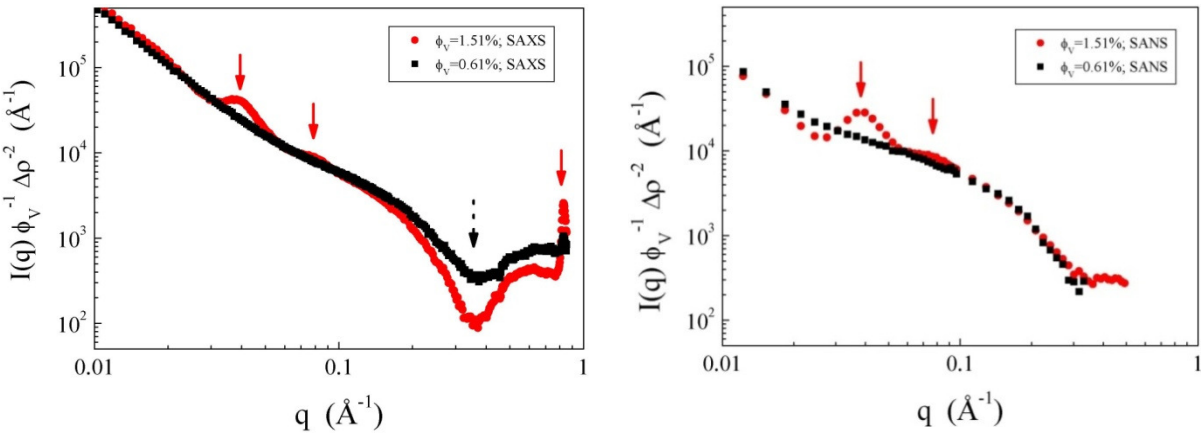

Figure II.37 a) SAXS and b) SANS curves of the solvent (a) H_2O; b) D_2O) and of the diluted (X_V = 0.61 %) and gelled (X_V = 1.50 %) solutions of complex $\mathbf{C_1}$. The absolute intensities renormalized by volume fraction and contrast are in ordinates. The dotted black arrow indicates an oscillation minimum of the form factor. The solid red arrows indicate the structure factor peaks in the curves of the gelled sample.

The contribution of interactions between objects to the overall scattering should be negligible in the diluted solution, as suggested by the un-gelled texture and the absence of structure factor peaks. The curves would then reflect the variation of the form factor and provide information upon the size and shape of objects. Indeed, the SANS curve in the Holzer representation contains an extended plateau region typical of a thin rod scattering regime (see figure II.38 a), which corresponds to the q vectors intermediate between the inverse half length, 2/L, and the inverse radius, 1/R, of the elongated objects. In this intermediate region, the form factor VP(q) of elongated objects can be approximated by the following relation, where A is cross-section area and R_G, the gyration radius, and which reduces to a simple q^{-1} dependence in the Holzer plateau range.[160]

$$VP(q) = \pi A\, q^{-1} \exp(-q^2 R_G^2 /2)$$

The deviation from the plateau observed at low q vectors might traduce the finite rod length setting the limit of the intermediate region and the cross over toward a regime dominated by the variation of the qL term. Alternatively, the q vectors then approach the reverse maximum distance between objects deduced from concentration ($1/D_{max} \approx 0.008$ Å^{-1}; vide infra) and it cannot be excluded that an interaction term then starts contributing to the scattering signal. At wide angles, but below the Guinier limit ($qR \approx 1$), the deviation from the Holzer plateau follows the decrease of the exponential factor, and the scattering intensity variation can therefore be approximated by a straight line in the

Guinier representation, which allows the direct determinations of R_G and A from slope and intercept (see Figure II.38.b). Remarkably, there is no significant discrepancy between the section area determined from Holzer plateau and intercept (A ≈ 180 Å^2) and the one determined from the gyration radius by assuming a cylindrical shape (R_G ≈ 5.6 Å = R/√2, A = πR^2 ≈ 200 Å^2). This excludes very dissymmetric cross-sections with large R_G^2 over A ratio, but confirms also the narrow shape polydispersity deduced from the observation of an un-damped form factor oscillation (vide infra), since the measured R_G^2 over A are respectively Z and weight averages of the distribution.

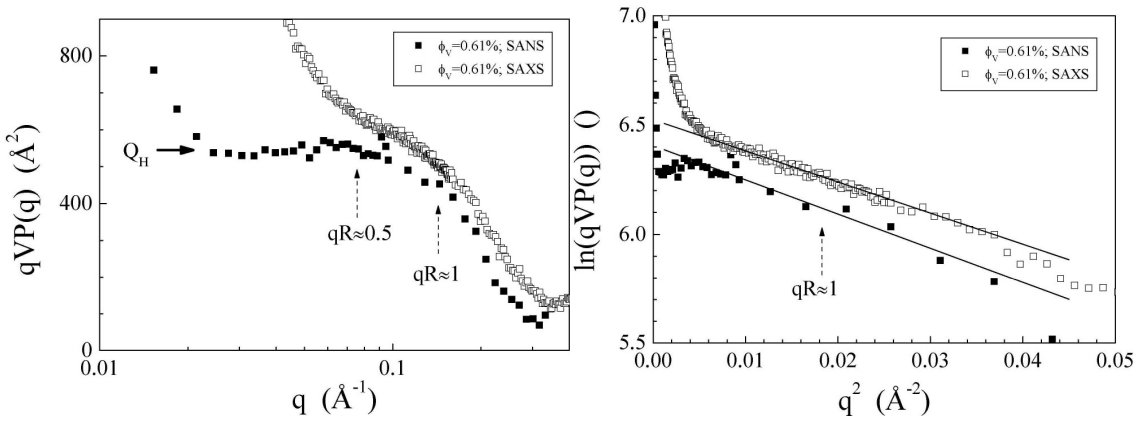

Figure II.38 Form factor variation of the diluted solution of complex **C_2** in D_2O (X_V = 0.61 %) in the intermediate region: a) Holzer representation; b) Guinier representation of the cylinder section.

The determined area is therefore representative of the elongated objects and may be compared to the columnar sub-lattice area in the crystalline phase (vide infra). The ratio close to 2 suggests for the object a strand structure made by the aggregation of two strings of piled complexes. Corollary, this would imply a deviation from cylindricality below the detectable shape dissymmetry (for instance, for an ideal ellipsoidal shape cross section with the experimental Holzer plateau area and a long to short axis ratio of 2: R_G ≈ 5.9 Å, 2πR_G^2 ≈ 220 Å^2). This strand structure would explain the similitude of SANS and SAXS curves despite the change of contrast with respect to the solvent, from a quite homogenous contrast all over the bulky hydrogenated ligands in SANS to a distribution of high electronic density zones centered onto iridium in SAXS. Thus, for single string of complexes, with the Iridium mainly located in the center of the piles, objects would appear much thinner in SAXS than in SANS. Conversely, the small discrepancy between both scattering curves reveals either the large distribution of Iridium in the cross section of strands or more realistically from a molecular point of view, the presence of several high electronic density zones in the cross

section. Indeed, the homogenous distribution of the electronic density of Iridium is excluded by the absence of the Holzer plateau evidenced in the SANS curve, the steep variation observed instead might then occur from the contribution of correlations between the high electronic density zones associated to Ir.

This general strand structure shows strong analogies with the one of wormlike micelles occurring in the concentration range 1 of phase diagrams of surfactants.[161] In both cases the objects are self-association polyelectrolytes which grow unidimensionally by keeping a quasi homogenous cross-section constituted by the association of a small and nearly constant number of molecules. In surfactants, this shape results from the segregation of the alkyl tails inside the micelles which curves the interfaces with polar heads and water toward cylinders. The complexes contain neither alkyl chains nor polar heads and the self association mechanism leading to the strand shape must involve another segregation process. Tentatively, it is suggested that this process follows the difference in nature and hydrophilicity of the bipyridine and phenylpyridine ligands, the former being preferentially rejected at the water interface and the latter being preferentially segregated inside the strands with the ligands of another complex.

Beyond the different mechanism leading to the shape analogy, strands and wormlike micelles differ in their behavior at higher concentration. Thus, in the concentration range 3 corresponding to the first birefringent gel, the micelles disappeared by fusing into large-size objects like ribbons or bilayers, those long-range ordered organization is at the origin of the gelling and of the birefringence. Quite the opposite, the similitude of the form factor variation in the dilute solution and in the gel (vide infra) indicates that the strands persist after the gelling. This again reflects the differences in molecular structure: the long, bulky and flexible aliphatic tails of surfactant micelles easily spread and merge with neighboring micelles into bigger structures with smaller interface areas, whilst the ligand periphery of complexes is short, compact and quite stiff, authorizing limited reorganizations in the segregation zone and at the water interface. This then preserves the strands in the birefringent gel phase, the long range-correlated structures at the origin of the gel properties consisting in close packing organizations of interacting polyelectrolyte strands, sheathed in their solvatation shell.

These long range-correlated structures might be elucidated with the structure factor, which can here be easily isolated by dividing the scattering curves of gelled and diluted solutions, since the form factor change caused by gelling is negligible. This looms up the correlation peaks already detected in the raw scattering curves (see Figure II.39). Apart from the peak at wide angle obviously related to the stacking of complexes along strands, several peaks are visible at small angles, the lowest-

angle one been located at 360-400 Å and the most intense one, at 150-160Å. Theses peaks probably occur from periodicities of strand rows alternating with water sublayers, but they may belong to different phases coexisting at the same concentration, as commonly the case in phase diagrams[161]. Moreover, the water content may be different in these structured phases, which may even coexist with amorphous zones, preventing the discussion of the packing. Thus, a nearer analysis of the gel structure would need a careful analysis of the phase diagram and the characterization of the dependence upon concentration of all structure factor peaks.

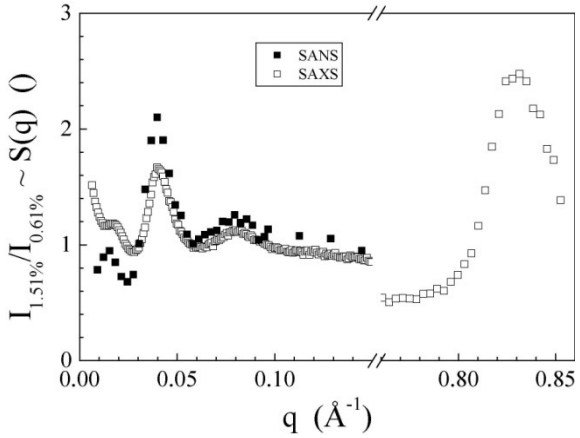

Figure II.39 Structure factor in the gelled solution of $[IrLig]^+AcO^-$ in D_2O (X_V = 1.50 %), from SAXS and SANS curves

II.4.4 Photophysical properties

II.4.4.1 Photophysical properties of cation $[Ir(ppy)_2(bpy)]^+$

The photophysical properties of complexes from class C were studied both in dichloromethane and in water solutions. Although several successive dilutions have been performed, all the solutions showed a multi exponential lifetime decays whose time constants were changing as a consequence of complex concentration. The observed behavior has been explained with the presence in solution of aggregates already existing in the dilute solution. In fact, as demonstrated by an accurate X-ray and neutron scattering diffraction analysis performed on complex **C_2**, these complexes at a concentration of 2.5% (w/w) organize themselves into columns formed by two strands of complexes. Moreover while in the gel phases these columns are strongly entangled through non-covalent interactions, in the dilute isotropic solution the columns are already formed and stable but they are smaller and less interacting with respect to what observed in the gel phase (see section II.4.3.3).

II.4.4.2 Photophysical properties of complexes C_2, C_3 and C_4 in gel phases

Aggregation phenomena can dramatically affect the photophysical properties of Iridium(III) complexes. In particular, for these complexes, changes in intermolecular interactions, environmental polarity and medium rigidity can significantly modify the observed spectroscopic features allowing to probe the environment around the metal centre by the use of both spectral- and time-resolved photophysical techniques[47, 138, 139, 162, 163, 164, 165, 166] Nevertheless, in order to effectively understand the photophysical behaviour of the complex in the aggregate phase (gel phase in our case) it is necessary to compare the photophysical behaviour of the aggregate with that of the corresponding monomeric solvated component. Since the photophysical properties of the complexes are independent from the counterions, the photophysical properties of class C compounds in the gel phases were compared to those of $[Ir(ppy)_2(bpy)]PF_6$, whose photophysical data were taken from literature (Table II.7).[37]

Table II.7 Phototophysical data[1] of cation $[Ir(ppy)_2(bpy)]^+$.

Complex	λ_{max} (nm)	τ[ns]	Φ(%)
$[(ppy)_2Ir(bpy)]PF_6$	590	τ = 180	1.8

The full photophysical data in water for complexes **C_2, C_3** and **C_4** are summarized in Table II.8.

Table II.8 The photophysical data for **C_2, C_3** and **C_4** in water.

Complex	Conc (% w/w)	λ_{max} (nm)	τ[ns]	Φ[%]
$[(ppy)_2Ir(bpy)]PF_6$		590	180	1.8
C_2: $[(ppy)_2Ir(bpy)]ac$	2.5	541	τ_1 = 212 (15.0%) τ_2 = 542 (85.0%)	11.0
C_3: $[(ppy)_2Ir(bpy)]ac$-C_2	2.5	541	τ_1 = 347 (18.3%) τ_2 = 624 (81.7%)	12.5
C_4:$[(ppy)_2Ir(bpy)]ac$-C_5	2.5	540	τ_1 = 70 (0.8%) τ_2 = 364 (23.0%) τ_3 = 619 (76.2%)	10.0

As illustrated in Table II.8, **C_2, C_3** and **C_4** complexes showed in the gel phase an evident blue shift of the emission maximum with respect to the monomeric solvated component. Moreover all the recorded luminescence decays turned out to be multi-exponential in nature. The blue shift of the emission maximum and the multi-exponentiality of the luminescence decays observed for **C_2, C_3** and **C4** can be associated to aggregates formation. As already observed for analogous compounds, the change in emission energy can be associated, to a progressive shift toward higher energy of the ^{3}MLCT state owing to a progressive change of the molecular environment and medium rigidity.[1a] Moreover the non-exponentiality of the luminescence decay can be associated to the presence in the gel phase of monomeric components and different sized columnar aggregate more or less entangled.

II.5 Complexes of class D

The functionalization of the *bpy* ligand with hydrophilic groups was further accomplished. As described previously in Chapter II.4, *bpy* is a particularly attractive oligopyridinea building block, being one of the most versatile ligand used for the preparation of supramolecular structures by coordinating a transitional metal center. This is because *bpy*may act as efficient proton acceptors in hydrogen bonding and can interact through π-stacking with other aromatic systems, providing many different intermolecular interactions useful for designing well-ordered arrays of functional supramolecules.The functionalization with long alkyl chains introduces a structural amphiphilicity which represent one of the basic properties needed for introducing lyotropic properties in the molecular structure. Furthermore, the introduction of OH groups by a proper functionalization of the *bpy* ancillary ligand increases the number of possible intermolecular interactions an may influence drastically the structure and properties of the final material. Finally, functionalization with a silica-based group is one of the strategies used in building mesostructured materials with the functional molecule situated in the walls of the inorganic structure.

Therefore a series of new functionalized *bpy*-based ligands able to coordinate to a metal ion while providing the hydrogen bonding interactions for organizing their complexes into extended networks through hydrogen bonds and increase their solubility in water to form hydrophilic Ir(III) complexes were prepared. Their versatility in complexation transition metals was tested using Zn(II) salts.This strategy permitted to investigate the stability of the ligands in different reaction conditions and the versatility towards complexation, through an easy one-step reaction. Furthermore, Zn (II) salts among the different transition metal studied are one of the most fascinating as it is very cheap and its 24th most abundant metal in the earth's crust.

II.5.1 Synthesis of 4,4'-substituted-2,2'-bipyridine and their versatility in complexation with Zn(II) salts

II.5.1.1 Synthesis

The functional *bpy*-based ligands were prepared by modifying literature processes under appropriate reaction conditions in good yields.[167] Their chemical structure and synthesis is presented in Scheme II.11.

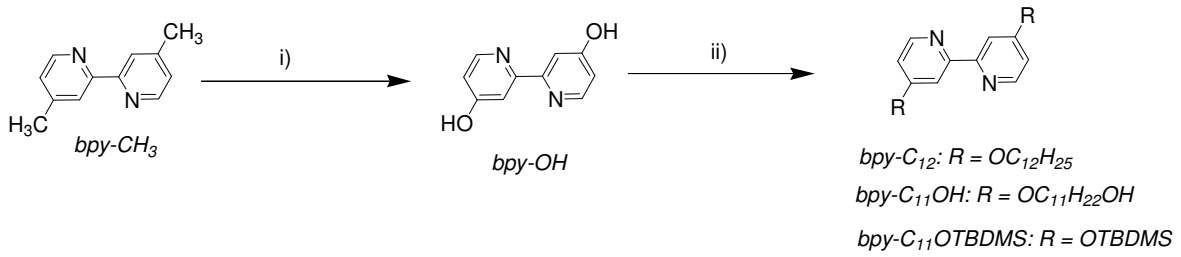

Scheme II.11 Synthesis of functionalized *bpy*-based ligands, i) HBr/CH_3COOH, ΔT, 48 hours, N_2; ii) RBr, DMF, KI, ΔT, 48 hours.

Furthermore, the versatility of the prepared ligands towards transition metal complexes was checked by using Zn(II) metal. Metal ions are powerful templates, which can gather ligands to build a variety of predetermined stereochemical arrangements. The metal-ligand distances reflects the properties of the metal complexes, namely the electronic distribution of the metal ion and the ligands, their polarizing ability and interactions, as well as the metal coordination number and coordination geometry which are the key factors governing the structure and reactivity of the metal complex. In this context, *bpy* ligands have been recently used for the molecular engineering of Zn complexes, due to their well-defined coordination ability. By contrast, since there is no ligand field stabilization effect, Zn(II) has the ability to expand its coordination sphere and therefore is known to give tetrahedral complexes or octahedral complexes with diimine ligands. Due to their electron-transporting ability, light-emitting efficiency, high thermal and redox stability and tunable electronic properties, Zn(II) complexes with N,N and N,O type chelating ligands have been widely applied in OLED technology.[168,169,170,171] Moreover, these peculiar physical and chemical properties, make Zn(II) complexes a very interesting and attractive alternative for the development of efficient molecular based optoelectronic devices.

The chemical structures of the new Zn (II) based complexes synthesised is presented in Figure II.40.

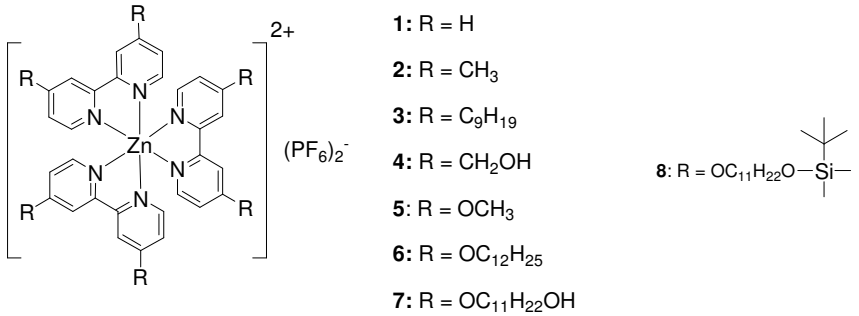

Figure II.40 Chemical structure of the octahedral ionic Zn(II) complexes of general formula $[Zn(bpy\text{-}R)_3](PF_6)_2$.

The substituents on the *bpy* ligands were selected owing to their different hydrogen bonding ability with the aim to modulate the final organizations and the photophysical properties of the resulting materials.

Synthesis of complexes

The synthesis of the ionic Zn(II) complexes of **1 – 8** were carried out by reaction of the zinc acetate dihydrate ($Zn(CH_3COO)_2{\cdot}2H_2O$) with 3.0 equivalents of *bpy-R* ligand in reflux condition in appropriate solvents as presented in the experimental part, followed by subsequently addition of 5-fold excess of NH_4PF_6 under inert nitrogen atmosphere (Scheme II.12).

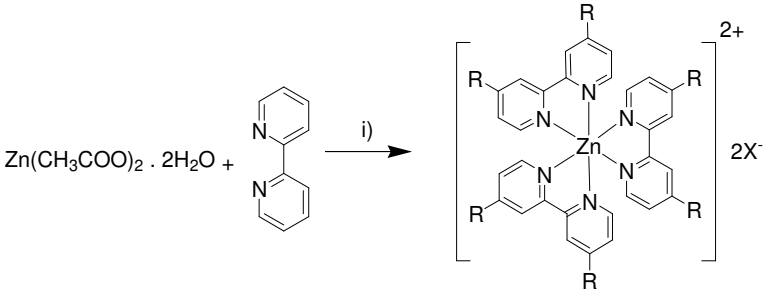

1. $[Zn(bpy)_3](PF_6)_2$. **2.** $[Zn(bpyCH_3)_3](PF_6)_2$.

3. $[Zn(bpyC_9H_{19})_3](PF_6)_2$. **4.** $\{[Zn(bpyCH_2OH)_3(PF_6)_2\}_2.bpyCH_2OH.4H_2O$

5. $[Zn(bpyOCH_3)_3](PF_6)_2$. **6.** $[Zn(bpy\text{-}C_{12})_3](PF_6)_2$.

7. $[Zn(bpy\text{-}Oc_{11}OH)_3](PF_6)_2$ **8.** $[Zn(bpy\text{-}C_{11}OTBDMS)_3](PF_6)_2$

Scheme II.12 Synthesis of octahedral ionic Zn (II) complexes **1 – 8:** i), ΔT, 24 hours, N_2; ii) NH_4PF_6, ΔT, 24 hours, N_2.

All ionic species are obtained as microcrystalline solid powders in good yields (61 – 85%), and will be referred as complexes **1 – 8** with the general formula $[Zn(bpy\text{-}R)_3](PF_6)_2$. The complexes were characterized by IR and ^1H NMR spectroscopies and elemental analysis.

II.5.1.2 Spectroscopic characterization

IR spectroscopy

In the IR spectra of complex **1 – 8,** the characteristic bands of the stretching frequencies of the aliphatic chains were identified around 2925 cm^{-1} and 2852 cm^{-1} more intense in case of complexes **3, 6, 7** and **8** that has long alkyl chains. Furthermore, the main bands of the C-O-C frequencies of the ether linkages were identified at 1292.4 cm^{-1} (C-O-C aysm. stretch.) and 1023.7 cm^{-1} (C-O-C sym. stretch.) for complex **5**, and respectively at 1273.51 cm^{-1} (C-O-C aysm. stretch.) and 1016.1 cm^{-1} (C-O-C sym. stretch.) for complex **6.** Whereas at 1258.17 cm^{-1} (C-O-C aysm. stretch.) and 1017.0 cm^{-1} (C-O-C sym. stretch.) for complex **7** and respectively complex **8** at 1256.3 C-O-C (aysm. stretch.) and 1023.7 cm^{-1} (C-O-C sym. stretch.). Moreover, the IR spectra of complexes **4**

and **7** showed one additional broad band at 3390 cm^{-1} and 3400.2 cm^{-1} regarding the –OH groups of *byCH_2OH* ligand and *byC11OH* respectively. Furthermore, for complex **8** one strong peak at 1102.2 cm^{-1} identified the O-Si-C stretching.

Finally, in the spectra of all complexes the main stretching frequency of the counterion was identified at around 845 cm^{-1}.

^{1}H NMR spectroscopy

For solubility reasons, the ^{1}H NMR spectra for complexes **1 – 3** and **5 – 8** were recorded in $CDCl_3$ and for complex **4** was recorded in DMSO-d_6. The aromatic region showed 18 protons of the ligands (*bpyCH3*, *byC_9H_{19}*, bpy-*C_{12}*, *bpy-CH_2OH* and *By-C_{11}OTBDMS*) in the range of 8.32 to 7.07 ppm for complexes **1**, **2** and **5 – 8**. Furthermore, for complex **1** addition two aromatic protons of the *bpy* ligand were identified in the aromatic region. The ^{1}H NMR spectra of the complex **2** was showed a singlet centered at 4.0 ppm. Furthermore, in the aliphatic region, the signals attributed to *byC_9H_{19},* bpy-*C_{12},* by-*$C_{11}OH$* and *by-C_{11}OTBDMS* ligands were identified in the range between 4.28 and 0.87 ppm for complex **3, 6, 7** and **8** respectively. Moreover, the signals attributed to tetrabutyldimethylsilyl (TBDMS) group of by-*C_{11}OTBDMS* ligand were identified as two singlets at 0.88 and 0.044 ppm in complex **8**.

In particular, in the ^{1}H NMR spectrum of complex **4**, two different kinds of aromatic signals were identified indicating the presence of different *bpy-CH_2OH* ligands, coordinated and co-crystallised. Upon coordination to the Zn(II) centre the protons of the bipyridines are shifted with respect to the uncoordinated $\mathbf{L_1}$ ligand (H6 proton up-field whereas H3 and H5 shifted to lower field). Moreover, the presence of the un-coordinated $\mathbf{L_1}$ ligand causes a significant broadening of all signals consistent with a certain degree of interaction. The integrals reveals the presence of one co-crystallised *bpy-CH_2OH* ligand to two molecules of complexes (respectively 6 coordinated *bpy-CH_2OH* ligands).

II.5.1.3 Thermal analysis

Furthermore, TGA analyses were performed in order to identify to possible solvents that are included in the molecular formula of the complexes **1 – 8**. The number of the solvent molecules was determined by the experimental weight loss. In particular, only the pristine powder complex **7** contains solvent molecules in the structure, its TGA scan showing an experimental mass loss of 2.45% corresponding to 3 molecule of water (calcd.2.50%).

II.5.2 Complexes of class D, [(ppy)$_2$Ir(bpy-R)](X), where X = PF$_6$, ac, bz

Furthermore the functionalized *bpy* ligands were used to obtain the complexes of class D. Hence, the complexes of class D contain two *ppy* as cyclometallating ligands and, as ancillary ligand, *bpy* functionalized in 4,4'-position (*bpy-R*) with either alkyl chains ending with the hydrophilic OH group or alkyl chains ending with the t-butyl-dimethylsilane (TBDMS) respectively. The functionalization of the *bpy* ligand may tune the redox, photophysical properties and supramolecular order of the Ir (III) complexes. The *bpy-R* has outstanding ability to form the stable complexes via 5 member metallocyclic rings with Ir metal centre. The use of functionalized *bpy-R* into the Ir(III) framework introduces the molecular functionalities, suitable for the generation of H-bonding interactions, one of the means to control molecular assembling and to engineer the structures of the resulting materials. Therefore, the potential of these ligands in the construction of new highly luminescent materials may be outstanding.

In particular, four new complexes were synthesized and characterized. Their chemical structure and proton numerotation are presented in Figure II.41.

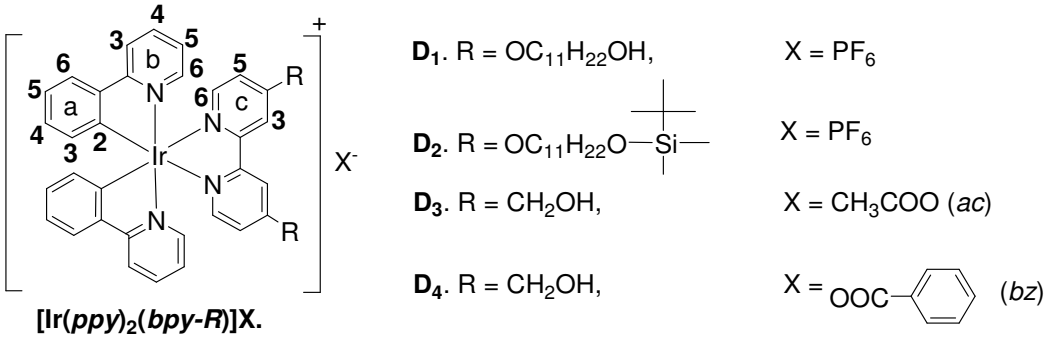

Figure II.41 Chemical structure of the complexes**D$_1$ - D$_4$** with the general formula [Ir(*ppy*)$_2$(*bpy-R*)]X, where X = hexafluorophosphate (PF_6), acetate (*ac*) and benzoate (*bz*).

II.5.3 Synthesis and characterization of complexes D_1 - D_4

II.5.3.1 Synthesis

For the synthesis of complexes of class D, previously a series of Ag(I) salts were prepared. Their synthesis was presented in the chapter II.2.1.1.

The synthesis of the functionalised bpy-R ligands was previously presented (II.5.1.1), whereas ligand bpy-CH_2OH was prepared by using a synthetic method found in the literature.[172]

Synthesis of complexes

The syntheses of the ionic Ir(III) complexes of **D_1 – D_4** were carried out by using the classical bridge-splitting reaction of the dimeric precursor $[Ir(ppy)_2]_2$-μCl_2 with 2.0 equivalents of *bpy-R* ligand, followed by subsequently addition of 5-fold excess of NH_4PF_6 obtaining tus complexes **D_1** and **D_2**, or by subsequently addition of 1.1 fold excess of Ag(I) salt containing the desired counterions *ac* and *bz* respectively for the synthesis of complexes **D_3** and **D_4** (Scheme II.13).

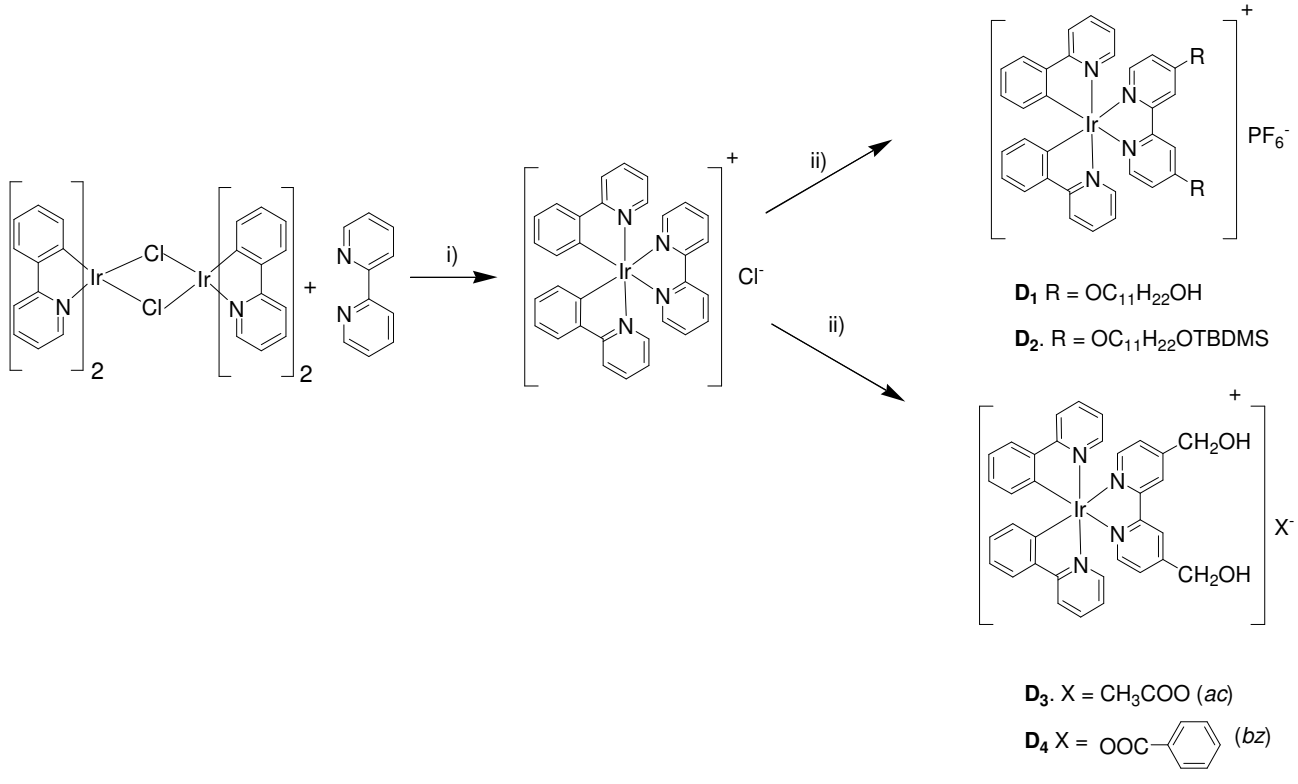

Scheme II.13 Synthesis of octahedral ionic Ir(III) complexes **D_1-D_4**: i) CH_2Cl_2/ MeOH (2:1 v/v), ΔT, 1 h, N_2; for complexes **D_1-D_4**: ii) NH_4PF_6, ΔT, 3h, N_2; for complexes **D_3-D_4**: ii) Ag_2X_2, ΔT, 3hours, N_2.

All ionic species are obtained as microcrystalline yellow powder solids in good yields (75-83%), and will be referred as complexes **D_1 – D_4** with the general formula $[Ir(ppy)_2(bpy\text{-}R)](X)$, as illustrated in Scheme II.13. In particular, complex **D_3** was water soluble. The complexes were fully

characterized by IR and ^{1}H NMR spectroscopies, conductivity measurements and elemental analysis. Conductivity measurements conducted in acetonitrile solution for complexes **D$_1$** and **D$_2$** assessed their 1:1 electrolyte nature. Indeed, the molar conductivities (109 $\Omega^{-1}\cdot cm^2\cdot mol^{-1}$ (**D$_1$**) and 103 $\Omega^{-1}\cdot cm^2\cdot mol^{-1}$ (**D$_2$**) respectively) are in the acceptable Λ_M ranges for univalent electrolytes in acetonitrile solution.[173] Furthermore, for solubility reasons, the conductivity measurements for complex **D$_3$** (53 $\Omega^{-1}\cdot cm^2\cdot mol^{-1}$) and **D$_4$** (58 $\Omega^{-1}\cdot cm^2\cdot mol^{-1}$) were performed in methanol solution. Again the value obtained is in the range of univalent electrolytes in methanol solution.[6]

II.5.3.2 Spectroscopic characterization

IR spectroscopy

In the IR spectra of complex **D$_1$** and **D$_2$**, the characteristic bands of the stretching frequencies of the aliphatic chains were identified around 2926 cm^{-1} and 2855 cm^{-1}. Furthermore, the main bands of the C-O-C frequencies of the ether linkages were identified at 1267.8 cm^{-1} (C-O-C abysm. stretch.) and 1030.8 cm^{-1} (C-O-C sym. stretch.) for complex **D$_1$** and respectively complex **D$_2$** at 1252.1 cm^{-1} (C-O-C asym. stretch.) and 1031.7 cm^{-1} (C-O-C sym. stretch.). In addition, the stretching frequencies for complex **D$_1$** of the OH groups were identified at 3224 cm^{-1} as large broad bands. Furthermore, for complex **D$_2$** one strong peak at 1100 cm^{-1} identifies the O-Si-C stretching. Finally, the main stretching frequency of the counterion (PF_6) was identified at around 845 cm^{-1}.

Regarding complexes **D$_3$** and **D$_4$**, the main bands of the C-O frequencies of the carboxylate anions are identified at 1560 cm^{-1} (C-O antisym. stretch.) and 1419 cm^{-1} (C-O sym. stretch.).

^{1}H NMR spectroscopy

The ^{1}H NMR spectra were recorded in $CDCl_3$ for all four complexes **D$_1$ – D$_4$**. The aromatic region showed the 16 protons of the *ppy* and the 6 protons of the functionalized ligands (*bpy-CH_2OH*, bpy-*$C_{11}OH$* and *bpy-C_{11}OTBDMS*) in the range of 9.51 ppy to 6.28 ppy. Furthermore, in the aliphatic region, the signals attributed to *by-$C_{11}OH$* and *by-C_{11}OTBDMS* ligands were identified in the range between 4.28 and 1.2 ppy for complexes **D$_1$** and **D$_2$** respectively. Moreover, the signals attributed to tetrabutyldimethylsilyl (TBDMS) group of by-*C_{11}OTBDMS* ligand were identified as two singlets at 0.88 and 0.044 ppy in complex **D$_2$**. Finally the signals contributed by -CH_2OH group of *bpy-CH_2OH* ligand were identified as singlets at 4.90 ppy and 3.90 ppm for complexes **D$_3$** and **D$_4$**.

Regarding the counterions, in the aliphatic region, the spectrum of complex **D$_3$** (with *ac* as counterion) showed singlet centered at 2.0 ppm. Furthermore, ^{1}H NMR spectrum of complex **D$_4$** showed in the aromatic region the additional signals regarding the 5 protons from *bz* as overlapped peaks in the range of 7.44 -7.65 ppm.

II.5.3.3 Thermal analysis

Furthermore, TGA analysis was performed in order to identify to possible solvents that are included in the molecular formula of the complexes $\mathbf{D_1}$ and $\mathbf{D_2}$**.** In particular, powder complexes $\mathbf{D_1}$ has no solvent molecules, whereas $\mathbf{D_2}$ powder complex contains solvent in its powder pristine solid, with an experimental mass loss of 1.29 % corresponding to 1 molecule of water (calcd.1.26%).

II.6 Complexes of class E, [(fppy)$_2$Ir(bpy)](X), where X = ac, bz, dos

In class E, the cyclometallating ligand was changed from *ppy* to 2-(2,4-difluorophenyl)pyridine (*fppy*). With respect to *ppy*, the *fppy* ligand possess two –F functionalities and an aromatic group, able, in principle, to direct the assembly of the complex cations through both H-bonding and aromatic interactions. The *bpy* was used as ancillary ligand while the counterions acetate (*ac*), benzoate (*bz*) and dodecylsulfate (*dos*) were used.

Their chemical structure and proton numerotations are presented in Figure II.42.

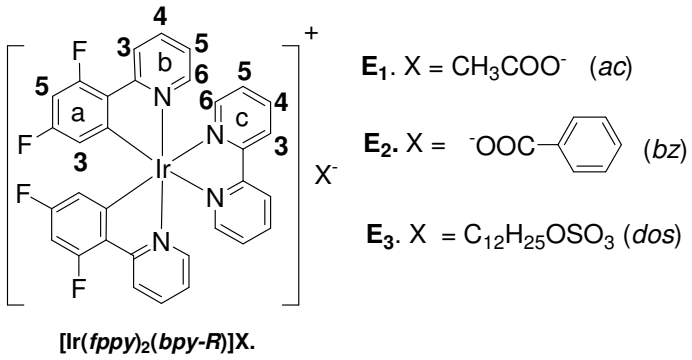

Figure II.42 Chemical structure of the octahedral Ir(III) ionic complexes of class E with the general formula [Ir(f*ppy*)$_2$ (*bpy*)](X), where X = acetate(*ac*), benzoate (*bz*) and dodecylsulfate (*dos*).

II.6.1 Synthesis and characterization of complexes E$_1$- E$_3$

II.6.1.1 Synthesis

For the synthesis of complexes of class E, previously a series of Ag(I) salts were prepared as discussed in chapter in the chapter II.2.1.1. Sodium dodecylsulfate was obtained from commercial sources and used as received without purification.

Furthermore, the synthesis of dichloro bridged precursor [Ir(*fppy*)$_2$]-μCl$_2$ was done using a modified method reported in literature.[174] In particular, Ir(III) chloride hydrate ($IrCl_3 \cdot 3H_2O$) and *f-.ppy* were dissolved in EtOEtOH/H_2O mixture under nitrogen atmosphere and refluxed for 20 hours. After cooling, the yellow precipitate formed was filtered out and washed with acetone and ethanol giving the desired product as a yellow greenish solid powder. The synthesis is presented in Scheme II.14.

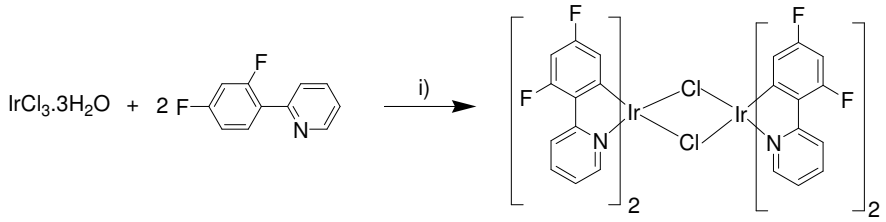

Scheme II.14 Synthesis of dichloro bridged precursor [Ir(*fppy*)$_2$]-μCl$_2$: i) 2-EtOEtOH/H$_2$O (3:1 v/v), ΔT, 20hours, N$_2$.

Synthesis of complexes

The synthesis of the ionic Ir(III) complexes of class E (**E$_1$** and **E$_2$**) were carried out by the classical bridge-splitting reaction of the dimeric precursor [Ir(*fppy*)$_2$]$_2$-μCl$_2$ with 2.0 equivalents of *bpy* ligand, followed by subsequently addition of 1.1-fold excess of Ag(I) salts that contains the appropriate counterions acetate (*ac*) and benzoate (*bz*) (Scheme II.15). The complex **E$_3$** was obtained by same classical bridge-splitting reaction of the dimeri precursor [Ir(p*py*)$_2$]$_2$-μCl$_2$ with 2.0 equivalents of *bpy* ligand, followed by subsequently addition of a 5-fold excess of sodium dodecylsolphate (Scheme II.15).

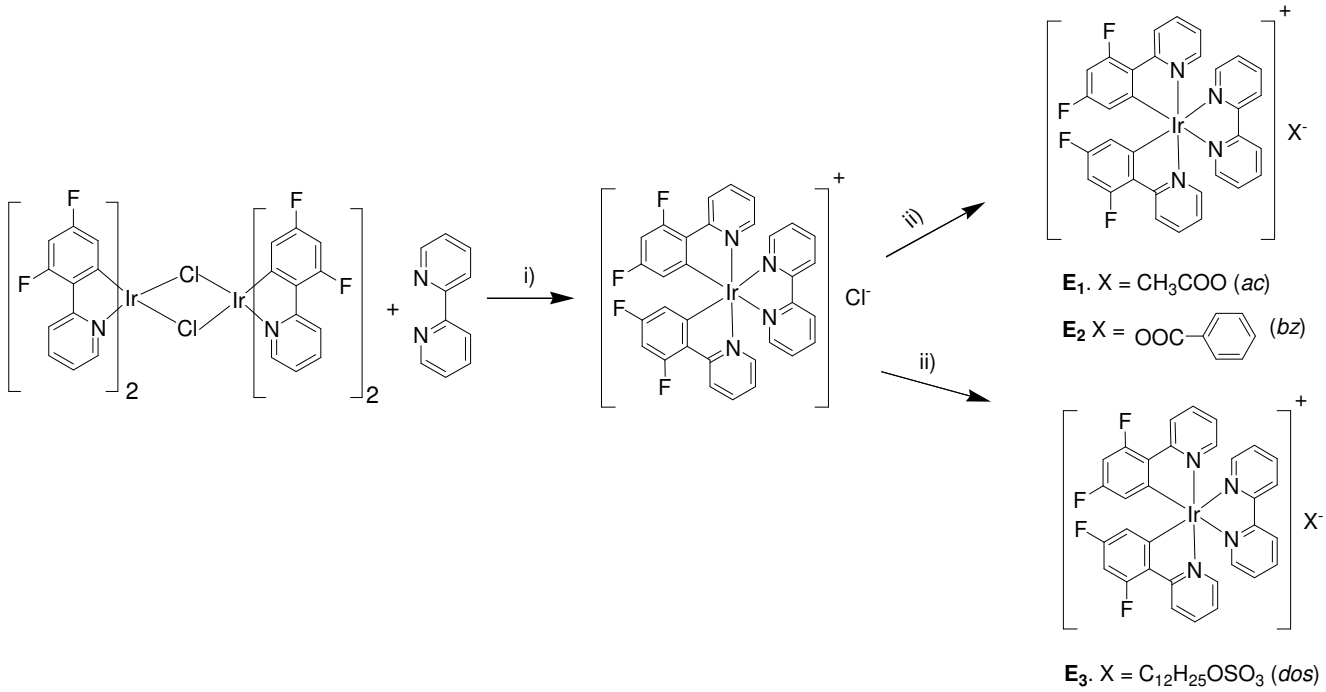

Scheme II.15 Synthesis of the octahedral ionic Ir(III) complexes **E$_1$ – E$_3$**: i) CH_2Cl_2/MeOH (3:1 v/v), ΔT, 4 h, N_2; ii) for complexes **E$_1$ – E$_2$**: ii) Ag_2X_2, ΔT, 3h, N_2; for complex **E$_3$**: ii) Na*dos*, ΔT, 24 h, N_2.

All ionic species are obtained as microcrystalline yellow powder solids in good yields (61-65%), and will be referred as complexes **E$_1$ – E$_3$** with the general formula [Ir(*fppy*)$_2$(bpy)]X, as illustrated in Scheme II.15. The complexes were fully characterized by IR and ^{1}H NMR spectroscopies,

conductivity measurements and elemental analysis. Conductivity measurements conducted in acetonitrile solution for complexes **E_1**, **E_2** and **E_3**, assessed their 1:1 electrolyte nature. Indeed, the molar conductivities [115 $\Omega^{-1}\cdot cm^2\cdot mol^{-1}$ (**E_1**), 103 $\Omega^{-1}\cdot cm^2\cdot mol^{-1}$ (**E_2**) and 119 $\Omega^{-1}\cdot cm^2\cdot mol^{-1}$ (**E_3**), respectively], are in the acceptable Λ_M ranges for univalent electrolytes in acetonitrile solution.[175]

II.6.1.2 Spectroscopic characterization

IR spectroscopy

In the IR spectra of complex **E_1** (*ac* as counterion) the main bands of the C-O frequencies of the carboxylate anions were identified at 1559 cm^{-1} (C-O antisym. stretch.) and 1384 cm^{-1} (C-O sym. stretch.) and respectively for complex **E_2** (*bz* as counterion) around 1558 cm^{-1} (C-O antisym. stretch.) and 1380 cm^{-1} (C-O sym. stretch.). Furthermore**,** IR spectra of complex **E_3,** the characteristic bands of the stretching SO_2 frequencies were identified at 1248 cm^{-1}(O=S=O asym. stretch.) and 1226 cm^{-1}(O=S=O sym. stretch) were identified.

^{1}H NMR spectroscopy

The ^{1}H NMR spectra were recorded in $CDCl_3$ for complexes **E_1 – E_3**. The aromatic region showed all 12 protons of the *fppy* and 8 protons of the *bpy* ligand in the range of 9.6 to 5.6 ppm. The spectra are characterized by a relatively large shift to low frequencies of proton 3A adjacent to the metallated carbon of the bidentate *fppy* ligand (*e.g*., for **E_1**, this proton resonates at 5.66 ppm).

Regarding the counterions, the singlet of the *ac* in complex **E_1** was centered at 2.0 ppm. Furthermore, the ^{1}H NMR spectrum of complex **E_2** showed in the aromatic region the additional signals regarding the 5 protons from *bz* as overlapped peaks in the range of 7.39-7.25 pp. In the aliphatic region, spectrum of complex **E_3** showed a triplate at 4.0, two multiplates at 1.60 and 1.3 ppm and singlet at 0.87 ppm**.**

II.7 Conclusions

As presented in the introduction chapter, the chemistry of cyclometallated Ir(III) complexes is a current topic of investigations because they display unique photophysical properties such as good photo- and thermal stability, high phosphorescence quantum efficiencies, relatively short lifetimes and simple colour tuning through ligand structure and control, and a set of key features for molecular-based light emitting devices applications.[26] However, it is also noteworthy that the actual performances of these molecular materials can be often severely limited because of the reduced emission efficiency in the solid state, owing to a concentration driven quenching.[176] Although different approaches, such as the dispersion of the emitters in a polymeric matrix or the introduction of sterically hindered substituents in the auxiliary ligands[177,178] have been explored to limit the concentration quenching effect, at present none of them seem to solve this problem satisfactorily. In this context, mesoporous materials can be a useful tool for the dispersion of the emitting Ir(III) complexes thus obtaining better performing Ir(III)-based luminescent materials.

Indeed, a homoleptic tris-cyclometallated Ir(III) surfactant has been recently employed in the synthesis of an amphiphile/silica co-assembled nanocomposite which was successfully used as an active layer for organic light-emitting diode. This provided a better performing device with respect to the one based on the pristine solid.[179]

In this thesis, the synthesis of hydrophilic Ir(III) luminescent complexes was followed by small changes in the molecular structure of the octahedral complex, in order to introduce different functional molecular parts able to induce a certain solubility in water of the final material. This strategy may allow an increased compatibility of the chromophore with water, or organic surfactant water systems, to yield functional structure directing agents (SDAs) for the construction of mesostructured materials.

Following the substitution of different molecular parts of the octahedral ionic Ir(III) systems with hydrophilic moieties, several water soluble complexes were obtained. Furthermore, using acetate and alkylcarboxylates as counterions, Ir(III) octahedral ionic complexes (**C_2**, **C_3** and **C_4** presented in Figure II.43) able to form supramolecular ordered systems in water were obtained.

Indeed, as demonstrated by POM measurements, ^{1}H and ^{2}H NMR spectroscopy and structural investigations made by WAXS, SAXS and SANS measurements (chapter II.4.3), these complexes form supramolecular columns made by two strands of complexes even at low concentration in water (>1.0 % w/w). On small increase of the concentration (<1.0 % w/w) a gellification of the solutions is visible. By increasing concentration of the Ir(III) complex, the columns grow unidimensionally

by keeping a quasi homogeneous cross-section constituted by the association of a small and nearly constant number of molecules. The origin of the gelification consists in close packing organisation of the interacting polyelectrolite strands, sheated in their solvatation shell.

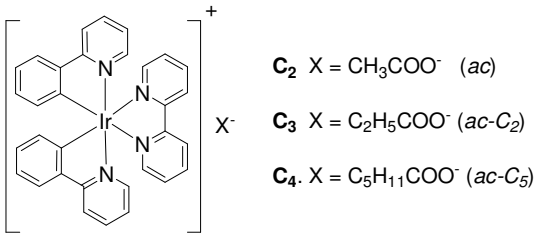

Figure II.43 Chemical structure of the complexes that show supramolecular organisations in water.

These peculiar supramolecular organisations in water, observed for the first time with Ir(III) complexes, cannot be beyond doubt classified in one of the acknowledged lyotropic, cromonic or hydrogel systems. While the lyotropism may be excluded because of the mechanism of formation and the amphiphilic molecular structure of the lyotropic sufractant molecules, these Ir(III) complexes may be classified in-between cromonics and hydrogels. Indeed, they have analogous polyeletrolite columnar structures formed by the chromonic molecules in water and show similar textures on POM, but the bulky voluminous shape of the octahedral Ir(III) complexes exclude the mechanism of the columns formation by the flat organic chromonic molecules, being more similar to the water swollen structures composed of hydrophilic self-assembled low molecular weight gelators.

These excellent results obtained for complexes **C_2 – C_4**, permit the use of the respective complexes directly as SDAs for the synthesis of functional mesoporous materials. Hence, we proceeded to the synthesis of the mesostructurated materials using complexes **C_2**, **C_3** and **C_4** directly as SDAs, employing the co-assembling process (CSA) that was described comprehensively in the introduction chapter.

II.7.1 Synthesis of mesostructured materials (MMs)

The synthesis of MMs by the co-assembling process (CSA) is based on the condensation of the inorganic source (in our case TEOS as silica source) on the low-concentration phase formed in water by the complexes **C_2**, **C_3** and **C_4** used directly as SDAs, under appropriate reaction conditions at suitable pH.

At a concentration of 1.0% in water, the complexes are organized in supramolecular columns, although at this concentration the columns are still disordered. The CSA method involves an

additional cooperative aggregation and phase separation leading to ordered organizations with molecular inorganic, which on further polymerization and condensation results in the MMs.

The use of complexes that have different chain length counterions may yield final MMs possibly with different pore sizes and hence it may contribute to its overall photophysical properties.

All mesoporous materials were prepared by a modified synthetical procedure reported in the literature.[101,180] In particular, here the synthesis of mesoporous materials using complex **C_2** is discussed further, the procedure is presented in Figure II.44.

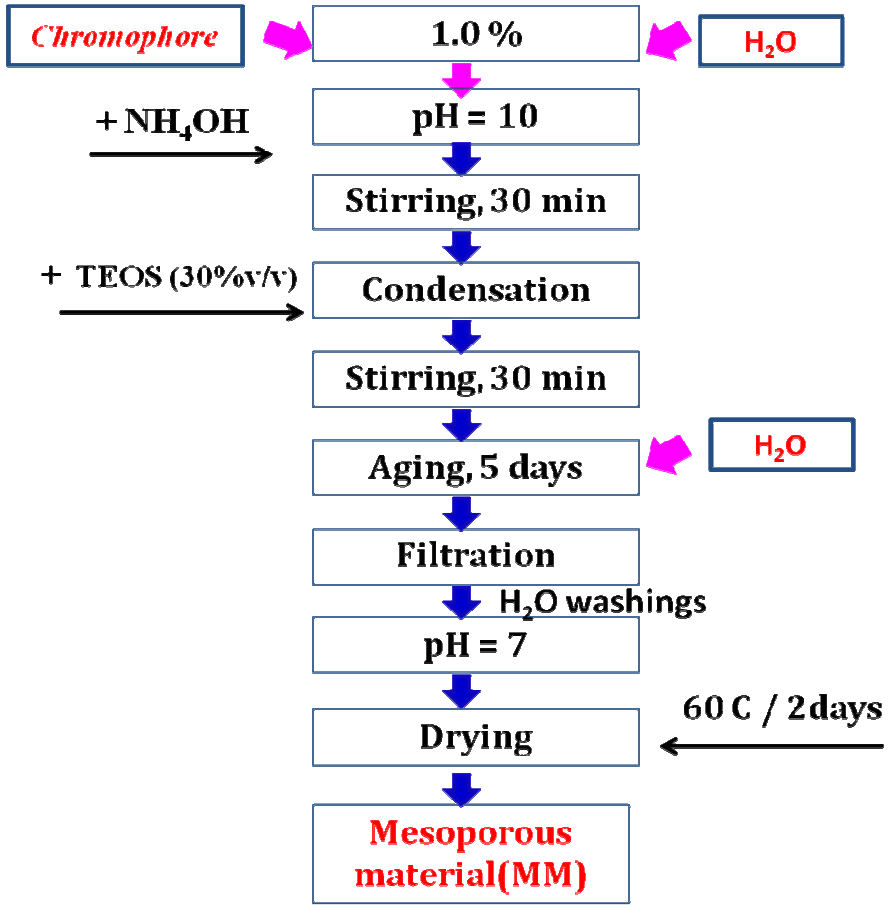

Figure II.44 Synthesis of mesoporous materials (MM) using complexes C_2, C_3 and C_4 and the CSA method

Procedure

Complex **C_2** (0.03 g, 0.04 mmol) dissolved in 3.0 g water resulted in a relatively viscous yellow-orange solution (1.0 % w/w) having the pH = 9, that was stirred well at 20°C for 2 hours. Then 0.04 ml NH_4OH (30% w/w) solution was added until pH = 10 and stirred well further for 10 minutes. Finally, 0.31 ml of tetraethoxy silane (TEOS, 1.39 mmol) was added leading to the formation of a sticky gel which was stirred for another 30 minutes. 1.0 g of water was added and the mixture was kept under vigorous stirring at 20°C for 5 days. A fine precipitate forms in time. The precipitate was

filtered out and washed with water until pH = 7. The obtained product was dried well at 60°C for 2 days.

The synthesis of all other MMs containing **C_3** and **C_4** complexes is presented in experimental section, (chapter III.5). In particular, the syntheses were conducted maintaining the same weight percentages.

The structural analysis of the mesostructured powders are still at work, whereas the photophysical properties are presented further.

II.7.2 Photophysical properties of the mesostructured materials (MM)

In order to investigate the photoluminescence properties of the newly synthesized mesostructured powder materials, a full photophysical investigation including emission spectra, phosphorescence quantum yield and time-resolved luminescence was performed for all the mesostructured materials obtained using the complexes **C_2**, **C_3** and **C_4.** The full photophysical data are summarized in Table II.9. In particular the obtained results have been compared with the photophysical properties of $[Ir(ppy)_2(bpy)]PF_6$ in THF solution.[37]

A significant blue shift of the emission maximum is observed on moving from solution to the mesostructured powders. Moreover the luminescent decay turned out to be multiexponential in nature.

Table II.9 Photophysical properties of the mesostructured powders of complexes **C_2, C_3** and **C_4**:

Complex	λ_{max}(nm)	τ[ns]	Φ[%]
[a] $[(ppy)_2Ir(bpy)]PF_6$	590	$\tau = 180$	1.8
C_2: $[(ppy)_2Ir(bpy)]ac$	539	$\tau_1 = 40$ (5.0%) $\tau_2 = 227$ (26.0%) $\tau_3 = 665$ (69.0%)	6.7
C_3: $[(ppy)_2Ir(bpy)]ac$-C_2	549	$\tau_1 = 39$ (5.0%) $\tau_2 = 290$ (28.7%) $\tau_3 = 633$ (66.3%)	5.4
C_4:$[(ppy)_2Ir(bpy)]ac$-C_5	549	$\tau_1 = 18$ (6.0%) $\tau_2 = 196$ (23.5%) $\tau_3 = 613$ (70.5%)	7.1

[a] Data concerning $[(ppy)_2Ir(bpy)]PF_6$ in air equilibrated THF solution taken from literature[37].

The change in emission energy observed on moving from solution to the mesostructures, can be associated to a shift toward higher energy of the ^{3}MLCT state owing to change of the molecular environment and medium rigidity[162], whereas the multi-exponential behaviour of the phosphorescence decays should results from the presence of different environments or different aggregation states experienced by the chromophore inside the materials.

Moreover, regarding phosphorescence quantum yield, mesostructured powders **C_2**, **C_3** and **C_4** showed, according to the observed rigidochromic behaviour, an enhanced efficiency with respect to solution.

III. Experimental section

III.1 Materials and methods

Ir(III) chloride hydrate ($IrCl_3$·xH2O) was purchased from Alfa-Aesar. 2-Phenylpyridine (*ppy*), ethylene diamine (*en*), 2-picolylamine (*pam*), 2,2'-bipyridine (*bpy*) , 2-(2,4-dichlorophenyl)pyridine (*fppy*), silver nitrate ($AgNO_3$), acetic acid (AcOH), propionic acid (C_2H_5COOH), hexanoic acid ($C_5H_{11}COOH$), octanoic acid ($C_7H_{15}COOH$), 1-bromooctane (C_8H_{17}), 1-bromododecane ($C_{12}H_{15}Br$), 11-bromoundecan-1-ol ($BrC_{11}H_{22}OH$), sodium dodecyl sulfate ($C_{12}H_{25}OSO_3Na$), trifluoroacetic acid (CF_3COOH), 4,4'-bis(methoxy)-2,2'-bipyridine (bpy-OCH_3), methyl 3,4,5-trihydroxybenzoate ($C_8H_8O_5$), tetraethoxy silane (TEOS), ammonium hydroxide (NH_4OH), ammonium hexaflourophosphate (NH_4PF_6) and potassium perchlorate ($KClO_4$) were purchased from Aldrich and used as received.

Counterions acetate (*ac*), benzoate (*bz*) and 3,4,5-tris-ocyloxybenzoate (*bz-C_8*), hexadecanoate (*ac-C_{15}*), and 3,4,5-tris-dodecyloxybenzoate (*bz-C_{12}*), propionate (*ac-C_2*), hexanoate (*ac-C_5*), octanoate (*ac-C_7*), trifluoroacetate (*tfa*) and dodecylsulfate (*dos*) were prepared by using literature processes.[132] The ligands 4,4'-bis(hydroxy)-2,2'-bipyridine (*bpy-OH*), 4,4'-bis(hydroxymethyl)-2,2'-bipyridine (bpy-CH_2OH), 4,4'-bis(dodecyloxy)-2,2'-bipyridine (*bpy-C_{12}*), 4,4'-bis(oxy-undecan-1-ol)-2,2'-bipyridine (*bpy-$C_{11}OH$*) and 4,4'-bis(tert-butyldimethylsilylundecyloxy)-2,2'-bipyridine (*bpy-$C_{11}OTBDMS$*) were also prepared by modifying the literature.[167,181] The solvents were used as received from commercial sources without further purification. All procedures involving $IrCl_3$·xH2O or any other Ir(III) species were carried out in an inert atmosphere. [Ir(*ppy*)$_2$]$_2$-μCl_2 precursor was prepared according to literature procedures.[66, 70]

^{1}H NMR spectra were acquired on a Bruker Avance DRX-300 spectrometer in deuterated solvents with TMS as internal standard. The ^{2}H-NMR spectrum was recorded at variable temperatures (298 K) on a Bruker Avance 500 MHz (11.74 T) instrument. Infrared spectra were recorded with a Spectrum 100 FT-IR Perkin-Elmer spectrometer (KBr pellets). Elemental analyses were performed with a Perkin-Elmer 2400 microanalyzer by the Microanalytical Laboratory at University of Calabria. Thermogravimetry (TGA) measurements were performed on a Perkin-Elmer TGA6 Thermogravimetric Analyser. The TGA traces were obtained on heating the samples at 10 °C min−1 from 25 to 350 °C.

Differential scanning calorimetry (DSC) measurements were made with a Perkin–Elmer Pyris 1 Differential Scanning Calorimeter. The DSC traces were obtained while heating the samples from 25 to 250 °C for DSC with heating-cooling rates: 10 °C/min.

Photophysical techniques

Spectrofluorimetric grade solvents were used for the photophysical investigations in solution for all the complexes. Absorption spectra were recorded with an UV-Vis Perkin-Elmer Lambda 900 spectrophotometer. Steady-state emission spectra were recorded on a Horiba JobinYvonFluorolog 3 spectrofluorimeter, equipped with a Hamamatsu R-928 photomultiplier tube. Emission quantum yields of a sample in solution were determined using the optically dilute method on deaerated solutions, whose absorbance at excitation wavelengths were <0.1; $Ru(bpy)_3Cl_2$ (*bpy* = 2,2′-bipyridine) in H_2O was used as standard (Φ= 0.028).[182,183] The experimental uncertainty on the emission quantum yields is 10%. The emission quantum yields of solid samples were obtained by means of a 102 mm diameter integrating sphere, coated with Spectralon® and mounted in the optical path of the spectrofluorimeter, using as excitation source a 450 W Xenon lamp coupled with a double-grating monochromator for selecting wavelengths.

X-ray crystallographic analysis

Single crystal XRD data were collected at room temperature with a Bruker-Nonius X8APEXII CCD area detector system equipped with a graphite monocromator with radiation Mo Kα (λ = 0.71073 Å). These data were processed through the SAINT[184] reduction and SADABS[185] absorption softwares. Nevertheless, an unsolved absorption effect, giving rise to high residual density peaks in the proximity of the Ir(III) metal centre, was observed during the final structure refinement of complex $\mathbf{A_1}$.

The structures were solved by direct methods through the *SHELXTL-NT*[186] structure determination package and refined by full-matrix least-squares based on F^2.

Generally, all non-hydrogen atoms were refined anisotropically and hydrogen atoms were included as idealized riding atoms. In the case of complexes $\mathbf{A_2}$ and $\mathbf{B_4}$, suitable hydrogen atoms were located from the difference map for the solvent water molecules and refined with restrain. In complex $\mathbf{A_1}$ and $\mathbf{B_6}$, two ($\mathbf{A_1}$) and four ($\mathbf{B_6}$) crystallization water molecules are present, but it was not possible to locate suitable hydrogen atoms from the difference map. In complex $\mathbf{C_1}$, three oxygen atoms of crystallized water molecules are located from the difference map, two of them with an occupancy factor of 0.5. Even in this case, it was not possible to locate suitable hydrogen atoms.

The final geometrical calculations and the graphical manipulations were performed using the XP utility of SHELXTL system and DIAMOND program.[187]

X-ray and neutron analysis

WAXS patterns were obtained by using a linear monochromatic Cu Kα1 beam (λ =1.5405 Å) from a sealed-tube generator equipped with a bent quartz monochromator and a curved Inel CPS120 detector. SAXS patterns were obtained at the Institut Charles Sadron (ICS), CNRS-UPR 22, France, with a S-MAX3000 system equipped with a MicroMax-007HF rotating anode from Rigaku-Elexience, for small scattering vectors (0.0065 to 0.16 $Å^{-1}$) and with a Nanostar setup of Bruker-AXS, equipped with a Fox-2D Xenocs mirror, for large scattering vectors (up to 0.85 $Å^{-1}$). In all cases, X-ray measurements were performed at room temperature on samples contained in home built sealed cells of 1 mm thickness and with mica windows. SANS patterns were conducted on the spectrometer PACE (Laboratoire Léon Brillouin, Saclay, France) at room temperature by using 2.5 mm thick quartz cells, in two configurations (λ =4.5 Å, detector to sample distances of 4.7 and 1 m, respectively), giving access to scattering vectors between 0.01 and 0.5 $Å^{-1}$. SAXS and SANS data were set in absolute scale with 10 percent maximum error on the intensity calibration.

III.2 Synthesis and structural characterization of the ligands

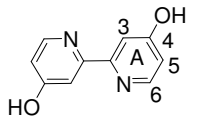

4,4'-bis(hydroxy)-2,2'-bipyridine *(bpy-OH)*: To a solution of 4,4′-dimethoxy-2,2′-bipyridine (2.95 g, 14 mmol) in 170 mL of glacial acetic acid was added 48 wt % HBr solution in water (24 mL, 140 mmol). The mixture was refluxed 48 hours. After the mixture had cooled to room temperature, solvent was removed in vacuum. The residue was dissolved in water and neutralized by adding aqueous ammonium hydroxide. This produced a white solid that was filtered and dried. This was used for the next step without further purification. Yield: 1.76 g (67%). M. p.: > 300°C. Anal. Calcd. for [$C_{10}H_8N_2O_2$] (188.18 g/mol): C, 63.82; H, 4.28; N, 14.89. Found: C, 63.76; H, 4.25; N, 14.80%. ^{1}H NMR [$(CD_3)_2SO$ 300 MHz)]: δ 8.19 (2H, d, ^3J = 6.24 Hz, H^{6a}), 7.25 (2H, d, ^4J = 2.21 Hz, H^{3a}), 6.76 (2H, dd, J = 6.23 Hz, 2.20 Hz, H^{5a}). IR (KBr/cm^{-1}): 3084.87, 3005.08 (C-H).

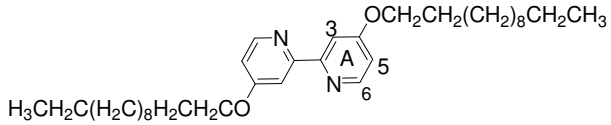

4,4'-bis(dodecyloxy)-2,2'-bipyridine (*bpy*-C_{12}): To a suspension of 4,4′-dihydroxy-2,2′-bipyridine *(bpy-OH)* (0.300 g, 1.559 mmol) in 60 mL of DMF was added 1-bromododecane (0.874 g, 3.507 mmol), anhydrous potassium carbonate (1.105 g, 7.997 mmol), and a catalytic amount of KI. The mixture was refluxed and stirred vigorously for 48 h. After the mixture had cooled at room temperature, the solid residue obtained was filtered and DMF was evaporated to dryness under reduced pressure. Then 50 ml $CHCl_3$ and 50 ml saturated NH_4Cl solution were added. The organic layer was separated and washed with 45 ml of water thrice (15x3). Finally organic layer passed dried over Na_2SO_4 and the pure product was obtained from recrystallization by $CHCl_3$/MeOH. Yield: 30% (0.252 g); M. p.: 99°C. Anal. Calcd. for [$C_{34}H_{56}N_2O_2$] (524.82 g/mol): C, 77.81; H, 10.76; N, 5.34. Found: C,77.75; H, 10.70; N, 5.25%. ^{1}H NMR ($CDCl_3$, 300 MHz): δ 5.49 (2H, d, J = 6.24 Hz, H^{6a}), 7.93 (2H, d, J = 2.21 Hz, H^{3a}), δ 6.81 (2H, dd, J = 5.49 Hz, J = 2.58 Hz, H^{5a}), δ 4.12 (4H, t, J = 6.6 Hz, OCH_2), δ 1.80 (4H, m, OCH_2CH_2), δ 1.61 (32H, m, $OCH_2CH_2(CH_2)_8$), δ 1.26 (4H, m, ($OCH_2CH_2(CH_2)_8CH_2$), δ 0.87 (6H, t, ^3J = 6.0 Hz, $OCH_2CH_2(CH_2)_8CH_2CH_3$). IR (KBr/cm^{-1}): 3430 (OH), 2919.4 ($\nu_{as}(CH_2)$), 2849 ($\nu_s(CH_2)$).

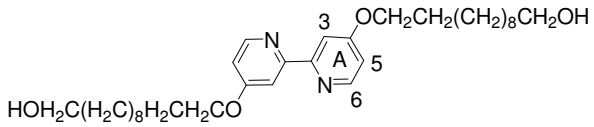

4,4'-bis(oxy-undecan-1-ol)-2,2'-bipyridine (*bpy-C$_{11}$OH*): To a suspension of 4,4′-dihydroxy-2,2′-bipyridine *(bpy-OH*) (0.500 g, 2.657 mmol) in 90 mL of DMF were added 11-bromoundecan-1-ol (*bpy*-$C_{11}OH$) (1.467 g, 5.845 mmol), anhydrous potassium carbonate (1.836 g, 13.285 mmol), and a catalytic amount of KI. The mixture was refluxed and stirred vigorously for 48 h. After the mixture had cooled to room temperature, the solid residue obtained was filtered and DMF was evaporated to dryness under reduced pressure. Then 50 ml $CHCl_3$ and 50 ml saturated NH_4Cl solution were added. The organic layer was separated and washed with 45 ml of water thrice (15x3). Finally organic layer passed through Na_2SO_4 and the pure product was obtained from recrystallization by $CHCl_3$/MeOH. Yield 54% (0.252 g); M. p.: 119°C. Anal. Calcd. for [$C_{32}H_{52}N_2O_4$] (528.77 g/mol): C, 72.69; H, 9.91; N, 5.30. Found: C,72.60; H,9.85; N, 5.20 %. ^{1}H NMR ($CDCl_3$, 300 Mz): δ 8.40 (2H, d, *J* = 5.87 Hz, H^{6a}), 7.90 (2H, d, *J* = 2.57 Hz, H^{3a}), δ 6.80 (2H, dd, *J* = 5.85 Hz, *J* = 2.57 Hz, H^{5a}), δ 4.12 (4H, t, *J* = 6.6 Hz, -OCH_2), δ 3.64 (4H, t, *J* = 6.6 Hz, -CH_2OH), δ 1.83 (4H, m, CH_2-$(CH_2)_8$), δ 1.51 (32H, m, -$(CH_2)_8CH_2OH$). IR (KBr/cm^{-1}): 3430 (OH), 2920.7 ($\nu_{as}(CH_2)$), 2850.8 ($\nu_s(CH_2)$).

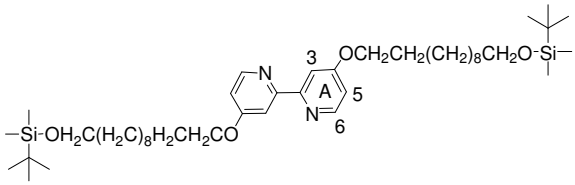

4,4'-bis(*tert*-butyldimethylsilylundecyloxy)- 2,2'-bipyridine (*bpy-C$_{11}$OTBDMS*): To a suspension of 4,4′-dihydroxy-2,2′-bipyridine *(bpy-OH*) (0.560 g, 2.976 mmol) in 90 mL of DMF were added [(11-bromoundecyl)oxy)(tert-butyl)dimethylsilane (2.176 g, 4.952 mmol), anhydrous potassium carbonate (2.056 g, 14.83 mmol), and a catalytic amount of KI. The mixture was refluxed and stirred vigorously for 48 h. After the mixture had cooled to room temperature, the solid residue obtained was filtered and DMF was evaporated to dryness under reduced pressure. Then 50 ml $CHCl_3$ and 50 ml saturated NH_4Cl solution were added. The organic layer was separated and washed with 45 ml of water thrice (15x3). Finally organic layer passed through Na_2SO_4 and the pure product was obtained from recrystallization by $CHCl_3$/MeOH. Yield: 65% (1.46 g); M. p.: 72 °C. Anal. Calcd. for [$C_{44}H_{80}N_2O_4Si_2$] (757.29 g/mol): C, 69.78; H, 10.65; N, 3.70. Found: C, 69.70; H, 10.70; N, 3.56 %: ^{1}H NMR ($CDCl_3$ 300 MHz): δ 8.45 (2H, d, *J* = 5.49 Hz, H^{6a}), 7.90 (2H, d, *J* = 2.58 Hz, H^{3a}), δ 6.80 (2H, dd, *J* = 5.85 Hz, *J* = 2.55 Hz, H^{5a}), δ 4.12 (4H, t, *J* = 6.42 Hz, -OCH_2), δ 3.59 (4H, t, *J* = 6.6 Hz, CH_2OCSi), δ 1.82 (4H, m, $CH_2(CH_2)_8$), δ 1.40 (32H, m, $(CH_2)_8CH_2O$), δ 0.89 (18H, s, $(CH_3)_3CSi$), δ 0.041 (12H, s, $(CH_3)_2CSi$). IR (KBr/cm^{-1}): 2927.6 ($\nu_{as}(CH_2)$, 2851.3 ($\nu_s(CH_2)$).

III.3 Synthesis and structural characterization of the Ag(I) salts containing the carboxylate counterions

All counterions were prepared similarly and one example is given. All counterions were obtained in yields ranging from 80–85%.

In particular, the corresponding acid precursor was reacted with NaOH in EtOH/H_2O solution, (scheme III.1). After two hours of stirring at r.t., an equimolecular amount of $AgNO_3$ was added and the mixture was further stirred for 2 hours. The products, formed as a white precipitates in the reaction mixture, were filtered out, washed with water, dried and used without further purification.

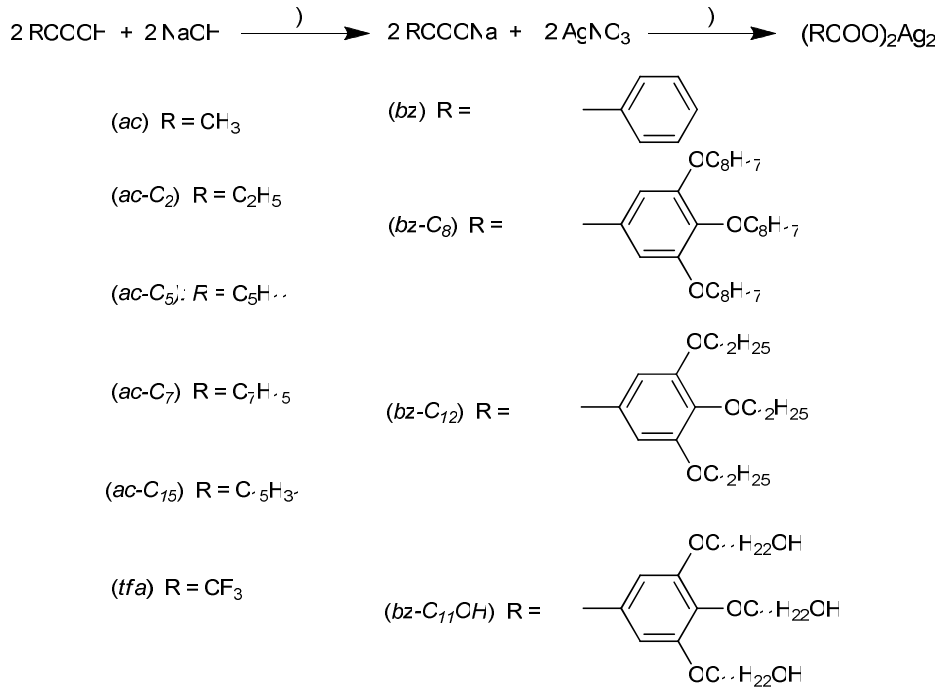

Scheme III.1 Synthesis and chemical Ag(I) salts: i) 2 hours, r.t, ii) 2 hours, r.t.

$Ag_2(ac)_2$: Yield: 86%. Anal. Calcd. $C_4H_6Ag_2O_4$ (FW 333.82 g/mol): C, 14.39; H, 1.81; found: C, 14.51; H, 1.74. IR(KBr): 1569.8 cm^{-1} ($\nu_{as}(COO^-)$); 1408.4 cm^{-1} ($\nu_s(COO^-)$).

$Ag_2(ac\text{-}C_2)_2$: Yield: 85%. Anal. Calcd. $C_6H_{10}Ag_2O_4$ (FW 361.88 g/mol): C, 19.91; H, 2.79; found: C, 19.82; H, 3.08. IR(KBr): 1571.0 cm^{-1} ($\nu_{as}(COO^-)$); 1418.5 cm^{-1} ($\nu_s(COO^-)$).

$Ag_2(ac\text{-}C_5)_2$: Yield 87%. Anal. Calcd. $C_{12}H_{22}Ag_2O_4$ (FW 446.04 g/mol): C, 32.31; H, 4.97; found: C, 32.42; H, 5.16. IR(KBr): 1563.5 cm^{-1} ($\nu_{as}(COO^-)$); 1411.9 cm^{-1} ($\nu_s(COO^-)$).

$Ag_2(ac\text{-}C_7)_2$: Yield: 84%. Anal. Calcd. $C_{16}H_{30}Ag_2O_4$ (502.14 g/mol): C, 38.27; H, 6.02; found: C, 38.61; H, 6.16. IR(KBr): 1564.6 cm^{-1} ($\nu_{as}(COO^-)$); 1415.2 cm^{-1} ($\nu_s(COO^-)$).

$Ag_2(ac\text{-}C_{15})_2$: Yield: 89%. Anal. Calcd. $C_{32}H_{62}Ag_2O_4$ (726.57 g/mol): C, 52.90; H, 8.60 %. Found: C, 52.85; H, 8.50 %. IR(KBr): 1519.0 cm^{-1} ($\nu_{as}(COO^-)$); 1419.9 cm^{-1} ($\nu_s(COO^-)$).

$Ag_2(tfa)_2$: Yield: 77%. Anal. Calcd. $C_4Ag_2F_6O_4$ (441.77 g/mol): C, 10.88 %. Found: C, 10.80 %. IR(KBr): 1687.9 cm^{-1} ($\nu_{as}(COO^-)$); 1200.0 cm^{-1} ($\nu_s(COO^-)$).

$Ag_2(bz)_2$: Yield: 82%. Anal. Calcd. $C_{14}H_{10}Ag_2O_4$ (457.96 g/mol): C, 36.72; H, 2.20 %. Found: C, 36.59; H, 2.18 %. IR(KBr): 1520.6 cm^{-1} ($\nu_{as}(COO^-)$); 1408.4 cm^{-1} ($\nu_s(COO^-)$).

$Ag_2(bz\text{-}C_8)_2$: Yield: 81%. Anal. Calcd. $C_{62}H_{106}Ag_2O_{10}$ (1227.24 g/mol): C,60.68; H, 8.71 %. Found: C, 60.59; H, 8.59 %. IR(KBr): 1552.2.8 cm^{-1} ($\nu_{as}(COO^-)$); 1383.7 cm^{-1} ($\nu_s(COO^-)$).

$Ag_2(bz\text{-}C_{12})_2$: Yield: 84%. Anal. Calcd. $C_{86}H_{154}Ag_2O_{10}$ (1563.87 g/mol): C, 66.05; H, 9.93 %. Found: C, 66.0; H, 9.50 %. IR(KBr): 1557.9 cm^{-1} ($\nu_{as}(COO^-)$); 1367.2 cm^{-1} ($\nu_s(COO^-)$).

$Ag_2(bz\text{-}C_{11}OH)_2$: Yield: 76%. Anal. Calcd. $C_{80}H_{142}Ag_2O_{16}$ (1575.71 g/mol): C, 62.13; H, 8.81 %. Found: C, 62.10; H, 8.75 %. IR(KBr): 1560.8 cm^{-1} ($\nu_{as}(COO^-)$); 1412.2 cm^{-1} ($\nu_s(COO^-)$).

III.4 Synthesis and structural characterization of the octahedral ionic Ir(III) complexes

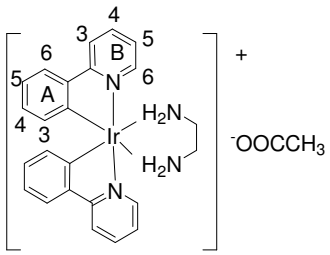

A_1. [Ir(*ppy*)$_2$(*en*)](*ac*)·1/2H$_2$O: The classical bridge-splitting reaction of the dimeric precursor [Ir(*ppy*)$_2$]$_2$-μCl$_2$ (0.150 g, 0.140 mmol) with 2,2'-bipyridine (0.017 g, 0.280mmol) in CH_2Cl_2/MeOH (20 ml, 3:1 v/v) was carried out for 4 hours under nitrogen atmosphere. Subsequently, the addition of 1.1 fold excess of Ag(I) salt containing *ac* (0.051 g, 0.154 mmol) was made and the reaction mixture, protected from light, was further stirred for 2 hours. Then the solvents were evaporated, CH_2Cl_2 was added and insoluble AgCl formed was filtered. The pure product was obtained by recrystallization from CH_2Cl_2/Hexane. Yield 0.145 g (82.3%). Dec. p.:250 ºC. Anal.Calcd. for: $[C_{26}H_{27}IrN_4O_2]$ ·1/2H_2O (628.75 g/mol): C, 49.67; H, 4.49; N, 8.91%. Found: C, 49.69; H, 4.37; N, 9.07 %. ^{1}H NMR (CD_3OD, 300 MHz): δ 8.77 (2H, d, *J* = 5.35 Hz, H^{3B}), δ 8.10 (2H, d, *J* = 7.69 Hz, H^{6A}), δ 7.93 (2H, td, *J* = 8.13 Hz, 1.38 Hz, H^{4B}), δ 7.66 (2H, dd, *J* =7.83, 0.96 Hz, H^{6B}), δ 7.38 (2H, m, H^{3B}), δ 6.82 (2H, td, *J* = 7.41 Hz, 1.05 Hz, H^{4A}), δ 6.66 (2H, td, *J* = 7.54 Hz, 1.24 Hz, H^{4B}), δ 6.23(2H, dd, *J* = 7.61 Hz, 0.75 Hz, H^{6B}), δ 4.60 (2H, m, NH_2), δ 3.8 (2H, m, NH_2), δ 2.90 (2H, m, CH_2), δ 2.70 (2H, m, CH_2), δ 1.88 (3H, S, CH_3). IR (KBr/cm^{-1}): 3381 (υ_{as}(NH)), 3237 (υ_s(NH)), 3059, 3037, 2966 (υ_{as}(CH_3)), 1562.2 (υ_{as} (COO^-)), 1417.9 (υ_s(COO^-)). Λ_M (c = 9.6·10^{-5}·mol·L^{-1}) = 127 Ω^{-1}·cm^2 ·mol^{-1} (acetonitrile). The TGA and DSC traces of complex **A_1** is shown in Figure III.1.

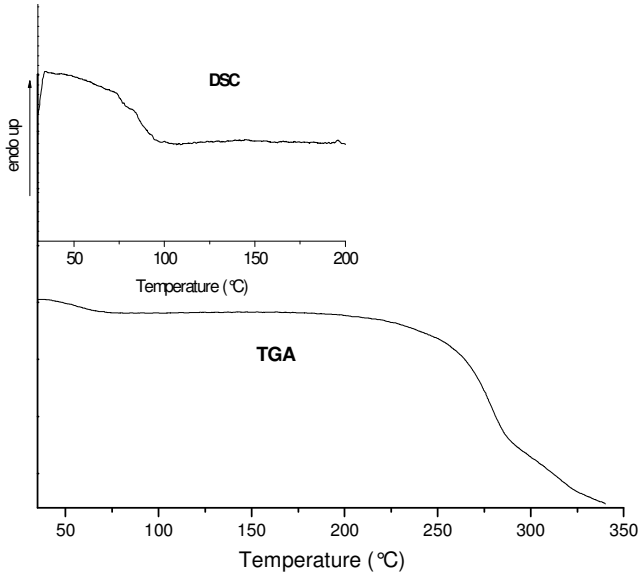

Figure III.1 TGA and DSC scans for complex $\mathbf{A_1}$, [Ir(*ppy*)$_2$(*en*)]ac·1/2H_2O: experimental weight loss of 1.29 % corresponding to 2 molecules of water (calcd. 1.13 %).

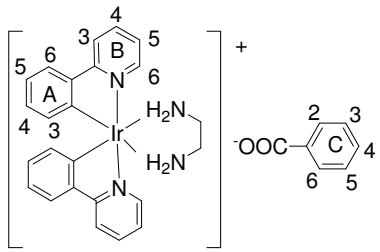

A_2. [Ir(*ppy*)$_2$(*en*)](*bz*)·2H_2O: A stirred suspension of [Ir(*ppy*)$_2$]$_2$-μCl_2 (0.150 g, 0.140 mmol) and ethylene diamine (0.017 g, 0.280 mmol) in CH_2Cl_2/MeOH (20 ml, 3:1 v/v) was carried out for 4 hours under nitrogen atmosphere. Subsequently, the addition of 1.1 fold excess of Ag(I) salt containing *bz* (0.070 g, 0.154 mmol) was made and the reaction mixture, protected from light, was further stirred for 2 hours. Then the solvents were evaporated, CH_2Cl_2 was added and insoluble AgCl formed was filtered. The pure product was obtained after recrystallization from CH_2Cl_2/Hexane. Yield: 0.163 g (81%). Dec. p.: 250 °C. Anal.Calcd. for [$C_{31}H_{29}IrN_4O_2$] ·2H_2O (717.84 g/mol): C, 51.87; H, 4.63; N, 7.80%. Found: C, 52.05; H, 4.40; N, 7.31%. ^{1}H NMR (CD_3OD, 300 MHz): δ 8.77 (2H, d, *J* = 5.86 Hz, H^{3B}), δ 8.09 (2H, *J* = 8.07 Hz, H^{6A}), δ 7.93 (4H, overlapped peaks, H^{4B}, H^{5A}), δ 7.66 (2H, d, *J* =7.71 H^{6B}), δ 7.36 (5H, overlapped peaks, H^{2C}, H^{3C}, H^{4C}, H^{5C}, H^{6C}), δ 6.81 (2H, t, *J* = 7.57 Hz, H^{5B}), δ 6.66 (2H, t, *J* = 7.06 Hz,H^{4A}), δ 6.23 (2H, d, *J* = 7.68, H^{6B}), δ 4.63 (2H, m, NH_2), δ 3.8 (2H, m, NH_2), δ 2.94 (2H, m, CH_2), δ 2.74 (2H, m, CH_2). IR (KBr/cm^{-1}): 3394 (υ_{as}(NH)), 3256 (υ_s(NH)), 3288.3, 3144.1, 3059.5 (C-H), 2966.8 (υ_{as}(CH_2)), 2888 (υ_s(CH_2)), 1552 (υ_{as}(COO^-)), 1382 (υ_s(COO^-)). Λ_M (*c* = 8.8·10^{-5} mol·L^{-1}) = 103 Ω^{-1}·cm^2·mol^{-1} (acetonitrile). The TGA and DSC traces of complex $\mathbf{A_2}$ is shown in Figure III.2.

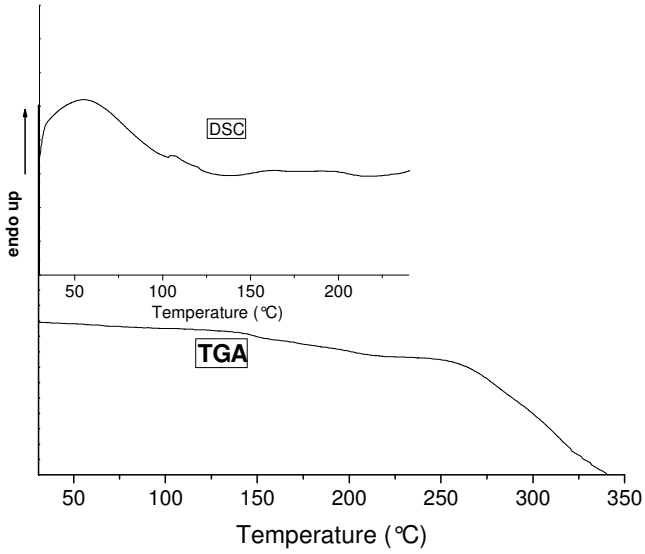

Figure III.2 TGA and DSC scans for complex $\mathbf{A_2}$, [Ir(*ppy*)$_2$(*en*)]ac·*2*H$_2$O: experimental weight loss of 5.13 % corresponding to 2 molecules of water (calc. 5.06 %).

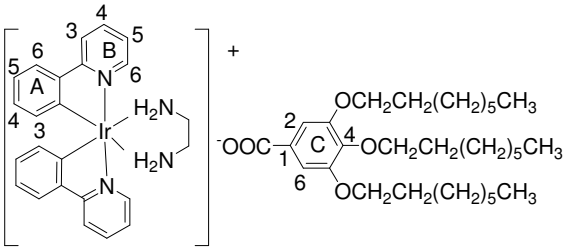

A_3. [Ir(*ppy*)$_2$(*en*)](*bz-C$_8$*)·xH_2O: A stirred suspension of [Ir(*ppy*)$_2$]$_2$-μCl$_2$ (0.150 g, 0.140 mmol) and ethyldiamine (0.017 g, 0.280 mmol) in CH_2Cl_2/MeOH (20 ml, 3:1 v/v) was carried out for 4 hours under nitrogen atmosphere. Subsequently, the addition of 1.1 fold excess of Ag(I) salt containing *ac* (0.180 g, 0.154 mmol) was made and the reaction mixture, protected from light, was further stirred for 2 hours. Then the solvents were evaporated, CH_2Cl_2 was added and insoluble AgCl formed was filtered. The pure product was obtained after recrystallization with CH_2Cl_2/Hexane. Yield: 0.230 g (75%). M. p.: 195°C. Anal.Calcd. for $[C_{55}H_{77}IrN_4O_5]$ ·3/2H_2O (1093.47 g/mol): C, 60.41; H, 7.37; N, 5.12%. Found: C, 60.13; H, 6.99; N, 4.91%. ^{1}H NMR ($CDCl_3$, 300 MHz): δ 8.91 (2H, d, *J* = 5.49 Hz, H^{6A}), δ 7.72 (4H, overlapped peacks, H^{6A}, H^{4B}), δ 7.33 (2H, *J* = 7.69 Hz, H^{6B}), δ 7.22 (2H, s, H^{2C}, H^{6C}), δ 7.08 (2H, t, *J* = 6.04 Hz, H^{5A}), δ 6.71 (2H, t, *J* = 7.51 Hz, H^{5B}), δ 6.57 (2H, t, *J* = 7.14 Hz, H^{4A}), δ 6.11 (2H, d, *J* = 7.14 Hz, H^{3A}), δ 4.79 (2H, m, NH_2), 3.94 (6H, m, OCH_2), δ 2.94 (2H, m, NH_2), 2.79 (2H, m, CH_2), 2.53(2H, m, CH_2), δ 1.76 (6H, m, OCH_2CH_2), δ 1.36 (30H, m, $OCH_2CH_2(CH_2)_5CH_3$), δ 0.87 (9H, t, ^3J = 6.6 Hz, $OCH_2CH_2(CH_2)_5CH_3$). IR (KBr/cm^{-1}): 3429 (υ_{as}(NH)), 3294 (υ_s(NH)), 2954.9 (υ_{as}(CH_3)), 2926.0 (υ_{as}(CH_2)), 2855.0 (υ_s(CH_2)), 1550 (υ_{as}(COO^-)), 1375 (υ_s(COO^-)). Λ_M (c = 9.37·10^{-5} mol·L^{-1})= 61 Ω^{-1}·cm^2·mol^{-1} (methanol).

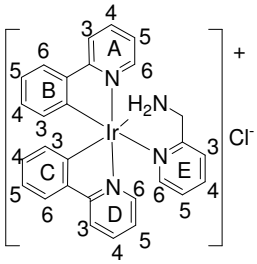

B_1. [Ir(*ppy*)$_2$(*pam*)](Cl)·1H_2O: The classical bridge-splitting reaction of the dimeric precursor [Ir(*ppy*)$_2$]$_2$-μCl_2 (0.153 g, 0.143 mmol) with 2-picolylamine (0.031 g, 0.285mmol) in CH_2Cl_2/MeOH (20 ml, 3:1 v/v) was carried out for 6 hours under nitrogen atmosphere. After 6 h the resulting yellow solution was cooled to room temperature and stirred overnight. Then the solvents were evaporated, CH_2Cl_2 was added and an insoluble white inorganic salt formed was filtered. The pure product was obtained by recrystallization from CH_2Cl_2/Hexane. Yield: 0.170 g (90%). Dec. p.: 180 °C. Anal. Calcd as solvate form: [$C_{28}H_{26}ClIrN_4O$] ·1H_2O, (662.2 g/mol): C, 50.79; H, 3.96; N, 8.46. Found: C, 50.85; H, 3.95; N, 8.49%. ^{1}H NMR ($CDCl_3$, 300 MHz): δ 9.76 (1H, d, J = 5.7 Hz, H^{6E}), δ 7.98–7.58 (9H, overlapped peaks, H^{6A}, H^{6D}, H^{5E}, H^{5A}, H^{5D}, H^{3A}, H^{3D}, H^{6B}, H^{6C}), δ 7.53 (1H, d, J = 6.6 Hz, H^{3E}), δ 7.32 (1H, t, J = 6.2 Hz, H^{4E}), δ 7.26 (1H, m, NH_2), δ 7.10–6.99 (2H, overlapped peaks, H^{4A}, H^{4D}), δ 6.94 (1H, t, J = 7.6 Hz, H^{5C}), δ 6.84–6.68 (3H, overlapped peaks, H^{5B}, H^{4B}, H^{4C}), δ 6.30 (1H, d, J = 7.6 Hz, H^{3B}), δ 6.21 (1H, d, J = 7.6 Hz, H^{3C}), δ 5.08 (1H, m, NH_2), δ 4.23 (1H, m, CH_2), δ 3.50 (1H, br, CH_2). IR (KBr/cm^{-1}): 3410 (υ_{as}(NH)), 3214 ((υ_s(NH)). Λ_M (c = 8.58·10^{-5} mol·L^{-1}) = 112 Ω^{-1}·cm^2·mol^{-1} (acetonitrile).

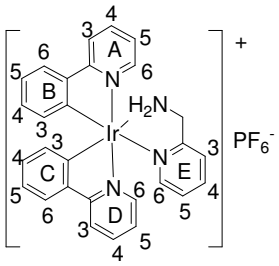

B_2. [Ir(*ppy*)$_2$(*pam*)](PF$_6$): The classical bridge-splitting reaction of the dimeric precursor [Ir(*ppy*)$_2$]$_2$-μCl_2 (0.153 g, 0.143 mmol) 2-picolylamine (0.031 g, 0.285 mmol) in CH_2Cl_2/MeOH (20 ml, 3:1 v/v) was carried out for 4 hours under nitrogen atmosphere. Subsequently, the addition of 5 fold excess of inorganic salt containing PF_6 (0.116 g, 0.714 mmol) was made and the reaction mixture, was further stirred for 2 hours. Then the solvents were evaporated, CH_2Cl_2 was added and insoluble salt formed was filtered. The pure product was obtained after recrystallisation from acetone/hexane. Yield: 0.175 g (81%). Dec. p.: 150 °C. Anal. Calcd for $C_{28}H_{24}F_6IrN_4P$ (753.70 g/mol): C, 44.62; H, 3.21; N, 7.42%. Found: C, 44.62; H, 3.13; N, 7.37%. ^{1}H NMR ($(CD_3)_2CO$, 300 MHz): δ 9.08 (1H, d, J = 5.9 Hz, H^{6E}), 8.28–8.20 (2H, overlapped peaks, H^{6A}, H^{6D}), 8.05–7.94 (5H, overlapped peaks, H^{5E}, H^{5A}, H^{5D}, H^{3A}, H^{3D}), δ 7.85–7.76 (3H, overlapped peaks, H^{6B}, H^{6C}, H^{3E}), δ 7.42–7.34 (2H, overlapped peaks, H^{4A}, H^{4D}), δ 7.30 (1H, td, J = 6.6 Hz, 1.5 Hz, H^{4E}), δ 6.96 (1H, td, J = 7.5 Hz, ^4J = 1.5 Hz, H^{5B}), δ 6.92–6.79 (2H, overlapped peaks, H^{5C}, H^{4B}), δ 6.75 (1H, td, J = 7.5 Hz, 1.5 Hz, H^{4C}), δ 6.32–6.24 (2H, overlapped peaks, H^{3B}, H^{3C}), δ 5.42 (1H, m, NH_2), δ 5.70–4.90 (2H, overlapped peaks, NH_2, CH_2), δ 4.77 (1H, m, CH_2). IR (KBr,

cm^{-1}): 3347 (υ_{as}(NH)), 3304.3 (υ_{s}(NH)). Λ_M (c = $8.98\cdot10^{-5}$ $mol\cdot L^{-1}$) = 122 $\Omega^{-1}\cdot cm^2\cdot mol^{-1}$ (acetonitrile).

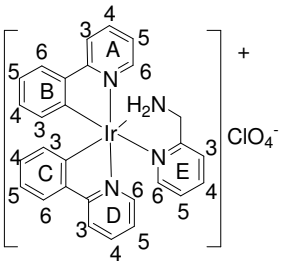

B_3. [Ir(*ppy*)$_2$(*pam*)](ClO$_4$): The classical bridge-splitting reaction of the dimeric precursor [Ir(*ppy*)$_2$]$_2$-μCl$_2$ (0.153 g, 0.143 mmol) and 2-picolylamine (0.031 g, 0.285 mmol)in CH_2Cl_2/MeOH (20 ml, 3:1 v/v) was carried out for 2 hours under nitrogen atmosphere. Subsequently, the addition of 5 fold excess of inorganic salt containing $KClO_4$ (0.100 g, 0.714 mmol) was made and the reaction mixture was further stirred for 4hours. Then the solvents were evaporated, CH_2Cl_2 was added and insoluble salt formed was filtered. The pure product was obtained by recrystallization from CH_2Cl_2/Hexane was washed with ethanol, yielding the pure product. Yield: 0.162 g (80%). Dec. p.: 270 °C. Anal. Calcd for [$C_{28}H_{24}ClIrN_4O_4$] (708.18 g/mol): C, 47.49; H, 3.42; N, 7.91%. Found: C, 47.51; H, 3.42; N, 7.68%. ^{1}H NMR ($(CD_3)_2CO$, 300 MHz): δ 9.13 (1H, d, ^3J = 5.6 Hz, H^{6E}), δ 8.27–8.18 (2H, overlapped peaks, H^{6A}, H^{6D}), δ 8.08–7.90 (4H, overlapped peaks, H^{5E}, H^{5A}, H^{5D}, H^{3A}), δ 7.85–7.75 (4H, overlapped peaks, H^{3D}, H^{6B}, H^{6C}, H^{3E}), δ 7.40–7.25 (3H, overlapped peaks, H^{4A}, H^{4D}, H^{4E}), δ 6.96 (1H, t, J = 7.3 Hz, H^{5B}), δ 6.90–6.80 (2H, overlapped peaks, H^{5C}, H^{4B}), δ 6.74 (1H, t, J = 7.4 Hz, H^{4C}), δ 6.35–6.25 (2H, overlapped peaks, H^{3B}, H^{3C}), δ 5.45 (1H, m, NH_2), 5.10–4.85 (2H, overlapped peaks, NH_2, CH_2), δ 4.75 (1H, m, CH_2). IR (KBr/cm^{-1}): 3309 (υ_{as}(NH)), 3278 (υ_{s}(NH)). Λ_M (c = $8.08\cdot10^{-5}$ $mol\cdot L^{-1}$) = 108 $\Omega^{-1}\cdot cm^2\cdot mol^{-1}$ (acetonitrile).

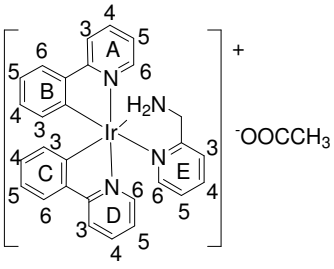

B_4. [Ir(*ppy*)$_2$(*pam*)](*ac*)·3/2H$_2$O: The classical bridge-splitting reaction of the dimeric precursor [Ir(*ppy*)$_2$]$_2$-μCl$_2$ (0.150 g, 0.140 mmol) with 2-picolylamine (0.030 g, 0.280 mmol)in CH_2Cl_2/MeOH (20 ml, 3:1 v/v) was carried out for 4 hours under nitrogen atmosphere. Subsequently, the addition of 1.1 fold excess of Ag(I) salt containing *ac* (0.051 g, 0.308 mmol) was made and the reaction mixture, protected from light, was further stirred for 2 hours. Then the solvents were evaporated, CH_2Cl_2 was added and insoluble AgCl formed was filtered. The pure product was obtained by recrystallization from CH_2Cl_2/Hexane. Yield: 0.152 g (78%). Dec. p.: 250 °C. Anal.Calcd as solate form [$C_{30}H_{27}IrN_4O_2$] ·3/2H_2O (694.81 g/mol): C, 51.86; H, 4.35; N, 8.06%. Found: C, 51.48; H, 4.33; N, 7.93%. ^{1}H NMR ($CDCl_3$, 300 MHz): δ 9.54

(1H, d, J = 5.29 Hz, H^{6E}), δ 9.53-7.57 (11H, overlappedpeaks, H^{6A}, H^{6D},H^{5E}, H^{5A}, H^{5D}, H^{3A}, H^{3D},H^{6B}, H^{6C},H^{3E}), δ 7.47 (1H, m, NH_2), δ 7.37 (1H, t, J = 6.6 Hz,H^{4E}), δ 7.11 (2H, t, J =6.6 Hz,H^{4A}, H^{4D}), δ 7.01 (1H, t, J = 7.4 Hz,H^{5C}), δ 6.95-6.80 (3H, overlapped peak, H^{5B}, H^{4B}, H^{4C}), δ 6.38 (1H, d, J = 6.75Hz, H^{3B}), δ 6.31(1H, d, J = 7.63 Hz, H^{3C}), δ 1.9 (3H, s, $OOCCH_3$). IR (KBr/cm^{-1}): 3398.5 (υ_{as}(NH)), 3210.1 (υ_s(NH)), 3107.4, 3057.9, ($\nu_{as}(CH_3)$), 1562.8 ($\nu_{as}(COO^-)$), 1417.9 ($\nu_s(COO^-)$). Λ_M ($c = 8.98\cdot10^{-5}$ mol·L^{-1}) = 122 $\Omega^{-1}\cdot cm^2\cdot mol^{-1}$ (acetonitrile).

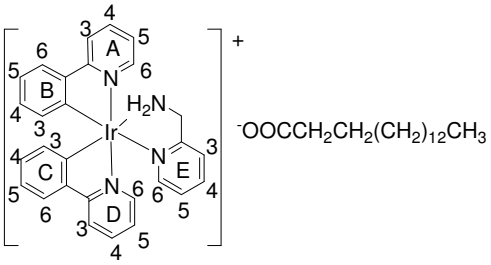

B_5. [Ir(*ppy*)$_2$(*pam*)](*ac-*C_{15})·3/2H_2O: The classical bridge-splitting reaction of the dimeric precursor [Ir(*ppy*)$_2$]$_2$-μCl_2 (0.150 g, 0.140 mmol) with 2-picolylamine (0.030 g,0.280mmol)in CH_2Cl_2/MeOH (20 ml, 3:1 v/v) was carried out for 4 hours under nitrogen atmosphere. Subsequently, the addition of 1.1 fold excess of Ag(I) salt containing ac-C_{15} (0.111 g, 0.308 mmol) was made and the reaction mixture, protected from light, was further stirred for 2 hours. Then the solvents were evaporated, CH_2Cl_2 was added and insoluble AgCl formed was filtered. The pure product was obtained by recrystallization from CH_2Cl_2/Hexane. Yield: 0.152 g (61%). Dec. p.: 150 °C. Anal.Calcd as solvate from: $[C_{44}H_{55}IrN_4O_2]\cdot$ 3/2H_2O (891.18 g/mol): C, 59.30; H, 6.56; N, 6.29%. Found: C, 59.15 H, 6.57; N, 6.43%. ^{1}H NMR ($CDCl_3$, 300 MHz): δ 9.63 (1H, d, J = 5.87 Hz, H^{6E}), δ 8.07-7.62 (10H, overlapped peaks, H^{6A}, H^{6D},H^{5E}, H^{5A}, H^{5D}, H^{3A}, H^{3D},H^{6B}, H^{6C}), δ 7.38-7.35 (2H, overlapped peak, H^{4E}, NH_2), δ 7.37 (1H, t, J = 5.86 Hz, H^{4A}), δ 7.10 (1H, t, J =6.6 Hz, H^{4D}), δ 7.08-6.79 (4H, overlapped peak, H^{5C}, H^{5B}, H^{4B}, H^{4C}), δ 6.34 (1H, d, J = 7.7Hz, H^{3B}), δ 6.30(1H, d, J = 8.8 Hz, H^{3C}), δ 5.23 (1H, m, NH_2), δ 4.31 (1H, m, CH_2), δ 3.38 (1H, overlapped peak, CH_2), δ 2.18 (2H, t, ^3J = 5.23 Hz, $OOCCH_2$), δ 1.60 (2H, m, $OOCCH_2CH_2$), δ 1.31 (24H, m, $OOCCH_2CH_2(CH_2)_{12}$), δ 0.94 (3H, t, ^3J = 6.23 Hz, $OOCCH_2CH_2(CH_2)_{12}CH_3$). IR (KBr/$cm^{-1}$): 3434.28 ($\upsilon_s$(NH)), 3259 ($\upsilon_s$(NH)), 3061.4 ($\nu_{as}(CH_3)$), 2919.9 ($\nu_{as}(CH_2)$), 2851.1 ($\nu_s(CH_2)$), 1562.3 ($\nu_{as}(COO^-)$), 1422.8($\nu_s(COO^-)$). Λ_M ($c = 9.39\cdot10^{-5}$ mol·L^{-1}) = 101 $\Omega^{-1}\cdot cm^2\cdot mol^{-1}$ (acetonitrile).

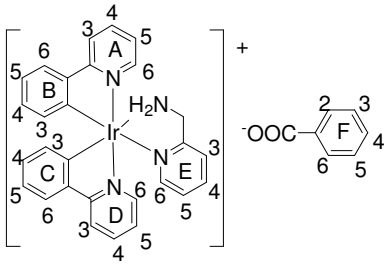

B_6. [Ir(*ppy*)$_2$(*pam*)](*bz*)·3/2H_2O: The classical bridge-splitting reaction of the dimeric precursor [Ir(*ppy*)$_2$]$_2$-μCl_2 (0.150 g, 0.140 mmol) with 2-picolylamine (0.030 g, 0.280 mmol) in CH_2Cl_2/MeOH (20 ml, 3:1 v/v) was carried out for 4 hours under nitrogen atmosphere. Subsequently, the addition of 1.1 fold excess of Ag(I) salt containing *bz* (0.070 g, 0.308mmol) was made and the reaction mixture, protected from light, was further stirred for 2 hours. Then the solvents were evaporated, CH_2Cl_2 was added and insoluble AgCl formed was filtered. The pure product was obtained by recrystallization from acetone/ethyl acetate. Yield: 0.175 g (82.5%). Dec. p.: 240 °C. Anal.Calcd for $[C_{35}H_{29}IrN_4O_2]$ ·3/2H_2O (756.87 g/mol): C, 55.54; H, 4.26; N, 7.40%. Found: C, 55.28; H, 4.28; N, 7.68%. ^{1}H NMR $(CD_3)_2CO$, 300 MHz): δ 9.86 (1H, d, J = 5.5 Hz, H^{6E}), δ 8.23 (3H, overlapped peaks, H^{6A}, H^{6D},H^{5E}), δ 8.0 (6H, overlapped peaks,H^{5A}, H^{5D}, H^{3A}, H^{3D}, H^{6B}, H^{6C}), δ 7.86 (1H, d, J =7.7 Hz, H^{3E}), δ 7.79 (3H, overlapped peaks, H^{4E},H^{4A}, H^{4D}), δ 7.42-7.27 (6H, overlapped peak, NH_2, H^{2F}, H^{6F}), δ 6.99 (1H, t, J = 7.52 Hz,H^{5C}), δ 6.92–6.85 (2H, overlapped peaks, H^{5B}, H^{4B}), δ 6.87 (1H, t, ^3J = 7.3 Hz, H^{4C}), δ 6.39 (1H,d, J = 7.71 Hz, H^{3B}), δ 6.39 (1H, d, ^3J = 7.71Hz, H^{3C}), δ 5.26 (1H, broad, NH_2), δ 5.70–4.65 (2H, overlapped peaks, NH_2, CH_2). IR (KBr/cm−1): 3548.4 (υ_{as}(NH)), 3259.2 (υ_s(NH)), 1557.8 ($\nu_{as}(COO^-)$), 1387.1($\nu_s(COO^-)$). Λ_M (c = 9.49·10^{-5} mol·L^{-1}) = 99 Ω^{-1}·cm^2·mol^{-1} (acetonitrile).

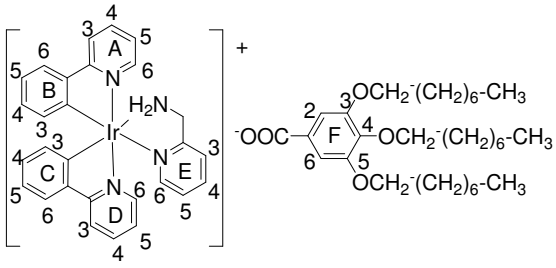

B_7. [Ir(*ppy*)$_2$(*pam*)](*bz-C$_8$*): The classical bridge-splitting reaction of the dimeric precursor [Ir(*ppy*)$_2$]$_2$-μCl_2 (0.150 g, 0.140 mmol) with and 2-picolylamine (0.030 g, 0.280 mmol) in CH_2Cl_2/MeOH (20 ml, 3:1 v/v) was carried out for 4 hours under nitrogen atmosphere. Subsequently, the addition of 1.1 fold excess of Ag(I) salt containing *bz-C$_8$* (0.188 g, 0.308mmol) was made and the reaction mixture, protected from light, was further stirred for 2 hours. Then the solvents were evaporated, CH_2Cl_2 was added and insoluble AgCl formed was filtered. The pure product was obtained by recrystallization from CH_2Cl_2/Hexane. Yield: 0.198 g (78.5%) m. p.: 150 °C. Anal.Calcd for $C_{59}H_{77}IrN_4O_5$ (1114.48 g/mol): C, 63.58; H, 6.98; N, 5.03%.Found: C, 63.07; H, 6.94; N, 4.84%. ^{1}H NMR ($CDCl_3$), 300 MHz): δ 9.58 (1H, d, J = 5.49 Hz, H^{6E}), δ 7.93-7.25 (12H, overlapped peaks, H^{6A}, H^{6D},H^{5E}, H^{5A}, H^{5D}, H^{3A}, H^{3D},H^{6B}, H^{6C},H^{3E}, H^{2F}, H^{6F}), δ 7.14 (1H, t, J =6.58 Hz, H^{4E}), δ 7.03-6.72 (7H, overlapped peaks, NH_2, H^{4A}, H^{4D}, H^{5C}, H^{5B},

H^{4B}, H^{4C}), δ 6.29 (1H, d, 3J = 7.68 Hz, H^{3B}), δ 6.25 (1H, t, *J* = 6.58 Hz, H^{3C}), δ 5.19 (1H, broad s, NH_2), δ 4.28 (1H,broad s, CH_2), δ 3.94 (6H, overlapped peak, OCH_2), δ 3.40 (1H, broad s, CH_2), δ 1.77-1.71 (6H, overlapped peak, OCH_2CH_2), δ 1.43-1.27 (36H, overlapped peak, $OCH_2CH_2(CH_2)_6$), δ 0.87 (3H, s, ^3J = 6.76 Hz, CH_3). IR (KBr, cm^{-1}): 3400.3 (υ_{as}(NH)), 3232.1 (υ_{as}(NH)), 3104.6, 3062.3, 3044.3 ($\nu_{as}(CH_3)$), 2925.0($\nu_{as}(CH_2)$), 2853.9 ($\nu_s(CH_2)$), 1560.2 ($\nu_{as}(COO^-)$), 1375.3 ($\nu_s(COO^-)$)1558.2 ($\nu_{as}(COO^-)$), 1365.1($\nu_s(COO^-)$). Λ_M (c = $8.97\cdot10^{-5}$ mol·L^{-1}) = 64 $\Omega^{-1}\cdot cm^2\cdot mol^{-1}$ (methanol).

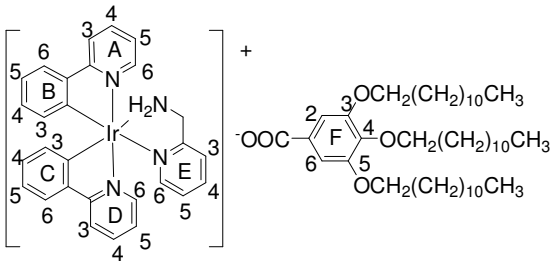

B_8. [Ir(*ppy*)$_2$(*pam*)](*bz-*C_{12}): The classical bridge-splitting reaction of the dimeric precursor [Ir(*ppy*)$_2$]$_2$-μCl_2 (0.150 g, 0.140 mmol) with 2-picolylamine (0.030 g,0.280mmol) in CH_2Cl_2/MeOH (20 ml, 3:1 v/v) was carried out for 4 hours under nitrogen atmosphere. Subsequently, the addition of 1.1 fold excess of Ag(I) salt containing containing ac-C_{12} (0.111 g, 0.308 mmol) was made and the reaction mixture, protected from light, was further stirred for 2 hours. Then the solvents were evaporated, CH_2Cl_2 was added and insoluble AgCl formed was filtered. The pure product was obtained by recrystallization from $CHCl_3$/Hexane. Yield: 0.152 g (66%). Dec. p.: 240 °C. Anal.Calcd for [$C_{44}H_{55}IrN_4O_2$] (864.15 g/mol): C, 61.15; H, 6.42; N, 6.48%. Found: C, 60.85 H, 6.27; N, 6.73%. ^{1}H NMR ($CDCl_3$, 300 MHz): δ 9.55 (1H, d, *J* = 5.49 Hz, H^{6E}), δ 7.92-7.47 (10H, overlapped peaks, H^{6A}, H^{6D},H^{5E}, H^{5A}, H^{5D}, H^{3A}, H^{3D},H^{6B}, H^{6C}, H^{3E}), δ 7.23 (2H, s, H^{2F}, H^{6F}), δ 7.19-7.15 (2H, overlapped peaks , NH_2, H^{4E}), δ 7.03-6.71 (6H, overlapped peaks, H^{4A}, H^{4D}, H^{5C}, H^{5B}, H^{4B}, H^{4C}), δ 6.28 (1H, d, *J* = 7.69 Hz, H^{3B}), δ 6.24 (1H, d, *J* = 6.58 Hz, H^{3C}), δ 5.18 (1H, m, NH_2), δ 4.29 (1H, m, CH_2), δ 3.38 (6H, m, OCH_2), δ 3.47 (1H, m, CH_2), δ 1.75 (6H, m, OCH_2), δ 1.33 (60H, m, $OCH_2(CH_2)_{10}$), δ 0.87 (9H, t, ^3J = 6.41 Hz, $OCH_2(CH_2)_{10}CH_3$). IR (KBr, cm^{-1}): 3104.6 (N–H), 3061.9 (N–H), 2919.94 (C-H), 2851.19 (C-H), 3104.6, 3061.9.3 ($\nu_{as}(CH_3)$), 1557.9 ($\nu_{as}(COO^-)$), 1367.9 ($\nu_s(COO^-)$). Λ_M (c = $8.2\cdot10^{-5}$ mol L^{-1} = 61 $\Omega^{-1}\cdot cm^2\cdot mol^{-1}$ (methanol).

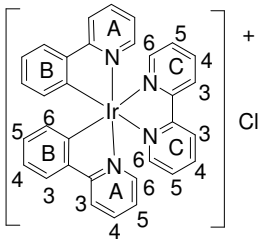

C_1. [Ir(*ppy*)$_2$(*bpy*)](Cl): The classical bridge-splitting reaction of the dimeric precursor [Ir(*ppy*)$_2$]$_2$-μCl$_2$ (0.150 g, 0.140 mmol) with 2,2'-bipyridine (0.043g, 0.280mmol) in CH_2Cl_2/MeOH (20 ml, 3:1 v/v) was carried out for 4 hours under nitrogen atmosphere. After evaporating the solvents, the yellow residue was dissolved with 10 mL of CH_2Cl_2 and filtered to remove the insoluble white inorganic salts. The pure product was obtained after recrystallization with CH_2Cl_2/Hexane. Yield: 0.160 g (83.5%). Dec. p.: 240 ºC. Anal.Calcd. for [$C_{32}H_{24}ClIrN_4$] (692.23 g/mol): C, 55.52; H, 3.49; N, 8.09%. Found: C, 55.87; H, 3.59; N, 7.80%. ^{1}H NMR ($CDCl_3$, 300MHz): δ 9.69 (2H, d, *J* =8.10 Hz, H^{3C}), δ 8.26 (2H, td, *J* = 8.25 Hz, 1.50 Hz, H^{4C}), δ 7.89 (4H, overlapped peaks, H^{3B}, H^{6C}), δ 7.75 (2H, td, *J* = 8.39 Hz, 1.38 Hz, H^{4B}), δ 7.68 (2H, dd, *J* = 7.83, 0.84 Hz, H^{6A}), δ 7.46 (2H, dd, *J* = 5.76Hz, 0.54 Hz, H^{6B}), δ 7.39 (2H, td, *J* = 6.45 Hz, 0.84 Hz, H^{5C}), δ 7.0 (4H, overlapped peaks, H^{5A}, H^{5B}), δ 6.91 (2H, td, *J* = 7.41 Hz, *J* = 1.23 Hz, H^{4A}), δ 6.29 (2H, dd, *J* = 7.21 Hz, 0.81 Hz, H^{3A}). Λ_M (*c* = 7.60·10^{-5} mol·L^{-1} in acetonitrile) = 139.2 Ω^{-1} cm^2·mol^{-1}.

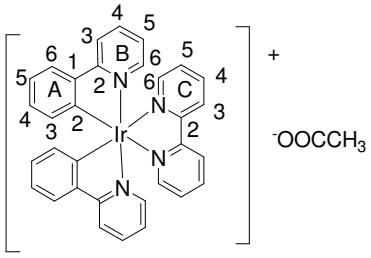

C_2. [Ir(*ppy*)$_2$(*bpy*)](*ac*)·xH_2O: The classical bridge-splitting reaction of the dimeric precursor [Ir(*ppy*)$_2$]$_2$-μCl$_2$ (0.150 g, 0.140 mmol) with 2,2'-bipyridine (0.043 g, 0.280mmol) in CH_2Cl_2/MeOH (20 ml, 3:1 v/v) was carried out for 4 hours under nitrogen atmosphere. Subsequently, the addition of 1.1 fold excess of Ag(I) salt containing *ac* (0.051 g, 0.154 mmol) was made and the reaction mixture, protected from light, was further stirred for 2 hours. Then the solvents were evaporated, CH_2Cl_2 was added and insoluble AgCl formed was filtered. The pure product was obtained by recrystallization from CH_2Cl_2/Hexane. Yield 0.169 g (80%). Dec. p.: 240 ºC. Anal.Calcd. as the solvent form: $C_{34}H_{27}IrN_4O_2·2H_2O$ (751.85 g/mol): C, 54.31; H, 4.16; N, 7.45%. Found: C, 54.17; H, 4.10; N, 7.20%. ^{1}H NMR ($CDCl_3$, 300MHz): δ 9.48 (2H, d, *J* =8.4 Hz, H^{3C}), δ 8.29 (2H, t, *J* = 7.52 Hz, H^{4C}), δ 7.90 (4H, overlapped peaks, H^{3B}, H^{6C}), δ 7.75 (2H, t, *J* = 7.2 Hz, H^{4B}), δ 7.68 (2H, d, *J* = 7.7, H^{6A}), δ 7.47 (2H, d, *J* = 5.5 Hz, H^{6B}), δ 7.37 (2H, t, *J* = 6.4 Hz, H^{5C}), δ 7.0 (4H, overlapped peaks, H^{5A}, H^{5B}), δ 6.91 (2H, t, *J* = 7.5 Hz, H^{4A}), δ 6.29 (2H, d, *J* = 7.7 Hz, H^{3A}), δ 2.03 (3H, s, CH_3COO). ^{13}C NMR ($CDCl_3$, 300 MHz): 177.2 (COO), 167.9 (C^{2B}), 156.2 (C^{2C}), 150.5 (C^{1A}), 149.7 (C^{6C}), 148.5 (C^{6B}), 143.4 (C^{2A}), 140.5 (C^{4C}), 137.9 (C^{4B}), 131.7 (C^{3A}), 130.8 (C^{4A}), 127.8 (C^{5C}), 127.3 (C^{6A}), 124.8 (C^{3C}), 123.2 (C^{5A}), 122.6 (C^{5B}), 119.6 (C^{3B}), 24.7 ($COOCH_3$).IR (KBr/cm^{-1}): 3392.2 (br H_2O), 3062.8,

3038.17, 2924.3, ($\upsilon_{as}(CH_3)$), 1562.6 ($\upsilon_{as}(COO^-)$), 1403.0 ($\upsilon_s(COO^-)$). Λ_M (c = 0.84·10^{-5} mol·L^{-1} in acetonitrile) = 122 Ω^{-1} cm^2·mol^{-1}, 55 Ω^{-1}·cm^2·mol^{-1} (water).

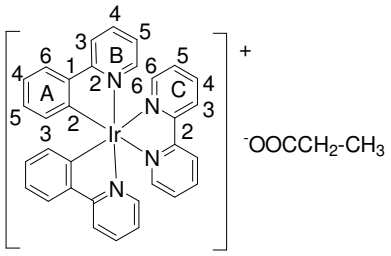

C_3. [Ir(*ppy*)$_2$(*bpy*)](*ac-C$_2$*)·xH_2O: The classical bridge-splitting reaction of the dimeric precursor [Ir(*ppy*)$_2$]$_2$-μCl$_2$ (0.150 g, 0.140 mmol) with 2,2'-bipyridine (0.043 g, 0.280mmol) in CH_2Cl_2/MeOH (20 ml, 3:1 v/v) was carried out for 4 hours under nitrogen atmosphere. Subsequently, the addition of 1.1 fold excess of Ag(I) salt containing *ac-C$_2$* (0.055 g, 0.154 mmol) was made and the reaction mixture, protected from light, was further stirred for 2 hours. Then the solvents were evaporated, CH_2Cl_2 was added and insoluble AgCl formed was filtered. The pure product was obtained by recrystallization from CH_2Cl_2/Hexane. Yield 0.178 g (83%). Dec. p.:240 ºC. Anal. Calcd. as the solvate form: [$C_{35}H_{29}IrN_4O_2$]·2H_2O (765.88 g/mol): C, 54.89; H, 4.34; N, 7.32%. Found: C, 54.73; H, 4.12; N, 7.45%. ^{1}H NMR ($CDCl_3$, 300 MHz): δ 9.66 (2H, d, J =8.2 Hz, H^{3C}), δ 8.29 (2H, td, J = 8.0 Hz, 1.4 Hz, H^{4C}), δ 7.91 (2H, d, J = 7.9 Hz, H^{3B}), δ 7.86 (2H, dd, J = 5.7 Hz, 1.1 Hz, H^{6C}), δ 7.75 (2H, td, J = 7.8, 1.5, H^{4B}), δ 7.68 (2H, dd, J = 7.9 Hz, 1.0 Hz, H^{6A}), δ 7.46 (2H, dd, J = 5.6 Hz, 1.0 Hz, H^{6B}), δ 7.36 (2H, td, J = 6.2 Hz, 1.0 Hz, H^{5C}), δ 7.0 (4H, overlapped peaks, H^{5A}, H^{5B}), δ 6.90 (2H, td, J = 7.34 Hz, 1.3 Hz, H^{4A}), δ 6.29 (2H, dd, J = 7.6 Hz, 1.0 Hz, H^{3A}), δ 2.32 (2H, q, OOC CH_2), δ 1.15 (3H, t, J =7.6 Hz, OOCCH_2CH_3). ^{13}C NMR ($CDCl_3$, 300 MHz): 179.7 (COO), 167.9 (C^{2B}), 156.2 (C^{2C}), 150.3 (C^{1A}), 149.3 (C^{6C}), 148.3 (C^{6B}), 143.3 (C^{2A}), 140.3 (C^{4C}), 137.7 (C^{4B}), 131.6 (C^{3A}), 130.6 (C^{4A}), 127.5 (C^{5C}), 127.4 (C^{6A}), 124.6 (C^{3C}), 122.9 (C^{5A}), 122.4 (C^{5B}), 119.3 (C^{3B}), 30.5 (OOC CH_2), 10.7 (OOCCH_2CH_3). IR (KBr/cm^{-1}): 3391.2 (br H_2O), 3066.0, 3043.9, 2973.7, ($\upsilon_{as}(CH_3)$), 2879.0 ($\upsilon_s(CH_3)$), 1562.2 ($\upsilon_{as}(COO^-)$), 1401.9 ($\upsilon_s(COO^-)$). Λ_M (c = 0.82·10^{-5} mol·L^{-1}) = 123 Ω^{-1}·cm^2·mol^{-1} (acetonitrile), 40 Ω^{-1}·cm^2·mol^{-1} (water). The TGA and DSC traces of complex **C_3** is shown in Figure III.3.

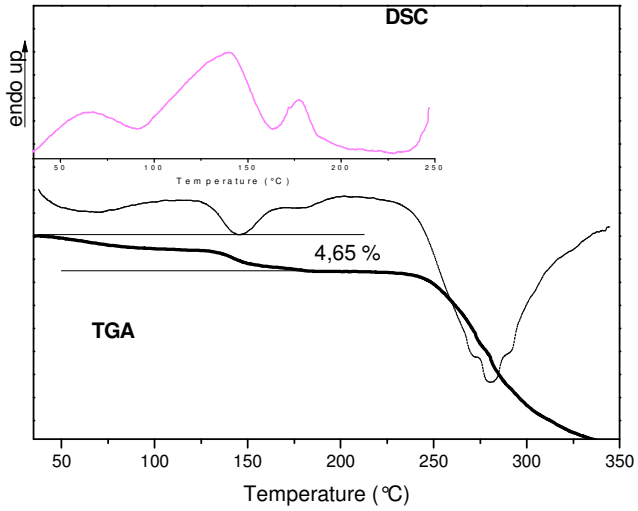

Figure III.3 TGA and DSC scans for complex **C_3**, [Ir(ppy)$_2$(bpy)]*ac-C$_2$*·2H$_2$O: experimental weight loss of 4.65 % corresponding to 2 molecules of water (calcd. 4.71 %).

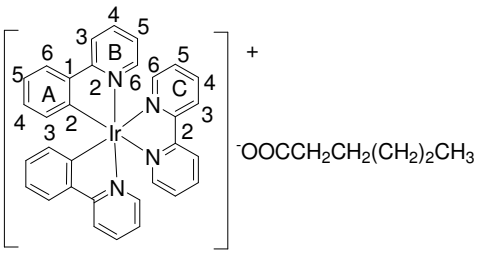

C_4. [Ir(*ppy*)$_2$(*bpy*)](*ac*_C_5)·xH_2O: The classical bridge-splitting reaction of the dimeric precursor [Ir(*ppy*)$_2$]$_2$-μCl_2 (0.150 g, 0.140 mmol) with 2,2'-bipyridine (0.043 g, 0.280 mmol) in CH_2Cl_2/MeOH (20 ml, 3:1 v/v) was carried out for 4 hours under nitrogen atmosphere. Subsequently, the addition of 1.1 fold excess of Ag(I) salt containing *ac-C$_5$* (0.068 g, 0.154 mmol) was made and the reaction mixture, protected from light, was further stirred for 2 hours. Then the solvents were evaporated, CH_2Cl_2 was added and insoluble AgCl formed was filtered. The pure product was obtained by recrystallization from CH_2Cl_2/Hexane. Yield 0.178 g (80%). Dec. p. :240 ºC. Anal. Calcd. as the solvate form: $[C_{38}H_{35}IrN_4O_2]\cdot H_2O$ (789.94 g/mol): C, 53.78; H, 4.72; N, 7.09%. Found: C, 53.73; H, 2.52; N, 7.45%. ^{1}H NMR ($CDCl_3$, 300MHz): δ 9.63 (2H, d, *J* =8.2 Hz, H^{3C}), δ 8.30 (2H, t, *J* = 7.7 Hz, H^{4C}), δ 7.87 (4H, overlapped peaks, H^{3B}, H^{6C}), δ 7.75 (2H, t, *J* = 7.8 Hz, H^{4B}), δ 7.68 (2H, d, *J* = 6.9, H^{6A}), δ 7.47 (2H, d, *J* = 4.9 Hz, H^{6B}), δ 7.36 (2H, t, *J* = 6.4 Hz, H^{5C}), δ 7.02 (4H, overlapped peaks, H^{5A}, H^{5B}), δ 6.90 (2H, t, *J* = 7.4Hz, H^{4A}), δ 6.29 (2H, d, *J* = 7.5 Hz, H^{3A}), δ 2.28 (2H, t, *J* = 7.7 Hz, $OOCCH_2$), δ 1.68 (2H, m, $OOCCH_2CH_2$), δ 1.28 (4H, m, $(OOCCH_2CH_2)_2$), δ 0.83 (3H, t, ^{3}*J* = 7.1 Hz, $OOCCH_2(CH_2)_2CH_3$). ^{13}C NMR ($CDCl_3$, 300 MHz): 180.2 (COO), 168.0 (C^{2B}), 156.4 (C^{2C}), 150.6 (C^{1A}), 149.5 (C^{6C}), 148.5 (C^{6B}), 143.5 (C^{2A}), 140.6

(C^{4C}), 137.9 (C^{4B}), 131.8 (C^{3A}), 130.8 (C^{4A}), 127.7 (C^{5C}), 127.6 (C^{6A}), 124.8 (C^{3C}), 123.1 (C^{5A}), 122.6 (C^{5B}), 119.6 (C^{3B}), 24.7 ($COOCH_3$). IR (KBr/cm^{-1}): 3392.2 (br, H_2O), 3062.8, 3035.9, 2955.6 ($\nu_{as}(CH_3)$), 2926.7 ($\nu_{as}(CH_2)$), 2859.4 ($\nu_s(CH_2)$), 1560.1 ($\nu_{as}(COO^-)$), 1391.8 ($\nu_s(COO^-)$). Λ_M (c = $0.78 \cdot 10^{-5}$ mol·L^{-1}): 111 $\Omega^{-1} \cdot cm^2 \cdot mol^{-1}$ (acetonitrile), 42 $\Omega^{-1} \cdot cm^2 \cdot mol^{-1}$ (water). The TGA and DSC traces of complex **C_4** is shown in Figure.III.4.

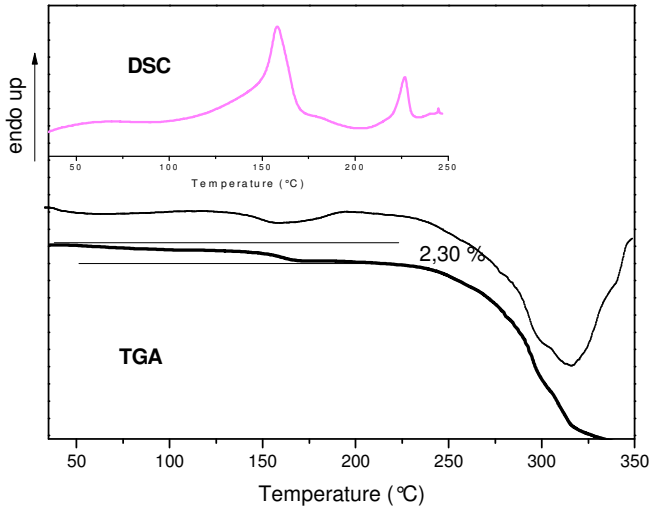

Figure III.4 TGA and DSC scans for complex **C_4**, [Ir(*ppy*)$_2$(*bpy*)]*ac-C*$_5$·1H_2O: experimental weight loss of 2.30 % corresponding to 1 molecule of water (calcd. 2.28 %).

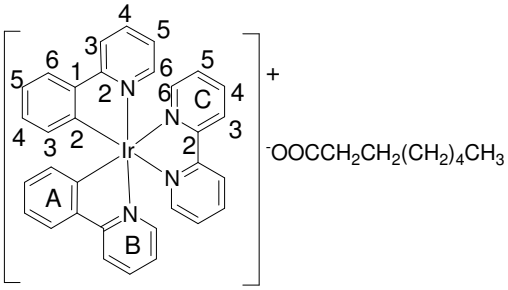

C_5. [Ir(*ppy*)$_2$(*bpy*)](*ac-C*$_7$)·xH_2O: The classical bridge-splitting reaction of the dimeric precursor [Ir(*ppy*)$_2$]$_2$-μCl_2 (0.150 g, 0.140 mmol) with 2,2'-bipyridine (0.043 g, 0.280 mmol) in CH_2Cl_2/MeOH (20 ml, 3:1 v/v) was carried out for 4 hours under nitrogen atmosphere. Subsequently, the addition of 1.1 fold excess of Ag(I) salt containing *ac-C*$_7$ (0.077 g, 0.154 mmol) was made and the reaction mixture, protected from light, was further stirred for 2 hours. Then the solvents were evaporated, CH_2Cl_2 was added and insoluble AgCl formed was filtered. The pure product was obtained by recrystallization from CH_2Cl_2/Hexane. Yield 0.190 mg (83%). Dec. p.: 245 ºC. Anal. Calcd. as the solvate form: $[C_{40}H_{39}IrN_4O_2]\cdot 1H_2O$ (818.00 g/mol): C, 58.83; H, 5.05; N, 6.85%. Found: C, 58.68; H, 4.95; N, 6.92%. ^{1}H NMR ($CDCl_3$, 300MHz): δ 9.67 (2H, d, *J* =8.2 Hz, H^{3C}), δ 8.30 (2H, t, *J* = 8.2 Hz, H^{4C}), δ 7.88 (4H, overlapped

peaks, H^{3B}, H^{6C}), δ 7.75 (2H, t, J = 7.8 Hz, H^{4B}), δ 7.68 (2H, d, J = 7.2, H^{6A}), δ 7.47 (2H, d, J = 5.3 Hz, H^{6B}), δ 7.36 (2H, t, J = 6.1 Hz, H^{5C}), δ 7.1 (4H, overlapped peaks, H^{5A}, H^{5B}), δ 6.91 (2H, t, J = 7.4 Hz, H^{4A}), δ 6.30 (2H, d, J = 7.6 Hz, H^{3A}), δ 2.28 (2H, t, $OOCCH_2$), δ 1.68 (2H, m, $OOCCH_2CH_2$), δ 1.25 (8H, m, $OOCCH_2CH_2(CH_2)_4$), δ 0.83 (3H, t, J = 7.1 Hz, $OOCCH_2CH_2(CH_2)_4CH_3$). ^{13}C NMR ($CDCl_3$, 300 MHz): 180.1 (COO), 168.0 (C^{2B}), 156.4 (C^{2C}), 150.6 (C^{1A}), 149.5 (C^{6C}), 148.5 (C^{6B}), 143.5 (C^{2A}), 140.6 (C^{4C}), 137.9 (C^{4B}), 131.8 (C^{3A}), 130.8 (C^{4A}), 127.8 (C^{5C}), 127.5 (C^{6A}), 124.8 (C^{3C}), 123.1 (C^{5A}), 122.6 (C^{5B}), 119.5 (C^{3B}), 39.2 ($COOCH_2$), 31.9 ($COOCH_2CH_2$), 30.1 ($COO(CH_2)_2CH_2$), 29.4 ($COO(CH_2)_3CH_2$), 27.3 ($COO(CH_2)_4CH_2$), 22.7 ($COO(CH_2)_5CH_2$), 14.1 ($COO(CH_2)_6CH_7$). IR (KBr/cm^{-1}): 3409.9 (br, H_2O), 3063.7, 3034.6, 2954.8 ($\nu_{as}(CH_3)$), 2925.3 ($\nu_{as}(CH_2)$), 2853.8 ($\nu_s(CH_2)$), 1563.1 ($\nu_{as}(COO^-)$), 1381.1 ($\nu_s(COO^-)$). Λ_M (c = $0.75 \cdot 10^{-5}$ mol·L^{-1}): 114 $\Omega^{-1} \cdot cm^2 \cdot mol^{-1}$ (acetonitrile). The TGA and DSC traces of complex **C_5** is shown in Figure III.5.

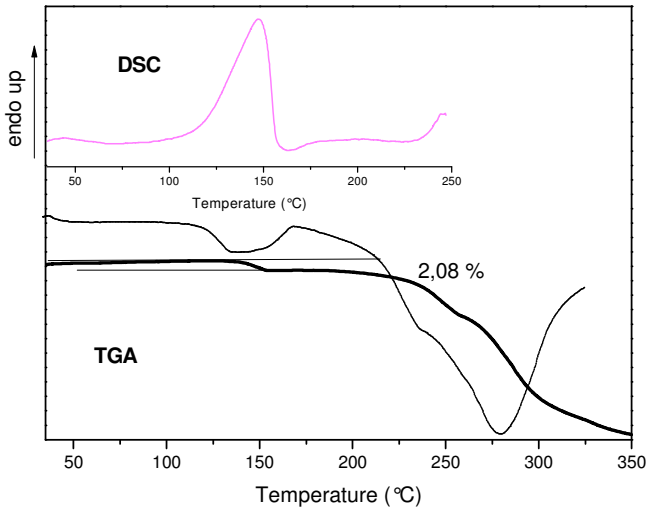

Figure III.5 TGA and DSC scans for complex **C_5**, [Ir(ppy)$_2$(bpy)]ac-C_7·1H_2O: experimental weight loss of 2.08 % corresponding to 1 molecule of water (calc. 2.20 %).

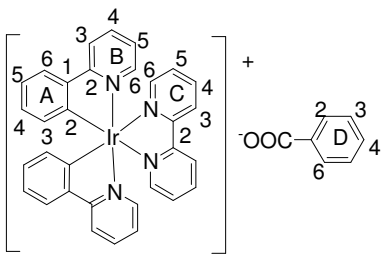

C_6. [Ir(ppy)$_2$(bpy)](bz)·1H_2O: The classical bridge-splitting reaction of the dimeric precursor [Ir(ppy)$_2$]$_2$-μCl_2 (0.150 g, 0.140 mmol) with 2,2'-bipyridine (0.043 g, 0.280mmol) in CH_2Cl_2/MeOH (20 ml, 3:1 v/v) was carried out for 4 hours under nitrogen atmosphere. Subsequently, the addition of 1.1 fold excess of Ag(I) salt containing bz (0.070 g, 0.154 mmol) was made and the reaction mixture, protected

from light, was further stirred for 2 hours. Then the solvents were evaporated, CH_2Cl_2 was added and insoluble AgCl formed was filtered. The pure product was obtained by recrystallization from CH_2Cl_2/Hexane. Yield 0.170 g (78%). Dec. p.:240 ºC. Anal.Calc.: $[C_{41}H_{33}IrN_4O_4]$ (795.91 g/mol): C, 58.85; H, 3.93; N, 7.04%. Found: C, 58.57; H, 4.11; N, 6.84%. ^{1}H NMR ($CDCl_3$, 300MHz)): δ 9.63 (2H, d, ^3J =8.23 Hz, H^{3C}), δ 8.2 (4H, m, H^{4C}, H^{5C}), δ 7.90 (2H, dd, ^3J = 7.41 Hz, 1.38 Hz, H^{6C}), δ 7.84 (2H, dd, ^3J = 5.49 Hz, 0.84 Hz H^{6A}), δ 7.74 (2H, td, ^3J = 7.41Hz, 1.38 H^{4B}), 7.67 (2H, dd, J = 7.95 Hz, 1.11 Hz H^{6B}), δ 7.46 (2H, d, J = 5.76 Hz, H^{3B}), δ 7.30 (5H, overlapped peaks, H^{2D}, H^{3D}, H^{4D}, H^{5D}, H^{6D}), δ 6.95 (6H, overlapped peaks, H^{5A}, H^{5B}, H^{4A}), δ 6.29 (2H, dd, J = 7.68 Hz, 0.84 Hz, H^{3A}). IR (KBr/cm^{-1}): 3387.9 (br, H_2O), 1559.7 ($\nu_{as}(COO^-)$), 1377.2 ($\nu_s(COO^-)$). Λ_M (c = $7.7\cdot10^{-5}$ mol·L^{-1}): 132 $\Omega^{-1}\cdot cm^2\cdot mol^{-1}$ (acetonitrile).

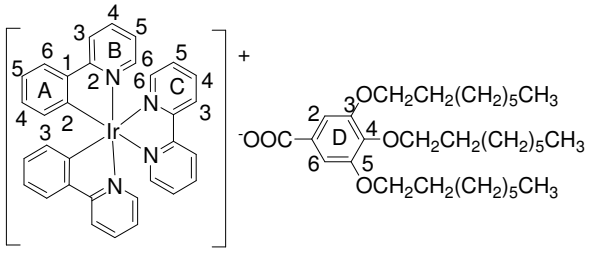

C_7. [Ir(*ppy*)$_2$(*bpy*)](*bz-C$_8$*)·5/2H$_2$O: The classical bridge-splitting reaction of the dimeric precursor $[Ir(ppy)_2]_2$-μCl_2 (0.150 g, 0.140 mmol) with 2,2'-bipyridine (0.043 g, 0.280mmol) in CH_2Cl_2/MeOH (20 ml, 3:1 v/v) was carried out for 4 hours under nitrogen atmosphere. Subsequently, the addition of 1.1 fold excess of Ag(I) salt containing *bz-C$_8$* (0.188 g, 0.154 mmol) was made and the reaction mixture, protected from light, was further stirred for 2 hours. Then the solvents were evaporated, CH_2Cl_2 was added and insoluble AgCl formed was filtered. The pure product was obtained by recrystallization from CH_2Cl_2/Hexane. Yield 0.230g (68%). M.p.: 195 ºC. Anal. Calcd. as solvate form: $[C_{63}H_{77}IrN_4O_5]\cdot5/2H_2O$ (1207.58 g/mol): C, 62.66; H, 6.84; N, 4.64%. Found: C, 62.46; H, 6.59; N, 5.05%. ^{1}H NMR ($CDCl_3$, 300MHz)): δ 9.38 (2H, d, ^3J =7.89 Hz, H^{3C}), δ 8.14 (2H, td, J = 8.22 Hz, 1.32 Hz, H^{4C}), δ 7.89 (2H, d, J =8.22 Hz, H^{3B}), δ 7.83 (2H, dd, J = 5.58 Hz, 1.29 Hz, H^{6C}), δ 7.74 (2H, td, J = 7.56, 1.32 Hz, H^{4B}), δ 7.67 (2H, dd, J = 7.56 Hz,0.99 Hz, H^{6A}), δ 7.48 (2H, s, H^{2D}, H^{6D}), δ 7.44 (2H, dd, J = 5.91 Hz, 0.66 Hz, H^{6B}), δ 7.30 (2H, td, J = 6.9 Hz, 0.96 Hz, H^{5C}), δ 7.0 (4H, overlapped peak, H^{5A}, H^{5B}), δ 6.90 (2H, t, ^3J = 7.56 Hz, 1.32 Hz, H^{4A}), δ 6.28 (2H, d, ^3J = 7.56 Hz, H^{3A}), δ 3.97 (6H, m, OCH_2), δ 1.72 (6H, m, OCH_2CH_2), δ 1.4 (30H, m, $OCH_2CH_2(CH_2)_5$), δ 0.87 (9H, t, ^3J = 6.7 Hz, $OCH_2CH_2(CH_2)_5CH_3$). IR (KBr/cm^{-1}): 3359.4 (br, H_2O), 3104.6, 3104.6, 3044.3 ($\nu_{as}(CH_3)$), 1560.2 ($\nu_{as}(COO^-)$), 1375.3 ($\nu_s(COO^-)$). Λ_M (c = $7.7\cdot10^{-5}$ mol·L^{-1}): 40 $\Omega^{-1}\cdot cm^2\cdot mol^{-1}$ (methanol).

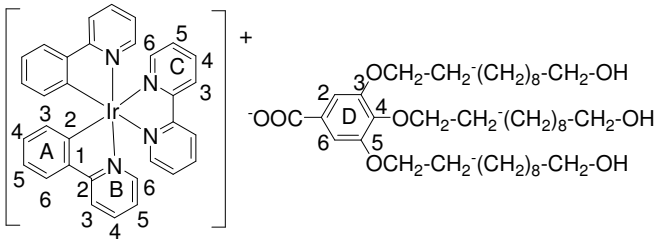

C_8. [Ir(*ppy*)$_2$(*bpy*)](*bz-C_{11}OH*): The classical bridge-splitting reaction of the dimeric precursor [Ir(*ppy*)$_2$]$_2$-μCl$_2$ (0.150 g, 0.140 mmol) with 2,2'-bipyridine (0.043 g, 0.280 mmol) in CH_2Cl_2/MeOH (20 ml, 3:1 v/v) was carried out for 4 hours under nitrogen atmosphere. Subsequently, the addition of 1.1 fold excess of Ag(I) salt containing *bz-C_{11}OH* (0.194 g, 0.154 mmol) was made and the reaction mixture, protected from light, was further stirred for 2 hours. Then the solvents were evaporated, CH_2Cl_2 was added and insoluble AgCl formed was filtered. The pure product was obtained by recrystallization from CH_2Cl_2/Hexane. Yield: 0.190g (65%). Dec. p.: 240 ºC. Anal.Calcd. as solvate form [$C_{71}H_{95}IrN_4O_8$] (1336.76 g/mol): C, 64.69; H, 7.16; N, 4.19%. Found: C, 64.27; H, 6.93; N, 3.89%. ^{1}H NMR ($CDCl_3$, 300MHz): δ 9.42 (2H, d, *J* = 7.69 Hz, H^{3C}), δ 8.16 (2H, t, *J* = 6.72, H^{4C}), δ 7.89 (2H, d, *J* = 8.0, H^{3B}), δ 7.83 (2H, d, *J* = 4.53 Hz, H^{6C}) δ 7.74 (2H, td, *J* = 7.41 Hz, 1.5 Hz, H^{4B}), δ 7.66 (2H, dd, *J* = 7.95, 1.11 Hz, H^{6A}), δ 7.45(4H, overlapped peaks, H^{2D}, H^{6D}, H^{6B}), δ 7.31 (2H, td, *J* = 5.49 Hz, 1.38 Hz, H^{5C}), δ 7.0 (4H, overlapped peaks, H^{5A}, H^{5B}), δ 6.90 (2H, td, *J* = 7.56 Hz, 1.23 Hz, H^{4A}), δ 6.28 (2H, d, *J* = 7.54 Hz, H^{3A}), δ 3.98 (6H, t, *J* = 5.91 Hz, OCH_2), δ 3.61 (6H, t, *J* = 6.65 Hz, CH_2OH), δ 1.73 (6H, m, OCH_2CH_2), δ 1.40 (48H, m, $OCH_2CH_2CH_2(CH_2)_8$). IR (KBr/cm^{-1}): 3309.2 (br, H_2O), 2926.8 ($\nu_{as}(CH_2)$), 2853.4 ($\nu_s(CH_2)$), 1562.7 ($\nu_{as}(COO^-)$), 1368.9 ($\nu_s(COO^-)$). Λ_M ($c = 7.20\cdot10^{-5}$ mol·L^{-1}) = 62.22 Ω^{-1}·cm^2·mol^{-1} (methanol).

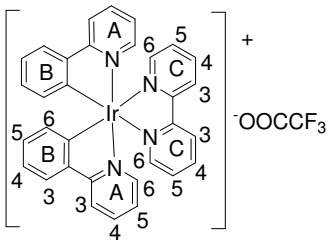

C_9. [Ir(*ppy*)$_2$(*bpy*)](*tfa*): The classical bridge-splitting reaction of the dimeric precursor [Ir(*ppy*)$_2$]$_2$-μCl$_2$ (0.150 g, 0.140 mmol) with 2,2'-bipyridine (0.043 g, 0.280mmol) in CH_2Cl_2/MeOH (20 ml, 3:1 v/v) was carried out for 4 hours under nitrogen atmosphere. Subsequently, the addition of 1.1 fold excess of Ag(I) salt containing *tfa* (0.068 g, 0.154 mmol) was made and the reaction mixture, protected from light, was further stirred for 2 hours. Then the solvents were evaporated, CH_2Cl_2 was added and insoluble AgCl formed was filtered. The pure product was obtained by recrystallization from CH_2Cl_2/Hexane. Yield: 0.160 g (80%). Dec. p.: 240 ºC. Anal. Calcd. for [$C_{34}H_{27}IrN_4O_2$] (769.79 g/mol): C, 53.05; H, 3.14; N, 7.28%. Found: C, 52.53; H, 2.90; N, 6.96%.^{1}H NMR ($CDCl_3$, 300MHz): δ 9.05 (2H, d, *J* =8.24 Hz, H^{3C}), δ 8.20 (2H, td, *J* = 7.95 Hz, 1.5 Hz, H^{4C}), δ 7.91 (4H, overlapped peaks, H^{3B}, H^{6C}), δ 7.76 (2H, td, *J* = 7.56 Hz, 1.37 Hz H^{4B}), δ 7.68 (2H, d, *J* = 7.70, H^{6A}), δ 7.49 (2H, d, *J* = 5.96 Hz, H^{6B}), δ 7.40 (2H, td, *J* =

5.76 Hz, 0.96 Hz, H^{5C}), δ 7.0 (2H, overlapped peaks, H^{5A}, H^{5B}), δ 6.93 (2H, td, *J* = 7.53 Hz, 1.23 Hz, H^{4A}), δ 6.84 (2H, d, ^3J = 7.2 Hz, H^{3A}). IR (KBr/cm^{-1}): 3408.5 (br H_2O), 1687.9 ($\nu_{as}(COO^-)$), 1200 ($\nu_s(COO^-)$). Λ_M ($c = 7.0\cdot10^{-5}$ mol·L^{-1}) = 108 $\Omega^{-1}\cdot cm^2\cdot mol^{-1}$ (acetonitrile).

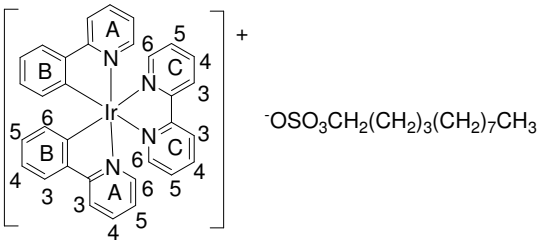

C_{10}. [Ir(*ppy*)$_2$(*bpy*)](*dos*): A stirred suspension of [Ir(*ppy*)$_2$(*bpy*)]ac (0.025 g, 0.0349 mmol) and 5.0 equivalents of *dos* (0.05 g, 0.174 mmol) in MeOH (15 ml) was heated to reflux. After 24 hours the resulting yellow solution was cooled to room temperature. Solvent was evaporated to dryness under reduced pressure, then 10 ml of CH_2Cl_2 was added, and insoluble white salt was filtered out. The pure product was obtained by recrystallization from CH_2Cl_2/Et_2O. Yield: 0.028 g (87.5%). Dec. p.: 240 ºC. Anal.Calcd. for [$C_{44}H_{49}IrN_4O_5S$] (922.17 g/mol): C, 57.81; H, 5.36; N, 6.08%. Found: C, 57.57; H, 5.29; N, 6.80%. ^{1}H NMR ($CDCl_3$, 300MHz): δ 9.26 (2H, d, *J* = 8.12 Hz, H^{3C}), δ 8.27 (2H, td, *J* = 7.8 Hz, 1.5 Hz, H^{4C}), δ 7.90 (4H, m, overlapped peaks H^{3B}, H^{6C}), δ 7.76 (2H, td, *J* = 7.20 Hz, 1.2 Hz, H^{4B}), δ 7.68 (2H, d, *J* = 7.20, H^{6A}), δ 7.49 (2H, td, *J* = 5.4 Hz, 1.5 Hz, H^{6B}), δ 7.38 (2H, t, *J* = 6.57 Hz, 1.5 Hz, H^{5C}), δ 7.85 (4H, overlapped peaks, H^{5A}, H^{5B}), δ 6.92 (2H, td, *J* = 7.0 Hz, 1.5 Hz, H^{4A}), δ 6.30 (2H, d, *J* = 7.54 Hz, H^{3A}), δ 4.11 (2H, t, *J* = 6.90 Hz, OSO_3CH_2), δ 1.74 (6H, m, $OSO_3CH_2(CH_2)_3$), δ 1.31 (14H, m, $OSO_3CH_2(CH_2)_3(CH_2)_7$), δ 0.87 (3H, t, *J* = 6. 9 Hz, $OSO_3CH_2(CH_2)_3(CH_2)_7CH_3$). IR (KBr/$cm^{-1}$): 3348.8 (OH), 3105, 3062.8, 3042.5 ($\nu_{as}(CH_3)$), 2924.5($\nu_{as}(CH_2)$), 2849.78 ($\nu_s(CH_2)$), 1247.8, 1227.31 ($\nu_s(SO_2)$). Λ_M ($c = 7.5\cdot10^{-5}$ mol·L^{-1}) = 68 $\Omega^{-1}\cdot cm^2\cdot mol^{-1}$ (methanol).

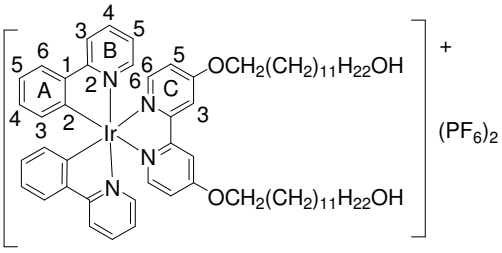

D_1. [Ir(*ppy*)$_2$(*bpy-C_{11}OH*)](PF$_6$)$_2$: The classical bridge-splitting reaction of the dimeric precursor [Ir(*ppy*)$_2$]$_2$-μCl_2 (0.100 g, 0.093 mmol) with *bpy-C_{11}OH* (0.0986g, 0.1865 mmol) in CH_2Cl_2/MeOH (20 ml, 2:1 v/v) was carried out for 1 hour under nitrogen atmosphere. Subsequently, the addition of 5.0 fold excess of inorganic salt containing PF_6 (0.076 g, 0.466 mmol) was made and the reaction mixture, protected from light, was further stirred for 3 hours. Then the solvents were evaporated, acetone was added and insoluble inorganic salt formed was filtered. The pure product was obtained by recrystallization from ethyl acetate/petroleum ether. Yield g (90%). Anal. Calcd.

for $C_{54}H_{68}F_6IrN_4O_4P$ (1174.32 g/mol): C, 55.23; H, 5.84; N, 4.77%. Found: C, 54.89; H, 5.55; N,4.50. ^{1}H NMR ($CDCl_3$, 300 MHz): δ 7.88 (4H, d, J = 6.97 Hz, H^{3C}, H^{3B}), δ 7.74 (2H, overlapped peaks, H^{6A}, H^{4B}), δ 7.65-7.63 (6H, overlapped peaks, H^{4B}, H^{6A}, H^{6B}), δ 7.05-6.98 (4H, overlapped peaks, H^{5C}, H^{5A}), δ 6.88-6.80 (4H, overlapped peaks, H^{5B}, H^{4B}), δ 6.28 (2H, d, J = 7.7 Hz , H^{3A}), δ 4.27 (4H, t, ^3J = 7.6 Hz, OCH_2), δ 3.63 (4H, t, ^3J = 7.6 Hz, CH_2O), δ 1.65 (36H, m, $OCH_2(CH_2)_8CH_2O$). IR (KBr/cm^{-1}): 2925.01 ($\nu_{as}(CH_2)$), 285.09 ($\nu_s(CH_2)$), 3434.79 (OH), 841.44 (PF_6). Λ_M (c = 7.0·10^{-5} mol·L^{-1})= 109 Ω^{-1}·cm^2·mol^{-1} (acetonitrile).

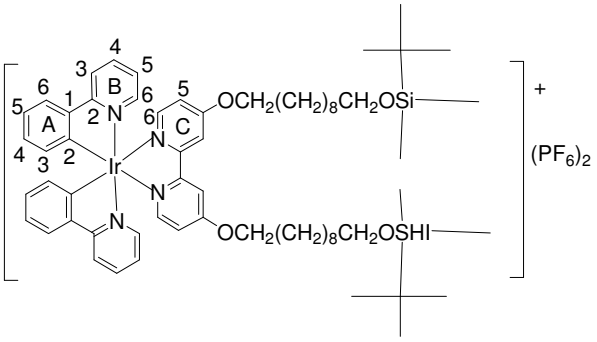

D$_2$. [Ir(*ppy*)$_2$(*bpy-C$_{11}$OTBDMS*)](PF$_6$)$_2$·H$_2$O: The classical bridge-splitting reaction of the dimeric precursor [Ir(*ppy*)$_2$]$_2$-μCl$_2$ (0.150 g, 0.140 mmol) with *bpy-C$_{11}$OH* (0.212g, 0.280 mmol) in CH_2Cl_2/MeOH (20 mL, 2 : 1 v/v) was carried out for 1 hours under nitrogen atmosphere. Subsequently, the addition of 5 fold excess of inorganic salt containing PF_6 (0.114 g, 0.070 mmol) was made and the reaction mixture, protected from light, was further stirred for 3 hour. Then the solvents were evaporated, CH_2Cl_2 was added and insoluble black salt formed was filtered. The pure product was obtained by recrystallization from acetone/diethyl ether. Yield 0.285g (71.6%). Dec. p.: 240 °C. Anal. Calcd. for $[C_{66}H_{96}F_6IrN_4O_4PSi_2]\cdot 1H_2O$ (1420.87 g/mol): C, 55.79; H, 6.95; N, 3.94%. Found: C, 55.69; H, 6.83; N,3.89%. ^{1}H NMR ($CDCl_3$, 300 MHz): δ 7.88 (4H, d, J = 6.97 Hz, H^{3C}, H^{3B}), δ 7.74 (2H, overlapped peaks, ^3J = 7.33 Hz, H^{6C}), 7.67-7.59 (6H, overlapped peaks, H^{4B}, H^{6A}, H^{6B}), δ 7.07-6.98 (4H, overlapped peaks, H^{5C}, H^{5A}), δ 6.91-6.81 (4H, overlapped peaks, H^{5B}, H^{4A}), δ 6.28 (2H, d, ^3J = 6.96 Hz ,H^{3A}), δ 4.27 (4H, t, ^3J = 6.03 Hz, OCH_2), δ 3.5 (4H, t, ^3J = 6.6 Hz, CH_2O), δ 1.80-1.26 (36H, m, $OCH_2(CH_2)_8CH_2O$), δ 0.88 (18H, s, $OCH_2(CH_2)_8CH_2OSiC(CH_3)_4$), δ 0.044 (12H, s, -$OCH_2(CH_2)_8CH_2OSiC(CH_3)_4(CH_3)_2$). IR (KBr/ cm^{-1}): 2928.49 ($\nu_{as}(CH_2)$), 2854.99 ($\nu_s(CH_2)$), 836.17 (PF_6). Λ_M (c = 7.0·10^{-5} mol·L^{-1}) = 103 Ω^{-1}·cm^2·mol^{-1} (acetonitrile).

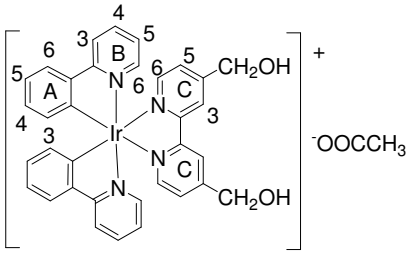

D$_3$. [Ir(*ppy*)$_2$(*bpyCH$_2$OH*)](*ac*): The classical bridge-splitting reaction of the dimeric precursor [Ir(*ppy*)$_2$]$_2$-μCl$_2$ (0.150 g, 0.140 mmol) with 4,4'-bis-(hydroxymethyl)-2,2'-bipyridine (0.060 g, 0.280 mmol) in CH_2Cl_2/MeOH (20 ml, 3:1 v/v) was carried out for 4 hours under nitrogen atmosphere. Subsequently, the addition of 1.1 fold excess of Ag(I) salt containing *ac* (0.052 g, 0.154 mmol) was made and the reaction mixture, protected from light, was further stirred for 2 hours. Then the solvents were evaporated, CH_2Cl_2 was added and insoluble AgCl formed was filtered. The pure product was obtained by recrystallization from CH_2Cl_2/Hexane. Yield 0.180 g (83%). Dec. p.:240 ºC. Anal.Calcd. for $C_{36}H_{31}IrN_4O_4$ (775.87 g/mol): C, 55.73; H, 4.03; N, 7.22%. Found: C, 55.47; H, 3.89; N, 6.80%. ^{1}H NMR ($CDCl_3$, 300MHz): δ 9.53 (2H, s, H^{3C}), δ 7.93 (2H, d, J = 8.31 H^{3B}), δ 7.84-7.79 (4H, overlapped peaks H^{6C}, H^{4B}), δ 7.74 (2H, d, J = 7.92 Hz, H^{6A}), δ 7.92 (2H, d, J = 7.58, H^{6B}), 7.28 (2H, d, J = 5.77 Hz, H^{5C}), δ 7.12-7.03 (4H, overlapped peaks , H^{5A}, H^{5B}), 7.33 (2H, td, ^3J = 7.35 Hz, 1.2 Hz, H^{4A}), δ 6.38 (2H, d, J = 7.63 Hz, H^{3A}), δ 4.94 (4H, s, CH_2), δ 3.91 (2H, br. s, CH_2OH), δ 2.04(3H, s, CH_3COO). IR (KBr/cm^{-1}): 3376 (OH), 2919.94($\nu_{as}(CH_2)$), 2849.78 ($\nu_s(CH_2)$). Λ_M (c = 7.7·10^{-5} mol ·L^{-1}) = 53.50 Ω^{-1}·cm^2·mol^{-1} (methanol).

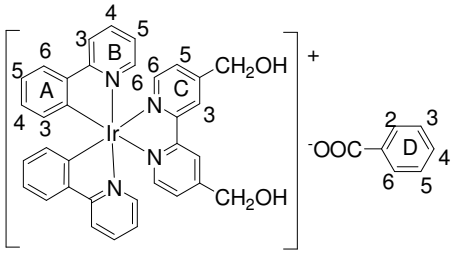

D$_4$. [Ir(*ppy*)$_2$(*bpy-CH$_2$OH*)](*bz*): The classical bridge-splitting reaction of the dimeric precursor [Ir(*ppy*)$_2$]$_2$-μCl$_2$ (0.150 g, 0.140 mmol) with 4,4'-bis-(hydroxymethyl)-2,2'-bipyridine (0.060 g, 0.280 mmol) in CH_2Cl_2/MeOH (20 ml, 3:1 v/v) was carried out for 4 hours under nitrogen atmosphere. Subsequently, the addition of 1.1 fold excess of Ag(I) salt containing *bz* (0.072 g, 0.154 mmol) was made and the reaction mixture, protected from light, was further stirred for 2 hours. Then the solvents were evaporated, CH_2Cl_2 was added and insoluble AgCl formed was filtered. The pure product was obtained by recrystallization from CH_2Cl_2/hexane. Yield 0.190 g (81%). Dec. p.:240 ºC. Anal.Calcd. for [$C_{41}H_{33}IrN_4O_4$](837.94 g/mol): C, 58.77; H, 3.97; N, 6.69%. Found: C, 58.87; H, 3.89; N, 6.80%. ^{1}H NMR ($CDCl_3$, 300MHz)): δ 9.60 (2H, s, H^{3C}), δ 8.04 (2H, d, J = 6.6 Hz, H^{3B}), δ 7.89 (2H, d, J = 7.7 Hz, H^{6C}), δ 7.74-7.65 (7H, overlapped peaks, H^{4B}, H^{2D}, H^{3D}, H^{4D}, H^{5D}, H^{6D}), δ 7.49 (2H, d, J = 5.5 Hz, H^{6A}), 7.30-7.25 (2H, overlapped peak, H^{6B}), δ 7.20 (2H, d, ^3J = 4.4 Hz, H^{5C}), 7.05-6.90 (6H, overlapped peaks, H^{5A}, H^{5B}, H^{4A}), δ 6.32 (2H, d, ^3J = 7.7 Hz, H^{3A}), δ 4.91

(4H, s, CH_2OH), δ 3.67 (2H, br. s, CH_2OH). IR (KBr/cm^{-1}): 3376 (OH), 2919.94 ($\nu_s(CH_2)$), 2849.78($\nu_{as}(CH_2)$). Λ_M ($c = 3.6\cdot10^{-5}$ mol·L^{-1}) = 58.87 $\Omega^{-1}\cdot cm^2\cdot mol^{-1}$ (methanol).

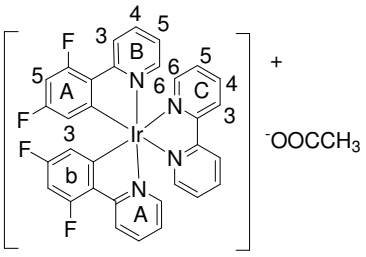

E_1. [Ir(*fppy*)$_2$(*bpy*)](*ac*): The classical bridge-splitting reaction of the dimeric precursor [Ir(*fppy*)$_2$]$_2$-μCl_2 (0.089 g, 0.073 mmol) with 2,2'-bipyridine (0.022 g, 0.146 mmol) in CH_2Cl_2/MeOH (20 ml, 3:1 v/v) was carried out for 4 hours under nitrogen atmosphere. Subsequently, the addition of 1.1 fold excess of Ag(I) salt containing *ac* (0.027 g, 0.080 mmol) was made and the reaction mixture, protected from light, was further stirred for 2 hours. Then the solvents were evaporated, CH_2Cl_2 was added and insoluble AgCl formed was filtered. The pure product was obtained by recrystallization from CH_2Cl_2/Hexane. Yield 0.70 g (61%). Dec. p.:250 ºC. Anal.Calcd for: [$C_{34}H_{23}F_4IrN_4O_4$] (787.78 g/mol): C, 51.84; H, 2.94; N, 7.11%. Found: C, 51.44; H, 2.84; N, 6.85%. ^{1}H NMR ($CDCl_3$, 300MHz): δ 9.59 (2H, d, J = 7.46 Hz, H^{3C}), δ 8.37-8.31 (4H, d, overlapped peaks , H^{3B}, H^{4C}), δ 7.89 (2H, d, J = 5.04 Hz, H^{4B}), δ 7.83 (2H, t, J = 7.68 Hz, H^{6B}), δ 7.49-7.44 (4H, overlapped peaks H^{6C}, H^{5C}), δ 7.05 (2H, t, J = 6.81 Hz, H^{5B}), δ 6.57 (2H, td , J = 9.0 Hz, 2.2 Hz, H^{5A}), δ 5.69 (2H, dd, ^3J = 8.4 Hz, 2.4 Hz, H^{3A}), δ 2.01 (3H, s, CH_3COO). IR (KBr/cm^{-1}): 3067.2, 2982.2, 2927.5 ($\upsilon_{as}(CH_3)$), 1559.3.6 ($\upsilon_{as}(COO^-)$), 1384.6 ($\upsilon_s(COO^-)$). Λ_M ($c = 3.0\cdot10^{-5}$ mol·L^{-1}) = 115 $\Omega^{-1}\cdot cm^2\cdot mol^{-1}$ (acetonitrile).

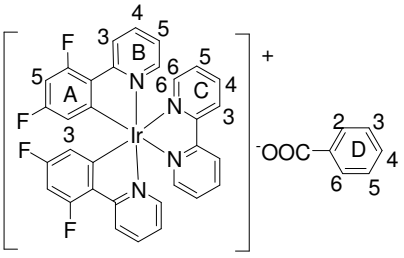

E_2. [Ir(*ppy*)$_2$(*bpy*)](*bz*): The classical bridge-splitting reaction of the dimeric precursor [Ir(*fppy*)$_2$]$_2$-μCl_2 (0.050 g, 0.041 mmol) with 2,2'-bipyridine (0.013 g, 0.082 mmol) in CH_2Cl_2/MeOH (20 ml, 3:1 v/v) was carried out for 4 hours under nitrogen atmosphere. Subsequently, the addition of 1.1 fold excess of Ag(I) salt containing *ac* (0.020 g, 0.045 mmol) was made and the reaction mixture, protected from light, was further stirred for 2 hours. Then the solvents were evaporated, CH_2Cl_2 was added and insoluble AgCl formed was filtered. The pure product was obtained by recrystallization from CH_2Cl_2/Hexane. Yield 0.043 g (62%). Dec. p.:240 ºC. Anal.Calcd. for $C_{39}H_{25}F_4IrN_4O_4$ (849.85 g/mol): C, 55.12; H, 2.97; N, 6.59%. Found: C, 55.87; H, 3.02; N, 6.80%. ^{1}H NMR ($CDCl_3$, 300MHz): δ 9.43 (2H, d, J = 8.1 Hz, H^{3C}), δ 8.29 (2H, d, J = 8.52 Hz, H^{3B}), δ 8.22 (2H, t, J = 7.53 Hz, H^{4B}), δ 8.06 (2H, d, J = 6.57 Hz, H^{6B}), δ 7.84-7.77 (4H, overlapped peaks H^{4C}, H^{5C}), δ 7.46 (2H, d, J = 5.76 Hz, H^{6C}), δ

7.39-7.25 (5H, overlapped peaks , H^{2D}, H^{3D}, H^{4D}, H^{5D}, H^{6D}), δ 7.02 (2H, t, *J* = 6.45 Hz, H^{5B}), δ 6.56 (2H, td, *J* = 9.06 Hz, 2.34 Hz, H^{5B}), δ 5.67 (2H, dd, *J* = 8.22 Hz, 2.19 Hz, H^{5B}). IR (KBr/cm^{-1}): 1558 ($\nu_{as}(COO^-)$), 1380 ($\nu_s(COO^-)$). Λ_M ($c = 3.6\cdot10^{-5}$ mol·L^{-1}) = 103 $\Omega^{-1}\cdot cm^2\cdot mol^{-1}$ (acetonitrile).

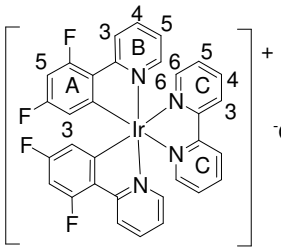

E_3. [Ir(*fppy*)$_2$(*bpy*)](*dos*): The classical bridge-splitting reaction of the dimeric precursor $[Ir(fppy)_2]_2$-μCl_2 (0.050 g, 0.041 mmol) with 2,2'-bipyridine (0.013 g, 0.082 mmol) in CH_2Cl_2/MeOH (20 ml, 3:1 v/v) was carried out for 4 hours under nitrogen atmosphere. Subsequently, the addition of 5 fold excess of inorganic salt containing *dos* (0.059 g, 0.205 mmol) was made and the reaction mixture, protected from light, was further stirred for 24 hours. Then the solvents were evaporated, CH_2Cl_2 was added and insoluble inorganic salt formed was filtered. The pure product was obtained by recrystallization from CH_2Cl_2/Hexane. Yield 0.057 g (70%). Dec. p.:240 ºC. Anal.Calcd. for $C_{44}H_{45}F_4IrN_4O_4S$ (994.13 g/mol): C, 53.16; H, 4.56; N, 5.64%. Found: C, 52.94; H, 4.79; N, 5.36%. ^{1}H NMR ($CDCl_3$, 300MHz): δ 9.33 (2H, d, *J* = 7.46 Hz, H^{3C}), δ 8.32 (4H, d, *J* = 7.41Hz, H^{3B}, H^{4C}), δ 7.89 (2H, d, *J* = 5.21 Hz, H^{4B}), δ 7.83 (2H, t, *J* = 8.22 Hz, H^{6B}), δ 7.49-7.45 (4H, overlapped peaks H^{6C}, H^{5C}), δ 7.07 (2H, t, ^3J = 6.24 Hz, H^{5B}), δ 6.58 (2H, td , *J* = 8.76 Hz, 1.92 Hz, H^{5A}), δ 5.70 (2H, dd, *J* = 8.23 Hz, 2.22 Hz, H^{3A}), δ 4.09 (2H, t, ^3J = 6.86 Hz, OSO_3CH_2), δ 1.74 (6H, m, $OSO_3CH_2(CH_2)_3$), δ 1.23 (14H, m, $OSO_3CH_2(CH_2)_3(CH_2)_7$), δ 0.85 (3H, t, ^3J = 6.69 Hz, $OSO_3CH_2(CH_2)_3(CH_2)_7CH_3$). IR (KBr,/$cm^{-1}$): 3075.9 ($\nu_{as}(CH_3)$), 2925.7 ($\nu_{as}(CH_2)$), 2854.6 ($\nu_s(CH_2)$), 1248.3, 1226.4 ($\nu_s(SO_2)$). Λ_M ($c = 3.3\cdot10^{-5}$ mol·L^{-1}) = 119 $\Omega^{-1}\cdot cm^2\cdot mol^{-1}$ (acetonitrile).

III.5 Synthesis and structural characterization of the octahedral ionic Zn(II) complexes

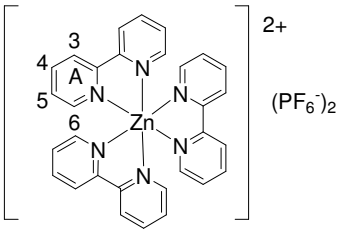

1. [Zn(*bpy*)$_3$](PF$_6$)$_2$: A suspension of *bpy* (0.500 g, 3.201 mmol) and Zn $(CH_3COO)_2{\cdot}2H_2O$ (0.234 g, 1.067 mmol) in 30 ml of methanol was heated to reflux under N_2 atmosphere. After 24 hours, clear solution formed was cooled to room temperature and NH_4PF_6 (0.860 g, 5.335 mmol) was added. The resulting faint pink suspension was again heated to reflux for 24 hours under N_2 atmosphere. Then the solvent was evaporated under vacuum, dichloromethane was added and the resulting mixture was filtered to remove inorganic salts. The pure product was obtained by recrystallization from CH_3CN/petroleum ether. Yield 0.660 g (75 %). M. p.: 300°C. Anal. Calcd. for $C_{30}H_{34}F_{12}N_6O_6P_2Zn$ (823.87 g/mol): C, 43.74; H, 2.94; N, 10.20%. Found: C, 42.99; H, 2.76; N, 10.25%. ^{1}H NMR (CD_3CN, 300 MHz): δ 8.49 (6H, d, *J* = 6.0 Hz, H^{3A}), δ 8.22 (6H, m, H^{4A}), δ 7.91 (6H, d, *J* = 5.13 Hz, H^{6A}), δ 7.55 (6H, m, H^{5A}). IR (KBr/cm^{-1}): 843.3 (PF_6).

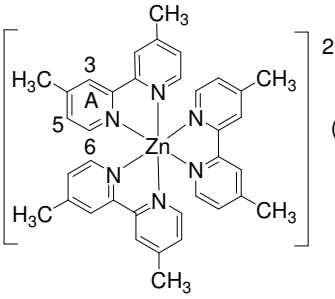

2. [Zn(*bpyCH$_3$*)$_3$](PF$_6$)$_2$: A suspension of *bpyCH$_3$* (0.200 g, 1.085 mmol) and Zn $(CH_3COO)_2{\cdot}2H_2O$ (0.079 g, 0.361 mmol) in 30 ml of methanol was heated to reflux under N_2 atmosphere. After 24 hours, clear solution formed was cooled to room temperature and NH_4PF_6 (0.294 g, 1.809 mmol) was added. The resulting faint pink suspension was again heated to reflux for 24 hours under N_2 atmosphere. Then the solvent was evaporated under *vacuum*, dichloromethane was added and the resulting mixture was filtered to remove inorganic salts. The pure product was obtained by recrystallization from CH_3CN/petroleum ether. Yield 0.262 g (80.0%). M. p.: >300°C. Anal. Calcd. for $C_{36}H_{36}F_{12}N_6O_6P_2Zn$ (908.03 g/mol): C, 47.62; H, 4.00; N, 9.26%; Found: C, 47.79; H, 4.16; N, 9.09%. ^{1}H NMR (CD_3CN, 300 MHz): δ 8.32 (6H, s, H^{3A}), δ 7.72 (6H, d, *J* = 5.13 Hz, H^{6A}), δ 7.34 (6H, d, *J* = 5.13 Hz, H^{5a}), δ 2.5 (6H, s, CH_3). IR (KBr/cm^{-1}): 3072.4, 2971.0, 2927.5 ($\upsilon_{as}(CH_3)$), 845.3 (PF_6).

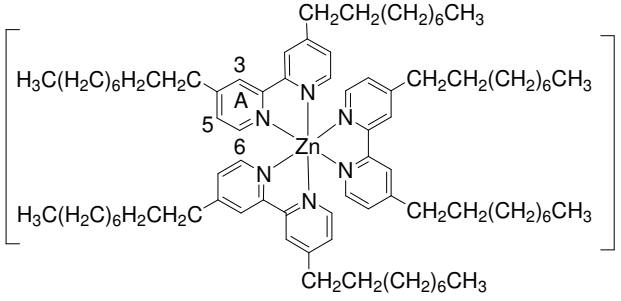

3. [Zn(*bpyC$_9$H$_{19}$*)$_3$](PF$_6$)$_2$: A suspension of *bpyC$_9$H$_{19}$* (0.250 g, 0.611 mmol) and Zn $(CH_3COO)_2{\cdot}2H_2O$ (0.044 g, 0.203 mmol) in 30 ml of methanol was heated to reflux under N_2 atmosphere. After 24 hours, clear solution formed was cooled to room temperature and NH_4PF_6 (0.166 g, 1.019 mmol) was added. The resulting faint pink suspension was again heated to reflux for 24 hours under N_2 atmosphere. Then the solvent was evaporated under vacuum, dichloromethane was added and the resulting mixture was filtered to remove inorganic salts. The pure product was obtained by recrystallization from CH_3CN/diethyl ether. Yield 0.222 g (70.0%). M. p.: 113°C. Anal. Calcd. for $C_{84}H_{132}F_{12}N_6O_6P_2Zn$ (1581.31 g/mol): C, 63.80; H, 8.41; N, 5.31%. Found: C, 63.79; H, 9.05; N, 5.57%. ^{1}H NMR ($CDCl_3$, 300 MHz): δ 8.05 (6H, s, H^{3A}), δ 7.81 (6H, d, *J* = 5.13 Hz, H^{6A}), δ 7.45 (6H, d, *J* = 5.13 Hz, H^{5A}), δ 2.78 (12H, s, CH_2), δ 1.67 (12H, m, CH_2CH_2), δ 1.26 (72H, m, CH_2CH_2 $(CH_2)_6$), δ 0.87 (18H, t, *J* = 6.78 Hz, $CH_2CH_2(CH_2)_6CH_3$). IR (KBr/cm^{-1}): 2926.6($\upsilon_{as}(CH_2)$), 2855.2 ($\upsilon_s(CH_2)$), 839.3 (PF_6).

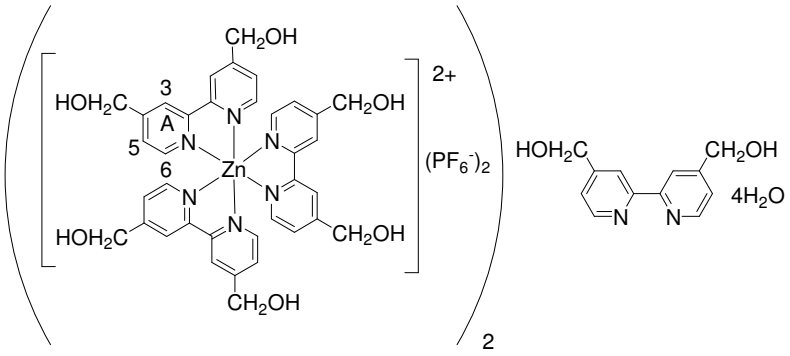

4. [Zn(*bpyC$_9$H$_{19}$*)$_3$](PF$_6$)$_2$: A suspension of *bpyCH$_2$OH* (0.250 g, 1.16 mmol) and Zn $(CH_3COO)_2{\cdot}2H_2O$ (0.084 g, 0.390 mmol) in 30 ml of methanol was heated to reflux under N_2 atmosphere. After 24 hours, clear solution formed was cooled to room temperature and NH_4PF_6 (0.318 g, 1.950 mmol) was added. The resulting faint pink suspension was again heated to reflux for 24 hours under N_2 atmosphere. Then the resulting mixture was filtered to remove inorganic salts, water added, and slow evaporation of water at room temperature gives pink crystals of the product. Yield 0.141 g (84.0%). M. p.: 225°C. Anal. Calcd. for $C_{84}H_{92}F_{24}N_{14}O_{18}P_4Zn$ (2006.42 g/mol): C, 42.93; H, 4.04; N, 8.54%. Found: C, 43.78; H, 3.99; N, 8.23%. ^{1}H NMR (DMSO-d_6, 300 MHz): δ 8.51 (14H, m, H^{3A}, H^{6A}), δ 7.64 (7H, m, H^{5a}), δ 5.67 (7H, s, -OH), δ 4.74 (14H, s, CH_2OH). IR (KBr/cm^{-1}): 3390 (-OH), 842 (PF_6).

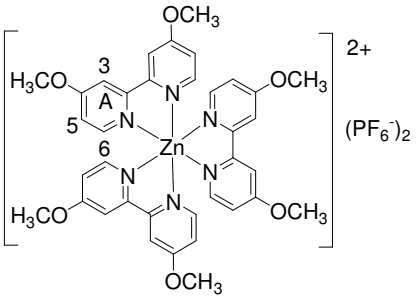

5. [Zn(*bpyOCH$_3$*)$_3$](PF$_6$)$_2$: A suspension of *bpyOCH$_3$* (250 mg, 1.16 mmol) and $Zn(CH_3COO)_2{\cdot}2H_2O$ (84 mg, 0.39 mmol) in 20 ml of methanol was heated to reflux under N_2 atmosphere. After 24 hours, the clear solution formed was cooled to room temperature and NH_4PF_6 (318 mg, 5.8 mmol) was added. The resulting pinkish suspension was again heated to reflux for 24 hours under N_2 atmosphere. Then the solvent was evaporated under vacuum, dichloromethane was added and the resulting mixture was filtered to remove inorganic salts. Recrystallization from CH_2Cl_2/diethyl ether yielded the pure product as a white crystalline solid. Yield 290 mg, 74 %). M.p. > 300°C. Anal. Calcd. for $C_{36}H_{36}F_{12}N_6O_6P_2Zn$ (1004.03 g/mol): C, 43.07; H, 3.61; N, 8.37%. Found: C, 42.99; H, 3.62; N, 8.11%. ^{1}H NMR (CD_3CN, 300 MHz): 7.72 (d, 3J = 6.24 Hz, 6H), 7.02 (dd, 3J = 6.24 hz, 4J = 2.58 Hz, 6H); 7.92 (d, 3J = 2.25, 6H); 4.00 (s,18H). IR(KBr/cm^{-1}): 2952.0 ($\upsilon_{as}(CH_2)$), 2847.0 ($\upsilon_s(CH_2)$), 848.0 (PF_6).

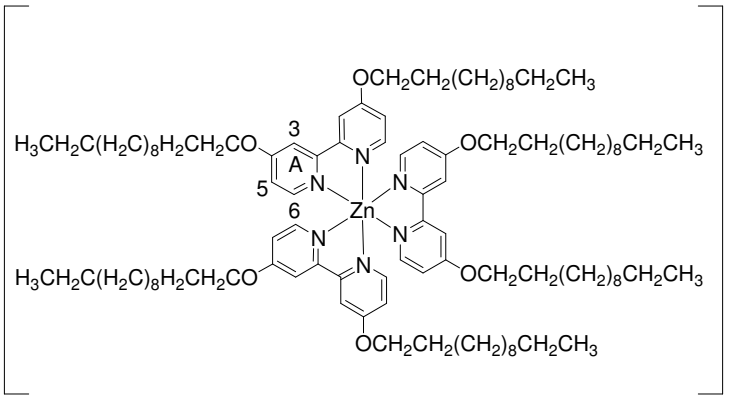

6. [Zn(*bpy-C$_{12}$*)$_3$](PF$_6$)$_2$: A suspension of *bpy-C$_{12}$* (0.150 g, 0.285 mmol) and Zn $(CH_3COO)_2{\cdot}2H_2O$ (0.021 g, 0.0953 mmol) in 30 ml of chloroform was heated to reflux under N_2 atmosphere. After 24 hours, faint yellow the clear solution formed was cooled to room temperature and NH_4PF_6 (0.077 g, 0.476 mmol) was added. The resulting faint yellow suspension was again heated to reflux for 24 hours under N_2 atmosphere. Then the solvent was evaporated under vacuum, dichloromethane was added and the resulting mixture was filtered to remove inorganic salts. Direct evaporation of solvent gives a sticky yellowish solid. Yield: 0.135 g (73.40 %). M. p.: 92°C. Anal. Calcd. for $C_{102}H_{168}F_{12}N_6O_6P_2Zn$ (1929.78 g/mol): C, 63.48; H, 8.77; N, 4.35%. Found: C, 63.84; H, 8.26; N, 4.05%. ^{1}H NMR ($CDCl_3$, 300 MHz): δ 7.79 (6H, d, *J* = 3.69 Hz, H^{6A}); δ 7.56 (6H, s, H^{3A}); δ 7.08 (6H, m, H^{5A}); δ 4.00 (12H, overlapped peaks, OCH_2), δ 1.80 (12H, m, CH_2CH_3), δ 1.470 (12H, m, $OCH_2CH_2(CH_2)_8$), δ 1.42 (96H, m, $OCH_2CH_2(CH_2)_8CH_2$), δ 0.87 (18H, t, *J* = 4.20 Hz,

$OCH_2CH_2(CH_2)_8CH_2CH_3$). IR (KBr/$cm^{-1}$): 2923.6 ($\upsilon_{as}(CH_3)$), 2853.3($\upsilon_s(CH_3)$), 1255.5($\upsilon_{as}$(C-O-C)), 1018.5 ($\upsilon_s$(C-O-C)), 837 ($PF_6$).

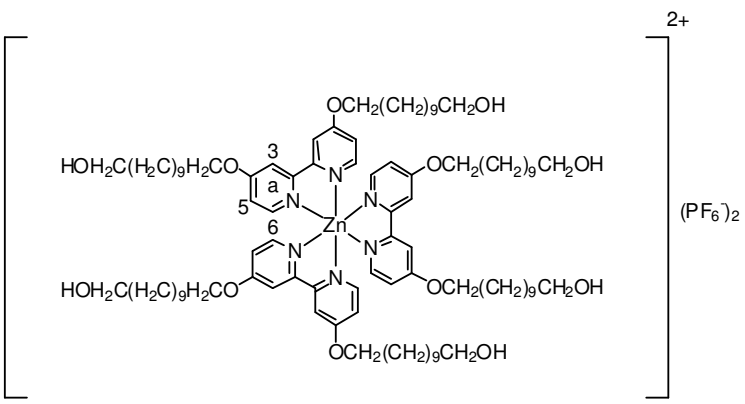

7. [Zn(*bpy-$C_{11}OH$*)$_3$](PF$_6$)$_2$: A suspension of *bpy-$C_{11}OH$* (0.100 g, 0.189 mmol) and Zn $(CH_3COO)_2{\cdot}2H_2O$ (0.013 g, 0.063 mmol) in MeOH/CH_2Cl_2 (2:1 v/v) was heated to reflux under N_2 atmosphere. After 24 hours, the clear solution formed was cooled to room temperature and NH_4PF_6 (0.051 g, 0.315 mmol) was added. The resulting clear solution was again heated to reflux for 24 hours under N_2 atmosphere. Then the solvent was evaporated under vacuum, dichloromethane was added and the resulting mixture was filtered to remove inorganic salts. The sticky product was obtained by recrystallization from CH_2Cl_2/ diethyl ether. Yield 0.069 g (66.3%). M. p.: 70°C. Anal. Calcd. for $C_{102}H_{168}F_{12}N_6O_6P_2Zn$ (1929.78 g/mol): C, 59.39; H, 8.10; N, 4.33%. Found: C, 59.46; H, 7.93; N, 4.57%. ^{1}H NMR ($CDCl_3$, 300 MHz): δ 7.73 (6H, d, *J* = 8.67 Hz, H^{6A}), δ 7.56 (6H, d, *J* = 2.19 Hz H^{3A}), δ 7.08 (6H, dd, *J* = 6.24 Hz, .22 Hz, H^{5A}), δ 4.00 (12H, overlapped peaks, OCH_2), δ 3.59 (12H, t, *J* = 6.6 Hz, CH_2OH), δ 1.46 (108H, m, $OCH_2(CH_2)_9CH_2OH$). IR (KBr/cm^{-1}): 2924.99 ($\upsilon_{as}(CH_3)$), 2852.8 ($\upsilon_s(CH_3)$), 1258.1(υ_{as}(C-O-C)), 1017.0 (υ_s(C-O-C)), 846.3 (PF_6).

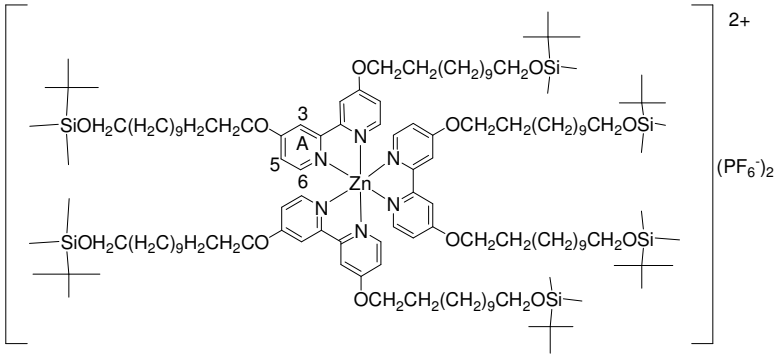

8. [Zn(*bpy-$C_{11}OTBDMS$*)$_3$](PF$_6$)$_2$: A suspension of *bpy-$C_{11}OTBDMS$* (0.100 g, 0.132 mmol) and Zn $(CH_3COO)_2{\cdot}2H_2O$ (0.010 g, 0.044 mmol) in MeOH/CH_2Cl_2 (2:1 v/v) was heated to reflux under N_2 atmosphere. After 24 hours, the clear solution formed was cooled to room temperature and NH_4PF_6 (0.035 g, 0.220 mmol) was added. The resulting clear solution was again heated to reflux for 24 hours under N_2 atmosphere. Then the

solvent was evaporated under vacuum, dichloromethane was added and the resulting mixture was filtered to remove inorganic salts. The sticky product was obtained by recrystallization from $CHCl_3$/hexane. Yield 0.069 g (73.40 %). M. p.: 105°C. Anal. Calcd. for $C_{138}H_{240}F_{12}N_6O_6P_2Si_6Zn$ (2699.24 g/mol): C, 61.41; H, 8.96; N, 3.11%. Found: C, 61.46; H, 8.84; N, 2.99%. ^{1}H NMR ($CDCl_3$, 300 MHz): δ 7.79 (6H, d, *J* = 5.88 Hz, H^{6A}), δ 7.57 (6H, d, *J* = 1.83 Hz H^{3A}), δ 7.08 (6H, d, *J* = 6.24 Hz, 2.22 Hz, H^{5A}), δ 4.14 (12H, overlapped peaks, OCH_2), δ 3.59 (12H, t, *J* = 6.6 Hz, $CH_2OSiC(CH_3)3(CH_3)_3$), δ 1.83 (12H, m, OCH_2CH_2), δ 1.37 (96H, m, $OCH_2CH_2(CH_2)_8CH_2O$), δ 0.90 (54H, s, $OCH_2CH_2(CH_2)CH_2OSiC(CH_3)_3$), 0.044 (36H, s, $OCH_2CH_2(CH_2)CH_2OSiC(CH_3)_3(CH_3)_2$). IR (KBr/$cm^{-1}$): 2919.1 ($\upsilon_{as}(CH_3)$), 2856.1 ($\upsilon_s(CH_3)$), 1256.3 ($\upsilon_{as}$(C-O-C)), 1023.7 ($\upsilon_s$(C-O-C)), 1102.2 (O-Si-C), 836.74 (PF_6).

III.6 Synthesis of the mesoporous materials

Synthesis of mesoporous material with C_3.

Complex **C_3** (0.030 g, 0.041 mmol) dissolved in 3.0 g water resulted in a relatively viscous yellow-orange solution (1.0 % w/w) having the pH = 9, that was stirred well at 20°C for 2 hours. Then 0.04 ml NH_4OH (30% w/w) solution was added until pH = 10 and stirred well further for 10 minutes. Finally, 0.31 ml of tetraethoxy silane (TEOS, 1.39 mmol) was added leading to the formation of a sticky gel which was stirred for another 30 minutes. 1.0 g of water was added and the mixture was kept under vigorous stirring at 20°C for 5 days. A fine precipitate forms in time. The precipitate was filtered out and washed with water until pH = 7. The obtained product was dried well at 60°C for 2 days.

Synthesis of mesoporous material with C_4.

Complex **C_3** (0.030 g, 0.038 mmol) dissolved in 3.0 g water resulted in a relatively viscous yellow-orange solution (1.0 % w/w) having the pH = 9, that was stirred well at 20°C for 2 hours. Then 0.04 ml NH_4OH (30% w/w) solution was added until pH = 10 and stirred well further for 10 minutes. Finally, 0.31 ml of tetraethoxy silane (TEOS, 1.39 mmol) was added leading to the formation of a sticky gel which was stirred for another 30 minutes. 1.0 g of water was added and the mixture was kept under vigorous stirring at 20°C for 5 days. A fine precipitate forms in time. The precipitate was filtered out and washed with water until pH = 7. The obtained product was dried well at 60°C for 2 days.

References:

1 D. L. Ma, W. L. Wong, W. H. Chung, F. Y. Chan, P. K. So, T. S. Lai, Z. Y. Zhou, Y. C. Leung and K. Y.Wong, *Angew. Chem., Int. Ed.*, **2008**, *47*, 3735–3739.

2 Q. Zhao, F. Y. Li and C. H. Huang, *Chem. Soc. Rev.*, **2010**, *39*, 3007–3030.

3 A. Kohler, J. S. Wilson and R. H. Friend, *Adv. Mater.*, **2002**, *14*, 701–707.

4 E. Holder, B. M. W. Langeveld and U. S. Schubert, *Adv. Mater.*, **2005**, *17*, 1109–1121.

5 R. D. Costa, E. Orti, H. J. Bolink, F. Monti, G. Accorsi, and Nicola Armaroli., *Angew. Chem. Int. Ed.* **2012**, *51*, 8178–8211.

6 H. J. Bolink, E. Coronado, R. D. Costa, N. Lardiés, E. Ortí, *Inorg. Chem.*, **2008**, *47*, 9149–9151.

7 Q. Zhao, L. Li, F. Y. Li, M. X. Yu, Z. P. Liu, T. Yi and C. H. Huang, *Chem. Commun.*, **2008**, 685–687.

8 K. W. Huang, H. Z. Wu, M. Shi, F. Y. Li, T. Yi and C. H. Huang, *Chem. Commun.*, **2009**, 1243–1245.

9 Y. You, H. S. Huh, K. S. Kim, S. W. Lee, D. Kim and S. Y. Park, *Chem. Commun.*, **2008**, 3998–4000.

10 C. H. Shin, J. O. Huh, S. J. Baek, S. K. Kim, M. H. Lee and Y. Do, *Eur. J. Inorg. Chem.*, **2010**, 3642–3651.

11 V. W. W. Yam, K. M. C. Wong and N. Zhu, *J. Am. Chem. Soc.*, **2002**, *124*, 6506–6507.

12 T. J. Wadas, Q. M. Wang, Y. J. Kim, C. Flaschenreim, T. N. Blanton and R. Eisenberg, *J. Am.Chem. Soc.*, **2004**, *126*, 16841–16849.

13 Y. Wan, H. Yang and D. Zhao, *Acc. Chem. Res.*, **2006**, *39*, 423 – 432.

14 Y. Wan and D. Zhao, *Chem. Rev.*, **2007**, *107*, 2821 – 2860.

15 T. Bessho, E. Yoneda, J. H. Yum, M. Guglielmi, I. Tavernelli, H. Imai, U. Rothlisberger, M. K. Nazeeruddin and M. Gratzel, *J. Am. Chem. Soc.*, **2009**, *131*, 5930–5934.

16 J. Slinker, D. Bernards, P. L. Houston, H. D. Abruna, S. Bernhard and G. G. Malliaras, *Chem. Commun.*, **2003**, 2392–2399.

17 Y. You and S. Y. Park, *Dalton Trans.*, **2009**, 1267–1282.

18 M. A. Baldo, D. F. O'Brien, Y. You, A. Shoustikov, S. Sibley, M. E. Thompson and S. R. Forrest, *Nature*, **1998**, *395*, 151–154.

19 K. A. Belmore, R. A. Vanderpool, J. C. Tsai, M. A. Khan and K. M. Nicholas*, J.Am. Chem. Soc*., **1988**, *110*, 2004–2005.

20 G. D. Marco, M. Lanza, A. Mamo, I. Stefio, C. Di Pietro, G. Romeo and S. Campagna, *Anal. Chem*., **1998**, *70*, 5019–5023.

21 K. K. W. Lo, C. K. Chung, T. K. M. Lee, L. H. Lui, K. H. K. Tsang and N. Y. Zhu, *Inorg. Chem*., **2003**, *42*, 6886–6897.

22 B. Norden, P. Lincoln, B. Akerman and E. Tuite, *Metal Ions in Biological Systems: Probing nucleic Acids by Metal Complexes of Small Molecules*, M. Decker, New York, **1996**.

23 Z. Li, H. Meng, *Organic Light-Emitting Materials and Devices*, CRC, Boca Raton, FL, **2007**.

24 C. Ulbricht, B. Beyer, C. Friebe, A. Winter and U. S. Schubert, *Adv. Mater*., **2009**, *21*, 4418–4441.

25 Q. B. Pei, Y. Yang, G. Yu, C. Zhang and A. J. Heeger, *J. Am. Chem. Soc*. **1996**, *118*, 3922–3929.

26 M. S. Lowry and S. Bernhard, *Chem. Eur. J*., **2006**, *12*, 7970–7977.

27 R. D. Costa, E. Ort, H. J. Bolink, S. Graber, S. Schaffner, M. Neuburger, C. E. Housecroft and E. C. Constable, *Adv. Funct. Mater*., **2009**, *19*, 3456–3463.

28 D. A. Bernards, T. Biegala, Z. A. Samuels, J. D. Slinker, G. G.Malliaras, S. F. Torres, H. D. Abruca and J. A. Rogers, *Appl. Phys. Lett*., **2004**, *84*, 3675–3677.

29 M. Buda, G. Kalyuzhny and A. J. Bard, *J. Am. Chem. Soc*., **2002**, *124*, 6090–6098.

30 D. A. Bernards, J. D. Slinker, G. G. Malliaras, S. Flores-Torres and H. D. AbruÇa, *Appl. Phys. Lett*., **2004**, *84*, 4980–4982.

31 J. D. Slinker, J. Rivnay, J. A. DeFranco, D. A. Bernards, A. A. Gorodetsky, S. T. Parker, M. P. Cox, R. Rohl, G. G. Malliaras, S. F. Torres and H. D. Abruca, *J. Appl. Phys*., **2006**, *99*, 074502–5.

32 Q. J. Sun, Y. F. Li and Q. B. Pei, *J. Disp. Technol*., **2007**, *3*, 211–224.

33 J. D. Slinker, J. Rivnay, J. S. Moskowitz, J. B. Parker, S. Bernhard, H. D. AbruÇa and G. G. Malliaras, *J. Mater. Chem*., **2007**, *17*, 2976–2988.

34 R. H. Friend, R. W. Gymer, A. B. Holmes, J. H. Burroughes, R. N. Marks, C. Taliani, D. D. C. Bradley, D. A. Dos Santos, J. L. Bredas, M. Logdlund and W. R. Salaneck, *Nature*., **1999**, *397*, 121–128.

35 H. Rudmann, S. Shimada, M. F. Rubner, *J. Am. Chem. Soc*., **2002**, *124*, 4918–4921.

36 V. Balzani, S. Campagna, *Topics in Current Chemistry*, Springer, Berlin, **2007**, *280*, 37–67.

37 L. Flamigni, A. Barbieri, C. Sabatini, B. Ventura and F. Barigelletti, *Top. Curr. Chem*., **2007**, *281*, 143–203.

38 A. Juris, V. Balzani, F. Barigelletti, S. Campagna, P. Belser and A. Von Zelewsky, *Coord. Chem. Rev*., **1988**, *84*, 85–77.

39 J. D. Slinker, A. A. Gorodetsky, M. S. Lowry, J. J. Wang, S. Parker, R. Rohl, S. Bernhard and G. G. Malliaras, *J. Am. Chem.Soc*., **2004**, *126*, 2763–2767.

40 G. G. Shan, Li. Y. Zhang, H. B. Li, S. Wang, D. X. Zhu, P. Li, C.G. Wang, Z.M. Su and Y. Liao, *Dalton Trans*., **2012**, *41*, 523–530.

41 K.. Ariga, H. Ito, J. P. Hill, H. Tsukube, *Chem. Soc. Rev*., **2012**, *41*, 5800–5835.

42 K.. Ariga, H. Ito, J. P. Hill, H. Tsukube, *Chem. Soc. Rev*., **2012**, *41*, 5800–5835.

43 C. Adachi, M. A. Baldo, M. E. Thompson and S. R. Forrest, *J. Appl. Phys*., **2001**, *90*, 5048–5051.

44 G. Zhou, C. L. Ho, W. Y. Wong, Q. Wang, D. Ma, X. Jing, F. Wang, Z. Lin, T. B. Marder and A. Beeby, *Adv. Funct. Mater*., **2008**, *18*, 499–511.

45 C. L. Ho, W. Y. Wong, Z. Q. Gao, C. H. Chen, K. W. Cheah, B. Yao, Z. Xie, Q. Wang, D. Ma, L. Wang, X. M. Yu, H. S. Kwok and Z. Lin, *Adv. Funct. Mater*., **2008**, *18*, 319–331.

46 C. L. Ho, W. Y.Wong, Q. Wang, D. Ma, L. Wang and Z. Lin, *Adv. Funct. Mater*., **2008**, *18*, 928–937.

47 H. J. Bolink, L. Cappelli, S. Cheylan, E. Coronado, R. D. Costa, N. Lardies, M. K. Nazeeruddin and E. Orti, *J. Mater. Chem*., **2007**, *17*, 5032–5041.

48 L. He, L. Duan, J. Qiao, G. F. Dong, L. D. Wang and Y. Qiu, *Chem.Mater*., **2010**, *22*, 3535–3542.

49 H. C. Su, F. C. Fang, T. Y. Hwu, H. H. Hsieh, H. F. Chen, G. H. Lee, S. M. Peng, K. T. Wong and C. C. Wu, *Adv. Funct. Mater*., **2007**, *17*, 1019–1027.

50 Y. Cheng-Han, C. Yi-Ming, C. Yun, H. Chia-Jung, F. Fu-Chuan, W. Ken-Tsung, C. Pi-Tai, C. Chih-Hao, T. Ming-Han and W. Chung-Chih, *Angew.Chem. Int. Ed.*, **2007**, *46*, 2418–2421.

51 A. B. Tamayo, B. D. Alleyne, P. I. Djurovich, S. Lamansky, I. Tsyba, N. N. Ho, R. Bau and M. E. Thompson, *J. Am. Chem. Soc*., **2003**, *125*, 7377–7387.

52 S. Q. Huo, J. C. Deaton, M. Rajeswaran and W. C. Lenhart, *Inorg Chem*., **2006**, *45*, 3155–3157.

53 P. Coppo, E. A. Plummer and L. De Cola, *Chem. Commun*., **2004**, 1774–1775.

54 M. Maestri, V. Balzani, C. D. Cornioley and A. V. Zelewsky, *Adv. Photochem*., **1992**, *17*.

55 K. Dedeian, P. I. Djurovich, F. O. Garces, G. Carlson and R. J. Watts, *Inorg Chem*., **1991**, *30*, 1685–1687.

56 F. O. Garces, K. A. King, R. J. Watts, *Inor. Chem*., **1988**, *27*, 3464–3471.

57 F. O Garces, R. J. Watts, *Magn. Reson. Chem*., **1993**, *31*, 529–536.

58 F. O. Graces, K. Dedian, N. L. Keder and R. J. Watts, *Acta Crystallogr*., **1993**, *49*, 1117–1120.

59 M. K. Nazeeruddin, R. H. Baker, D. Berner, S. Rivier, L. Zuppiroli, and M. Graetzel, *J. Am. Chem. Soc.*, **2003**, *125*, 8790–8797.

60 Y. You and S. Y. Park, *J. Am. Chem. Soc*., **2005**, *127*, 12438–12439.

61 J. A. G. Williams, A. J. Wilkinson and V. L. Whittle, *Dalton Trans*., **2008**, 2081–2099.

62 V. Adamovich, J. Brooks, A. Tamayo, A. M. Alexander, P. I. Djurovich, B. W. D'Andrade, C. Adachi, S. R. Forrest and M. E. Thompson, *New J. Chem*., **2002**, *26*, 1171–1178.

63 R. Ragni, E. A. Plummer, K. Brunner, J. W. Hofstraat, F. Babudri, G. M. Farinola, F. Naso and L. De Cola, *J. Mater. Chem*., **2006**, *16*, 1161–1170.

64 A. B. Tamayo, B. D. Alleyne, P. I. Djurovich, S. Lamansky, I. Tsyba, N. N. Ho, R. Bau and M. E. Thompson, *J. Am. Chem. Soc*., **2003**, *125*, 7377–7387.

65 A. R. McDonald, M. Lutz, L. S. von Chrzanowski, G. P. M. van Klink, A. L. Spek and G. van Koten, *Inorg. Chem*., **2008**, *47*, 6681–6691.

66 M. Nonoyama, *Bull. Chem. Soc. Jpn*., **1974**, 47, 767–768.

67 M. A. Bennett and T. R. B. Mitchell, *Inorg. Chem*., **1976**, *15*, 2936–2938.

68 H.C. Bottcher, M. Graf, H. Krüger and C. Wagner, *Inorg. Chem. Commun*., **2005**, *8*, 278–280.

69 S. Lamansky, P. Djurovich, D. Murphy, F. Abdel-Razzaq, R. Kwong, I. Tsyba, M. Bortz, B. Mui, R. Bau and M. E. Thompson*, Inorg. Chem*., **2001**, *40*, 1704–1711.

70 S. Sprouse, K. A. King, P. J. Spellane and R. J. Watts, *J. Am. Chem. Soc*., **1984**, *106*, 6647–6653.

71 J. N. Demas and B. A. DeGraff, *Coord. Chem. Rev*., **2001**, *211*, 317–351.

72 Y. H. Song, Y. C. Chiu, Y. Chi, Y. M. Cheng, C. H. Lai, P. T. Chou, K. T. Wong, M. H.Tsai and C. C. Wu, *Chem. Eur. J*., **2008**, *14*, 5423–5434.

73 J. Li, P. I. Djurovich, B. D. Alleyne, M. Yousufuddin, N. N. Ho, J. C.Thomas, J. C. Peters, R. Bau and M. E. Thompson, *Inorg. Chem*., **2005**, *44*, 1713–1727.

74 X. D. Liu, J. K. Feng, A. M. Ren, L. Yang, B. Yang and Y. G. Ma, *Opt. Mater*., **2006**, *29*, 231–238.

75 T. Tsuzuki, N. Shirasawa, T. Suzuki and S. Tokito, *Adv. Mater*., **2003**, *15*, 1455–1458.

76 X. Gu, T. Fei, H. Y. Zhang, H. Xu, B. Yang, Y. G. Ma and X. D. Liu, *Eur. J. Inorg. Chem*., **2009**, 2407–2414.

77 Q. Zhao, S. Liu, M. Shi, C. Wang, M. Yu, L. Li, F. Li, T. Yi and C. Huang, *Inorg. Chem*., **2006**, *45*, 6152–6160.

78 M. L. Xu, R. Zhou, G. Y. Wang and J. Y. Yu, *Inorg. Chim. Acta*, **2009**, *362*, 515–518.

79 H. W. Hong and T. M. Chen, *Mater. Chem. Phys*, **2007**, *101*, 170–176.

80 L. He, L. Duan, J. Qiao, R. J. Wang, P. Wei, L. D. Wang and Y. Qiu, *Adv. Funct. Mater.,* **2008**, *18*, 2123–2131.

81 G. G. Shan, D. X. Zhu, H. B. Li, P. Li, Z. M. Su and Y. Liao, *Dalton Trans*., **2011**, *40*, 2947–2953.

82 R. E. Harding, S. C. Lo, P. L. Burn and I. D. W. Samuel, *Org. Electron*., **2008**, *9*, 377–384.

83 C. H. Yang, S. W. Li, Y. Chi, Y.M. Cheng, Y. S. Yeh, P. T. Chou, G. H. Lee, C. H. Wang and C. F. Shu, *Inorg. Chem*., **2005**, *44*, 7770–7780.

84 Y.S. Park, J. W. Kang, D. M. Kang, J. W. Park, Y. H. Kim, S. K. Kwon and J.J. Kim, *Adv. Mater*., **2008**, *20*, 1957–1961.

85 P. T. Chou and Y. Chi, *Chem.–Eur. J*., **2007**, *13*, 380–395.

86 F. M. Hwang, H. Y. Chen, P.S. Chen, C. S. Liu, Y. Chi, C. F. Shu, F. I. Wu, P. T. Chou, S. M. Peng and G. H. Lee, *Inorg. Chem*., **2005**, *44*, 1344–1353.

87 S. Takizawa, J. Nishida, T. Tsuzuki, S. Tokito and Y. Yamashita, *Inorg. Chem*., **2007**, *46*, 4308–4319.

88 G.Q. Lu and X. S. Zhao, *Nanoporous Materials, science and engineering, Series of chemical engeneering*, Imperial college Press, London, **2004**, *4*.

89 H.S. Nalwa, *Handbook of Organic-Inorganic Hybrid Materials and Nanocomposites*, American Scientific Publishers, North Lewis Way, **2003,** *1*.

90 K. S. W. Sing, *Pure and Applied Chemistry.,* **1985,** *57*, 603–619.

91 C. Wang, Y. Mao, D. Wang, Q. Qu, G. Yang and X. Hu, C. Wang, *J. Mater. Chem.,* **2008**, *18*, 683–690.

92 P. C. A. Alberius, K. L. Frindell, R. C. Hayward, E. J. Kramer, G. D. Stucky and B. F. Chmelka, *Chem. Mater.*, **2002**, *14*, 3284–3294.

93 C. T. Kresge, M. E. Leonowicz, W. J. Roth, J. C. Vartuli and J. S. Beck, *Nature*, **1992**, *359*, 710–712.

94 J. S. Beck, J. C. Vartuli, W. J. Roth, *J. Am. Chem. Soc*., **1992**, *114*, 10834–10843.

95 F. Schuth and W. Schmidt, *Adv. Mater.* **2002**, *14*, 629–638.

96 J. Y. Ying, C. P. Mehnert and M. S. Wong, *Angew. Chem. Int. Ed.,* **1999**, *38*, 56–77.

97 F. Schuth, *Chem. Mater.,* **2001**, *13*, 3184–3195.

98 K. Holmberg, B. Jonsson, B. Kronberg and B. Lindman, *Surfactants and polymers in aqueous solution.,* England, 2nd ed. John Wiley & Sons Ltd. **2003**.

99 C. J. Brinker, G. W. Scherer, *Sol-gel science*. London: Academic Press **1990**, 97–234.

100 J. C. Vartuli, C. T. Kresge, M. E. Leonowicz, A. S. Chu, S. B. McCullen, I. D. Johnson, and E. W. Sheppardt, *Chem Mater.,* **1994**, *6*, 2070–2077.

101 G. S. Attard, J. C. Glyde and C. G. Goltner, *Nature*, **1995**, *378*, 366–368.

102 B. A. Ammundsen, G. R. Burns, D. J. Jones and J. Rozière*, J. Sol–Gel Sci. Technol*., **1997,** *8*, 331–336.

103 C. G. Goltner and M. Antonietti, *Adv. Mater.,* **1997**, *9*, 431–436.

104 B. Smarsly, S. Polarz and M. Antonietti, *J. Phys. Chem. B,* **2001**, *105*, 10473–10483.

105 J. Rozière, M. Brandhorst, R. Dutartre, M. Jacquin, D.J. Jones, P. Vitse and J. Zajac, *J. Mater. Chem*., **2001,** *11*, 3264–3275.

106 J. L. Blin, A. Leonard and B. L. Su, *Chem. Mater.,* **2001**, *13*, 3542–3553.

107 Q. S. Huo, D. I. Margolese, U. Ciesla, P. Y. Feng, T. E. Gier, P. Sieger, R. Leon, P. M. Petroff, F. Schuth, G. D. Stucky, *Nature,* **1994**, *368*, 317–321.

108 A. Stein, B. J. Melde and R.k C. Schroden, *Adv. Mater*., **2000**, *12*, 1403–1419.

109 G. Kickelbick, *Hybrid Materials, Synthesis, Characterization, and Applications*, Wiley-VCH Verlag GmbH & Co. KGaA, Weinheim, **2007**.

110 Y. M. Setoguchi, Y. Teraoka, I. Moriguchi and S. Kagawa, *J Porous Mater*, **1997**, *4*, 129–134.

111 S. Che, H. Li,S. Lim,Y. Sakamoto, O. Terasaki, And Takashi Tatsumi, *Chem. Mater*., **2005**, *17*, 4103–4113.

112 Y. Sakamoto, M. Kaneda, O. Terasaki, D. Y. Zhao, J. M. Kim, G. Stucky, H. J. Shim and R. Ryoo, *Nature,* **2000**, *408*, 449–453.

113 S. D. Shen, A. E. Garcia-Bennett, Z. Liu, Q. Y. Lu, Y. F. Shi, Y. Yan, C. Z. Yu, W. C. Liu, Y. Cai, O. Terasaki and D. Y. Zhao, *J. Am. Chem. Soc.,* **2005**, *127*, 6780–6787.

114 B. Tan, A. Dozier, H. J. Lehmler, B. L. Knutson and S. E. Rankin, *Langmuir.,* **2004**, *20*, 6981–6984.

115 S. A. Bagshaw, E. Prouzet and T. J. Pinnavaia, *Science*, **1995**, *269*, 1242–1244.

116 M. Templin, A. Franck, A. DuChesne, H. Leist, Y. M. Zhang, R. Ulrich, V. Schadler and U. Wiesner, *Science*, **1997**, *278*, 1795–1798.

117 G. M. Whitesides, J. P. Mathias and C. T. Seto, *Science*, **1991**, *254*, 1312–1319.

118 Y. Wan, Y. Shia and D. Zhao. *Chem. Commun.*, **2007**, 897–926.

119 M. G. Colombo, A. Hauser and A. U. Gudel, *Top. Curr. Chem.*, **1994**, *171*, 144.

120 G. R Desiraju, *Angew. Chem. Int. Ed.*, **2007**, *46*, 8342–8356.

121 J. A. Theobald, N. S. Oxtoby, M. A. Phillips, N. R. Champness and P. H. Beton, *Nature*, **2003**, *424*, 1029–1031.

122 P. A. Staniec, L. M. A. Perdigao, A. Saywell, N. R. Champness and P. H. Beton, *ChemPhysChem*., **2007**, *8*, 2177–2181.

123 M. Stohr, M. Wahl, H. Spillmann, L. H. Gade and T. A. Jung, *Small*, **2007**, *3*, 1336–1340.

124 K. Tahara, S. Furukawa, H. Uji-I, T. Uchino, T. Ichikawa, J. Zhang, W. Mamdouh, M. Sonoda, F. C. De Schryver, S. De Feyter and Y. Tobe, *J. Am. Chem. Soc*., **2006**, *128*, 16613–16625.

125 K. G. Nath, O. Ivasenko, J. A. Miwa, H. Dang, J. D. Wuest, A. Nanci, D. F. Peripchka and F. Rosei, *J. Am. Chem. Soc*., **2006**, *128*, 4212–4213.

126 S. Griessl, M. Lackinger, M. Edelwirth, M. Hietschold and W. M. Heckl, *Single Mol*., **2002**, *3*, 25–31.

127 B. B. Bozic-Weber, E.C. Constable, N. Hostettler, C. E. Housecroft, R. Schmitt and E. Schonhofer, *Chem. Commun*., **2012**, *48*, 5727–5729.

128 A. Barbieri, G. Accorsi and N. Armaroli, *Chem. Commun*., **2008**, 2185–2193.

129 Y. Marcus, *Chem. Rev*., **1988**, *88*, 1475–1498.

130 I. L. Alberts, K. Nadassy, S. J. Wodak, *Protein sci*. **1988**, *7*, 1700–1716.

131 A. Santoro, A. M. Prokhorov, V. N. Kozhevnikov, A. C. Withwood. B. Donnio and D. W. Bruce, *J. Am. Chem. Soc*., **2011**, *133*, 5248 – 5251.

132 K. D. Berlin and D. E. Gibbs, *Proc. of the Okla. Acad. of Sci*., **1963**, *44*, 89–94.

133 L. P. Olson, D. R. Whitcomb, M. Rajeswaran, T. N. Blanton and B. J. Stwertka, *Chem. Mater*., **2006**, *18*, 1667–1674.

134 B. T. Usubaliev, E. M. Movsumov, I. R. Amiraslanov, A. I. Akhmedov, A. A. Musaev and K. S. Mamedov. *J. Structural Chem*., **1981**, 22, 73–77.

135 K. E. Rowe and D. W. Bruce, *J. Mater. Chem*., **1998**, *8*, 331–341.

136 W. J. Geary, *Coord. Chem. Rev.,* **1971**, *7*, 81–122.

137 A. M. Talarico, E. I. Szerb, I. Aiello, T. F. Mastropietro, A. Crispini and M. Ghedini, *Dalton Trans.,* **2012**, *41*, 8899–8907.

138 A. M. Talarico, E. I. Szerb, I. Aiello, T. F. Mastropietro, A. Crispini and M. Ghedini, *Dalton Trans.,* **2012**, *41*, 4919–4926.

139 A. M. Talarico, I. Aiello, A. Bellusci, A. Crispini, M. Ghedini, N. Godbert, T. Pugliese and E. I. Szerb, *Dalton Trans*., **2010**, *39*, 1709–1712.

140 M. Yoshizawa, M. Nagao, K. Umemoto, K. Biradha, M. Fujita, S. Sakamoto and K. Amaguchi, *Chem. Commun.*, **2003**, 1808–1809.

141 K. Umemoto, K. Yamaguchi and M. Fujita, *J. Am. Chem. Soc.,* **2000**, *122*, 7150–7151.

142 M. Fujita, N. Fujita, K. Ogura and K. Yamaguchi, *Nature*, **1999**, *400*, 52–55.

143 C. Peinador, V. Blanoo and J. M. Quintela, *J. Am. Chem. Soc.*, **2009**, *131*, 920–921.

144 PLATON, *A Multipurpose Crystallographic Tool*, Utrecht University, Utrecht, The Netherlands, A. L. Spek, **1998**.

145 G. G. Evans and J. A. Boeyens, *Acta Cryst., Sect. B: Struct. Sci*., **1989**, *45*, 581–590.

146 I. Dance and M. J. Scudder, *J. Chem. Soc., Dalton Trans*., **1998**, 1341.

147 J. Breu, C. Kratzer and H. Yersin, *J. Am. Chem. Soc*., **2000**, *122*, 2548–2555.

148 W. Huanga and T. Ogawaa, *Polyhedron*, **2006**, *25*, 1379–1385.

149 H. D. Flack and G. Bernardinelli, *Chirality*, **2008**, *20*, 681–690.

150 S. Gonella, J. Mahieux, M. Sanselme and G. Coquerel*, Org. Process Res. Dev*., **2012**, *16*, 286–293.

151 D. Cremer and J. A. Pople, *J. Am. Chem. Soc*., **1975**, *97*, 1354–1358.

152 K. K. Chacko and W. Saenger, *J. Am. Chem. Soc*., **1981**, *103*, 1708–1715.

153 V. Zabel, W. Saenger and S. A. Mason*, J. Am. Chem. Soc*., **1986**, *108*, 3664–3673.

154 J. Xu, E. Radkov, M. Ziegler and K. N. Raymond, *Inorg. Chem*., **2000**, *39*, 4156–4164.

155 L.S. Long, Y.R. Wu, R.B. Huang and L.Z. Zheng, *Inorg. Chem*., **2004**, *43*, 3798–3800.

156 M. Zuhayra, W. U. Kampen, E. Henze, Z. Soti, L. Zsolnai, G. Huttner and F. Oberdorfer, *J. Am. Chem. Soc*., **2006**, *128*, 424–425.

157 It is worthy to mention that the letters N and M, used to designate the two principal types of chromonic phase, originated in the appearance of these two optical textures—the letter 'N' from the similarity of the texture shown by this to that formed by thermotropic nematic systems—the letter 'M' because herringbone textures had been previously seen in the 'middle' phases of conventional amphiphile systems

158 J. Lydon, *J. Mater. Chem*., **2010**, *20*, 10071–10099.

159 W. Lu, Y. Chen, V. A. L. Roy, S. S. Chui and C. Che, Angew. Chem. Int. Ed. **2009**, *48*, 7621–7625.

160 R. Schmidt, M. Schmutz, A. Mathis, G. Decher, M. Rawiso, Ph. J. Mésini, *Langmuir,* **2012**, *18***,** 7167–7173.

161 R. Oda, I. Huc, J.-C. Homo, B. Heinrich, M. Schmutz, S. Candau, Langmuir, **1999**, *15*, 2384–2390.

162 E. I. Szerb, A. M. Talarico, I. Aiello, A. Crispini, N. Godbert, D. Pucci, T. Pugliese and M. Ghedini, *Eur. J. Inorg. Chem.*, **2010**, 3270–3277.

163 D. Aiello, A. M. Talarico, F. Teocoli, E. I. Szerb, I. Aiello, F. Testa and M. Ghedini, *New J. Chem.,* 2011**, 35,** 141–148.

164 A. Guerrero-Martınez, Y. Vida, D. Domínguez-Gutiérrez, R. Q. Albuquerque and L. De Cola, *Inorg. Chem.*, **2008**, *47*, 9131–9133.

165 H. Wang, Q. Liao, H. Fu, Y. Zeng, Z. Jiang, J. Ma and J. Yao, *J. Mater. Chem*., **2009**, *19*, 89–96.

166 C. H. Shin, J. O. Huh, M. H. Lee and Y. Do, *Dalton Trans*., **2009**, *33,* 6476–6479.

167 Y. R. Hong and C. B. Gorman, *J. Org. Chem*., **2003**, *68*, 9019–9025

168 F. Morale, R. L. Finn, S. R. Collinson, A. J. Blake, C. D. Wilson, W. Bruce, D. Guillon, B. Donnio, M. Schroder., *New J.Chem.,* **2008**, *32*, 297-305.

169 I.Aiello, A. Bellusci, A. Crispini, M. Ghedini, D. Pucci, T. Spataro, *Mol. Cryst. Liq.Cryst.,* **2008**, *481*, 1-13.

170 G. Barberio, A. Bellusci, A. Crispini, M. Ghedini, A.Golemme, P. Prus, D. Pucci, *Eur. J. Inorg.Chem.,* **2005**, 181-188.

171 E. Terrazzi, J.-M. Bénech, J.P. Rivera, G. Bernardinelli, B. Donnio, D. Guillon, C. Piguet, *Dalton Trans.,* **2003**, 769-772.

172 G. Will, G. Boschloo, S. N. Rao, and D. Fitzmaurice, *J. Phys. Chem. B*, **1999**, *103*, 8067–8079.

173 W. J. Geary, *Coord. Chem. Rev.,***1971**, *7*, 81-122.

174 Y. You and S.Young Park, J. Am. Chem. Soc., **2005**, *127*, 12438-12439.

175 W. J. Geary, *Coord. Chem. Rev.,***1971**, *7*, 81 – 122.

176 Y. Kawamura, J. Brooks, J. J. Brown, H. Sasabe and C. Adachi, *Phys. Rev. Lett*., **2006**, *96*, 017404.

177 C. Rothe, C. J. Chiang, V. Jankus, K. Abdullah, X. Zeng, R. Jitchati, A. S. Batsanov, M. R. Bryce and A. P. Monkman, *Adv. Funct. Mater*., **2009**, *19*, 2038–2044.

178 C. H. Chang, C. C. Chen, C. C. Wua, C. H. Yang and Y. Chi,*Org. Electron.,* **2009**, *10*, 364–1371.

179 C.-H. Yang, S. H. Yang and C.S. Hsu, *Nanotechnology*, **2009**, *20*, 315601–315606.

180 K. E. Amos, N. J. Brooks, N. C. King, S. Xie, J. C. Vazquez, M. J. Danks, H. B. Jervis, W. Zhou, J. M. Seddon, and D. W. Bruce, *J. Mater. Chem*., **2008**, *18*, 5282–5292.

181 G. Will, G. Boschloo, S. N. Rao, and D. Fitzmaurice, *J. Phys. Chem. B*, **1999**, *103*, 8067–8079

182 N. Demas and G. A. Crosby, *J. Phys. Chem*., **1971**, *75*, 991–1024.

183 K. Nakamaru, *Bull. Chem. Soc. Jpn*., **1982**, *5*, 2697–2705.

184 *SAINT*, Version 6.45 Copyright (c) 2003, Bruker Analytical X-ray Systems Inc.

185 G.M. Sheldrick, *SADABS*. Version 2.10, Bruker AXS Inc., Madison, WI, USA, 2003.

186 *SHELXTL-NT*, Version 5.1 Copyright (c) 1999, Bruker Analytical X-ray Systems Inc.

187 DIAMOND 3.1b, Crystal Impact GbR, CRYSTAL IMPACT K; Brandeburg & H. Putz GBR: Bonn, Germany, 2006.